Retrospective Cost-based Adaptive Spacecraft Attitude Control

by

Gerardo E. Cruz Ortiz

A dissertation submitted in partial fulfillment
of the requirements for the degree of
Doctor of Philosophy
(Aerospace Engineering)
in the University of Michigan
2015

Doctoral Committee:

Professor Dennis S. Bernstein, Chair
Assistant Professor James R. Forbes
Professor Ilya V. Kolmanovsky
Professor A. Galip Ulsoy

2015

Para mis abuelos Gerardo y Estela. Gracias por inspirarme hasta el final. Descansen en paz.

A C K N O W L E D G M E N T S

I would like to thank my adviser Professor Dennis Bernstein for pushing me to strive for more and the countless revisions of our papers. I want to thank Professor Ilya Kolmaonvsky for giving me the opportunity to grade for his different courses, and for being on my committee. I also want to thank Professor James Forbes for the invaluable predefense suggestions and Professor Galip Ulsoy for taking the time to be part of my defense committee.

I am grateful for the funding from the Gates Millenium Scholars program which has enabled me to pursue an excellent education for the last 10 years. Also thanks to the Department of Aerospace Engineering and the Rackham Graduate School at the University of Michigan for the summer funding during my last two years.

Thanks for the love and support of my mom Estela, and my godmother Yayi who are always there for me despite the distance. Also, to my siblings, Francisco, Juan Jose, and Stella, who one way or another taught me to work with others and are the source of my love of teaching.

To my friends, Sasha, Rose, Eduardo, Matt, Amy, and Kenny, thank you for your support, the advice, and all the good times. To Laura and the Dance Revolution community for providing a home and a loving atmosphere in which to unwind and share my passion.

To those who blazed the trail before me, Asad and Alex, who not only inspired me to pursue a PhD but also helped me get through it. To my colleagues in Professor Bernstein's research group especially Frant Sobolik with whom I had the pleasure of many productive discussions.

James O'Donnell, Neerav Shah, and all the people at Goddard Spaceflight Center's Attitude Control Systems Engineering Branch for providing me a window into the real world of engineering while I worked on my degree.

Last but not least I thank my math teacher and mentor, Nelson Ciprian, whose lessons and encouragement have led me here and which I carry everywhere I go.

TABLE OF CONTENTS

LIST OF FIGURES

LIST OF TABLES

ABSTRACT

Retrospective Cost-based
Adaptive Spacecraft Attitude Control

by

Gerardo E. Cruz Ortiz

Chair: Dennis S. Bernstein

Fixed gain attitude control laws are sensitive to modeling errors and actuator nonlinearities. Adaptive control can solve many of these challenges. We present a retrospective cost-based adaptive spacecraft attitude controller designed using the system's impulse response as modeling information. The performance metric is based on rotation matrices and thus, the controller does not suffer from singularities or discontinuities present in vector attitude representations.

We demonstrate robustness to inertia and actuator scaling as well as actuator misalignment and nonlinearities, unknown disturbances, sensor noise and bias for thrusters and reaction wheels through numerical simulations. We implement an averaged Markov parameter and decentralized control to address the problem of the singular input matrix of magnetic torquers. For control moment gyros, we develop a hybrid linearization and impulse response-based Markov parameter and present new guidelines to evaluate the feasibility of desired rest-to-rest maneuvers.

Finally, we address the problem of angular velocity-free attitude control of a flexible spacecraft with noncollocated sensors and actuators. We present a new approach to controlling harmonic nonminimum-phase systems using the step and impulse response of the linearized system. We demonstrate robustness to model uncertainty through system analysis and numerical simulations.

CHAPTER 1

Introduction

Spacecraft play an important yet mostly invisible role in our everyday lives. Communications, GPS, and weather predictions are only possible because of orbiting satellites. Science also benefits immensely from space-based observations; spacecraft provide valuable data which has furthered mankind's understanding of not only planet Earth but of the solar system and beyond. The instruments used for these measurements and tasks need to be precisely pointed at different spots on Earth, the stars, or other spacecraft. This is attitude control.

Spacecraft attitude control is a nonlinear control problem due to the quadratic nonlinearity in the dynamics (Euler's) equation and the kinematic nonlinearities due to the special orthogonal group SO(3) of 3×3 rotation matrices [1]. Although using rotation matrices for control synthesis seems like an obvious choice, memory constraints in space-qualified computers, difficulties propagating the matrices in estimators, and complicated control analysis have rendered this choice unpopular [2]. Therefore, rotation matrices are usually parameterized using 3 or 4 component vector representations [3].

Quaternions remain the standard representation for many spacecraft missions [4]. This 4×1 vector parameterization avoids the singularities inherent in the dynamics of 3×1 representations, and requires less memory than rotation matrices. However, quaternions cover SO(3) twice, that is, every rotation matrix in SO(3) can be represented by two different quaternions. Furthermore, careful control design is required to avoid unwinding, a phenomenon where the controller will rotate 359 deg clockwise to achieve a counterclockwise rotation of 1 deg [5, 6]. To avoid issues with quaternions and other parameterizations we develop our control laws using rotation matrices. Although matrix operations are memory and resource heavy, we present an algorithm which does not require propagation of the rotation matrices and in which terms involving the matrices can be easily computed using quaternions or other vector attitude representations.

The attitude of a spacecraft in low-Earth orbit can be either passively stabilized or actively controlled. Passive methods exploit environmental torques to achieve a stable

attitude. However, the range of reachable attitudes is limited by the specific method utilized [7]. Active attitude control is achieved by changing the angular momentum of the spacecraft through torque generation or momentum redistribution [8]. In practice, nonlinearities arise from the type of actuation implemented on the spacecraft. Thrusters change the angular momentum of the spacecraft due to the forces they apply to the spacecraft. However, they usually operate in an on-off mode which is nonlinear and may have limited accuracy. Magnetic torquers can change the total angular momentum of the spacecraft by creating a local magnetic dipole which interacts with the Earth's magnetic field. Unfortunately, magnetic torquers are highly nonlinear due to the fact that the available torque at each instant is confined to a plane that is perpendicular to the direction of the Earth's magnetic field, which is also time-varying. Furthermore, the accuracy of control laws for magnetic torquers depends on limited knowledge of the Earth's magnetic field or the accuracy of magnetometers.

In contrast to thrusters and magnetic torquers, reaction wheels cannot change the total angular momentum of the spacecraft. Each reaction wheel spins about an axis that is fixed in the spacecraft body frame and can redistribute the body-frame angular momentum by changing the speed at which they spin relative to the spacecraft bus. However, as disturbance torques accumulate, reaction wheels spin up and may saturate. Thus, thrusters or torquers may be needed for desaturation [9, 10].

An alternative to reaction wheels is to spin a wheel at a constant rate about its axis and then rotate the wheel axis about a direction that is orthogonal to the wheel axis. This gimbaled-wheel is a control moment gyro (CMG). Although the dynamics of CMG's are significantly more complex than reaction wheels, the torques they can produce are substantially higher [11].

Attitude control laws can be separated into two categories. The first type of controller considers the actuator dynamics in the control synthesis [12–16]. The second type of controller only considers the problem of control torque synthesis and deals with the whether or not that control torque is implementable separately [17–19]. We implement a control law which uses a minimal model of the actuator dynamics in order to synthesize an appropriate command. That is, force for thrusters, wheel acceleration for reaction wheels, magnetic dipole for magnetic torquers, and gimbal speed for CMG's.

Different control laws can be used for detumbling [20, 21] , attitude reorientation to a desired attitude [22–25], or attitude tracking [26, 27]. Modern control methods, such as nonlinear feedback linearization [28, 29], gain scheduling [30, 31], optimal control [32, 33], among many others [34, 35] have been successfully applied to the attitude control problem. Tuning these control laws often requires knowledge of the mass properties of the spacecraft,

information about actuator placement and orientation, as well as a characterization of the spacecraft's operating environment. This information is sometimes used to build a high-fidelity model of both the spacecraft and the environment which is then used to determine controller performance.

Although high fidelity modeling, Monte Carlo testing, and stability analysis are effective techniques, they require significant time and effort. Uncertainty may arise due to imprecisely modeled mass and modal properties [36, 37]; nonlinearity may arise due to large-angle and high-rate kinematics; and high dimensionality may arise due to the continuum mechanics of flexible appendages [38] and propellant slosh [39]. Spacecraft projects with limited resources can benefit from control algorithms that require little to no modeling and are forgiving to modeling error.

Adaptive control can provide robustness to model uncertainty, unknown parameters, unmodeled dynamics, and disturbances [40–42]. There are two types of adaptive controllers. Indirect adaptive control attempts to estimate system parameters in order to apply a fixed gain control law. Direct adaptive control takes a given controller structure, proportional-integral control (PID) for example, and updates the controller gains based on available measurements. These techniques allow the controller to tune itself to the spacecraft and actuator dynamics, the maneuver type, and environmental disturbances. Thus, adaptive control is useful when a sufficiently accurate model of the spacecraft is not available for fixed-gain controller synthesis.

Adaptive techniques for spacecraft attitude control have been used to provide robustness to errors in mass property models [43–46], improve the performance of proportional-derivative (PD) laws [47–49], reject disturbances [50–52], handle unknown nonlinearities [53], and maintain control during unexpected failures [54–56]. These techniques, though effective, may require assumptions on persistency of excitation, bounded disturbances, or bounds on the uncertainty in the mass properties. Also, many of these methods are designed to work with specific actuators or are constrained to certain maneuver types such as small angle rotations. Moreover the majority of control laws in the literature, adaptive or otherwise, use quaternions, or other 3 and 4 parameter attitude representations.

Developing attitude control laws on SO(3) avoids the singularities and other problems inherent in vector attitude representations [57]. This can simplify the control law significantly since there is no need for discontinuous switching to avoid singularities or to choose the "right" quaternion. The SO(3) adaptive controllers in [58, 59] provide almost-global stabilization without using inertia information. However, they are limited to continuous thrusters and reaction wheels. Furthermore, they require a priori knowledge of the disturbance frequencies.

We propose an adaptive control law which is robust to mass property uncertainty, actuator nonlinearities, unknown disturbances, and is developed on SO(3). Furthermore, the controller requires limited modifications in order to be applied to different actuators.

Retrospective cost adaptive control (RCAC) is a multi-input, multi-output direct adaptive controller that utilizes an input-output plant model and previous performance data to update a dynamic compensator using recursive least squares. RCAC has been applied to systems with unknown nonminimum-phase (NMP) zeros [60–62] for stabilization, command following, and disturbance rejection. Furthermore, RCAC can be modified to handle uncertain nonlinearities in Hammerstein [63] and Weiner systems [64]. RCAC has also been tested on nonlinear plants such as multiple linkages [65, 66], and aircraft [67–69]. We apply RCAC to the problem of spacecraft attitude control. Since RCAC was originally designed for linear discrete-time plants, we develop methods to extract the necessary input-output model, that is the Markov parameters, from the nonlinear system equations of spacecraft controlled with thrusters, reaction wheels, magnetic torquers, and control moment gyros (CMG's).

First, we describe and expand two different implementations of RCAC. Then, we derive the dynamics for spacecraft controlled using thrusters, reaction wheels, magnetic torquers, or control moment gyros. These dynamics are then used to obtain linearized and discretized system equations which provide the Markov parameters to use in RCAC. For thrusters, reaction wheels, and magnetic torquers, inertia-free control is demonstrated by replacing the spacecraft inertia matrix in the Markov parameter formulation with the identity matrix. Robustness to actuator nonlinearities, actuator misalignment, unmodeled disturbances, and sensor noise is demonstrated through numerical simulations. Finally, we successfully apply RCAC to simplified model of flexible spacecraft with noncollocated actuators.

1.1 Contributions to the Spacecraft Attitude Control Literature

1. Successfully applied RCAC to detumble, slew, and spin rigid body spacecraft using thrusters, reaction wheels, magnetic torquers, and control moment gyros [70–72].

2. Numerically demonstrated robustness to unknown inertia modeling errors, actuator misalignment, unmodeled disturbances, and unknown saturation for both thrusters and reaction wheel controlled spacecraft [70–73].

3. Demonstrated robustness to actuator nonlinearities and their effect on settling time

for slew maneuvers using thrusters [73].

4. Qualified the effect of noise and bias in the angular velocity measurements for attitude control using reaction wheels. [71]

5. Developed two RCAC formulations to handle the input matrix rank deficiency problem inherent in magnetic torquers [72].

6. Successfully applied decentralized RCAC on a spacecraft with magnetic torquers aligned with the rigid body's principal axes [72].

7. Clearly derived the dynamics of a rigid body spacecraft controlled by CMG's using Newton-Euler methods without relying on simplifying assumptions commonly found in literature [74, 75].

8. Developed a new result relating the reachability of a desired rest attitude given the initial CMG configuration [75].

9. Successfully implemented a novel approach to CMG attitude control which directly commands gimbal speed without the need for a separate control law for torque synthesis, singularity avoidance methods, or steering laws [74, 75].

10. Demonstrated output-feedback adaptive control of a linearized planar dual rigid-body and developed guidelines for robustness to modeling errors in the joint stiffness and body inertias [76].

1.2 Contributions to the Adaptive Control Literature

1. Demonstrated the applicability of RCAC to control nonlinear continuous-time systems by using Markov parameters obtained through linearization and simple difference discretization [70–75].

2. Developed a new approach to control nonminimumphase systems which have a single NMP zero using RCAC [76].

3. Developed the equations to allow for separate performance, control, and retrospective control filters in the retrospective performance of RCAC.

4. Derived the equations to include a new control penalty in the 1-Step implementation of RCAC [74–76].

5. Improved the numerical robustness of RCAC by implementing sequential updates and a QR-decomposition method in the recursive least squares-based controller parameter update [76].

1.3 Chapter Summary

Chapter 2 presents the retrospective cost concept and describes the two different RCAC implementations used in this thesis. The two-step version of RCAC is used in Chapters 4, 5, and 6, to control a spacecraft with thrusters, reaction wheels, and magnetic torquers, respectively. The one-step method is used in Chapters 7 and 8 to control the CMG-actuated spacecraft and the planar dual-rigid body. Chapter 2 also presents improvements to the recursive least squares implementation in RCAC based on numerical robustness and computational efficiency techniques in the system identification and Kalman filtering literature.

Chapter 3 derives the dynamics for a rigid-body spacecraft using different types of actuators and presents an overview of the spacecraft inertias and control scenarios tested in this thesis. Furthermore, we present a detailed description of the attitude control problem, that is the desired attitude and angular velocity as well as the error parameters which are used in the following chapters.

Chapters 4 and 5 present the implementation of RCAC on a spacecraft actuated by thrusters and reaction wheels, respectively, and presents robustness results for each actuator. Robustness to model uncertainty is tested by scaling and rotating the spacecraft inertia and actuator matrices. Different actuator dynamics and nonlinearities are included in the robustness studies. We test the effect of saturation levels on steady state performance. Furthermore, we examine the effect of on-off thrusters, reaction wheel speed saturation, CMG singularities.

In Chapter 6 we cover the problem of attitude control using magnetic torquers. Two solutions are presented which enable the application of the 2-Step method despite the rank deficiency of the input matrix. However, the results in this chapter are require knowledge of the principal axes of the spacecraft.

Chapter 7 includes a detailed derivation of the Newton-Euler dynamics for a spacecraft controlled with CMG's. Special cases are explored and we introduce a new result on the reachability of desired rest attitudes. Unlike in Chapters 4, 5, and 6, the linearization of the system dynaics is achieved using variations. Furthermore, a hybrid linear/nonlinear approach to Markov parameters is presented where the system dynamics are assumed to be linear but the system output nonlinearities are preserved.

Chapter 8 deals with the problem of controlling a flexible spacecraft with noncolocated

sensors and actuators. The linearized dynamics of the planar dual rigid-body spacecraft model are nonminimum phase and present additional challenges for adaptive control. A novel method of selecting the Markov parameters to model the NMP behavior is presented and guidelines for robustness are given for this special type of NMP system.

CHAPTER 2

Retrospective Cost Adaptive Control

RCAC is a discrete-time output-feedback controller that minimizes the error given by a performance variable. RCAC does not require detailed plant information, instead, it uses knowledge of the system's impulse response as described by Markov parameters [77]. Although RCAC is derived for linear systems, we apply it to the nonlinear spacecraft model by using Markov parameters from the linearized dynamics.

2.1 The System

Consider the strictly causal multi-input multi-output (MIMO) discrete-time system

$$x(k) = Ax(k-1) + Bu(k-1) + Fw(k-1), \tag{2.1}$$

$$y(k) = Cx(k) + v(k), \tag{2.2}$$

$$z(k) = Ex(k) - r(k), \tag{2.3}$$

where $x(k) \in \mathbb{R}^{l_x}$, $y(k) \in \mathbb{R}^{l_y}$, $u(k) \in \mathbb{R}^{l_u}$, $w(k) \in \mathbb{R}^{l_w}$ is a disturbance signal, $v(k) \in \mathbb{R}^{l_v}$ is the measurement noise, $z(k) \in \mathbb{R}^{l_z}$ is a performance metric, $r(k) \in \mathbb{R}^{l_r}$ is the command, and $k \geq 1$.

2.1.1 Transfer Function as a Laurent Expansion

The transfer function G_{zu} is given by [78]

$$G_{zu}(\mathbf{q}) \stackrel{\triangle}{=} E(\mathbf{q} - A)^{-1}B, \tag{2.4}$$

$$= \sum_{0}^{\infty} \frac{H_i}{\mathbf{q}^i}, \tag{2.5}$$

$$\approx \sum_{0}^{n_H} \frac{H_i}{\mathbf{q}^i}, \tag{2.6}$$

where $\mathbf{q}$ is the forward-shift operator and the Markov parameters H_i are given by

$$H_i \stackrel{\triangle}{=} EA^{i-1}B,\ i \geq 1. \tag{2.7}$$

2.1.2 Convolution and Markov Parameters

Let $n \geq 1$ be an integer. Then, for all $k \geq n$, we can express $x(k)$ in (2.1) as

$$x(k) = A^n x(k-n) + \sum_{i=1}^{n} A^{i-1} \left[Bu(k-i) + Fw(k-i) \right]. \tag{2.8}$$

Thus, the performance $z(k)$ is given by

$$z(k) = EA^n x(k-n) + E\sum_{i=1}^{n} A^{i-1}Bu(k-i) + E\sum_{i=1}^{n} A^{i-1}Fw(k-i) - r(k), \tag{2.9}$$

$$= EA^n x(k-n_H) + \sum_{i=1}^{n} H_i u(k-i) + \sum_{i=1}^{n} H_i' w(k-i) - r(k),$$

$$= \frac{EA^n}{\mathbf{q}^n} x(k) + \sum_{i=1}^{n} \frac{H_i}{\mathbf{q}^i} u(k) + \sum_{i=1}^{n} \frac{H_i'}{\mathbf{q}^i} w(k) - r(k), \tag{2.10}$$

where for $i = 1, \ldots, n$, H_i' are the Markov parameters of G_{wu}.

2.2 The Controller

Let the controller be given by

$$u(k) = \Phi(k)\theta(k) = \Theta(k)\phi(k), \tag{2.11}$$

where

$$\Phi(k) \stackrel{\triangle}{=} I_{l_u} \otimes \phi(k), \quad \theta(k) = \text{vec}\, \Theta(k) \tag{2.12}$$

$\Phi(k)$ is the regressor matrix and $\theta(k)$ is a vector of controller parameters and $\otimes$ represents the Kronecker product .

2.2.1 Strictly Proper Controller

Define a strictly proper dynamic compensator as the time series controller

$$u(k) \stackrel{\triangle}{=} \sum_{i=1}^{n_c} P_i(k)u(k-i) + \sum_{i=1}^{n_c} Q_i(k)y'(k-i), \tag{2.13}$$

where for all $i = 1, \ldots, n_c$, $P_i \in \mathbb{R}^{l_u \times l_u}, Q_i \in \mathbb{R}^{l_u \times l_{y'}}$ are unknown gain matrices. Note that (2.13) is an infinite-impulse-response (IIR) controller. We rewrite (2.13) as

$$u(k) = \Phi(k)\theta(k), \tag{2.14}$$

where the regressor is given by,

$$\phi(k) = \begin{bmatrix} u(k-1) \\ \vdots \\ u(k-n_c) \\ y'(k-1) \\ \cdots \\ y'(k-n_c) \end{bmatrix} \in \mathbb{R}^{l_u \times l_\theta}, \tag{2.15}$$

the regressor variable $y'(x(k))$ is a function of the state, $\theta(k) \in \mathbb{R}^{l_\theta}$ is a vector of controller parameters which contains the elements of all the gain matrices $P_i(k)$ and $Q_i(k)$, and $l_\theta = n_c l_u (l_u + l_{y'})$.

2.2.2 Proper Controller

In some cases it is of interest to apply a proper controller. Then, the time-series is given by

$$u_{\text{prop}}(k) \triangleq \sum_{i=1}^{n_c} P_i(k)u(k-i) + \sum_{i=0}^{n_c} Q_i(k)y'(k-i) \tag{2.16}$$

$$= \Phi_{\text{prop}}(k)\theta(k). \tag{2.17}$$

and the regressor becomes,

$$\Phi_{\text{prop}}(k) \triangleq I_{l_u} \otimes \begin{bmatrix} u(k-1) \\ \vdots \\ u(k-n_c) \\ y'(k) \\ \cdots \\ y'(k-n_c) \end{bmatrix}^{\text{T}} \in \mathbb{R}^{l_u \times l_\theta}, \tag{2.18}$$

and $l_\theta = l_u\left(n_c l_u + (n_c+1)l_{y'}\right)$.

2.2.2.1 Zeroth-order Controller

A special case of the proper controller is the zeroth-order, $n_c = 0$, controller. This type of controller enables output and state feedback control laws. Thus, the time series (2.13) is replaced by,

$$u_0(k) \triangleq Q_0 y'(k), \tag{2.19}$$

$$= \Phi_0(k)\theta(k). \tag{2.20}$$

Then the regressor matrix becomes,

$$\Phi_0(k) \triangleq I_{l_u} \otimes y'(k)^{\text{T}} \in \mathbb{R}^{l_u \times l_u l_{y'}}. \tag{2.21}$$

2.2.3 FIR Controller

Although an IIR compensator offers flexibility there are situations where a finite-impulse-response (FIR) controller is more appropriate. In these cases (2.13) simplifies to

$$u_{\mathrm{FIR}}(k) \triangleq \sum_{i=k_0}^{n_c} Q_i(k) y'(k-i), \tag{2.22}$$

$$= \Phi_{\mathrm{FIR}}(k)\theta(k). \tag{2.23}$$

where we use $k_0 = 0$ for a proper controller and $k_0 = 1$ for a strictly proper controller. The regressor matrix is then given by,

$$\Phi_{\mathrm{FIR}}(k) \triangleq I_{l_u} \otimes \begin{bmatrix} y'(k-k_0) \\ \cdots \\ y'(k-n_c) \end{bmatrix}^{\mathrm{T}} \in \mathbb{R}^{l_u \times l_\theta}, \tag{2.24}$$

where $l_\theta = (n_c + 1 - k_0) l_u l_{y'}$.

2.2.4 Integrator

In order to add an integrator to the controller we must introduce an integrator state,

$$\gamma(k) = \gamma(k-1) + z(k). \tag{2.25}$$

Then, we include this new state in the controller time series,

$$u_{\mathrm{int}}(k) \triangleq \sum_{i=1}^{n_c} P_i(k) u(k-i) + \sum_{i=k_0}^{n_c} Q_i(k) y'(k-i) + K_{\mathrm{I}} \gamma(k) \tag{2.26}$$

$$= \Phi_{\mathrm{int}}(k)\theta(k), \tag{2.27}$$

where the regressor is given by

$$\Phi_{\text{int}}(k) \stackrel{\triangle}{=} I_{l_u} \otimes \begin{bmatrix} u(k-1) \\ \vdots \\ u(k-n_c) \\ y'(k-k_0) \\ \cdots \\ y'(k-n_c) \\ \gamma(k) \end{bmatrix}^{\mathrm{T}} \in \mathbb{R}^{l_u \times l_\theta}, \tag{2.28}$$

where as before, $k_0 = 0$ corresponds to a proper controller and $k_0 = 1$ corresponds to a strictly proper controller and $l_\theta = l_u\,(n_c l_u + (n_c + 1 - k_0) l_{y'} + l_z)$.

2.3 The 2-Step Algorithm

We can rewrite (2.10) as [62]

$$z(k) = E_1 A^n x(k-n) + \tilde{H}(\tilde{\sigma}) U(k, \tilde{\sigma}) + E_1 \sum_{i=1}^{n} A^{i-1} F w(k-i) - E_0 r(k), \tag{2.29}$$

where

$$\tilde{H}(\tilde{\sigma}) \stackrel{\triangle}{=} \begin{bmatrix} H_{\tilde{\sigma}_1} & H_{\tilde{\sigma}_2} & \cdots & H_{\tilde{\sigma}_{n+1}} \end{bmatrix} = \begin{bmatrix} H_1 & \cdots & H_n \end{bmatrix} \in \mathbb{R}^{l_z \times n l_u}, \tag{2.30}$$

$$U(k, \tilde{\sigma}) \stackrel{\triangle}{=} \begin{bmatrix} u(k-\tilde{\sigma}_1) \\ \vdots \\ u(k-\tilde{\sigma}_{n+1}) \end{bmatrix} = \begin{bmatrix} u(k-1) \\ \vdots \\ u(k-n) \end{bmatrix} \in \mathbb{R}^{n l_u}, \tag{2.31}$$

and

$$\tilde{\sigma} \stackrel{\triangle}{=} \begin{bmatrix} 1 & \cdots & n \end{bmatrix}. \tag{2.32}$$

2.3.1 Choice of Markov Parameters

We can rewrite (2.29) with an integer delay $q \geq 0$ and $n = n_q \geq 1$. Then, for all $k \geq n_q + q$,

$$z(k-q) = E_1 A^{n_q} x(k-n_q-q) + \tilde{H}(\tilde{\sigma}) U(k-q,\tilde{\sigma}) + E_1 \sum_{i=1}^{n_q} A^{i-1} F w(k-q-i) - E_0 r(k-q). \tag{2.33}$$

At each step $k-q$, we can select which Markov parameters and corresponding controls we wish to use for optimization. Thus, we partition $\tilde{H}(\tilde{\sigma})$ and $U(k-q,\tilde{\sigma})$ so that

$$\tilde{H}(\tilde{\sigma}) U(k-q,\tilde{\sigma}) = \tilde{H}(\sigma_q) U(k-q,\sigma_q) + \tilde{H}(\bar{\sigma}_q) U(k-q,\bar{\sigma}_q). \tag{2.34}$$

The selected Markov parameters are grouped into

$$\tilde{H}(\sigma_q) \triangleq \left[\begin{array}{cccc} H_{\sigma_{q,1}} & H_{\sigma_{q,2}} & \cdots & H_{\sigma_{q,m_q}} \end{array} \right] \in \mathbb{R}^{l_z \times m_q l_u}, \tag{2.35}$$

where m_q is a positive integer,

$$\sigma_q \triangleq \left[\begin{array}{cccc} \sigma_{q,1} & \sigma_{q,2} & \cdots & \sigma_{q,m_q} \end{array} \right], \tag{2.36}$$

and the components of σ_q are distinct positive integers that satisfy

$$\sigma_{q,1} < \sigma_{q,2} < \cdots < \sigma_{q,m_q}.$$

The corresponding control inputs are

$$U(k-q,\sigma_q) \triangleq \left[\begin{array}{c} u(k-q-\sigma_{q,1}) \\ u(k-q-\sigma_{q,2}) \\ \vdots \\ u(k-q-\sigma_{q,m_q}) \end{array} \right] \in \mathbb{R}^{m_q l_u}. \tag{2.37}$$

The remaining Markov parameters and controls are grouped into $\tilde{H}(\bar{\sigma}_q) \in \mathbb{R}^{l_z \times (n_q - m_q + 1) l_u}$ and $U(k-q,\bar{\sigma}_q) \in \mathbb{R}^{(n_q - m_q + 1) l_u}$, respectively, where

$$\bar{\sigma}_q \triangleq \left[\begin{array}{cccc} \bar{\sigma}_{q,1} & \bar{\sigma}_{q,2} & \cdots & \bar{\sigma}_{q,n_q-m_q+1} \end{array} \right]. \tag{2.38}$$

The components of $\bar{\sigma}_q$ are distinct positive integers that satisfy

$$\bar{\sigma}_{q,1} < \bar{\sigma}_{q,2} < \cdots < \bar{\sigma}_{q,m_q}.$$

Next, we rewrite (2.33) as

$$z(k-q) = \mathcal{S}(k-q, \bar{\sigma}_q) + \tilde{H}(\sigma_q)U(k-q, \sigma_q), \tag{2.39}$$

where

$$\begin{aligned}\mathcal{S}(k-q, \bar{\sigma}_q) \triangleq\ & E_1 A^{n_q} x(k-q-n_q) + \tilde{H}(\bar{\sigma}_q)U(k-q, \bar{\sigma}_q) \\ & + E_1 \sum_{i=1}^{n} A^{i-1} F w(k-q-i) - E_0 r(k-q).\end{aligned} \tag{2.40}$$

2.3.2 Extended Performance

We stack the delayed performance variables and define the *extended performance* as

$$Z(k, \tilde{q}) \triangleq \begin{bmatrix} z(k-q_1) \\ z(k-q_2) \\ \vdots \\ z(k-q_s) \end{bmatrix} \in \mathbb{R}^{sl_z}, \tag{2.41}$$

where the components of $\tilde{q} = \begin{bmatrix} q_1 & \cdots & q_s \end{bmatrix}$ are distinct nonnegative integers that satisfy

$$q_1 < q_2 < \cdots < q_s.$$

Similar in form to (2.39), we can write the extended performance as

$$Z(k, \tilde{q}) = \tilde{\mathcal{S}}(k, \tilde{q}) + \tilde{\mathcal{H}}\tilde{U}(k, \tilde{q}), \tag{2.42}$$

where

$$\tilde{\mathcal{H}} \triangleq \begin{bmatrix} \tilde{H}(\sigma_{q_1}) & & & \\ & \tilde{H}(\sigma_{q_2}) & & \\ & & \ddots & \\ & & & \tilde{H}(\sigma_{q_s}) \end{bmatrix} \in \mathbb{R}^{sl_z \times \left(\sum_{i=1}^{s} m_{q_i}\right) l_u} \tag{2.43}$$

is block diagonal,

$$\tilde{H}(\sigma_{q_i}) = \left[\begin{array}{cccc} H_{\sigma_{q_i,1}} & H_{\sigma_{q_i,2}} & \cdots & H_{\sigma_{q_i,m_{q_i}}} \end{array} \right] \in \mathbb{R}^{l_z \times m_{q_i} l_u}, \tag{2.44}$$

and

$$\tilde{U}(k,\tilde{q}) \triangleq \left[\begin{array}{c} U(k-q_1,\sigma_{q_1}) \\ U(k-q_2,\sigma_{q_2}) \\ \vdots \\ U(k-q_s,\sigma_{q_s}) \end{array} \right] \in \mathbb{R}^{\left(\sum_{i=1}^{s} m_{q_i}\right) l_u}. \tag{2.45}$$

2.3.2.1 Consolidating Repeated Entries in the Retrospective Controls

Depending on the components of $\tilde{q}$ and σ_{q_i}, the components of $\tilde{U}(k,\tilde{q})$ might contain repeated entries. For example, if we choose

$$\tilde{q} = \left[\begin{array}{cc} q_1 & q_2 \end{array} \right] = \left[\begin{array}{cc} 0 & 1 \end{array} \right], \qquad \sigma_{q_1} = \sigma_0 = \left[\begin{array}{cc} 1 & 3 \end{array} \right], \qquad \sigma_{q_2} = \sigma_1 = \left[\begin{array}{c} 0 \end{array} \right],$$

then

$$\tilde{\mathcal{H}} = \left[\begin{array}{ccc} H_1 & H_3 & 0 \\ 0 & 0 & H_0 \end{array} \right]$$

and

$$\tilde{U}(k,\tilde{q}) = \left[\begin{array}{c} u(k-1) \\ u(k-3) \\ u(k-1) \end{array} \right].$$

Note that $u(k-1)$ is repeated.

To remove the repeated entries in $\tilde{U}(k,\tilde{q})$, define the *extended control* $\mathcal{U}(k,\tilde{g}) \in \mathbb{R}^{pl_u}$, which contains all of the required entries $u(k-g_i)$ without repetition. Then, define the corresponding Markov parameter matrix $\mathcal{H} \in \mathbb{R}^{sl_z \times pl_u}$ such that

$$Z(k,\tilde{q}) = \tilde{\mathcal{S}}(k,\tilde{q}) + \mathcal{H}\mathcal{U}(k,\tilde{g}), \tag{2.46}$$

where the components of $\tilde{g} = \left[\begin{array}{cccc} g_1 & \ldots & g_p \end{array} \right]$ are distinct positive integers that satisfy

$$g_1 < g_2 < \cdots < g_p.$$

For the above example,

$$\tilde{g} = \begin{bmatrix} 1 & 3 \end{bmatrix},$$
$$\mathcal{U}(k, \tilde{g}) = \begin{bmatrix} u(k-1) \\ u(k-3) \end{bmatrix},$$

and the Markov parameter matrix is

$$\mathcal{H} = \begin{bmatrix} H_1 & H_3 \\ H_0 & 0 \end{bmatrix}.$$

2.3.3 Retrospective Cost Optimization

Given the extended control vector $\mathcal{U}(k, \tilde{g})$ and the Markov parameter matrix $\mathcal{H}$, we use (2.46) to define the *retrospective performance*

$$\hat{Z}(k, \tilde{q}) \triangleq \tilde{\mathcal{S}}(k, \tilde{q}) + \mathcal{H}\hat{\mathcal{U}}(k, \tilde{g}), \tag{2.47}$$

where the *retrospective controls* $\hat{\mathcal{U}}(k, \tilde{g})$ replace the past controls in $\mathcal{U}(k, \tilde{g})$. Subtracting (2.46) from (2.66) yields

$$\hat{Z}(k, \tilde{q}) = Z(k, \tilde{q}) - \mathcal{H}\mathcal{U}(k, \tilde{g}) + \mathcal{H}\hat{\mathcal{U}}(k, \tilde{g}). \tag{2.48}$$

We define the *retrospective cost function*

$$\hat{J}(k) \triangleq \hat{Z}(k, \tilde{q})^{\mathrm{T}} R_Z(k) \hat{Z}(k, \tilde{q}) + \hat{\mathcal{U}}(k, \tilde{g})^{\mathrm{T}} R_U(k) \hat{\mathcal{U}}(k, \tilde{g}), \tag{2.49}$$

where $R_Z(k) \in \mathbb{R}^{sl_z \times sl_z}$ is a positive-definite performance weight and $R_U(k) \in \mathbb{R}^{pl_u \times pl_u}$ is a positive-semidefinite control weight. We use (2.48) to expand (2.49),

$$\hat{J}(k) = \hat{\mathcal{U}}(k, \tilde{g})^{\mathrm{T}} \mathcal{A}(k) \hat{\mathcal{U}}(k, \tilde{g}) + \mathcal{B}(k)^{\mathrm{T}} \hat{\mathcal{U}}(k, \tilde{g}) + \mathcal{C}(k), \tag{2.50}$$

where

$$\mathcal{A}(k) \triangleq \mathcal{H}^{\mathrm{T}} R_Z(k) \mathcal{H} + R_U(k),$$
$$\mathcal{B}(k) \triangleq 2\mathcal{H}^{\mathrm{T}} R_Z(k) \left[Z(k, \tilde{q}) - \mathcal{H}\mathcal{U}(k, \tilde{g}) \right],$$
$$\mathcal{C}(k) \triangleq \left[Z(k, \tilde{q}) - \mathcal{H}\mathcal{U}(k, \tilde{g}) \right]^{\mathrm{T}} R_Z(k) \left[Z(k, \tilde{q}) - \mathcal{H}\mathcal{U}(k, \tilde{g}) \right].$$

The minimizer $\hat{\mathcal{U}}^*(k,\tilde{g})$ of (2.50) satisfies

$$2\mathcal{A}(k)\hat{\mathcal{U}}^*(k,\tilde{g}) + \mathcal{B}(k) = 0.$$

Thus, if $\mathcal{A}(k)$ is invertible, then

$$\hat{\mathcal{U}}^*(k,\tilde{g}) = -\frac{1}{2}\mathcal{A}(k)^{-1}\mathcal{B}(k). \tag{2.51}$$

Therefore, the *retrospectively optimized control* is given by

$$\hat{\mathcal{U}}^*(k,\tilde{g}) = \left[\mathcal{H}^{\mathrm{T}}R_Z(k)\mathcal{H} + R_U(k)\right]^{-1}\mathcal{H}^{\mathrm{T}}R_Z(k)\left[\mathcal{H}\mathcal{U}(k,\tilde{g}) - Z(k)\right], \tag{2.52}$$

$$= \begin{bmatrix} \hat{u}_k(k-g_1) \\ \vdots \\ \hat{u}_k(k-g_p) \end{bmatrix} \tag{2.53}$$

where $\hat{u}_k(k-g_i)$ denotes the reconstructed control $u(k-g_i)$ using information from the kth step. We use the retrospectively optimized control $\hat{\mathcal{U}}^*(k,\tilde{g})$ to update the controller coefficients $\Theta(k)$.

2.3.4 Least Squares Controller Construction

To obtain $\Theta(k)$, we use previous measurements and define a least squares problem by horizontally stacking the retrospective controls $\hat{u}_k(k-g_i)$ contained in $\hat{\mathcal{U}}^*(k,\tilde{g})$ over m previous iterations. Thus,

$$\Gamma_u(k) = \Theta(k)\Gamma_\phi(k), \tag{2.54}$$

where

$$\Gamma_u(k) \triangleq$$
$$[\hat{u}_k(k-g_1)\ \cdots\ \hat{u}_k(k-g_p)\ \cdots\ \hat{u}_{k-m}(k-g_1-m)\ \cdots\ \hat{u}_{k-m}(k-g_p-m)] \in \mathbb{R}^{l_u\times p(m+1)}$$

and

$$\Gamma_\phi(k) \triangleq$$
$$[\phi(k-g_1)\ \cdots\ \phi(k-g_p)\ \cdots\ \phi(k-g_1-m)\ \cdots\ \phi(k-g_p-m)] \in \mathbb{R}^{n_c(l_u+l_v)\times p(m+1)}.$$

Given a right-invertible $\Gamma_\phi(k)$, the controller coefficients are given by

$$\Theta(k) = \Gamma_u(k)\Gamma_\phi(k)^{\mathrm{T}} \left[\Gamma_\phi(k)\Gamma_\phi(k)^{\mathrm{T}}\right]^{-1}, \tag{2.55}$$

which yields the RCAC control input

$$u(k) = \Theta(k)\phi(k). \tag{2.56}$$

The result in (2.55) and (2.56) requires a complete history of the previous performance and control data as well as the inversion of a $n_{\mathrm{c}}(l_u + l_v) \times n_{\mathrm{c}}(l_u + l_v)$ matrix. To reduce computational complexity we utilize a recursive approach.

2.3.4.1 Recursive Least Squares

$\Theta(k-1)$	controller coefficients at beginning of each step
$\mathcal{P}(k-1)$	information matrix at beginning of each step
$\Theta_{g_i}(k)$	controller coefficients after update using $\hat{u}(k-g_i)$, for $i = 0, \ldots, p$,
$\mathcal{P}_{g_i}(k)$	information matrix after update using $\hat{u}(k-g_i)$, for $i = 0 \ldots p$,
$\Theta(k)$	updated controller coefficients,
$\mathcal{P}(k)$	updated information matrix.

Table 2.1: Notation for controller construction using recursive least squares.

We can obtain the controller coefficients using *recursive least squares*. We use the notation in Table 2.1 to specify the update sequence. For $i' = 1, 2, \ldots, p$, define the cumulative cost function

$$\begin{aligned} J_{\mathrm{R}}(\Theta_{g_{i'}}(k), k) \triangleq & \sum_{i=1}^{i'} \|\hat{u}_k(k-g_i) - \Theta_{g_{i'}}(k)\phi(k-g_i)\|^2 \\ & + \sum_{i=1}^{p}\sum_{j=1}^{m} \|\hat{u}_{k-j}(k-g_i-j) - \Theta_{g_{i'}}(k)\phi(k-g_i-j)\|^2. \end{aligned} \tag{2.57}$$

For $i' = 1, 2, \ldots, p$, the minimizer of (2.57) is given by

$$\Theta^*_{g_{i'}}(k) \triangleq \Theta_{g_{i'-1}}(k) + \frac{\hat{u}_k(k-g_{i'}) - \Theta_{g_{i'-1}}(k)\phi(k-g_{i'})}{1 + \phi^{\mathrm{T}}(k-g_{i'})\mathcal{P}_{g_{i'-1}}(k)\phi(k-g_{i'})}\phi(k-g_{i'})^{\mathrm{T}}\mathcal{P}_{g_{i'-1}}(k), \tag{2.58}$$

where the information matrix is updated by

$$\mathcal{P}_{g_{i'}}(k) \triangleq \mathcal{P}_{g_{i'-1}}(k) - \frac{\mathcal{P}_{g_{i'-1}}(k)\phi(k-g_{i'})\phi(k-g_{i'})^{\mathrm{T}}\mathcal{P}_{g_{i'-1}}(k)}{1+\phi^{\mathrm{T}}(k-g_{i'})\mathcal{P}_{g_{i'-1}}(k)\phi(k-g_{i'})} \tag{2.59}$$

and

$$\mathcal{P}_{g_0}(k) \triangleq \mathcal{P}(k-1), \tag{2.60}$$

$$\Theta_{g_0}(k) \triangleq \Theta(k-1). \tag{2.61}$$

information matrix

$$\Theta(k) \triangleq \Theta_{g_p}(k), \tag{2.62}$$

$$\mathcal{P}(k) \triangleq \mathcal{P}_{g_p}(k). \tag{2.63}$$

Finally, the RCAC control is

$$u(k) = \Theta(k)\phi(k). \tag{2.64}$$

2.4 1-Step Algorithm

2.4.1 Retrospective Performance

Define the *retrospective control* as [79]

$$\hat{u}(k) \triangleq \Phi(k)\hat{\theta}, \tag{2.65}$$

and the corresponding *retrospective performance* as,

$$\hat{z}(k) \triangleq z_{\mathrm{f}}(k) + \Phi_{\mathrm{f}}(k)\hat{\theta} - u_{\mathrm{f}}(k) \tag{2.66}$$

where $z_{\mathrm{f}}(k)$, $\Phi_{\mathrm{f}}(k)$, and $u_{\mathrm{f}}(k)$ result from filtering $z(k)$, $\Phi(k)$, and $u(k)$ respectively, that is

$$\begin{aligned} z_{\mathrm{f}}(k) &\stackrel{\triangle}{=} G_z(\mathbf{q})z(k) = \mathcal{D}_z(\mathbf{q})^{-1}\mathcal{N}_z(\mathbf{q})z(k), \\ &= \sum_{i=0}^{n_z} N_{z_i} z(k-i) - \sum_{i=1}^{\bar{n}_z} D_{z_i} z_{\mathrm{f}}(k-i), \\ &= \bar{N}_z \bar{Z}(k) - \bar{D}_z \bar{Z}_{\mathrm{f}}(k) \end{aligned} \tag{2.67}$$

$$\begin{aligned} \Phi_{\mathrm{f}}(k) &\stackrel{\triangle}{=} G_\phi(\mathbf{q})\Phi(k) = \mathcal{D}_\phi(\mathbf{q})^{-1}\mathcal{N}_\phi(\mathbf{q})\Phi(k), \\ &= \sum_{i=0}^{n_\phi} N_{\phi_i} \Phi(k-i) - \sum_{i=1}^{\bar{n}_\phi} D_{\phi_i} \Phi_{\mathrm{f}}(k-i), \\ &= \bar{N}_\phi \bar{\Phi}(k) - \bar{D}_\phi \bar{\Phi}_{\mathrm{f}}(k) \end{aligned} \tag{2.68}$$

$$\begin{aligned} u_{\mathrm{f}}(k) &\stackrel{\triangle}{=} G_u(\mathbf{q})u(k) = \mathcal{D}_u(\mathbf{q})^{-1}\mathcal{N}_u(\mathbf{q})u(k), \\ &= \sum_{i=1}^{n_u} N_{u_i} u(k-i) - \sum_{i=1}^{\bar{n}_u} D_{u_i} u_{\mathrm{f}}(k-i), \\ &= \bar{N}_u \bar{u}(k) - \bar{D}_u \bar{u}_{\mathrm{f}}(k). \end{aligned} \tag{2.69}$$

Each filter $G_z(\mathbf{q}), G_\phi(\mathbf{q}), G_u(\mathbf{q})$ is defined as the quotient of two FIR filters, for all three filters the denominator is defined as

$$\mathcal{D}_{(\cdot)}(\mathbf{q}) \stackrel{\triangle}{=} I_{l_z} + \sum_{i=1}^{\bar{n}_{(\cdot)}} D_{(\cdot)_i} \mathbf{q}^{-i} \in \mathbb{R}^{l_z \times l_z}. \tag{2.70}$$

The numerator for both the z and ϕ filters is defined as

$$\mathcal{N}_{z,\phi}(\mathbf{q}) \stackrel{\triangle}{=} \sum_{i=0}^{n_{z,\phi}} N_{z,\phi_i} \mathbf{q}^{-i} \in \mathbb{R}^{l_z, l_u \times l_u}, \tag{2.71}$$

for the u filter the numerator is defined as

$$\mathcal{N}_u(\mathbf{q}) \stackrel{\triangle}{=} \sum_{i=1}^{n_u} N_{u_i} \mathbf{q}^{-i} \in \mathbb{R}^{l_u \times l_u}, \tag{2.72}$$

The matrices of filter coefficients is where

$$\tilde{N} \stackrel{\triangle}{=} \begin{bmatrix} N_1 & \cdots & N_{n_{\mathrm{f}}} \end{bmatrix} \in \mathbb{R}^{l_z \times n_{\mathrm{f}} l_u}, \qquad \tilde{D} \stackrel{\triangle}{=} \begin{bmatrix} D_1 & \cdots & D_{n_{\mathrm{f}}} \end{bmatrix} \in \mathbb{R}^{l_z \times n_{\mathrm{f}} l_z}. \tag{2.73}$$

Next, we define the *extended regressor*, and *extended control* as

$$\tilde{\Phi}(k) \triangleq \begin{bmatrix} \bar{\Phi}(k) \\ \bar{\Phi}_{\mathrm{f}}(k) \end{bmatrix} \in \mathbb{R}^{n_{\mathrm{f}}(l_z+l_u)\times l_\theta}, \qquad \tilde{U}(k) \triangleq \begin{bmatrix} \bar{U}(k) \\ \bar{U}_{\mathrm{f}}(k) \end{bmatrix} \in \mathbb{R}^{n_{\mathrm{f}}(l_z+l_u)}, \tag{2.74}$$

where

$$\bar{\Phi}(k) \triangleq \begin{bmatrix} \Phi(k-1) \\ \vdots \\ \Phi(k-n_{\mathrm{f}}) \end{bmatrix} \in \mathbb{R}^{n_{\mathrm{f}}l_u\times l_\theta}, \quad \bar{\Phi}_{\mathrm{f}}(k) \triangleq \begin{bmatrix} \Phi_{\mathrm{f}}(k-1) \\ \vdots \\ \Phi_{\mathrm{f}}(k-n_{\mathrm{f}}) \end{bmatrix} \in \mathbb{R}^{n_{\mathrm{f}}l_z\times l_\theta}, \tag{2.75}$$

$$\bar{U}(k) \triangleq \begin{bmatrix} u(k-1) \\ \vdots \\ u(k-n_{\mathrm{f}}) \end{bmatrix} \in \mathbb{R}^{n_{\mathrm{f}}l_u}, \qquad \bar{U}_{\mathrm{f}}(k) \triangleq \begin{bmatrix} u_{\mathrm{f}}(k-1) \\ \vdots \\ u_{\mathrm{f}}(k-n_{\mathrm{f}}) \end{bmatrix} \in \mathbb{R}^{n_{\mathrm{f}}l_z}. \tag{2.76}$$

Therefore, we can write the retrospective performance $\hat{z}(k)$ in (2.66) in terms of the filter matrix $\tilde{G}$, the extended control $\tilde{U}(k)$, and the extended regressor $\tilde{\Phi}(k)$,

$$\hat{z}(k) = z(k) + \tilde{G}\left[\tilde{\Phi}(k)\hat{\theta} - \tilde{U}(k)\right]. \tag{2.77}$$

2.4.2 Alternative Formulation for IIR Filters

We can reformulate an IIR $G_{\mathrm{f}}(\mathbf{q})$ as two separate FIR filters. First, we multiply by $\mathbf{q}^{-n_{\mathrm{f}}}\mathcal{D}_{\mathrm{f}}(\mathbf{q})$ on the left which results in

$$\mathbf{q}^{-n_{\mathrm{f}}}\mathcal{D}_{\mathrm{f}}(\mathbf{q})\hat{z}(k) = \mathbf{q}^{-n_{\mathrm{f}}}\mathcal{D}_{\mathrm{f}}(\mathbf{q})z(k) + \mathbf{q}^{-n_{\mathrm{f}}}\mathcal{N}_{\mathrm{f}}(\mathbf{q})\left[\Phi(k)\hat{\theta} - u(k)\right]. \tag{2.78}$$

Thus, we define the *filtered retrospective performance*,

$$\hat{z}_{\mathrm{f}}(k) \triangleq \mathbf{q}^{-n_{\mathrm{f}}}\mathcal{D}_{\mathrm{f}}(\mathbf{q})\hat{z}(k), \tag{2.79}$$

$$= z_{\mathrm{f}}(k) + \Phi'_{\mathrm{f}}(k)\hat{\theta} - u'_{\mathrm{f}}(k), \tag{2.80}$$

where

$$\Phi'_{\mathrm{f}}(k) = \tilde{N}\bar{\Phi}(k), \qquad u'_{\mathrm{f}}(k) = \tilde{N}\bar{U}(k), \tag{2.81}$$

and

$$z_{\mathrm{f}}(k) = \begin{bmatrix} I_{l_z} & -\tilde{D} \end{bmatrix} \bar{Z}(k), \qquad \bar{Z}(k) \triangleq \begin{bmatrix} z(k) \\ \vdots \\ z(k-n_{\mathrm{f}}) \end{bmatrix} \in \mathbb{R}^{(n_{\mathrm{f}}+1)l_z}. \tag{2.82}$$

2.4.3 The Retrospective Filter

We demonstrate two special cases for building the filter $G_{\mathrm{f}}(\mathbf{q})$ to use in (2.66). Both methods described result in a FIR filter. Other filters can be built as needed.

2.4.3.1 Markov Parameter-based FIR filter

A straightforward approach to building the filter $G_{\mathrm{f}}9\mathbf{q})$ is to use the convolution in (2.10) and define the retrospective performance as

$$\hat{z}(k) = \frac{EA^{n_H}}{\mathbf{q}^{n_H}} x(k) + \sum_{i=1}^{n_H} \frac{H_i}{\mathbf{q}^i} \hat{u}(k) - \sum_{i=1}^{n_H} \frac{H_i}{\mathbf{q}^i} u(k). + \sum_{i=1}^{n_H} \frac{H_i'}{\mathbf{q}^i} w(k) - r(k), \tag{2.83}$$

We rewrite (2.83) using (2.10) and (2.65) and obtain

$$\hat{z}(k) = z(k) + \sum_{i=1}^{n_H} \frac{H_i}{\mathbf{q}^i} \left(\Phi(k)\hat{\theta} - u(k) \right). \tag{2.84}$$

Thus, the filter is given by the Markov parameters,

$$G_{\mathrm{f}}(\mathbf{q}) = \sum_{i=1}^{n_H} \frac{H_i}{\mathbf{q}^i}. \tag{2.85}$$

Using (2.85) we can construct the filter coefficient matrix,

$$\tilde{G}_H = \begin{bmatrix} H_1 & H_2 & \cdots & H_{n_H} \end{bmatrix}, \tag{2.86}$$

The extended regressor then is,

$$\tilde{\Phi}_{\mathrm{FIR}}(k) = \bar{\Phi}(k). \tag{2.87}$$

Similarly the extended control is

$$\tilde{U}_{\mathrm{FIR}}(k) = \bar{U}(k). \tag{2.88}$$

2.4.3.2 Nonminimum-phase Zeros for SISO systems

We can include modeling information of the zeros of the transfer function $G_{zu}(\mathbf{z})$. Note that the zeros of the transfer function are all values of $\mathbf{z}$ that satisfy,

$$0 = G_{zu}(\mathbf{z}). \tag{2.89}$$

Using a truncated Laurent expansion, we can write,

$$\begin{aligned} 0 &= \sum_{i=0}^{n_H} \frac{H_i}{\mathbf{z}^i} \\ &= \frac{H_0\mathbf{z}^{n_H} + H_1\mathbf{z}^{n_H-1} + \cdots + H_d\mathbf{z}^{n_H-d} + \cdots + H_{n_H}}{\mathbf{z}^{n_H}} \approx \frac{(\mathbf{z} - {}_1)\,(\mathbf{z} - {}_2)\cdots(\mathbf{z} - {}_{n_z})}{\mathbf{z}^{n_H}} \end{aligned} \tag{2.90}$$

where ${}_i$ is the ith zero of G_{zu} and n_z is the number of known nonminimum-phase zeros of G_{zu}.

We combine the knowledge of the Markov parameters and the nonminimum-phase zeros to obtain new parameters for the filter G_{f}. For causal systems, $H_0 = 0$, therefore,

$$0 = H_1\mathbf{z}^{n_H-1} + \cdots + H_d\mathbf{z}^{n_H-d} + \cdots + H_{n_H}. \tag{2.91}$$

Next, denote by H_d the first nonzero Markov parameter, then

$$0 = H_d\mathbf{z}^{n_H-d} + H_{d+1}\mathbf{z}^{n_H-d-1} + \cdots + H_{n_H}. \tag{2.92}$$

Note that the leading term of the polynomial on the far right side of (8.33), that is $\mathbf{z}^{n_z}$, has a unit coefficient. Thus, in order to match the polynomial coefficients, we normalize (2.92) using H_d, thus,

$$0 = \mathbf{z}^{n_H-d} + \frac{H_{d+1}}{H_d}\mathbf{z}^{n_H-d-1} + \cdots + \frac{H_{n_H}}{H_d}. \tag{2.93}$$

Where $n_H - d = n_z$, thus,

$$0 = \mathbf{z}^{n_z} + \frac{H_{d+1}}{H_d}\mathbf{z}^{n_z-1} + \cdots + \frac{H_{n_z+d}}{H_d}. \tag{2.94}$$

We define a new set of parameters K_i for $i = 1, \ldots, n_z + 1$ such that $K_1 \triangleq H_d$ and

$$\mathbf{z}^{n_z} + \frac{K_2}{K_1}\mathbf{z}^{n_z-1} + \cdots + \frac{K_{n_z+1}}{K_1} = (\mathbf{z} - {}_1)(\mathbf{z} - {}_2)\cdots(\mathbf{z} - {}_{n_z}). \tag{2.95}$$

In order to identify the coefficients K_i we expand the polynomial on the far right side of (2.95).

$$(\mathbf{z} - {}_1)(\mathbf{z} - {}_2)\cdots(\mathbf{z} - {}_{n_z}) = \mathbf{z}^{n_z} - \left(\sum_{j=1}^{n_z} {}_j\right)\mathbf{z}^{n_z-1} + \cdots + (-1)^{n_z}\prod_{j=1}^{n_z} {}_j. \tag{2.96}$$

Thus, we can obtain the second and the last coefficients,

$$K_2 = -H_d\sum_{j=1}^{n_z} {}_j, \qquad\qquad K_{n_z+1} = (-1)^{n_z} H_d\prod_{j=1}^{n_z} {}_j. \tag{2.97}$$

The remaining coefficients can be obtained by expanding the polynomial on the right side of (2.95) given the number of zeros in the transfer function.

Using the parameters $K_1, K_2, \ldots, K_{n_z+1}$ we can build an FIR filter to use in (2.66),

$$G_{\mathrm{f}}(\mathbf{q}) = \sum_{i=1}^{n_{\mathrm{f}}} \frac{K_i}{\mathbf{q}^i}. \tag{2.98}$$

This results in the filter coefficient matrix

$$\tilde{G}_0 = \begin{bmatrix} K_1 & K_2 & \cdots & K_{n_H} \end{bmatrix} \tag{2.99}$$

with the extended regressor and performance defined as in (2.87) and (2.88), respectively.

2.4.4 Retrospective Cost Function

We define a cumulative cost function to minimize the retrospective performance $\hat{z}$. By minimizing $\hat{z}$ RCAC attempts to minimizes $z(k)$, the actual performance. The cumulative cost function used in the 1-Step version of RCAC in [68] which itself is an expansion of

the cost function in [77] is given by

$$J_{\mathrm{D}}(k,\theta(k)) \triangleq \sum_{i=k_0}^{k} \lambda^{k-i} \left(\hat{z}(i)^{\mathrm{T}} \hat{z}(i) + \eta(i) \left[\Phi_{\mathrm{f}}(i)\hat{\theta} \right]^{\mathrm{T}} \Phi_{\mathrm{f}}(i)\hat{\theta} \right) + \lambda^{k} \left[\hat{\theta} - \theta(0) \right]^{\mathrm{T}} P(0)^{-1} \left[\hat{\theta} - \theta(0) \right], \tag{2.100}$$

where k_0 is the first time-step in which $\Phi_{\mathrm{f}}(k)$ is available, $\lambda \in (0,1]$ is a forgetting factor, and η is a penalty on the filtered control.

Replacing the filtered control term with a penalty on the control input $u(k) = \Phi(k)\hat{\theta}$ and adding a penalty to changes in θ yields the retrospective cost function

$$\begin{aligned} J(k,\hat{\theta}) \triangleq & \sum_{i=k_0}^{k} \hat{z}(i)^{\mathrm{T}} R_z(k,i) \hat{z}(i) \\ & + \sum_{i=k_0}^{k} \left[\Phi_{\mathrm{f}}(i)\hat{\theta} \right]^{\mathrm{T}} R_{u_{\mathrm{f}}}(k,i) \left[\Phi_{\mathrm{f}}(i)\hat{\theta} \right] + \left[\Phi(i)\hat{\theta} \right]^{\mathrm{T}} R_u(k,i) \left[\Phi(i)\hat{\theta} \right] \\ & + \left[\hat{\theta} - \theta(0) \right]^{\mathrm{T}} R_\theta(k) \left[\hat{\theta} - \theta(0) \right] + \left[\hat{\theta} - \theta(k-1) \right]^{\mathrm{T}} R_\Delta(k) \left[\hat{\theta} - \theta(k-1) \right]. \end{aligned} \tag{2.101}$$

where k_0 is the first time-step in which $\Phi_{\mathrm{f}}(k)$ is available and $R_z(k,i), R_u(k,i), R_\Delta(k), R_\theta(k)$ are symmetric and positive semi-definite for all k, i.

The cost function in (2.101) has three purposes, the first line is the a cost for the performance history, the second line penalizes the control effort, and the third line penalizes the control parameter transient. Furthermore, note that the control penalty can be applied to both the control input and the filtered controls.

2.4.5 Minimizer for J

We compute the derivative of (2.101) with respect to $\hat{\theta}$ and obtain

$$\begin{aligned} \frac{\partial J_{\mathrm{G}}}{\partial \hat{\theta}} &= 2 \sum_{i=k_0}^{k} \left(\hat{z}(i)^{\mathrm{T}} R_z(k,i) \Phi_{\mathrm{f}}(i) + \left[\Phi(i)\hat{\theta} \right]^{\mathrm{T}} R_u(k,i) \Phi(i) + \left[\Phi_{\mathrm{f}}(i)\hat{\theta} \right]^{\mathrm{T}} R_{\mathrm{f}}(k,i) \Phi_{\mathrm{f}}(i) \right) \\ &\quad + 2 \left[\hat{\theta} - \theta(0) \right]^{\mathrm{T}} R_\theta + 2 \left[\hat{\theta} - \theta(k-1) \right]^{\mathrm{T}} R_\Delta(k), \qquad (2.102) \\ &= 2\mathcal{A}(k)^{\mathrm{T}} + 2\hat{\theta}^{\mathrm{T}} \mathcal{P}(k)^{-1}, \qquad (2.103) \end{aligned}$$

where

$$\mathcal{A}(k) \triangleq \sum_{i=k_0}^{k} \left(\Phi_{\mathrm{f}}(i)^{\mathrm{T}} R_z(k,i) \left[z_{\mathrm{f}}(i) - u_{\mathrm{f}}(i) \right] \right) - R_\theta(k)\theta(0) - R_\Delta(k)\theta(k-1), \tag{2.104}$$

$$\mathcal{P}(k) \triangleq \left[\sum_{i=k_0}^{k} \left(\Phi_{\mathrm{f}}(i)^{\mathrm{T}} \left[R_z(k,i) + R_{\mathrm{f}}(k,i) \right] \Phi_{\mathrm{f}}(i) + \Phi(i)^{\mathrm{T}} R_u(k,i) \Phi(i) \right) + R_\theta(k) + R_\Delta(k) \right]^{-1}. \tag{2.105}$$

Therefore, the minimizer must satisfy

$$\mathcal{P}(k)^{-1} \hat{\theta}(k) + \mathcal{A}(k) = 0. \tag{2.106}$$

Thus, for all invertible $\mathcal{P}(k)$,

$$\hat{\theta} = -\mathcal{P}(k)\mathcal{A}(k). \tag{2.107}$$

Therefore, the controller parameters are given by

$$\theta(k) = \hat{\theta}. \tag{2.108}$$

We examine special cases which enable us to obtain a recursive expression for the controller parameters.

2.4.5.1 Constant Weights

Let the weights only depend on the current step i such that,

$$R_z(k,i) = R_z(i), \quad R_u(i) = R_u(i), \quad R_{\mathrm{f}}(k,i) = R_{\mathrm{f}}(i), \quad R_\Delta(k) = R_\Delta, \quad R_\theta(k) = R_\theta. \tag{2.109}$$

Then,

$$\begin{aligned} \mathcal{A}(k) &= \mathcal{A}(k-1) + \Phi_{\mathrm{f}}(k)^{\mathrm{T}} R_z(k) \left[z(k) - u_{\mathrm{f}}(k) \right] + R_\Delta \left[\theta(k-2) - \theta(k-1) \right] \\ &= \mathcal{A}(k-1) + X(k)^{\mathrm{T}} \bar{R}(k) z'(k) + R_\Delta \left[\theta(k-2) - \theta(k-1) \right] \end{aligned} \tag{2.110}$$

where

$$X(k) \triangleq \begin{bmatrix} \Phi_{\mathrm{f}}(k) \\ \Phi(k) \end{bmatrix} \in \mathbb{R}^{(l_z+l_u)\times l_\theta}, \tag{2.111}$$

$$\bar{R}(k) \triangleq \begin{bmatrix} R_z(k) & 0 \\ 0 & R_u(k) \end{bmatrix} \in \mathbb{R}^{(l_z+l_u)\times(l_z+l_u)}, \quad z'(k) \triangleq \begin{bmatrix} z(k) - u_{\mathrm{f}}(k) \\ 0 \end{bmatrix} \in \mathbb{R}^{l_z+l_u}. \tag{2.112}$$

Furthermore,

$$\begin{aligned} \mathcal{P}(k) &= \left[\mathcal{P}(k-1)^{-1} + \Phi_{\mathrm{f}}(k)^{\mathrm{T}} R_z(k) \Phi_{\mathrm{f}}(k) + \Phi(k)^{\mathrm{T}} R_u(k) \Phi(k)\right]^{-1}, \\ &= \left[\mathcal{P}(k-1)^{-1} + X(k)^{\mathrm{T}} \bar{R}(k) X(k)\right]^{-1}, \\ &= \mathcal{P}(k-1) - \mathcal{P}(k-1) X(k)^{\mathrm{T}} \Gamma(k)^{-1} X(k) \mathcal{P}(k-1), \end{aligned} \tag{2.113}$$

where

$$\Gamma(k) \triangleq \left[\bar{R}(k)^{-1} + X(k) \mathcal{P}(k-1) X(k)^{\mathrm{T}}\right] \tag{2.114}$$

and $R_z(k)$, $R_u(k)$, and $R_\theta + R_\Delta$ are positive definite. We combine (2.110) and (7.49) to compute $\theta(k)$,

$$\theta(k) = -\mathcal{P}(k)\mathcal{A}(k) \tag{2.115}$$

$$\begin{aligned} &= \left[\mathcal{P}(k-1) X(k)^{\mathrm{T}} \Gamma(k)^{-1} X(k) \mathcal{P}(k-1) - \mathcal{P}(k-1)\right] \cdot \\ &\left[\mathcal{A}(k-1) + X(k)^{\mathrm{T}} \bar{R}(k) z'(k) + R_\Delta \left[\theta(k-2) - \theta(k-1)\right]\right]. \end{aligned} \tag{2.116}$$

After some algebra we obtain the recursive solution

$$\begin{aligned} \theta(k) &= \theta(k-1) + \mathcal{P}(k-1) X(k)^{\mathrm{T}} \Gamma(k)^{-1} \varepsilon(k) \\ &+ \mathcal{P}(k-1) R_\Delta \left[X(k)^{\mathrm{T}} \Gamma(k)^{-1} X(k) \mathcal{P}(k-1) - I_{l_\theta}\right] \left(\theta(k-2) - \theta(k-1)\right), \end{aligned} \tag{2.117}$$

where

$$\varepsilon(k) \triangleq z'(k) - X(k)\theta(k-1). \tag{2.118}$$

The initial values are given by

$$\theta(k_0) = \theta_0, \quad \mathcal{P}(k_0) = \left[R_\theta + R_\Delta\right]^{-1}, \tag{2.119}$$

where θ_0 is chosen arbitrarily.

2.4.5.2 Zero Control Penalty

If we let $R_u(k)$ be zero, then the recursive solutions simplify,

$$\mathcal{A}(k) = \mathcal{A}(k-1) + \Phi_{\mathrm{f}}(k)^{\mathrm{T}} R_z(k) \left[z(k) - u_{\mathrm{f}}(k)\right] + R_\Delta \left[\theta(k-2) - \theta(k-1)\right], \tag{2.120}$$

$$\begin{aligned}\mathcal{P}(k) &= \mathcal{P}(k-1) - \mathcal{P}(k-1)\Phi_{\mathrm{f}}(k)^{\mathrm{T}} \left[\left(R_z(k) + R_{\mathrm{f}}(k)\right)^{-1} + \Phi_{\mathrm{f}}(k)\mathcal{P}(k-1)\Phi_{\mathrm{f}}(k)^{\mathrm{T}}\right]^{-1} \Phi_{\mathrm{f}}(k)\mathcal{P}(k-1), \\ &= \mathcal{P}(k-1) - \mathcal{P}(k-1)\Phi_{\mathrm{f}}(k)^{\mathrm{T}}\Gamma(k)^{-1}\Phi_{\mathrm{f}}(k)\mathcal{P}(k-1). \end{aligned} \tag{2.121}$$

Where

$$\Gamma(k) \stackrel{\triangle}{=} \left(R_z(k) + R_{\mathrm{f}}(k)\right)^{-1} + \Phi_{\mathrm{f}}(k)\mathcal{P}(k-1)\Phi_{\mathrm{f}}(k)^{\mathrm{T}}. \tag{2.122}$$

Thus, the simplified recursive solution is given by

$$\begin{aligned}\theta(k) = \theta(k-1) &+ \mathcal{P}(k-1)\Phi_{\mathrm{f}}(k)^{\mathrm{T}}\Gamma(k)^{-1}\varepsilon(k) \\ &+ \mathcal{P}(k-1)R_\Delta \left[\Phi_{\mathrm{f}}(k)^{\mathrm{T}}\Gamma(k)^{-1}\Phi_{\mathrm{f}}(k)\mathcal{P}(k-1) - I_{l_\theta}\right] \left(\theta(k-2) - \theta(k-1)\right), \end{aligned} \tag{2.123}$$

where

$$\varepsilon \stackrel{\triangle}{=} \left(R_z(k) + R_{\mathrm{f}}(k)\right)^{-1} R_z \left(u_{\mathrm{f}}(k) - z(k)\right) - \Phi_{\mathrm{f}}(k)\theta(k-1). \tag{2.124}$$

The initial conditions are given by (2.119).

2.4.5.3 Forgetting Factor

Next, we let the weight matrices be given by

$$R_z(k,i) = \lambda^{k-i} R_z(i), \quad R_u(k,i) = \lambda^{k-i} R_u(i), \quad R_\theta(k) = \lambda^k R_\theta, \quad R_\Delta(k) = 0. \tag{2.125}$$

Then, the recursive relations become,

$$\mathcal{A}(k) = \lambda\mathcal{A}(k-1) + \Phi_{\mathrm{f}}(k)^{\mathrm{T}} R_z(k) \left[z(k) - u_{\mathrm{f}}(k)\right], \tag{2.126}$$

$$\begin{aligned}\mathcal{P}(k) &= \left[\lambda\mathcal{P}(k-1)^{-1} + X(k)^{\mathrm{T}}\bar{R}(k)X(k)\right]^{-1}, \\ &= \frac{1}{\lambda}\mathcal{P}(k-1) - \frac{1}{\lambda}\mathcal{P}(k-1)X(k)^{\mathrm{T}}\Gamma(k)^{-1}X(k)\mathcal{P}(k-1).\end{aligned} \tag{2.127}$$

Which yield the recursive relation for θ,

$$\theta(k) = \theta(k-1) + \mathcal{P}(k-1)X(k)^{\mathrm{T}}\Gamma(k)^{-1}\varepsilon(k), \tag{2.128}$$

where $z'(k)$ and $\bar{R}(k)$ are given by (2.112), and

$$\Gamma(k) \triangleq \lambda\bar{R}(k)^{-1} + X(k)\mathcal{P}(k-1)X(k)^{\mathrm{T}}, \tag{2.129}$$

$$\varepsilon \triangleq \bar{R}(k)^{-1}\bar{R}'(k)z'(k) - X(k)\theta(k-1). \tag{2.130}$$

2.4.5.4 Kalman Filter

The measurement update step of the Kalman filter is given by

$$\hat{x}(k) = \hat{x}_{k|k-1} + K(k)\epsilon(k), \tag{2.131}$$

$$P(k) = \left(I - K(k)H(k)\right)P_{k|k-1}. \tag{2.132}$$

Where the estimate and information matrix $\hat{x}_{k|k-1}, P_{k|k-1}$ are given by the prediction step and

$$K(k) \triangleq P_{k|k-1}H(k)^{\mathrm{T}}\left(R(k) + H(k)P_{k|k-1}H(k)^{\mathrm{T}}\right)^{-1}, \tag{2.133}$$

$$\epsilon(k) \triangleq y(k) - H(k)\hat{x}_{k|k-1}. \tag{2.134}$$

Compare (2.131), (2.132) with a specialized form of (2.123) where $R_{\mathrm{f}}(k) = R_{\Delta}(k) = 0$, that is,

$$\theta(k) = \theta(k-1) + \mathcal{P}(k-1)\Phi_{\mathrm{f}}(k)^{\mathrm{T}}\Gamma(k)^{-1}\varepsilon(k), \tag{2.135}$$

$$\mathcal{P}(k) = \left(I - \mathcal{P}(k-1)\Phi_{\mathrm{f}}(k)^{\mathrm{T}}\Gamma(k)^{-1}\Phi_{\mathrm{f}}(k)\right)\mathcal{P}(k-1), \tag{2.136}$$

where

$$\Gamma(k) \triangleq R_z(k)^{-1} + \Phi_{\mathrm{f}}(k)\mathcal{P}(k-1)\Phi_{\mathrm{f}}(k)^{\mathrm{T}}, \tag{2.137}$$

$$\varepsilon(k) \triangleq (u_{\mathrm{f}}(k) - z(k)) - \Phi_{\mathrm{f}}(k)\theta(k-1). \tag{2.138}$$

Notice that the both equations are equal in structure, $\varepsilon(k)$ in (2.135) is an analogue to $\epsilon(k)$ in (2.131), similarly the analogue of $K(k)$ in (2.131) is $\mathcal{P}(k-1)\Phi_{\mathrm{f}}(k)^{\mathrm{T}}\Gamma(k)^{-1}$ in (2.135).

We introduce a prediction step for the controller parameters θ by first defining a dynamic system

$$\theta^*(k) = A^*(k-1)\theta^*(k-1) + w(k) \tag{2.139}$$

where $A^*(k)$ is stable for all k and $w(k)$ is a random process. The prediction step for the Kalman filter is given by

$$\hat{x}_{k|k-1} = A(k-1)\hat{x}(k-1), \tag{2.140}$$

$$P_{k|k-1} = A(k-1)P(k-1)A(k-1)^{\mathrm{T}} + Q(k-1). \tag{2.141}$$

Thus, the corresponding prediction step for the controller parameter is,

$$\theta_{k|k-1} = A^*(k-1)\theta(k-1), \tag{2.142}$$

$$\mathcal{P}_{k|k-1} = A^*(k-1)\mathcal{P}(k-1)A^*(k-1)^{\mathrm{T}} + Q(k-1). \tag{2.143}$$

we then compute the measurement update using the output of the prediction step,

$$\theta(k) = \theta_{k|k-1} + \mathcal{P}_{k|k-1}\Phi_{\mathrm{f}}(k)^{\mathrm{T}}\Gamma(k)^{-1}\left[(u_{\mathrm{f}}(k) - z(k)) - \Phi_{\mathrm{f}}(k)\theta_{k|k-1}\right], \tag{2.144}$$

$$\mathcal{P}(k) = \left(I - \mathcal{P}_{k|k-1}\Phi_{\mathrm{f}}(k)^{\mathrm{T}}\Gamma(k)^{-1}\Phi_{\mathrm{f}}(k)\right)\mathcal{P}_{k|k-1}. \tag{2.145}$$

2.5 RLS Implementation

2.5.1 Sequential Updates

When $l_z > 1$ or $R_u \neq 0$, $\Gamma(k)$ in (2.114), (2.122), (2.129), and (2.137) becomes a matrix. The numerical matrix inversion can cause the information matrix $\mathcal{P}$ to lose its positive definite or symmetric properties. To avoid matrix inversion we process each component of ϵ separately [80].

Consider the least squares problem

$$\begin{bmatrix} a_{11} & a_{12} & \cdots & a_{1n} \end{bmatrix} x = b_1. \tag{2.146}$$

where, for $i > 0$, a_i, b_i are scalars and $x \in \mathbb{R}^n$ is the quantity to be estimated. After k steps, (2.146) becomes

$$\begin{bmatrix} a_{1,1} & a_{1,2} & \cdots & a_{1,n} \\ \vdots & \vdots & \ddots & \vdots \\ a_{k,1} & a_{k,2} & \cdots & a_{k,n} \end{bmatrix} x = \begin{bmatrix} b_1 \\ \vdots \\ b_k \end{bmatrix}. \tag{2.147}$$

Note that both the matrix on the left side and the vector on the right side of (2.148) grow by one row after each step.

Next, consider a similar problem given by

$$\begin{bmatrix} A_{1,1} & A_{1,2} & \cdots & A_{1,n} \\ \vdots & \vdots & \ddots & \vdots \\ A_{k,1} & A_{k,2} & \cdots & A_{k,n} \end{bmatrix} x = \begin{bmatrix} B_1 \\ \vdots \\ B_k \end{bmatrix}. \tag{2.148}$$

Instead of scalar measurements and row vector regressors we have vector measurements B_i and matrix regressors $A_i = \begin{bmatrix} A_{i,1} & \cdots A_{i,n} \end{bmatrix}$. Note that

$$A_{i,j} = \begin{bmatrix} a_{i,j,1} & \cdots & a_{i,j,p} \end{bmatrix}^{\mathrm{T}}, \tag{2.149}$$

$$B_i = \begin{bmatrix} b_{i,1} & \cdots & b_{i,p} \end{bmatrix}^{\mathrm{T}}, \tag{2.150}$$

that is, the each matrix regressor A_i and vector measurement B_i have the same number of rows p. Thus at each step the matrix on the left and the vector on the right grow by p rows. When solving for x recursively these problems involve a matrix inversion of size $p \times p$. This matrix inversion can deteriorate the condition of the information matrix compromising its positive-definite and symmetry.

These difficulties can be avoided by processing the vector measurements row by row.

When the $k+1$st measurement is acquired we solve the modified problem

$$\begin{bmatrix} A_{1,1} & A_{1,2} & \cdots & A_{1,n} \\ \vdots & \vdots & \ddots & \vdots \\ A_{k,1} & A_{k,2} & \cdots & A_{k,n} \\ a_{k+1,1,1} & a_{k+1,2,1} & \cdots & a_{k+1,n,1} \end{bmatrix} x = \begin{bmatrix} B_1 \\ \vdots \\ B_k \\ b_{k+1,1} \end{bmatrix}. \tag{2.151}$$

Iterating over the p rows yields the solution to

$$\begin{bmatrix} A_{1,1} & A_{1,2} & \cdots & A_{1,n} \\ \vdots & \vdots & \ddots & \vdots \\ A_{k+1,1} & A_{k+1,2} & \cdots & A_{k+1,n} \end{bmatrix} x = \begin{bmatrix} B_1 \\ \vdots \\ B_{k+1} \end{bmatrix}. \tag{2.152}$$

2.5.2 Sequential Update in RCAC

Consider the update equation

$$\theta(k) = \theta(k-1) + \mathcal{P}(k-1)X(k)^{\mathrm{T}}\Gamma(k)^{-1}\varepsilon(k), \tag{2.153}$$

where $\varepsilon(k) \in \mathbb{R}^p$. Instead of using (2.153) we process each row of $X(k)$ and $\varepsilon(k)$ sequentially. Let

$$\theta(k-1)^1 = \theta(k-1), \tag{2.154}$$

$$\mathcal{P}^1(k-1) = \mathcal{P}(k-1). \tag{2.155}$$

Then for all $i = 2, \ldots, p$

$$\theta(k-1)^i = \theta(k-1)^{i-1} + \mathcal{P}^{i-1}(k-1)X_i(k)^{\mathrm{T}}\Gamma^{i-1}(k)^{-1}\varepsilon_i(k), \tag{2.156}$$

where X_i, ε_i are the ith rows of X and ε respectively and

$$\Gamma^i(k) = R_{i,i} + X_i(k)^{\mathrm{T}}\mathcal{P}^{i-1}(k-1)X_i(k), \tag{2.157}$$

$$\mathcal{P}^i(k-1) = \mathcal{P}^{i-1}(k-1) - \mathcal{P}^{i-1}(k-1)X_i(k)^{\mathrm{T}}\Gamma^{i-1}(k)^{-1}X_i(k)\mathcal{P}^{i-1}(k-1), \tag{2.158}$$

where $R_{i,i}$ is the (i,i) entry of R. Note that Γ_i is a scalar and thus there is no longer a matrix inverse in the update of $\mathcal{P}^i(k-1)$. The updated control parameters and information matrix are given by

$$\theta(k) = \theta_p(k-1), \tag{2.159}$$

$$\mathcal{P}(k) = \mathcal{P}^p(k-1). \tag{2.160}$$

CHAPTER 3

Spacecraft Attitude Dynamics

In this chapter we derive the kinematics and dynamics of a spacecraft controlled by either torque generating actuators (thrusters, magnetic torquers) or momentum exchange devices (reaction wheels, control moment gyros). Throughout the chapter, the vector $\vec{r}_{\mathrm{b/a}}$ represents the position of point b relative to point a, the vector $\vec{v}_{\mathrm{b/a/X}}$ denotes the velocity of point b relative to point a with respect to the frame $\mathrm{F_X}$, and the vector $\vec{\omega}_{\mathrm{Y/X}}$ is the angular velocity of frame $\mathrm{F_Y}$ relative to frame $\mathrm{F_X}$. All frames are orthogonal and right-handed.

3.1 Rigid Body Dynamics

We derive the dynamics for a rigid spacecraft bus actuated by rigidly attached actuators. The dynamics are derived using Newtonian methods [8, 81]. First, we define two frames, an inertial frame $\mathrm{F_I}$ and a body frame $\mathrm{F_B}$ fixed to the spacecraft bus. We describe the dynamics of the spacecraft using Euler's equation

$$\overset{\mathrm{B}\bullet}{\vec{H}}_{\mathrm{sc/c/I}} = -\vec{\omega}^{\times}_{B/I}\vec{H}_{\mathrm{sc/c/I}} + \vec{M}_{\mathrm{sc}}, \tag{3.1}$$

where $\vec{H}_{\mathrm{sc/c/I}}$ is the combined angular momentum of the spacecraft bus and the actuators relative to the spacecraft's center of mass c with respect to the inertial frame, $\vec{\omega}_{\mathrm{B/I}}$ is the angular velocity of the body frame relative to the inertial frame, and $\vec{M}_{\mathrm{sc}}$ is the sum of external torques applied to the spacecraft.

The angular momentum of the spacecraft relative to its center of mass with respect to $\mathrm{F_I}$ is given by

$$\vec{H}_{\mathrm{sc/c/I}} = \vec{H}_{\mathrm{b/c/I}} + \sum_{i=1}^{n_{\mathrm{A}}} \vec{H}_{\mathrm{a}_i\mathrm{/c/I}}, \tag{3.2}$$

where n_{A} is the number of actuators and the angular momentum $\vec{H}_{\mathrm{b/c/I}}$ of the spacecraft bus b relative to c with respect to $\mathrm{F_I}$ is given by

$$\vec{H}_{\mathrm{b/c/I}} = \vec{J}_{\mathrm{b/c}}\vec{\omega}_{\mathrm{B/I}}, \tag{3.3}$$

where $\vec{J}_{\mathrm{b/c}}$ is the physical inertia matrix of the bus relative to the center of mass of the spacecraft c, and $\vec{J}_{\mathrm{b/c}}$ is the angular velocity of $\mathrm{F_B}$ relative to $\mathrm{F_I}$. The angular momentum $\vec{H}_{\mathrm{a}_i\mathrm{/c/I}}$ of actuator i relative to c with respect to $\mathrm{F_I}$ depends on the actuator type.

To obtain the equations of motion, we expand the derivative on the left-hand side of (7.22) with (7.14), which yields

$$\overset{\mathrm{B}\bullet}{\vec{H}}_{\mathrm{sc/c/I}} = \vec{J}_{\mathrm{b/c}}\overset{\mathrm{B}\bullet}{\vec{\omega}}_{\mathrm{B/I}} + \sum_{i=1}^{n_{\mathrm{A}}} \overset{\mathrm{B}\bullet}{\vec{H}}_{\mathrm{a}_i\mathrm{/c/I}}\,. \tag{3.4}$$

Then, we combine (7.22), (7.14), and (3.4) to obtain

$$\vec{J}_{\mathrm{b/c}}\overset{\mathrm{B}\bullet}{\vec{\omega}}_{\mathrm{B/I}} + \sum_{i=1}^{n_{\mathrm{A}}} \overset{\mathrm{B}\bullet}{\vec{H}}_{\mathrm{a}_i\mathrm{/c/I}} = -\vec{\omega}_{B/I} \times \left[\vec{J}_{\mathrm{b/c}}\vec{\omega}_{\mathrm{B/I}}, + \sum_{i=1}^{n_{\mathrm{A}}} \vec{H}_{\mathrm{a}_i\mathrm{/c/I}},\right] + \vec{M}_{\mathrm{sc}}. \tag{3.5}$$

In the following sections we compute the actuator-specific terms $\vec{H}_{\mathrm{a}_i\mathrm{/c/I}}$ and $\overset{\mathrm{B}\bullet}{\vec{H}}_{\mathrm{a}_i\mathrm{/c/I}}$.

3.1.1 On the inertia matrix

To study the ability of RCAC to control different rigid bodies we define different spacecraft bus inertias [73].

Lemma 1. *Let $\mathcal{B}$ be a rigid body composed of particles that are not colinear and define a point w, a frame $\mathrm{F_A}$, and the inertia matrix $J \triangleq \vec{J}_{\mathcal{B}/w}\Big|_{\mathrm{A}}$. Then*

1. *J is positive definite,*
2. *There exists a frame $\mathrm{F_B}$ such that $\vec{J}_{\mathcal{B}/w}\Big|_{\mathrm{B}}$ is diagonal.*

Lemma 2. *Let J be a diagonal inertia matrix defined by*

$$J \triangleq \mathrm{diag}(\lambda_1,\ \lambda_2, \lambda_3). \tag{3.6}$$

Where the principal moments of inertia $\lambda_1, \lambda_2, \lambda_3$ satisfy

1. $\lambda_1 \geq \lambda_2 \geq \lambda_3 > 0$,

2. $\lambda_1 \leq \lambda_2 + \lambda_3$, *the triangle inequality.*

Given a body with major principal moment of inertia λ_1, the triangle inequality yields all possible relations between the principal moments of inertia. Thus, all possible inertia combinations can be described by the triangle in Figure 3.1.

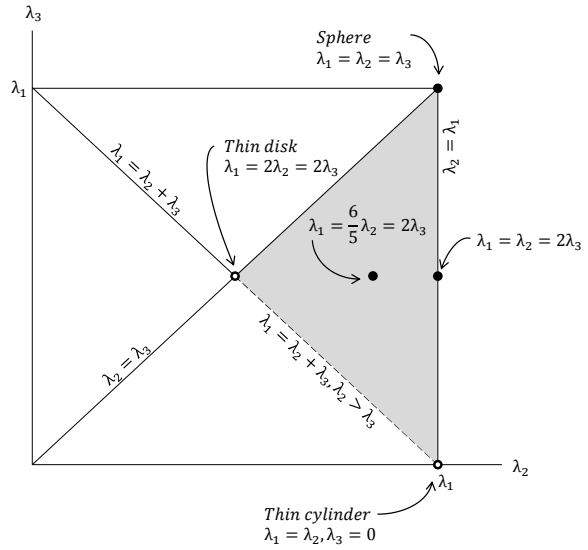

Figure 3.1: Feasible region for λ_2, λ_3 given λ_1. The shaded region satisfies both the triangle inequality $\lambda_1 \leq \lambda_2 + \lambda_3$ and $\lambda_1 \geq \lambda_2 \geq \lambda_3 > 0$. The open dots and dashed lines represent nonphysical cases.

Let $\lambda_1 = 10$kg-m^2, based on Figure 3.1, we define five diagonal inertias which correspond to common spacecraft bus shapes.

1. $J_1 \triangleq 10I_3$ kg-m^2, for a sphere or a cube,
2. $J_2 \triangleq \mathrm{diag}(10,\ 10,\ 5)$ kg-m^2, for a cylinder
3. $J_3 \triangleq \mathrm{diag}(10,\ 25/3,\ 5)$ kg-m^2, for the centroid of the triangle,
4. $J_4 \triangleq \mathrm{diag}(10,\ 5,\ 5)$ kg-m^2, for a thin disk
5. $J_5 \triangleq \mathrm{diag}(10,\ 10,\ 0)$ kg-m^2, for a thin cylinder.

Note that both J_4 and J_5 violate the triangle inequality and thus are not physical inertias.

3.2 Attitude and Angular Velocity Measurements

We assume that both rate (inertial) and attitude (noninertial) measurements are available. Gyro measurements $y_{\rm rate} \in \mathbb{R}^3$ provide measurements of the angular velocity resolved in the spacecraft frame, that is,

$$y_{\rm rate} = \vec{\omega}_{\rm B/I}\Big|_{\rm B}. \tag{3.7}$$

For simplicity, we assume that rate measurements are available without noise and bias. In practice, rate bias can be corrected by using attitude measurements and filtering techniques.

Attitude is measured indirectly using sensors such as star trackers. The attitude measurement is determined to be

$$y_{\rm attitude} = \vec{R}_{\rm B/I}\Big|_{\rm B}. \tag{3.8}$$

3.3 The Attitude Control Problem

The objective of the attitude control problem is to determine control inputs such that the spacecraft attitude given by R follows a commanded attitude trajectory given by a possibly time-varying C^1 rotation matrix $R_{\rm d}(t)$ [58].

3.3.1 Desired Attitude and Attitude Error

The control objective is to have the spacecraft attitude R follow the commanded attitude trajectory given by

$$\dot{R}_{\rm d} = \frac{\rm d}{{\rm d}t}\left(\vec{R}_{\rm d/I}\Big|_{\rm d}\right) = \overset{\rm d\bullet}{\vec{R}}_{\rm d/I}\Big|_{\rm d} = \vec{R}_{\rm d/I}\Big|_{\rm d}\,\vec{\omega}_{\rm d/I}\Big|_{\rm d}^{\times} = R_{\rm d}\omega_{\rm d}^{\times}, \tag{3.9}$$

where $\vec{R}_{\rm d/I}$ is the physical rotation matrix that transforms $\mathrm{F_I}$ into $\mathrm{F_d}$, $\vec{\omega}_{\rm d/I}$ is the angular velocity of $\mathrm{F_d}$ relative to $\mathrm{F_I}$, d$\bullet$ indicates the derivative with respect to $\mathrm{F_d}$, and

$$R_{\rm d} \triangleq \vec{R}_{\rm d/I}\Big|_{\rm d}, \qquad \omega_{\rm d} \triangleq \vec{\omega}_{\rm d/I}\Big|_{\rm d}. \tag{3.10}$$

The error between R and $R_{\rm d}$ is given in terms of the attitude-error rotation matrix

$$\tilde{R} \triangleq \vec{R}_{\rm B/d}\Big|_{\rm B} = R_{\rm d}^{\rm T}R, \tag{3.11}$$

which satisfies

$$\dot{\tilde{R}} = \frac{\mathrm{d}\tilde{R}}{\mathrm{d}t} = \overset{\mathrm{B}\bullet}{\vec{R}}_{\mathrm{B/d}}\Big|_{\mathrm{B}} = \vec{R}_{\mathrm{B/d}}\Big|_{\mathrm{B}}\, \vec{\omega}_{\mathrm{B/d}}\Big|_{\mathrm{B}}^{\times} = \tilde{R}\tilde{\omega}^{\times}, \tag{3.12}$$

where $\vec{R}_{\mathrm{B/d}}$ is the physical rotation matrix that transforms $\mathrm{F_d}$ into $\mathrm{F_B}$, $\vec{\omega}_{\mathrm{B/d}}$ is the angular velocity of $\mathrm{F_B}$ relative to $\mathrm{F_{B_d}}$, and the angular-velocity error $\tilde{\omega}$ is given by

$$\tilde{\omega} \triangleq \vec{\omega}_{\mathrm{B/d}}\Big|_{\mathrm{B}} = \left(\vec{\omega}_{\mathrm{B/I}} - \vec{\omega}_{\mathrm{d/I}}\right)\Big|_{\mathrm{B}} = \omega - \tilde{R}^{\mathrm{T}}\omega_{\mathrm{d}}. \tag{3.13}$$

3.3.1.1 Vector Representation of Attitude Error

A vector representation of the attitude error $\tilde{R}$ in (5.29) is given by [58]

$$S \triangleq \sum_{i=1}^{3} a_i(\tilde{R}^{\mathrm{T}}e_i) \times e_i = \begin{bmatrix} a_3\tilde{R}_{32} - a_2\tilde{R}_{23} \\ a_1\tilde{R}_{13} - a_3\tilde{R}_{31} \\ a_2\tilde{R}_{21} - a_1\tilde{R}_{12} \end{bmatrix} \in \mathbb{R}^3, \tag{3.14}$$

where a_1, a_2, a_3 are distinct positive numbers. Note that S depends on the off-diagonal entries of the error matrix $\tilde{R}$ in (5.29).

3.3.2 Performance Metrics

To study the performance of the algorithm we define a scalar attitude error metric by using the eigenaxis attitude-error.

$$\theta_{\mathrm{eig}} \triangleq \cos^{-1}\frac{1}{2}\left(\mathrm{tr}\ \tilde{R} - 1\right), \tag{3.15}$$

The eigenangle θ_{eig} is the rotation angle about the eigenaxis which rotates $R(t)$ to the desired attitude $R_{\mathrm{d}}(t)$. To evaluate the closed-loop performance, we define the settling time T as the time needed to bring the eigenaxis attitude-error within a bound θ_{ss}, that is,

$$\theta_{\mathrm{eig}}(t) \leq \theta_{\mathrm{ss}}, \quad \text{for all } t \geq T. \tag{3.16}$$

3.4 Maneuver Types

We study two maneuver types namely, motion-to-rest (M2R) and motion-to-spin (M2S). For both maneuvers, the spacecraft starts at an arbitrary attitude spinning at a given angular rate. Thus, the spacecraft is tumbling in a scenario representative of the spacecraft attitude after launch vehicle separation. In M2R maneuvers, the goal of the controller is to bring the spacecraft to rest at a desired attitude. In M2S the goal of the spacecraft is to bring the spacecraft to a specified time-varying attitude, this includes common maneuvers such as Nadir pointing and spins about a specified body axis pointed inertially. Both maneuvers have a simplified variant, rest-to-rest (R2R) and rest-to-spin (R2S) respectively. In these variants the spacecraft begins at rest. The R2R maneuver represents a slew, the R2S represents a spin up maneuver. These maneuver types encompass, step, ramp, and arbitrary time-dependent attitude commands.

CHAPTER 4

Thrusters

We apply RCAC to spacecraft attitude control using thrusters. First, RCAC is implemented as a regulator for the angular velocity of a rigid body governed by Euler's equation. This type of controller can be used to detumble a spacecraft after launch-vehicle separation; this is the rate-only motion-to-rest (M2R-R) problem. Then, we consider commanded spins about an arbitrary body axis; this constitutes the rate-only motion-to-spin (M2S-R) problem. Initially, we use knowledge of the inertia and actuator alignment to compute the parameters required by RCAC. Then, RCAC is tested for robustness to scaling of the inertia and actuator matrices.

The angular velocity controllers are then extended to attitude control. Attitude kinematics are included in the spacecraft model, and motion-to-rest (M2R) and motion-to-spin (M2S) maneuvers are tested. For M2R, the spacecraft has an initial attitude and angular velocity, and the objective is to bring the spacecraft to rest at a specified attitude. For M2S, the spacecraft has an arbitrary initial attitude and angular velocity, and the objective is to bring the spacecraft to spin about a specified body axis that is pointed inertially. The body spin axis need not be a principal axis. As in the angular velocity control case, both problems are first examined using complete knowledge of the inertia and actuator alignment. Robustness is then examined through scaling and misalignments.

4.1 Spacecraft Model

Thrusters produce a force which results in a moment applied to the spacecraft. We consider only the rotational motion of the spacecraft while ignoring the translational motion of the spacecraft's center of mass; therefore we consider only the torque applied by the force actuators. Furthermore, we ignore the effects of fuel slosh on the angular momentum as well as the problem of thruster placement.

Since thrusters do not store angular momentum, the terms $\vec{H}_{\mathrm{a}_i/\mathrm{c}/\mathrm{I}}, \overset{\mathrm{B}\bullet}{\vec{H}}_{\mathrm{a}_i/\mathrm{c}/\mathrm{I}}$ in (3.5) are

zero. Define a body-fixed frame $\mathrm{F_B}$, whose origin is chosen to be the center of mass, and specify an inertial frame $\mathrm{F_I}$ to determine the attitude of the spacecraft. Then, the dynamics for a spacecraft with thrusters are given by

$$\vec{J}_{\mathrm{b/c}} \overset{\mathrm{B}\bullet}{\vec{\omega}}_{\mathrm{B/I}} = -\vec{\omega}_{B/I} \times \vec{J}_{\mathrm{b/c}} \vec{\omega}_{\mathrm{B/I}} + \vec{M}_{\mathrm{thrust}} + \vec{M}_{\mathrm{b}}, \tag{4.1}$$

where $\vec{M}_{\mathrm{thrust}}$ is the torque produced by the thrusters and $\vec{M}_{\mathrm{b}}$ is the sum of all disturbance torques acting on the spacecraft bus.

We define the notation

$$R \triangleq \vec{R}_{\mathrm{B/I}}\Big|_{\mathrm{B}}, \quad \omega \triangleq \vec{\omega}_{\mathrm{B/I}}\Big|_{\mathrm{B}}, \quad \dot{\omega} \triangleq \overset{\mathrm{B}\bullet}{\vec{\omega}}_{\mathrm{B/I}}\Big|_{\mathrm{B}}, \quad \tau_{\mathrm{dist}} \triangleq \vec{M}_{\mathrm{b}}\Big|_{\mathrm{B}}, \quad J \triangleq \vec{J}_{\mathrm{b/c}}\Big|_{\mathrm{B}}. \tag{4.2}$$

Resolving (4.1) in the body frame yields Euler's equation for a spacecraft actuated by thrusters,

$$J\omega = -\omega^{\times} J\omega + B_{\mathrm{sc}} u + \tau_{\mathrm{dist}}, \tag{4.3}$$

where $B_{\mathrm{sc}} u \triangleq \vec{M}_{\mathrm{thrust}}\Big|_{\mathrm{B}}$, $\omega \in \mathbb{R}^3$ is the angular velocity of the spacecraft frame with respect to the inertial frame resolved in the spacecraft frame and $J \in \mathbb{R}^{3\times 3}$ is the constant, positive-definite inertia matrix of the spacecraft, that is, the inertia dyadic of the spacecraft relative to the spacecraft center of mass resolved in the spacecraft frame. The spacecraft attitude evolves according to Poisson's equation [81]

$$\dot{R} = R\omega^{\times}. \tag{4.4}$$

whereq, $R \in \mathbb{R}^{3\times 3}$ is the proper orthogonal matrix (that is, the rotation matrix) that transforms the components of a vector resolved in the spacecraft frame into the components of the same vector resolved in the inertial frame, and $\omega^{\times}$ is the skew-symmetric cross-product matrix of ω.

The components of the vector $u \in \mathbb{R}^{l_u}$ represent independent control inputs, while the matrix $B_{\mathrm{sc}} \in \mathbb{R}^{3\times l_u}$ determines the applied torque about each axis of the spacecraft frame due to u as given by the product $B_{\mathrm{sc}} u$. The vector τ_d represents disturbance torques, that is, all internal and external torques applied to the spacecraft aside from control torques. These disturbances may be due to onboard components, gravity gradients, solar pressure, atmospheric drag, or the ambient magnetic field. For convenience in (4.3), (4.4) we omit the argument t, recognizing that ω, R, u, and τ_{rmdist} are time-varying quantities.

4.1.1 Attitude and Angular Velocity Error

Let the attitude and angular velocity errors be given by

$$\tilde{R} = R_{\mathrm{d}}^{\mathrm{T}} R, \quad \tilde{\omega} = \omega - \tilde{R}^{\mathrm{T}} \omega_{\mathrm{d}} \tag{4.5}$$

where $R_{\mathrm{d}}, \omega_{\mathrm{d}}$ are the desired attitude and angular velocity, respectively. Using (4.5) to rewrite (4.3) and (4.4) yields

$$J\dot{\tilde{\omega}} = [J(\tilde{\omega} + \tilde{R}^{\mathrm{T}}\omega_{\mathrm{d}})] \times (\tilde{\omega} + \tilde{R}^{\mathrm{T}}\omega_{\mathrm{d}}) + J(\tilde{\omega} \times \tilde{R}^{\mathrm{T}}\omega_{\mathrm{d}} - \tilde{R}^{\mathrm{T}}\dot{\omega}_{\mathrm{d}}) + B_{\mathrm{sc}}u + \tau_d, \tag{4.6}$$

$$\dot{\tilde{R}} = \tilde{R}\tilde{\omega}^{\times}. \tag{4.7}$$

4.2 Markov Parameters for Angular Velocity Control

For the linear, discrete-time plant

$$x(k) = Ax(k-1) + Bu(k-1), \quad z(k) = Cx(k) - r(k)$$

the Markov parameters are given by

$$H = CA^{i-1}B \tag{4.8}$$

for all $i \geq 1$. However, the angular velocity and attitude control problems are governed by nonlinear, continuous-time equations. Thus, for angular velocity control we linearize and discretize (4.6) to obtain the required Markov parameters to use in RCAC.

For the angular velocity control problem the attitude error is ignored. Let $\tilde{R} = I_3$, then the performance variable becomes

$$z = \omega - \omega_d. \tag{4.9}$$

Next, we linearize Euler's equation in (4.6) about a desired equilibrium $\tilde{\omega}_e$, which yields the Jacobian

$$A_c(\tilde{\omega}_e, \omega_d) = \frac{\partial \dot{\tilde{\omega}}}{\partial \tilde{\omega}} = J^{-1}\left[-\left(\tilde{\omega}_e + \omega_d\right)^{\times} J + \left[J\left(\tilde{\omega}_e + \omega_d\right)\right]^{\times}\right] - \omega_d^{\times}, \tag{4.10}$$

Similarly, the input matrix for the linearized system is given by

$$B_c = \frac{\partial \dot{\omega}}{\partial u} = J^{-1} B_{SC}. \tag{4.11}$$

For the angular velocity control problem the output matrices are given by $C = I$ and $D = 0$.

We obtain the discrete-time dynamics matrix from

$$A = e^{A_c h}, \tag{4.12}$$

where A_c is given by (4.10) and h is the controller time step. The discrete-time input matrix is given by

$$B = \int_0^h e^{A\tau} B_c d\tau. \tag{4.13}$$

Using (4.13) in (4.8) yields the first Markov parameter

$$H_1 = CB. \tag{4.14}$$

4.3 Numerical Examples for Angular Velocity Control

Consider a rigid spacecraft with the inertia matrix

$$J = \begin{bmatrix} 5 & -0.1 & -0.5 \\ -0.1 & 2 & 1 \\ -0.5 & 1 & 3.5 \end{bmatrix} \text{ kg-m}^2 \tag{4.15}$$

and let the spacecraft be fully actuated such that $B_{SC} = I_3$. Furthermore, let all disturbances be zero. The RCAC parameters used are shown in Table 4.2.

The Markov parameter H_1 is computed using the Jacobian (4.10) evaluated at $\tilde{\omega}_e = 0$ and ω_{d} which depends on the type of maneuver.

We consider angular velocity control for both detumbling (M2R-R) and spin (M2S-R) maneuvers. For each maneuver we examine robustness to unknown changes in the inertia by using modified Markov parameters.

Parameter	Value
n_c	3
P_0	$100I$
R	I
s	1
k_s	1
θ_0	0
$\lambda(k)$	1
h	0.1
k_{on}	54

Table 4.1: RCAC Parameters for Thruster Control.

4.3.1 M2R-R Maneuvers

Let the initial motion of the spacecraft be described by

$$\omega(0) = \frac{0.1}{\sqrt{3}} \begin{bmatrix} 1 & -1 & 1 \end{bmatrix}^{\mathrm{T}} \text{ rad/sec.} \tag{4.16}$$

The goal of the controller is to bring the spacecraft to rest, that is,

$$\omega_d = \begin{bmatrix} 0 & 0 & 0 \end{bmatrix}^{\mathrm{T}} \text{ rad/sec.} \tag{4.17}$$

Given the output matrix $E_1 = I$, the discrete-time dynamics matrix in (4.12) evaluated at $\tilde{\omega}_e = 0$ and $\omega_d = 0$ so that $A_c = 0$, and the input matrix in (4.13), the Markov parameter in (4.14) is given by

$$H_1 = B = hJ^{-1}B_{SC}. \tag{4.18}$$

Figure 4.1 shows the closed-loop performance for this maneuver. The angular velocity about each axis is shown in Figure 4.1a and the controller coefficients $\theta(k)$ are shown in Figure 4.1b.

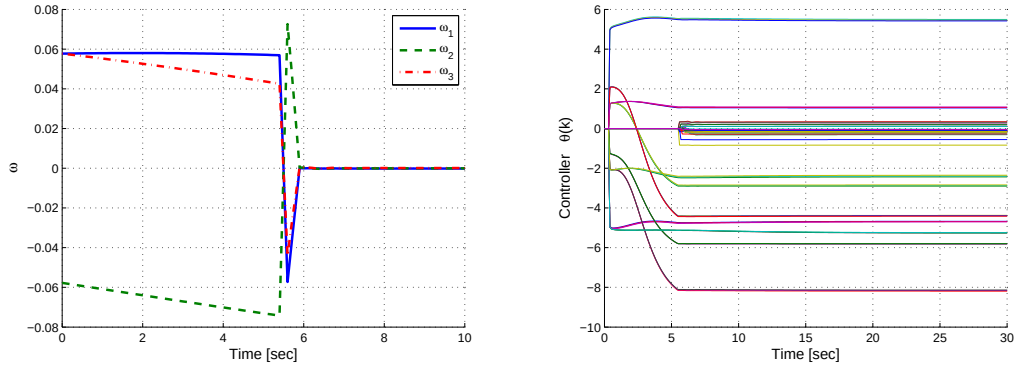

(a) angular velocity $[\mathrm{rad/sec}]$ (b) Controller Coefficients

Figure 4.1: RCAC closed-loop performance for M2R-R using the Markov parameter H_1 in (4.18).

4.3.2 Effect of the Markov Parameters on Convergence

The Markov parameter in (4.18) shows that, for M2R-R, we utilize three pieces of information: the mass distribution, the actuator alignments, and the controller time step. We wish to limit the information used by constructing an arbitrary Markov parameter. We define a matrix $\hat{H}_1$ to use in place of the Markov parameter H_1. Then, since that the time step h is a scaling parameter, we can replace it with a positive scalar α and tune the controller. Thus, we begin with

$$\hat{H}_1 = \alpha J^{-1} B_{SC}, \tag{4.19}$$

where α is a positive number. We test this choice of $\hat{H}_1$ by varying the parameter α.

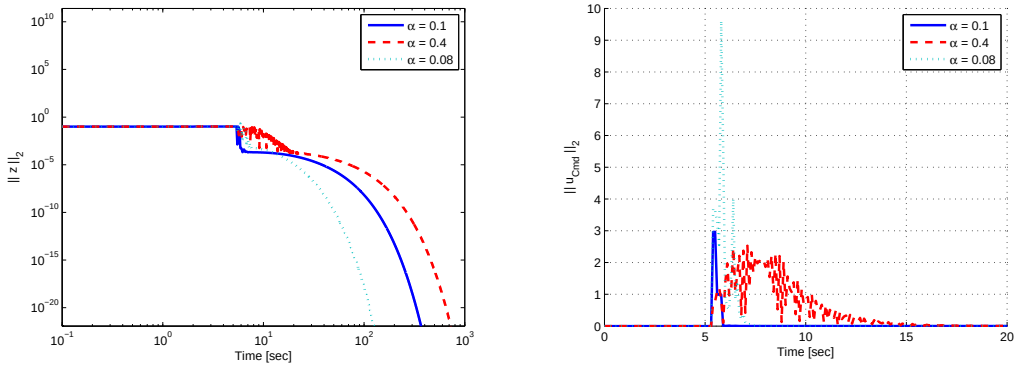

(a) Log Plot of Euclidean Norm of Performance (b) Euclidean Norm of Control Input

Figure 4.2: Comparison of performance variable and commanded control input for RCAC for the M2R-R maneuver using various values of α in the Markov parameter $\hat{H}_1$ in (4.19).

Figure 4.2 shows the results of this analysis. Note that, as α increases, the controller

applies less torque to the spacecraft, whereas as α decreases, more torque is applied. However, as we move away from the nominal value of $\alpha = h$ the controller diverges. Figure 4.3 shows how values of α that are both larger and smaller than the nominal value cause the controller coefficients θ to diverge. Thus, the control inputs also diverge. Note that the smaller value of α in Figures 4.3b and 4.3d is close to the working value of $\alpha = 0.08$ in Figure 4.2 which suggests that RCAC is sensitive to scaling of H_1.

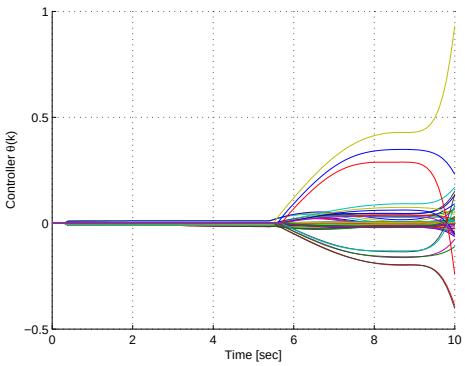

(a) Controller Coefficients for $\alpha = 50$

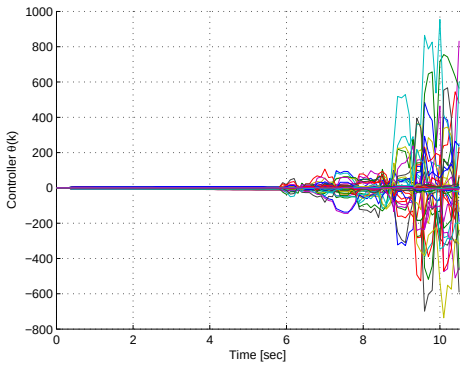

(b) Controller Coefficients for $\alpha = 0.074$

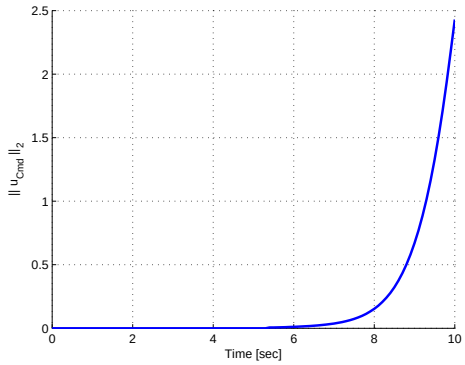

(c) Euclidean Norm of Control Input for $\alpha = 50$

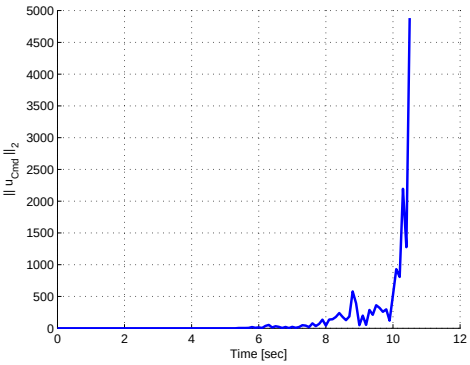

(d) Euclidean Norm of Control Input for $\alpha = 0.074$

Figure 4.3: Controller divergence for off-nominal values of $\alpha = 50$ and $\alpha = 0.074$ for M2R-R using Markov parameter $\hat{H}_1$ in (4.19).

To overcome this problem we introduce a proportional saturation in the control input

by scaling the control vector as

$$u_{\text{sat}} = \begin{cases} u, & u \in \mathcal{B}, \\ \\ \eta u, & u \notin \mathcal{B}, \end{cases} \tag{4.20}$$

where $\mathcal{B}$ is a boundary defined by the saturation limits and η is the maximum scaling possible such that $u_{sat} \in \mathcal{B}$, that is,

$$\eta = \max_{\eta \in (0,1]} \{\eta : \eta u \in \mathcal{B}\}. \tag{4.21}$$

Figure 4.4 shows that this method enables RCAC to bring the system to rest using significantly off-nominal Markov parameters.

Note that varying α corresponds to changing the scale of the inertia, the actuator matrix, or both. Define a scaled inertia $J' = \beta_J J$ and a scaled actuator matrix $B'_{SC} = \beta_B B_{SC}$, where β_J and β_B are positive numbers. Then, we can set $\alpha = \frac{\beta_B}{\beta_J}$ and obtain

$$\hat{H}_1 = J'^{-1} B'_{SC} = \frac{\beta_B}{\beta_J} J^{-1} B_{SC} = \alpha J^{-1} B_{SC}.$$

Thus, if RCAC is robust to changes in α, it is robust to scaling of the inertia and the actuator matrices. Therefore, saturation increases the robustness of RCAC to scaling errors in the inertia J and the actuator matrix B_{SC} for M2R-R maneuvers. Furthermore, for a given saturation level, α can also be used as a tuning parameter for control authority.

With the saturation method added to the controller, we eliminate the inertia information used in $\hat{H}_1$ by removing J from (4.19) and obtain

$$\hat{H}_1 = \alpha B_{SC}. \tag{4.22}$$

Removing the inertia from $\hat{H}_1$ hides information about the spacecraft axes coupling from RCAC. Figure 4.5 shows that RCAC completes the M2R-R maneuver considered in Figure 4.1 for various values of α. Notice that, as expected, decreasing α increases the control input.

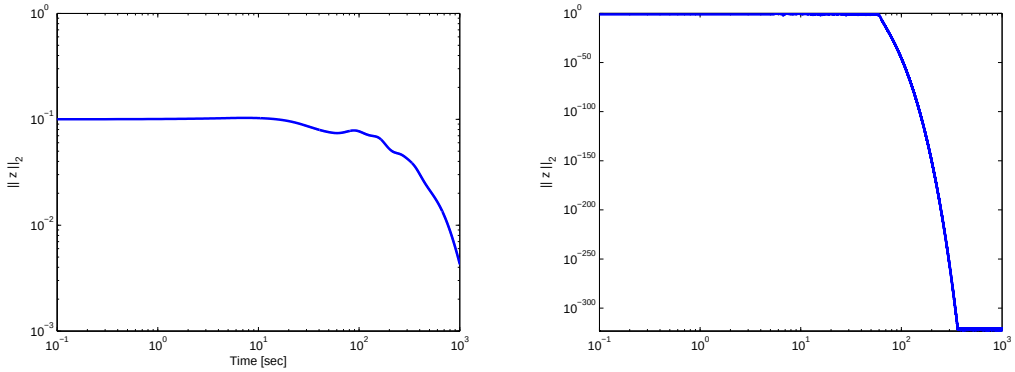

(a) $\alpha = 1000$, Saturation 0.001 N-m (b) $\alpha = 0.001$, Saturation 10 N-m

Figure 4.4: Log plots of the Euclidean norm of performance, $\|z\|_2$, for M2R-R for off-nominal values of $\alpha = 1000$ and $\alpha = 0.001$ in the Markov parameter $\hat{H}_1$ in (4.19) with a saturation level of 1 N-m.

4.3.3 M2S-R Maneuvers

To expand on the M2R-R example, we command the spacecraft to spin about an arbitrary body axis and examine the M2S-R problem. The initial angular velocity is described by (4.16), and the controller goal is to make the spacecraft spin at the desired angular velocity of

$$\omega_d = \frac{0.1}{\sqrt{3}} \begin{bmatrix} -1 & 1 & 1 \end{bmatrix}^{\mathrm{T}} \text{ rad/sec.} \tag{4.23}$$

The spacecraft has the inertia matrix in (4.15) with the initial angular velocity in (4.16). The RCAC parameters are chosen as in Table 4.2. Figure 4.6 compares the performance for the maneuver using the Markov parameters in (4.18) and (4.22). For both Markov parameter choices, RCAC completes the maneuver. However, the lack of information increases the settling time for the case using the inertia-free Markov parameter.

4.4 RCAC Parameters for Attitude Control

We extend the results from Section V and include the attitude kinematics. Since RCAC requires a vector performance, the rotation matrix governed by Poisson's equation (4.4), cannot be used directly.

Thus, we formulate the attitude error dynamics by using the vector function of the attitude error matrix presented in [58]. For $i = 1, 2, 3$, let e_i denote the ith column of the 3×3 identity matrix and let $A_{\mathrm{att}} = \mathrm{diag}(a_1, a_2, a_3)$ be a diagonal positive-definite matrix,

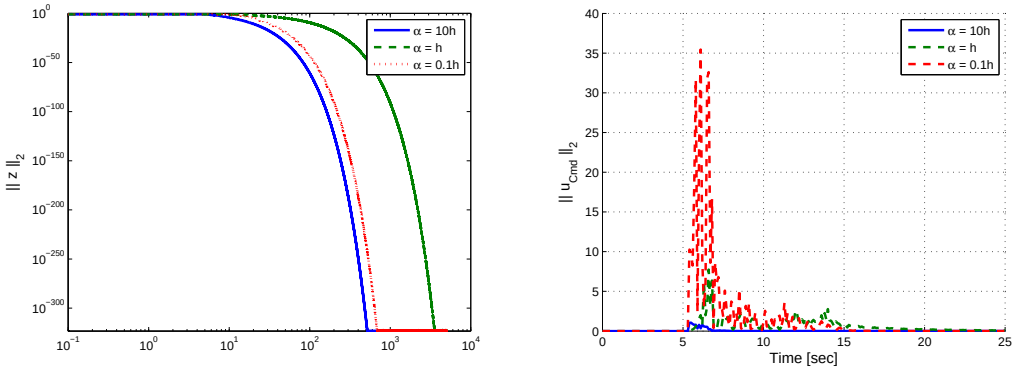

(a) Euclidean Norm of Performance (b) Euclidean Norm of Unsaturated Control Input

Figure 4.5: Inertia-free RCAC performance for various values of α for M2R-R. Euclidean norm of performance, $\|z\|_2$ and unsaturated controller input, $\|u_{\rm cmd}\|$ using the Markov parameter $\hat{H}_1$ in (4.22). The saturation level is set to 1 N-m and $h = 0.1$ sec.

then

$$z_a \triangleq \sum_{1}^{3} a_i \left(\tilde{R}^{\rm T} e_i\right) \times e_i, \tag{4.24}$$

is a 3×1 vector measure of attitude error. Note that $z_a = 0$ when $\tilde{R} = I_3$. Thus, we use z_a as the attitude performance variable. The attitude error affects the rate error given as shown in (5.31). We redefine the angular velocity performance as

$$z_\omega \triangleq \omega - \tilde{R}^{\rm T} \omega_d. \tag{4.25}$$

The combined performance variable for the attitude control problem is given by

$$z = \begin{bmatrix} z_\omega \\ \\ z_a \end{bmatrix}. \tag{4.26}$$

4.4.1 Parameterization of R

The Markov parameters required by RCAC serve as a mapping between the control input and the performance variable. To obtain the Markov parameters, we represent the SO(3) attitude kinematics as vector equations. Thus, we parameterize the SO(3) attitude as a vector composed by the rows of the rotation matrix. Therefore, we express the attitude

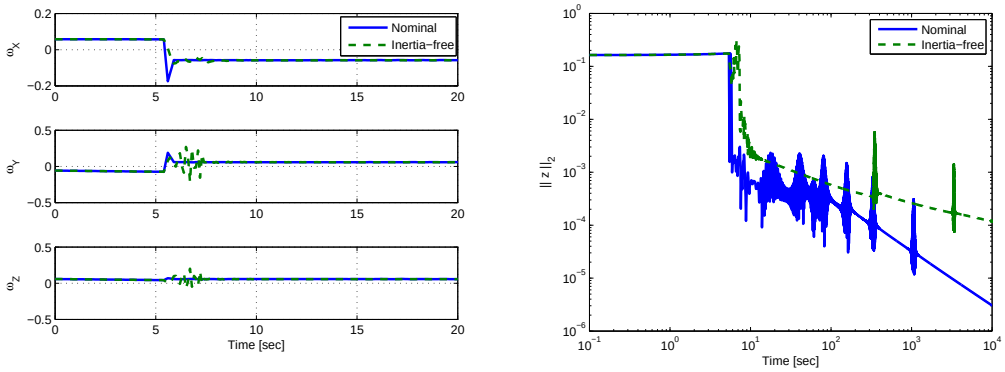

(a) angular velocity $[\mathrm{rad/sec}]$ (b) Log Plot of Euclidean Norm of Performance

Figure 4.6: angular velocity, ω, and Euclidean norm of performance, $\|z\|_2$ for M2S-R. Plots compare convergence for RCAC using Markov parameters derived from the linearized dynamics in (4.18) with RCAC using inertia-free Markov parameters in (4.22) with a saturation level of 10 N-m and $\alpha = 0.1$.

error matrix $\tilde{R}$ as

$$\tilde{R} = \begin{bmatrix} \tilde{r}_1 \\ \tilde{r}_2 \\ \tilde{r}_3 \end{bmatrix}, \tag{4.27}$$

where, for $i = 1, 2, 3$, $\tilde{r}_i \in \mathbb{R}^{1\times 3}$ is a row of $\tilde{R}$. Using (4.27), the new attitude parameter is given by

$$\tilde{r} = \begin{bmatrix} \tilde{r}_1 & \tilde{r}_2 & \tilde{r}_3 \end{bmatrix}^{\mathrm{T}}. \tag{4.28}$$

Expressing the performance variable (4.26) in terms of $\tilde{r}$ yields

$$z_a = \sum_{1}^{3} a_i \left(\tilde{R}^{\mathrm{T}} e_i \right) \times e_i = -M_a R_a \tilde{r}, \tag{4.29}$$

$$z_\omega = \omega - \mathcal{D}(\omega_d)\tilde{r}, \tag{4.30}$$

where

$$M_a = \begin{bmatrix} e_1^\times & e_2^\times & e_3^\times \end{bmatrix} \in \mathbb{R}^{3\times 9}, \tag{4.31}$$

$$R_a = \begin{bmatrix} a_1 I_3 & & \\ & a_2 I_3 & \\ & & a_3 I_3 \end{bmatrix} \in \mathbb{R}^{9\times 9}, \tag{4.32}$$

and, for $x \in \mathbb{R}^3$ with components x_1, x_2, x_3,

$$\mathcal{D}(x) \triangleq \begin{bmatrix} x_1 I_3 & x_2 I_3 & x_3 I_3 \end{bmatrix}. \tag{4.33}$$

4.4.2 Markov parameter

Rewriting (4.6) and (4.7) using $\tilde{r}$ yields

$$\begin{aligned} \dot{\tilde{\omega}} = {} & J^{-1}\left[\left[J\left(\tilde{\omega} + \mathcal{D}(\omega_d) r\right)\right] \times \left(\tilde{\omega} + \mathcal{D}(\omega_d) r\right)\right] + \tilde{\omega} \times \left[\mathcal{D}(\omega_d) r\right] - \mathcal{D}(\dot{\omega}_d) r \\ & + J^{-1}\left(B_{\mathrm{sc}} u + z_d\right), \end{aligned} \tag{4.34}$$

and

$$\dot{\tilde{r}} = \begin{bmatrix} -\tilde{\omega}^\times & & \\ & -\tilde{\omega}^\times & \\ & & -\tilde{\omega}^\times \end{bmatrix} \tilde{r}. \tag{4.35}$$

We compute the discrete-time system matrices A, B, C by linearizing (4.34) and (4.39) about $\tilde{\omega}_e = 0$ and $\tilde{R} = I_3$ followed by discretization with the controller time step h.

To obtain the Jacobian we stack the angular velocity error $\tilde{\omega}$ and the attitude-error parameter $\tilde{r}$ to form a state vector. Next, we differentiate (4.39) and (4.34) with respect to this new state and evaluate it at a given equilibrium $\begin{bmatrix} \tilde{\omega}_e \\ \tilde{r}_e \end{bmatrix}$. For the rotational dynamics in (4.34) the derivative with respect to $\tilde{\omega}$ is given by

$$\frac{\partial \dot{\tilde{\omega}}}{\partial \tilde{\omega}} = J^{-1}\left[-\left(\tilde{\omega}_e + \mathcal{D}(\omega_d)\tilde{r}_e\right)^\times J + \left[J\left(\tilde{\omega}_e + \mathcal{D}(\omega_d)\tilde{r}_e\right)\right]^\times\right] - \left(\mathcal{D}(\omega_d)\tilde{r}_e\right)^\times. \tag{4.36}$$

Similarly, the derivative with respect to $\tilde{r}$ is given by

$$\frac{\partial \dot{\tilde{\omega}}}{\partial \tilde{r}} = J^{-1}\left[-\left(\tilde{\omega}_e + \mathcal{D}(\omega_d)\tilde{r}_e\right)^{\times} J\mathcal{D}(\omega_d) + \left[J\left(\tilde{\omega}_e + \mathcal{D}(\omega_d)\tilde{r}_e\right)\right]^{\times}\mathcal{D}(\omega_d)\right] + \tilde{\omega}_e^{\times}\mathcal{D}(\omega_d) - \mathcal{D}(\dot{\omega}_d). \tag{4.37}$$

Thus, we construct the Jacobian for the angular velocity dynamics

$$A_{\omega} = \begin{bmatrix} \frac{\partial \dot{\tilde{\omega}}}{\partial \tilde{\omega}} & \frac{\partial \dot{\tilde{\omega}}}{\partial \tilde{r}} \end{bmatrix}. \tag{4.38}$$

For the attitude kinematics, we partition (4.39) for each row $\tilde{r}_i$ of $\tilde{R}$ as

$$\dot{\tilde{r}}_i = (\tilde{r}_i \times \tilde{\omega})^{\mathrm{T}}. \tag{4.39}$$

Differentiating with respect to to $\tilde{\omega}$ yields

$$\frac{\partial \dot{\tilde{r}}_i}{\partial \tilde{\omega}} = -\tilde{r}_{e,i}^{\times}, \text{ for } i = 1, 2, 3. \tag{4.40}$$

Differentiating (4.39) with respect to $\tilde{r}_j$ yields

$$\frac{\partial \dot{\tilde{r}}_i}{\partial \tilde{r}_j} = \left[-\tilde{\omega}^{\times}\frac{\partial \tilde{r}_i}{\partial \tilde{r}_j} + \tilde{r}_i^{\times}\frac{\partial \tilde{\omega}}{\partial \tilde{r}_j}\right]^{\mathrm{T}}, \tag{4.41}$$

where

$$\frac{\partial \tilde{r}_i}{\partial \tilde{r}_j} = \begin{cases} I_3, & i = j, \\ 0_{3\times 3}, & i \neq j, \end{cases} \tag{4.42}$$

and

$$\frac{\partial \tilde{\omega}}{\partial \tilde{r}_j} = \begin{cases} \mathcal{D}(\omega_d)\begin{bmatrix} I_3 & 0 & 0 \end{bmatrix}^{\mathrm{T}}, & j = 1, \\ \mathcal{D}(\omega_d)\begin{bmatrix} 0 & I_3 & 0 \end{bmatrix}^{\mathrm{T}}, & j = 2, \\ \mathcal{D}(\omega_d)\begin{bmatrix} 0 & 0 & I_3 \end{bmatrix}^{\mathrm{T}}, & j = 3. \end{cases} \tag{4.43}$$

Finally, we obtain the Jacobian for the attitude kinematics

$$A_a = \begin{bmatrix} \frac{\partial \dot{\tilde{r}}_1}{\partial \tilde{\omega}} & \frac{\partial \dot{\tilde{r}}_2}{\partial \tilde{\omega}} & \frac{\partial \dot{\tilde{r}}_3}{\partial \tilde{\omega}} \\ \frac{\partial \dot{\tilde{r}}_1}{\partial \tilde{r}_1} & \frac{\partial \dot{\tilde{r}}_2}{\partial \tilde{r}_1} & \frac{\partial \dot{\tilde{r}}_3}{\partial \tilde{r}_1} \\ \frac{\partial \dot{\tilde{r}}_1}{\partial \tilde{r}_2} & \frac{\partial \dot{\tilde{r}}_2}{\partial \tilde{r}_2} & \frac{\partial \dot{\tilde{r}}_3}{\partial \tilde{r}_2} \\ \frac{\partial \dot{\tilde{r}}_1}{\partial \tilde{r}_3} & \frac{\partial \dot{\tilde{r}}_2}{\partial \tilde{r}_3} & \frac{\partial \dot{\tilde{r}}_3}{\partial \tilde{r}_3} \end{bmatrix}^{\mathrm{T}}. \tag{4.44}$$

Thus, the dynamics matrix for the linearized continuous-time system is

$$A_{\mathrm{c}}(\tilde{\omega}_e, \tilde{r}_e, \omega_d) = \begin{bmatrix} A_\omega \\ A_a \end{bmatrix}. \tag{4.45}$$

And the continuous time, linear system matrices are given by

$$A_c = \begin{bmatrix} 0_{3\times 3} & 0_{3\times 9} \\ -M_a^{\mathrm{T}} & 0_{9\times 9} \end{bmatrix}, \tag{4.46}$$

$$B_c = \begin{bmatrix} J^{-1}B_{\mathrm{sc}} \\ 0_{9\times 3} \end{bmatrix}, \tag{4.47}$$

$$C = \begin{bmatrix} I_3 & 0_{3\times 9} \\ 0_{3\times 3} & -M_a R_a \end{bmatrix}. \tag{4.48}$$

Discretization of A_c, B_c, with the controller time step h yields

$$A = e^{A_c h} = \begin{bmatrix} I_3 & 0_{3\times 9} \\ -hM_a^{\mathrm{T}} & I_9 \end{bmatrix}, \tag{4.49}$$

$$B = \left(\int_0^h A d\tau \right) B_c = \begin{bmatrix} hJ^{-1}B_{\mathrm{sc}} \\ -\frac{h^2}{2} M_a^{\mathrm{T}} J^{-1} B_{\mathrm{sc}} \end{bmatrix}. \tag{4.50}$$

The Markov parameter corresponding to the performance in (4.26) is given by

$$H_1 = \begin{bmatrix} hJ^{-1}B_{\rm sc} \\ \frac{1}{2}h^2 M_a R_a M_a^{\rm T} J^{-1} B_{\rm sc} \end{bmatrix}. \tag{4.51}$$

4.5 Attitude Control Examples

Let the spacecraft inertia matrix be defined as in (4.15), $B_{SC} = I_3$, and $A_{\rm att} = I$. We use the RCAC parameters in Table 4.2. The Markov parameter is given by the linearized system in Section VI evaluated at $\tilde{R}_e = I_3$ and $\tilde{\omega}_e = 0$, ω_d depends on the maneuver. We examine slew (M2R) and spin (M2S) maneuvers. For each maneuver we examine robustness to changes in the inertia using arbitrary Markov parameters.

4.5.1 M2R Maneuvers

Let the initial motion of the spacecraft be described by (4.16) and the initial attitude be given by

$$R(0) = I_3. \tag{4.52}$$

The goal of the controller is to bring the spacecraft to rest, that is $\omega_d = 0$, with the inertial attitude

$$R_d = \begin{bmatrix} 0.5000 & 0.5000 & 0.7071 \\ 0.5000 & 0.5000 & -0.7071 \\ -0.7071 & 0.7071 & 0.0000 \end{bmatrix}. \tag{4.53}$$

Figure 4.7 shows the closed-loop performance for the M2R maneuver using the Markov parameter H_1 in (4.51). Note that the linear controller coefficients converge smoothly and quickly.

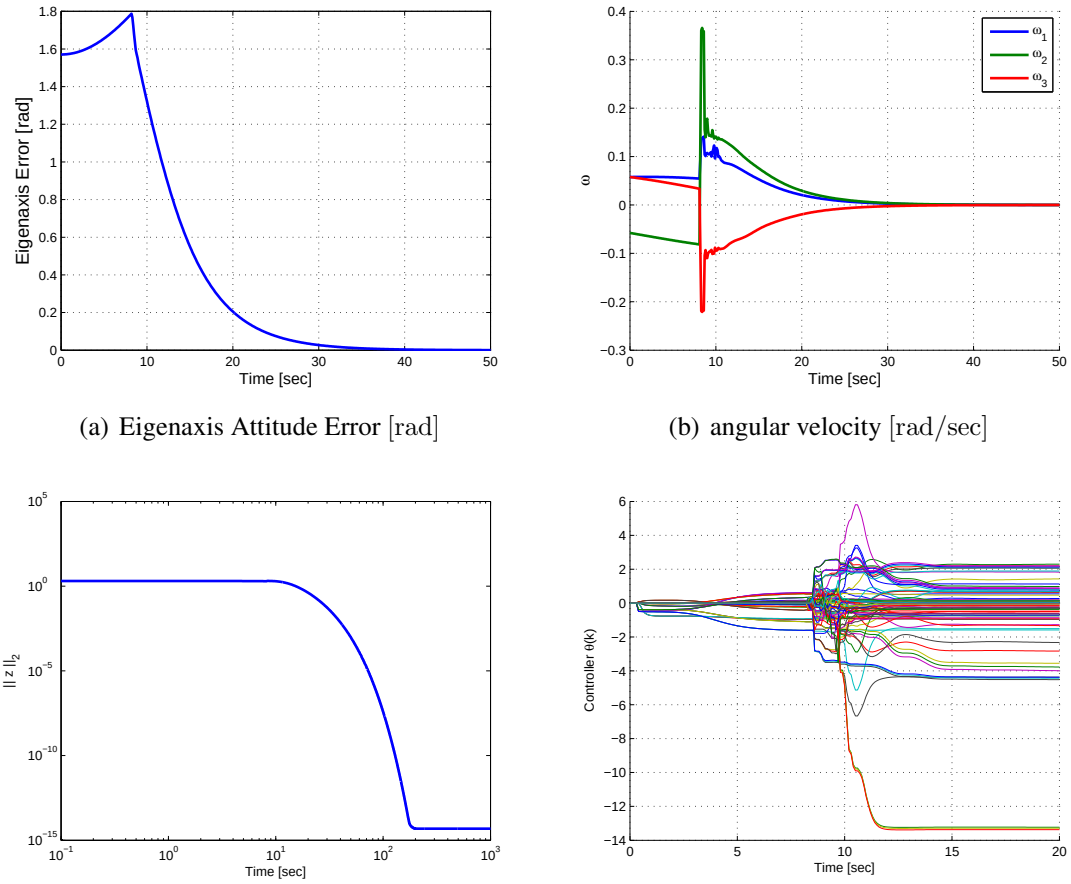

(a) Eigenaxis Attitude Error $[\mathrm{rad}]$

(b) angular velocity $[\mathrm{rad/sec}]$

(c) Euclidean Norm of Performance

(d) Controller Coefficients

Figure 4.7: RCAC performance for M2R using Markov parameter H_1 in (4.51).

4.5.2 Effect of the Markov Parameters on Convergence

We use H_1 in (4.51) to define the arbitrary Markov parameter

$$\hat{H}_1 = \begin{bmatrix} \alpha B_{\mathrm{sc}} \\ \frac{1}{2}\alpha^2 M_a R_a M_a^{\mathrm{T}} B_{\mathrm{sc}} \end{bmatrix} \tag{4.54}$$

where we have removed the inertia matrix and replaced the time step h with a positive scaling parameter α. As in the M2R-R case, off-nominal values of α cause the controller to diverge. Thus, we implement the saturation method in (4.20) to mitigate this problem.

Figure 4.8 shows the controller's performance using various values of α. Note that, unlike the M2R-R case, saturation does not provide robustness to changes of α outside of the nominal value $\alpha = h$, especially for values greater than 1. This is due to the nonlinear

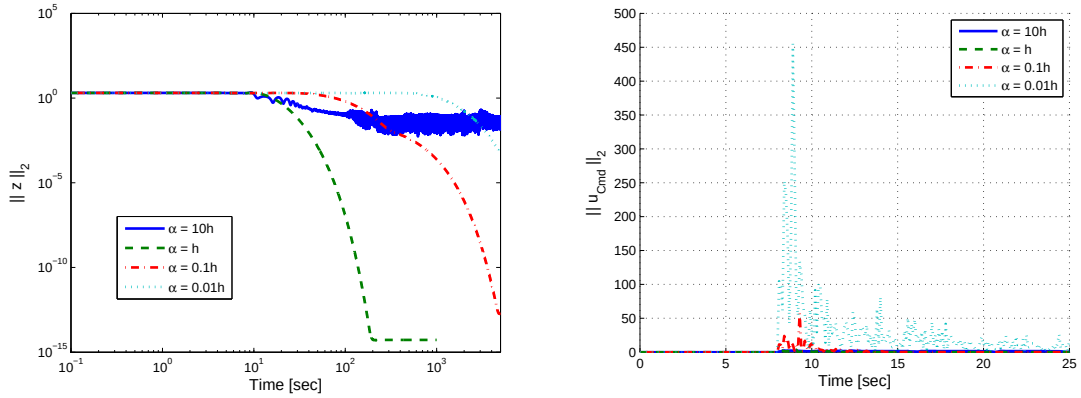

(a) Euclidean Norm of Performance

(b) Euclidean Norm of Unsaturated Control Input

Figure 4.8: Inertia-free RCAC performance for M2R using Markov parameter $\hat{H}_1$ in (4.54) with $h = 0.1$ sec and a saturation level of 1 N-m.

term, α^2 in the lower portion of the matrix $\hat{H}_1$ in (4.54). When $\alpha \neq h$ the ratios between the entries in the top and bottom halves of the matrix $\hat{H}_1$ change from their nominal values, thus affecting the internal structure of the Markov parameter. Thus, we redefine the Markov parameter as

$$\hat{H}_1' = \alpha \begin{bmatrix} hB_{\rm sc} \\ \frac{1}{2}h^2 M_a R_a M_a^{\rm T} B_{\rm sc} \end{bmatrix}. \tag{4.55}$$

This scaling maintains the matrix element ratios at their nominal values.

The M2R maneuver in Figure 4.9 examines the effect of the Markov parameter $\hat{H}_1'$ given by (4.55). The trajectory for $\alpha = 1$ corresponds to the unscaled inertia-free Markov parameter. As shown by the performance variable plot in Figure 4.9a, RCAC is robust to changes in the inertia and to scaling of the input matrix $B_{\rm sc}$. As expected, decreasing α increases the commanded control input.

4.5.3 M2R Robustness Studies

Consider the M2R maneuver given by an eigenaxis rotation of 40 deg about the body fixed direction $\begin{bmatrix} 1 & 1 & 1 \end{bmatrix}^{\rm T}$. Let the spacecraft be initially at $R(0) = I_3$. Assume there are no disturbances.

The RCAC parameters used are shown in Table 4.2. For the M2R problem, we utilize the inertia-free Markov parameter $\hat{H}_1'$ in (4.55)

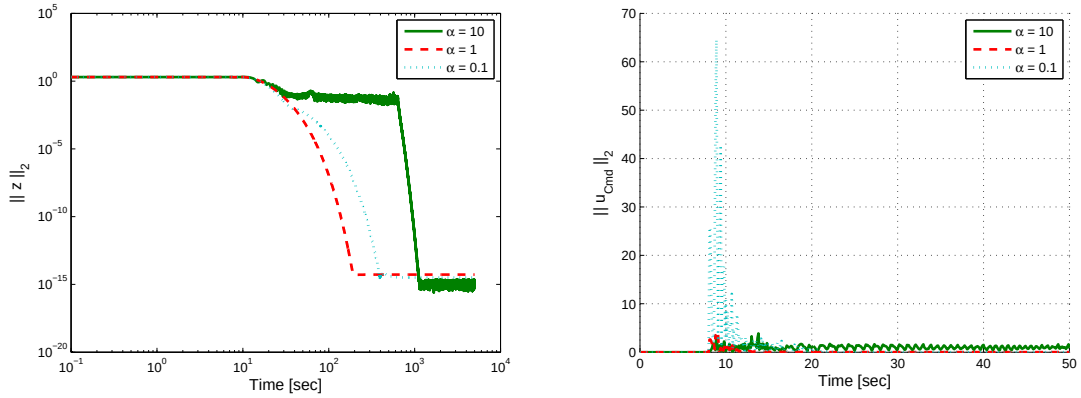

(a) Euclidean Norm of Performance

(b) Euclidean Norm of Unsaturated Control Input

Figure 4.9: Inertia-free RCAC performance for M2R using the inertia-free Markov parameter $\hat{H}_1'$ in (4.55) with $h = 0.1$ sec. The controller is robust to scaling of H_1.

4.5.3.1 Robustness to Changes in the Inertia Matrix

We use two approaches to examine the effect of unmodeled inertia variations on the M2R settling time. Let the centroid inertia matrix be given by $J_3 = \text{diag}\ (10, 8.33, 5)$. Then we set the spacecraft inertia to be a value between J_3 and other inertias according to

$$J = (1 - \alpha)J_3 + \alpha J_i, \text{ for} \tag{4.56}$$

where, for $i = 1, 2, 4, 5$, J_i is given by

$$J_1 = 10I_3, \quad J_2 = \text{diag}\ (10, 10, 5) \quad J_4 = \text{diag}(10, 5, 5) \quad J_5 = \text{diag}(10, 10, 0.1),$$

J_1 represents a sphere, J_2 is a cylinder, J_4 is a thin disk and J_5 is a thin cylinder.

Figures 4.10 and 4.11 show how the settling time changes as a function of α. Each point on the curves represents a different spacecraft inertia. Note that RCAC is using the same model for all simulations, that is the inertia used in the Markov parameter is given by $\hat{J} = I_3$. Thus, Figures 4.10 and 4.11 demonstrate RCAC's robustness to unmodeled inertia variations when using thrusters to achieve M2R maneuvers.

Parameter	Description	Value
n_c	Controller order	3
P_0	Initial error covariance used in the RLS update	$100I$
R	Performance weighting to compute the retrospective cost function	I
s	Number of data points used for retrospective cost computation	1
k_s	Delay used to construct the extended performance vector	1
θ_0	Initial controller coefficients	0
$\lambda(k)$	Forgetting factor	1
h	Controller time step	0.1
k_{on}	Number of time steps to wait before applying first control action	81
A_{att}	Weighting on the attitude error matrix $\tilde{R}$ used in z_a	I_3

Table 4.2: RCAC Parameters.

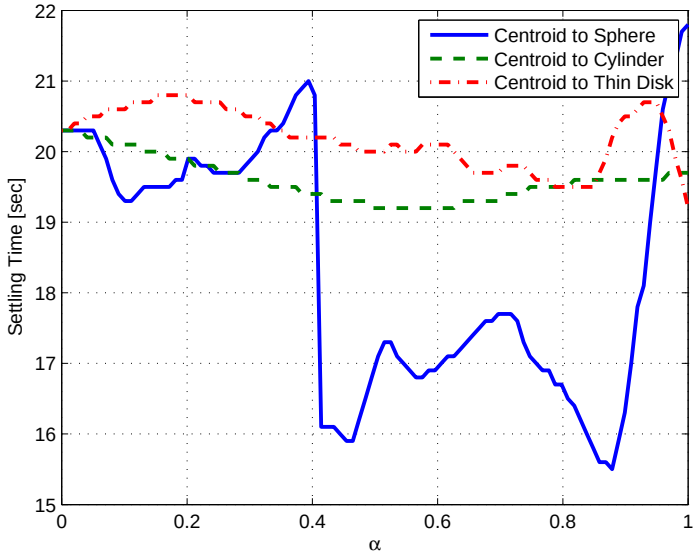

Figure 4.10: M2R settling time for RCAC using thrusters. The inertia J starts at the centroid value J_3 and moves toward the sphere J_1, cylinder J_2, and thin disk J_4 inertias according to (4.56). The saturation level is set at 1 N-m.

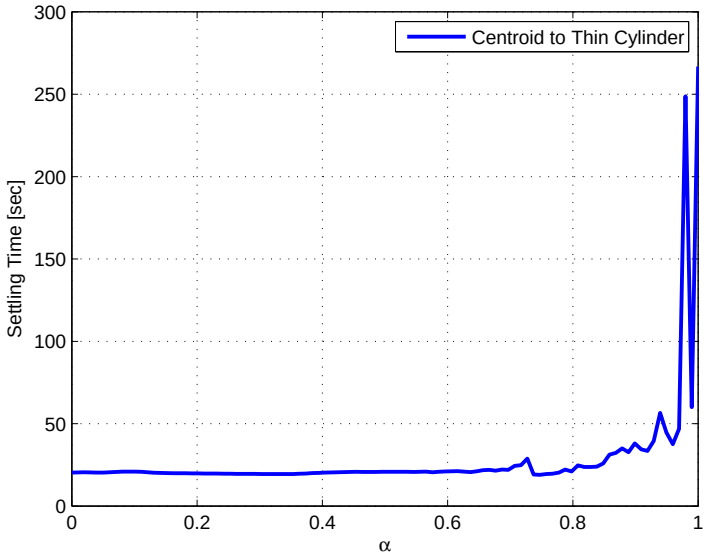

Figure 4.11: M2R settling time for RCAC using thrusters. The inertia J starts at the centroid value J_3 and moves toward the thin cylinder inertia J_5 according to (4.56). The saturation level is set at 1 N-m.

Next, we examine the M2R settling time as the actuator and sensor axes are rotated away from the principal axes according to

$$J = R_i(\phi) J_3 R_i(\phi)^{\mathrm{T}}. \tag{4.57}$$

Where $R_i(\phi) \in \mathbb{R}^{3\times 3}$ for $i = 1, 2, 3$ is the rotation matrix given by

$$\mathcal{R}(\phi, e_i) = \cos(\phi) I_3 + (1 - \cos(\phi)) e_i e_i^{\mathrm{T}} + \sin(\theta) e_i^{\times}, \tag{4.58}$$

where ϕ is the misalignment angle and e_i is the ith column of the 3×3 identity matrix. Figure 4.12 shows that RCAC can handle the coupling effects introduced by the off diagonal entries that appear in (4.57) as ϕ moves away from zero.

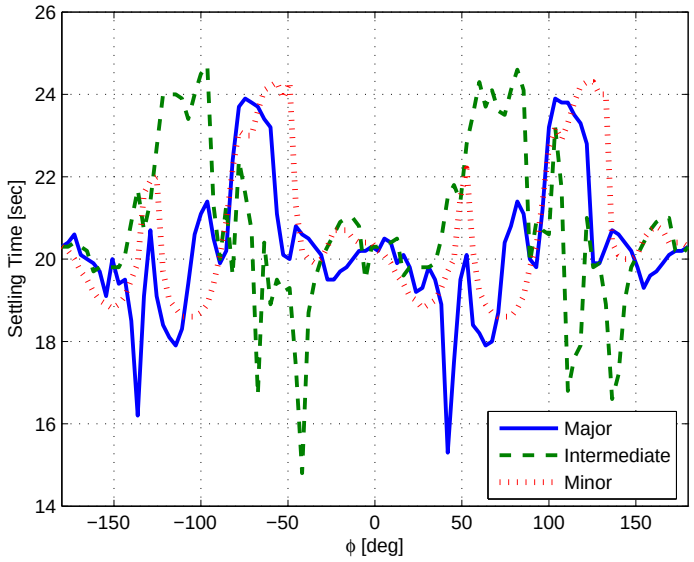

Figure 4.12: M2R settling time for RCAC using thrusters. The inertia J starts at the centroid value J_3 and is rotated about each principal axis by ϕ. The saturation level is set at 1 N-m on each axis.

4.5.3.2 Actuator Misalignment

We examine the robustness of RCAC for the M2R maneuver to actuator misalignment. We misalign each actuator in different directions by varying angles. For a spacecraft with three actuators, the input matrix is given by

$$B_{\mathrm{sc}} = \begin{bmatrix} R_1 e_1 & R_2 e_2 & R_3 e_3 \end{bmatrix}. \tag{4.59}$$

Each $R_i \in \mathbb{R}^{3\times 3}$ for $i = 1, 2, 3$ in (4.59) is a rotation matrix given by Rodrigues' equation

$$\mathcal{R}(\theta_B, n_B) = \cos(\theta_B) I_3 + (1 - \cos(\theta_B)) n_B n_B^{\mathrm{T}} + \sin(\theta_B) n_B^{\times}, \tag{4.60}$$

where θ_B is the misalignment angle and $n_B \in \mathbb{R}^3$ is a unit vector which corresponds to the misalignment axis.

The initial conditions and RCAC parameters used are given in Section VII. First, we test a misalignment of $\theta_B = 30$ deg on each actuator with different misalignment axes so that the rotation matrices in (4.59) are

$$R_1 = \mathcal{R}(\theta_B, e_3), \tag{4.61}$$

$$R_2 = \mathcal{R}(\theta_B, e_1), \tag{4.62}$$

$$R_3 = \mathcal{R}(\theta_B, e_2). \tag{4.63}$$

where e_i for $i = 1, 2, 3$ is the ith column of I_3. Figure 4.13 compares the closed-loop performance using RCAC with full inertia and actuator knowledge given by the Markov parameter H_1 in (4.51) with RCAC using the inertia and misalignment-free Markov parameter $\hat{H}_1'$ in (4.55).

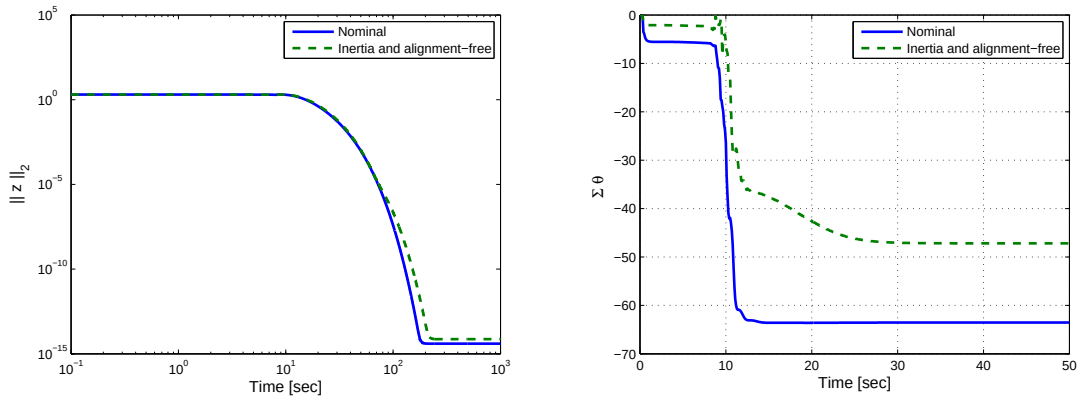

(a) Euclidean Norm of Performance

(b) Sum of Controller Coefficients

Figure 4.13: Comparison of RCAC performance for M2R with $\theta_B = 30$ deg. Plots compare RCAC using Markov parameter H_1 in (4.51) without saturation versus RCAC using the inertia and alignment-free Markov parameter $\hat{H}_1$ in (4.54) with $\alpha = 1$, $h = 0.1$ sec, and a saturation limit of 1 N-m.

RCAC can complete the M2R maneuver without using knowledge of the misalignments in the actuator matrix B_{SC}. As shown in Figure 4.13b the lack of alignment information results in a longer settling time. To evaluate robustness, we test RCAC with larger misalignment angles.

Figure 4.14 shows the closed-loop performance when using the Markov parameter $\hat{H}_1$ in (4.54) for different misalignment angles. We increase the misalignment angle until the controller fails to complete the M2R maneuver. As shown in Figure 4.15, for angles greater than 60 deg or less than -40 deg, the controller coefficients converge but the system settles into a limit cycle.

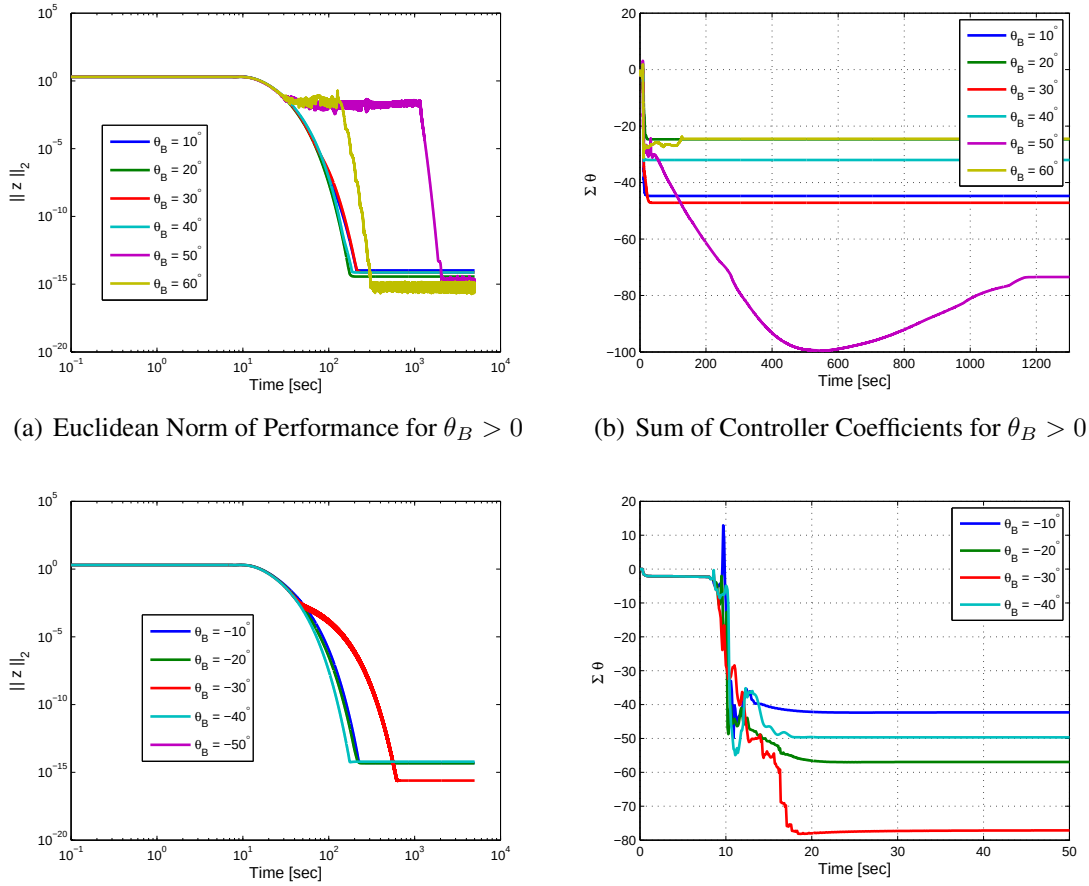

(a) Euclidean Norm of Performance for $\theta_B > 0$

(b) Sum of Controller Coefficients for $\theta_B > 0$

(c) Euclidean Norm of Performance for $\theta_B < 0$

(d) Sum of Controller Coefficients for $\theta_B < 0$

Figure 4.14: Comparison of RCAC performance for M2R for various misalignment angles θ_B. Plots compare the closed-loop performance using the inertia and alignment-free Markov parameter $\hat{H}_1$ in (4.54) with $\alpha = 1$, $h = 0.1$ sec, and a saturation limit of 1 N-m.

4.5.3.3 Saturation Level

We examine the M2R settling time for RCAC under varying levels of saturation. We define the boundary $\mathcal{B}$ in (4.20) by setting saturation limits for each axis

$$u_{\text{lim}} = u_{\text{max}} \begin{bmatrix} 1 & 1 & 1 \end{bmatrix}^{\text{T}} \text{N-m.} \tag{4.64}$$

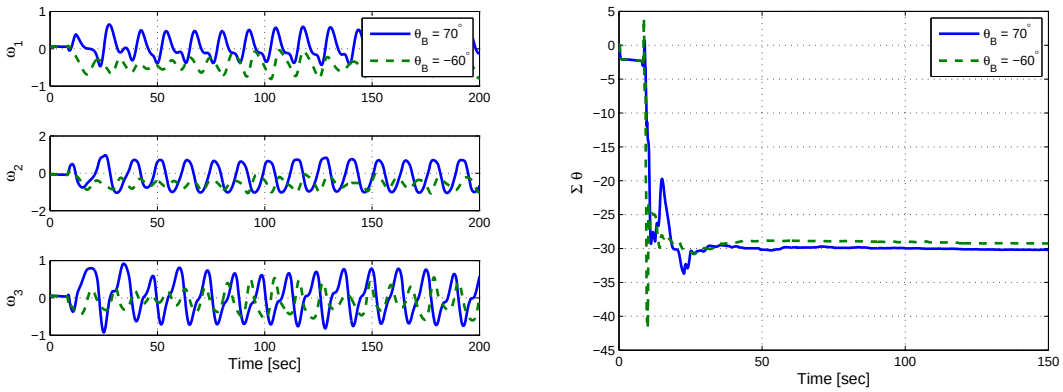

(a) Angular Velocity

(b) Sum of Controller Coefficients

Figure 4.15: RCAC performance for M2R for misalignment angles $\theta_B = 70$ deg and $\theta_B = -60$ deg using the inertia and alignment-free Markov parameter $\hat{H}_1$ in (4.54) with $\alpha = 1$ and a saturation limit of 1 N-m. Although the controller coefficients converge, the system enters a limit cycle as shown by the angular velocity plot.

We let $J = J_3$ and vary $u_{\max}$. Figure 4.16 shows the settling time as a function of saturation level.

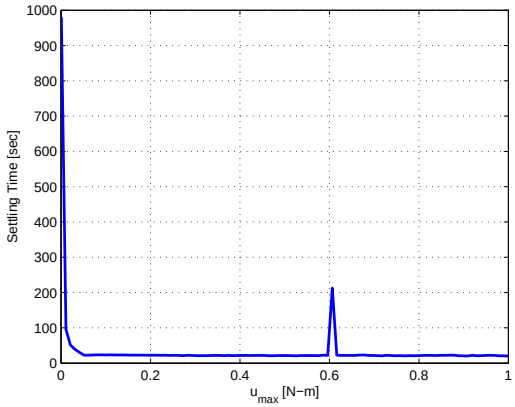

Figure 4.16: M2R settling time as a function of saturation level $u_{\max}$.

4.5.3.4 On-Off Thrusters

We introduce an input nonlinearity in the form of on-off thrusters. The control torque applied to the spacecraft is given by

$$u = \text{sign}(u_{\text{cmd}})u_{\text{on}} \tag{4.65}$$

where u_{on} is a positive scalar and u_{cmd} is the commanded torque computed using RCAC. We examine the effect of the on-off nonlinearity on the M2R settling time. We let $J = J_3$ and vary the thruster torque u_{on}. Figure 4.17 shows that as u_{on} increases the spacecraft takes more time to complete the maneuver.

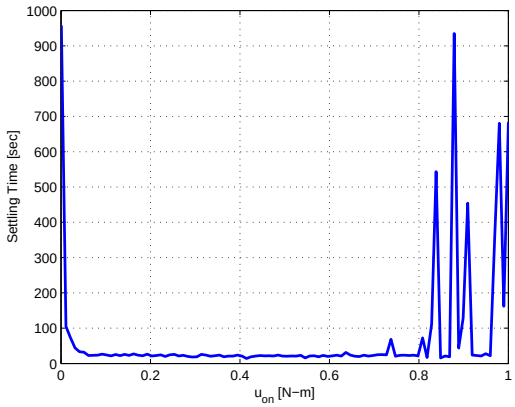

Figure 4.17: M2R settling time for RCAC using on-off thrusters as a function of the thrust level u_{on}.

4.5.3.5 Constant Disturbance

We examine the effect of disturbances on the M2R settling time. We let $J = J_3$ and consider a constant unknown disturbance τ_{dist} about each principal axis of the form

$$\tau_{\text{dist}} = \beta e_i, \tag{4.66}$$

where e_i is the ith column of the 3×3 identity matrix. We vary the disturbance level β and examine its effect on M2R settling time. Figure 4.18 shows the settling time as a function of the disturbance level β.

4.5.4 M2S Maneuvers

To expand the M2R example we command the spacecraft to spin about a specified body axis aligned with a specific inertial attitude. Let the initial state of the spacecraft be as in the examples in the previous section, set the controller parameters as in Table 4.2, and let the desired angular velocity ω_d be as described in (4.23). Since the commanded angular velocity is non-zero the desired attitude evolves over time according to

$$\dot{R}_{\text{d}} = R_{\text{d}} \omega_{\text{d}}^{\times}. \tag{4.67}$$

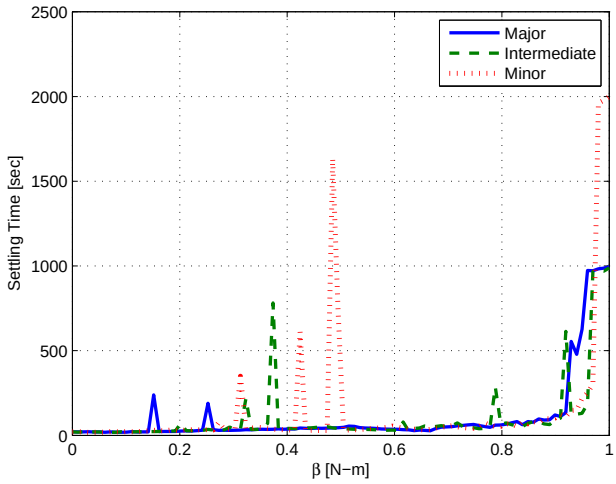

Figure 4.18: M2R closed-loop performance for RCAC using thrusters. Settling time as a function of the constant disturbance magnitude β about each principal axis. The number of previous time steps in the retrospective cost is set to $s = 1$. The saturation level is set at 1 N-m, which is sufficient to reject the disturbance for all $\beta \in [0, 1]$.

Figure 4.19 compares the performance of RCAC using the nominal Markov parameter in (4.51) with RCAC using the inertia-free Markov parameter (4.55) with saturation for the M2S maneuver.

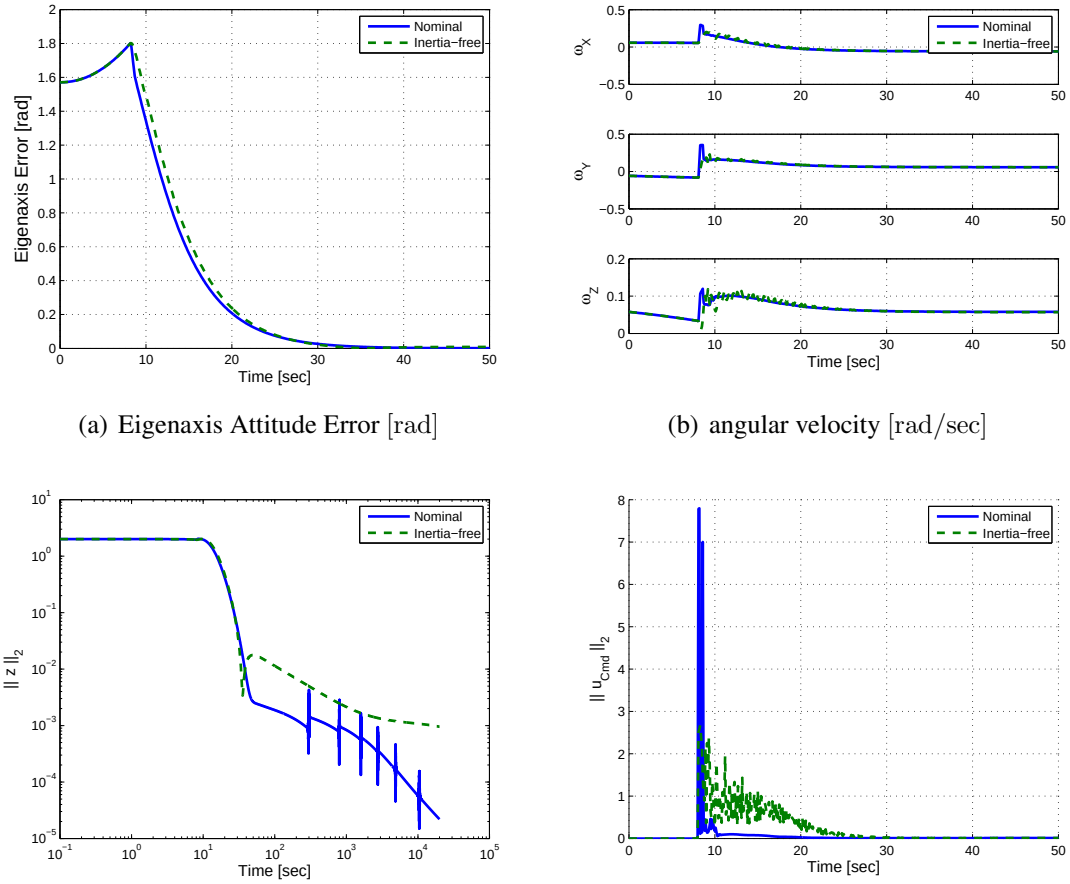

(a) Eigenaxis Attitude Error $[\mathrm{rad}]$

(b) angular velocity $[\mathrm{rad/sec}]$

(c) Euclidean Norm of Performance

(d) Euclidean Norm of Unsaturated Control Input

Figure 4.19: Comparison of RCAC performance for M2S. Plots compare RCAC using Markov parameter H_1 in (4.51) without saturation versus RCAC using the inertia-free Markov parameter $\hat{H}_1'$ in (4.55) with $\alpha = 1$, $h = 0.1$ sec, and a saturation limit of 1 N-m.

4.6 Conclusions

RCAC algorithm is able to control spacecraft angular velocity and attitude using Markov parameters derived from the linearized Euler and Poisson equations. Numerical simulations indicate that the inertia information can be removed from the Markov parameter to obtain inertia-free attitude control. We noticed an increased settling time for both M2R-R and M2R maneuvers when the controller time step was unknown.

We demonstrated robustness to scaling errors in the inertia and actuator models, if the inertia model is smaller The results for inertia scaling showed increase control input when the inertia was underestimated. When the modeling errors are on similar orders of magnitude the impact on the settling time is small, on the order of 5 seconds difference from nominal. Furthermore, incorrect modeling of the off-diagonal entries did not had a similarly small effect on settling time.

These results sugggest that RCAC can be used as an inertia-free angular velocity and attitude controller for detumbling (M2R-R), slews (M2R), and spinning maneuvers (M2S-R and M2S) as long as the order of magnitude of the spacecraft inertia is known.

Robustness to actuator misalignments was also examined. Simulation results indicate that RCAC is robust to thruster misalignments of up to 50 deg in all directions. Larger misalignment errors result in RCAC entering a limit cycle due to the incorrect input-output information provided by the Markov parameter.

The results for robustness to unmodeled but known saturation indicate that RCAC can perform well regardless of the saturation level. Similarly unmodled on-off behavior is only a problem with thrust resolutions higher then 0.5N-m.

Finally the results for unmodeled disturbances indicate that RCAC can reject a disturbance constant in the body frame as long as the available torque is greater than the disturbance magnitude. However, larger disturbance torques increase the settling time.

In summary, RCAC is a suitable method for attitude control using thrusters. Furthermore, the controller provides robustness to many common spacecraft design problems such as mass property modeling error. Inaccurate alignment information on-off thruster behavior and unmodeled disturbances.

CHAPTER 5

Reaction Wheels

We extend the thruster control approach in [70] by utilizing reaction wheels with momentum-storage capabilities as actuators. The momentum stored in the wheels introduces additional nonlinearities in Euler's equation as shown in [59]. These nonlinearities present an additional challenge for the linear compensator produced by RCAC. The goal of this work is to control the spacecraft without knowledge of the spacecraft or reaction-wheel inertias. Specifically, we evaluate the closed-loop performance for motion-to-rest (M2R) maneuvers. For these maneuvers the spacecraft has an arbitrary initial attitude and angular-velocity, and the objective is to bring the spacecraft to rest at a specified inertial attitude. We examine the relation between the spacecraft inertia, the reaction-wheel inertia, and the closed-loop settling time. Furthermore, we investigate the effect of inertially constant disturbance torques as well as noise and bias on the angular-velocity measurement.

First, we show that RCAC can complete the M2R maneuver using full information of the mass properties of the spacecraft. Then, we remove the spacecraft and reaction-wheel inertia information from the controller and examine the closed-loop settling time for off-nominal spacecraft inertias. Thus, the controller uses limited knowledge of the system. Finally, the algorithm is tested in the presence of disturbances, unknown actuator misalignment, and noise and bias in the angular-velocity measurement.

5.1 Nonlinear Equations of Motion

We consider a single rigid body controlled by n reaction wheels w_i which provide on-board momentum storage. The translational motion of the spacecraft's center of mass is not considered. We assume that a body-fixed frame $\mathrm{F_B}$ is defined for the spacecraft, whose origin is chosen to be the center of mass c, and that an inertial frame $\mathrm{F_I}$ is specified for determining the attitude of the spacecraft. Furthermore, for $i = 1, \ldots, n$, where n is the number of reaction wheels, we define a wheel frame $\mathrm{F_{W_i}}$ which is attached to $\mathrm{w_i}$.

Reaction wheels change the attitude of the spacecraft by changing the direction of the total angular momentum in the body frame. Since reaction wheels store angular momentum, (3.5) becomes,

$$\vec{J}_{\mathrm{b/c}} \overset{\mathrm{B}\bullet}{\vec{\omega}}_{\mathrm{B/I}} + \sum_{i=1}^{n} \overset{\mathrm{B}\bullet}{\vec{H}}_{\mathrm{w}_i/\mathrm{c/I}} = -\vec{\omega}_{\mathrm{B/I}} \times \left[\vec{J}_{\mathrm{b/c}} \vec{\omega}_{\mathrm{B/I}}, + \sum_{i=1}^{n} \vec{H}_{\mathrm{w}_i/\mathrm{c/I}} \right] + \vec{M}_{\mathrm{b}}. \tag{5.1}$$

where n is the number of reaction wheels on the spacecraft and the angular momentum $\vec{H}_{\mathrm{w}_i/\mathrm{c/I}}$ of the ith reaction wheel relative to c with respect to $\mathrm{F_I}$, is given by

$$\begin{aligned} \vec{H}_{\mathrm{w}_i/\mathrm{c/I}} &= \vec{J}_{\mathrm{w}_i/\mathrm{c}} \vec{\omega}_{\mathrm{B/I}} + \vec{H}_{\mathrm{w}_i/\mathrm{c/B}} \\ &= \vec{J}_{\mathrm{w}_i/\mathrm{c}} \vec{\omega}_{\mathrm{B/I}} + \vec{H}_{\mathrm{w}_i/\mathrm{c}_i/\mathrm{B}} + \vec{r}_{\mathrm{c/c}_i} \times m_i \vec{v}_{\mathrm{c/c}_i/\mathrm{B}} \\ &= \vec{J}_{\mathrm{w}_i/\mathrm{c}} \vec{\omega}_{\mathrm{B/I}} + \vec{H}_{\mathrm{w}_i/\mathrm{c}_i/\mathrm{B}} \end{aligned} \tag{5.2}$$

where $\vec{J}_{\mathrm{w}_i/\mathrm{c}}$ is the physical inertia matrix of reaction wheel i relative to the spacecraft center of mass, m_i is the mass of the ith reaction wheel, and $\vec{r}_{\mathrm{c/c}_i}$ is the vector from the center of mass of the ith wheel to the center of mass of the spacecraft. The velocity $\vec{v}_{\mathrm{c}_i/\mathrm{c/B}}$ of c_i relative to c with respect to $\mathrm{F_B}$ is zero since the actuators are rigidly attached to the spacecraft bus.

We expand the inertia term $\vec{J}_{\mathrm{w}_i/\mathrm{c}}$ using Lemma 16

$$\vec{J}_{\mathrm{w}_i/\mathrm{c}} = \vec{J}_{\mathrm{w}_i/\mathrm{c}_i} - m_i(\vec{r}^{\times}_{\mathrm{c/c}_i})^2, \tag{5.3}$$

where $\vec{J}_{\mathrm{w}_i/\mathrm{c}_i}$ is the physical inertia matrix of reaction wheel i relative to its center of mass c_i. The angular momentum $\vec{H}_{\mathrm{w}_i/\mathrm{c}_i/\mathrm{B}}$ of reaction wheel i relative to c_i with respect to $\mathrm{F_B}$ is given by

$$\vec{H}_{\mathrm{w}_i/\mathrm{c}_i/\mathrm{B}} = \vec{J}_{\mathrm{w}_i/\mathrm{c}_i} \vec{\omega}_{\mathrm{W}_i/\mathrm{B}}. \tag{5.4}$$

where $\vec{\omega}_{\mathrm{W}_i/\mathrm{B}}$ is the angular velocity of $\mathrm{F}_{\mathrm{W}_i}$ relative to $\mathrm{F_B}$. Therefore, the angular momentum of the w_i relative to c with respect to $\mathrm{F_I}$ is given by

$$\vec{H}_{\mathrm{w}_i/\mathrm{c/I}} = \left[\vec{J}_{\mathrm{w}_i/\mathrm{c}_i} - m_i(\vec{r}^{\times}_{\mathrm{c/c}_i})^2 \right] \vec{\omega}_{\mathrm{B/I}} + \vec{J}_{\mathrm{w}_i/\mathrm{c}_i} \vec{\omega}_{\mathrm{W}_i/\mathrm{B}}, \tag{5.5}$$

By differentiating (5.5) we obtain

$$\begin{aligned}\overset{\mathrm{B}\bullet}{\vec{H}}_{\mathrm{w}_i/\mathrm{c}/\mathrm{I}} = &\left[\overset{\mathrm{B}\bullet}{\vec{J}}_{\mathrm{w}_i/\mathrm{c}_i} - m_i(\vec{v}^{\times}_{\mathrm{c}/\mathrm{c}_i/\mathrm{B}})^2\right]\vec{\omega}_{\mathrm{B}/\mathrm{I}} + \left[\vec{J}_{\mathrm{w}_i/\mathrm{c}_i} - m_i(\vec{r}^{\times}_{\mathrm{c}/\mathrm{c}_i})^2\right]\overset{\mathrm{B}\bullet}{\vec{\omega}}_{\mathrm{B}/\mathrm{I}} \\ &+ \overset{\mathrm{B}\bullet}{\vec{J}}_{\mathrm{w}_i/\mathrm{c}_i}\vec{\omega}_{\mathrm{W}_i/\mathrm{B}} + \vec{J}_{\mathrm{w}_i/\mathrm{c}_i}\overset{\mathrm{B}\bullet}{\vec{\omega}}_{\mathrm{W}_i/\mathrm{B}} \\ = &\overset{\mathrm{B}\bullet}{\vec{J}}_{\mathrm{w}_i/\mathrm{c}_i}\vec{\omega}_{\mathrm{B}/\mathrm{I}} + \vec{J}_{\mathrm{w}_i/\mathrm{c}}\overset{\mathrm{B}\bullet}{\vec{\omega}}_{\mathrm{B}/\mathrm{I}} + \vec{J}_{\mathrm{w}_i/\mathrm{c}_i}\overset{\mathrm{B}\bullet}{\vec{\omega}}_{\mathrm{W}_i/\mathrm{B}}\,. \end{aligned} \tag{5.6}$$

Since the alignment of the wheel frame and the body frame is fixed with respect to F_{B}, the inertia matrix frame derivative $\overset{\mathrm{B}\bullet}{\vec{J}}_{\mathrm{w}_i/\mathrm{c}_i}$ is zero. Furthermore, we command the reaction wheel acceleration, thus we define the ith wheel control input as

$$\vec{u}_i \triangleq \overset{\mathrm{B}\bullet}{\vec{\omega}}_{\mathrm{W}_i/\mathrm{B}}\,. \tag{5.7}$$

Therefore, the reaction wheel angular momentum derivative is given by

$$\overset{\mathrm{B}\bullet}{\vec{H}}_{\mathrm{w}_i/\mathrm{c}/\mathrm{I}} = \vec{J}_{\mathrm{w}_i/\mathrm{c}}\overset{\mathrm{B}\bullet}{\vec{\omega}}_{\mathrm{B}/\mathrm{I}} + \vec{J}_{\mathrm{w}_i/\mathrm{c}_i}\vec{u}_i. \tag{5.8}$$

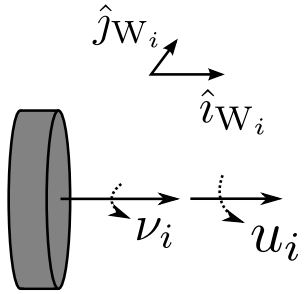

Figure 5.1: Wheel frame $\mathrm{F}_{\mathrm{W_i}}$, wheel angular velocity ν_i, and control input u_i.

We resolve the quantities in (5.5) and (5.8) in the body frame F_{B}. First, we resolve the angular velocities in the in the ith wheel frame as shown in Figure 5.1,

$$\vec{\omega}_{\mathrm{W}_i/\mathrm{B}}\Big|_{\mathrm{W}_i} = \nu_i e_1, \qquad\qquad \vec{u}_i\Big|_{\mathrm{W}_i} = u_i e_1, \tag{5.9}$$

where e_i is the ith column of the 3×3 identity matrix, $u_i \in \mathbb{R}$ is the acceleration command to the ith wheel, and the ith wheel spins with an angular velocity $\nu_i \in \mathbb{R}$ about the $\hat{\imath}$ axis of

$\mathrm{F}_{\mathrm{W}_i}$ which is evolves according to

$$\dot{\nu}_i = u_i \tag{5.10}$$

Furthermore, we assume that each wheel is radially symmetric and let its spin axis moment of inertia be α_i, thus,

$$J_{\mathrm{W}_i} \triangleq \vec{J}_{\mathrm{w}_i/\mathrm{c}_i}\Big|_{\mathrm{W}_i} = \begin{bmatrix} \alpha_i & 0 & 0 \\ 0 & \beta_i & 0 \\ 0 & 0 & \beta_i \end{bmatrix}, \tag{5.11}$$

where β_i denotes the moment of inertia about the remaining axes. Next, we resolve these quantities in the body frame and obtain

$$\vec{\omega}_{\mathrm{W}_i/B}\Big|_{\mathrm{B}} = \mathcal{O}_i e_1 \nu_i, \qquad \vec{u}_i\Big|_{\mathrm{B}} = \mathcal{O}_i e_1 u_i, \qquad \vec{J}_{\mathrm{w}_i/\mathrm{c}_i}\Big|_{\mathrm{B}} = \mathcal{O}_i J_{\mathrm{W}_i} \mathcal{O}_i^{\mathrm{T}}, \tag{5.12}$$

where the orientation matrix

$$\mathcal{O}_i \triangleq \vec{R}_{\mathrm{B}_i/\mathrm{W}_i}\Big|_{\mathrm{B}}^{\mathrm{T}}, \qquad \dot{\mathcal{O}}_i = u_i e_1^{\times} \mathcal{O}_i, \tag{5.13}$$

transforms vectors resolved in $\mathrm{F}_{\mathrm{W}_i}$ into vectors resolved in F_{B}. Finally, we define the notation

$$R \triangleq \vec{R}_{\mathrm{B/I}}\Big|_{\mathrm{B}}, \qquad \omega \triangleq \vec{\omega}_{\mathrm{B/I}}\Big|_{\mathrm{B}}, \qquad \dot{\omega} \triangleq \overset{\mathrm{B}\bullet}{\vec{\omega}}_{\mathrm{B/I}}\Big|_{\mathrm{B}},$$

$$\tau_{\mathrm{dist}} \triangleq \vec{M}_{\mathrm{b}}\Big|_{\mathrm{B}}, \qquad J_{\mathrm{b}} \triangleq \vec{J}_{\mathrm{b/c}}\Big|_{\mathrm{B}}, \qquad r_i \triangleq \vec{r}_{\mathrm{c/c}_i}\Big|_{\mathrm{B}}.$$

Resolving the reaction wheel angular momentum (5.5) in the body frame yields

$$\begin{aligned} \vec{H}_{\mathrm{w}_i/\mathrm{c/I}}\Big|_{\mathrm{B}} &= \left[\mathcal{O}_i J_{\mathrm{W}_i} \mathcal{O}_i^{\mathrm{T}} - m_i (r_i^{\times})^2\right] \omega + \mathcal{O}_i J_{\mathrm{W}_i} \mathcal{O}_i^{\mathrm{T}} \mathcal{O}_i e_1 \nu_i, \\ &= \left[\mathcal{O}_i J_{\mathrm{W}_i} \mathcal{O}_i^{\mathrm{T}} - m_i (r_i^{\times})^2\right] \omega + \mathcal{O}_i e_1 \alpha_i \nu_i, \end{aligned} \tag{5.14}$$

its body-frame derivative (5.8) resolved in $\mathrm{F_B}$ is

$$\begin{aligned}\overset{\mathrm{B}\bullet}{\vec{H}}_{\mathrm{w}_i/\mathrm{c}/\mathrm{I}}\Big|_{\mathrm{B}} &= \left[\mathcal{O}_i J_{\mathrm{W}_i}\mathcal{O}_i^{\mathrm{T}} - m_i(r_i^{\times})^2\right]\dot{\omega} + \mathcal{O}_i J_{\mathrm{W}_i}\mathcal{O}_i^{\mathrm{T}}\mathcal{O}_i e_1 u_i \\ &= \left[\mathcal{O}_i J_{\mathrm{W}_i}\mathcal{O}_i^{\mathrm{T}} - m_i(r_i^{\times})^2\right]\dot{\omega} + \mathcal{O}_i e_1 \alpha_i u_i. \end{aligned} \tag{5.15}$$

We use (5.14) and (5.15) to evaluate the summation terms in (5.1) . Thus,

$$\begin{aligned}\sum_{i=1}^{n}\vec{H}_{\mathrm{w}_i/\mathrm{c}/\mathrm{I}}\Big|_{\mathrm{B}} &= \sum_{i=1}^{n}\left[\mathcal{O}_i J_{\mathrm{W}_i}\mathcal{O}_i^{\mathrm{T}} - m_i(r_i^{\times})^2\right]\omega + \mathcal{O}_i e_1 \alpha_i \nu_i \\ &= \sum_{i=1}^{n}\left[\mathcal{O}_i J_{\mathrm{W}_i}\mathcal{O}_i^{\mathrm{T}} - m_i(r_i^{\times})^2\right]\omega + B_{\mathrm{W}}\nu \end{aligned} \tag{5.16}$$

where the ith column of B_{W} is given by

$$B_{\mathrm{W}_i} \triangleq \alpha_i \mathcal{O}_i e_1 \in \mathbb{R}^3 \tag{5.17}$$

and

$$\nu \triangleq \begin{bmatrix} \nu_1 & \nu_2 & \cdots & \nu_n \end{bmatrix}^{\mathrm{T}} \in \mathbb{R}^n. \tag{5.18}$$

Similarly, the frame derivative summation term is given by

$$\begin{aligned}\sum_{i=1}^{n}\overset{\mathrm{B}\bullet}{\vec{H}}_{\mathrm{w}_i/\mathrm{c}/\mathrm{I}}\Big|_{\mathrm{B}} &= \sum_{i=1}^{n}\left[\mathcal{O}_i J_{\mathrm{W}_i}\mathcal{O}_i^{\mathrm{T}} - m_i(r_i^{\times})^2\right]\dot{\omega} + \mathcal{O}_i e_1 \alpha_i u_i \\ &= \sum_{i=1}^{n}\left[\mathcal{O}_i J_{\mathrm{W}_i}\mathcal{O}_i^{\mathrm{T}} - m_i(r_i^{\times})^2\right]\dot{\omega} + B_{\mathrm{W}}u, \end{aligned} \tag{5.19}$$

where

$$u \triangleq \begin{bmatrix} u_1 & u_2 & \cdots & u_n \end{bmatrix}^{\mathrm{T}}. \tag{5.20}$$

Finally, resolving (5.1) in $\mathrm{F_B}$ yields

$$J_{\mathrm{b}}\dot{\omega} + \sum_{i=1}^{n}\overset{\mathrm{B}\bullet}{\vec{H}}_{\mathrm{w}_i/\mathrm{c}/\mathrm{I}}\Big|_{\mathrm{B}} = -\omega^{\times}\left(J_{\mathrm{b}}\omega + \sum_{i=1}^{n}\vec{H}_{\mathrm{w}_i/\mathrm{c}/\mathrm{I}}\Big|_{\mathrm{B}}\right) + \tau_{\mathrm{dist}}. \tag{5.21}$$

Substituting (5.16) and (5.19) into (5.21) yields the equation of motion,

$$J_{\mathrm{b}}\dot{\omega} + \sum_{i=1}^{n} \left[\mathcal{O}_i J_{\mathrm{W}_i} \mathcal{O}_i^{\mathrm{T}} - m_i (r_i^{\times})^2\right] \dot{\omega} + B_{\mathrm{W}} u = \\ - \omega^{\times} \left(J_{\mathrm{b}}\omega + \sum_{i=1}^{n} \left[\mathcal{O}_i J_{\mathrm{W}_i} \mathcal{O}_i^{\mathrm{T}} - m_i (r_i^{\times})^2\right] \omega + B_{\mathrm{W}} \nu \right) + \tau_{\mathrm{dist}}.$$

Therefore Euler's equation for a spacecraft actuated by reaction wheels is given by

$$J\dot{\omega} = -\omega^{\times} \left(J\omega - B_{\mathrm{sc}}\nu\right) + B_{\mathrm{sc}} u + \tau_{\mathrm{dist}}, \tag{5.22}$$

where $\omega \in \mathbb{R}^3$ is the angular-velocity of the spacecraft frame with respect to the inertial frame resolved in the spacecraft frame, $J \in \mathbb{R}^{3\times 3}$ is the constant, positive-definite inertia matrix of the spacecraft, given by

$$J \triangleq J_{\mathrm{b}} + \sum_{i=1}^{n} \left[\mathcal{O}_i J_{\mathrm{W}_i} \mathcal{O}_i^{\mathrm{T}} - m_i (r_i^{\times})^2\right], \tag{5.23}$$

$$B_{]rmsc} = -B_{\mathrm{W}}, \tag{5.24}$$

and $\tau_{\mathrm{dist}} \in \mathbb{R}^3$ represents all internal and external disturbance torques applied to the spacecraft bus. The equations of motion for a spacecraft actuated by reaction wheels are given by Euler's equation (5.22), Poisson's equation,

$$\dot{R} = R\omega^{\times}, \tag{5.25}$$

and the reaction-wheel dynamics

$$\dot{\nu} = u, \tag{5.26}$$

where $\nu \in \mathbb{R}^{n_w}$ is a vector composed of the angular-rate of each reaction-wheel with respect to the spacecraft frame, $u \in \mathbb{R}^{n_w}$ is a vector composed of the control input to each wheel, which has units of angular acceleration.

Furthermore, $R \in \mathbb{R}^{3\times 3}$ is the proper orthogonal matrix (that is, the rotation matrix) that transforms the components of a vector resolved in the spacecraft frame into the components of the same vector resolved in the inertial frame and $\omega^{\times}$ is the skew-symmetric cross-product matrix of ω. Finally, α_i is the positive moment of inertia about the rotation axis of

the ith reaction-wheel, $\mathcal{O}_i \in \mathbb{R}^{3\times3}$ is the rotation matrix that transforms the components of a vector resolved in the ith reaction-wheel frame into the components of the same vector resolved in the spacecraft body frame, and $e_{W_i} \in \mathbb{R}^3$ is the unit vector that represents the direction of the ith reaction-wheel's spin axis resolved in the ith wheel frame. For convenience, in (5.22), (5.25), and (5.26) we omit the argument t, recognizing that ω, R, ν, u, and τ_{dist} are time-varying quantities.

5.1.1 Error Dynamics

The objective of the attitude control problem is to determine control inputs such that the spacecraft attitude given by R follows a commanded attitude trajectory given by a possibly time-varying C^1 rotation matrix $R_{\mathrm{d}}(t)$. For $t \geq 0$, $R_{\mathrm{d}}(t)$ is given by

$$\dot{R}_{\mathrm{d}}(t) = R_{\mathrm{d}}(t)\omega_{\mathrm{d}}(t)^{\times}, \tag{5.27}$$

$$R_{\mathrm{d}}(0) = R_{\mathrm{d0}}, \tag{5.28}$$

where ω_{d} is the desired, possibly time-varying angular velocity of the spacecraft relative to the inertial frame. The attitude error, that is, the rotation between $R(t)$ and $R_{\mathrm{d}}(t)$, is given by

$$\tilde{R} \stackrel{\triangle}{=} R_{\mathrm{d}}^{\mathrm{T}} R, \tag{5.29}$$

which satisfies Poisson's equation

$$\dot{\tilde{R}} = \tilde{R}\tilde{\omega}^{\times}, \tag{5.30}$$

where the angular-velocity error $\tilde{\omega}$ is defined by

$$\tilde{\omega} \stackrel{\triangle}{=} \omega - \tilde{R}^{\mathrm{T}}\omega_{\mathrm{d}}. \tag{5.31}$$

We rewrite (5.22) in terms of the angular-velocity error as

$$\begin{aligned} J\dot{\tilde{\omega}} =& [J(\tilde{\omega} + \tilde{R}^{\mathrm{T}}\omega_{\mathrm{d}}) - B_{\mathrm{sc}}\nu] \times (\tilde{\omega} + \tilde{R}^{\mathrm{T}}\omega_{\mathrm{d}}) \\ &+ J(\tilde{\omega} \times \tilde{R}^{\mathrm{T}}\omega_{\mathrm{d}} - \tilde{R}^{\mathrm{T}}\dot{\omega}_{\mathrm{d}}) + B_{\mathrm{sc}}u + z_{\mathrm{dist}}. \end{aligned} \tag{5.32}$$

5.2 RCAC Parameters for Attitude Control

RCAC requires a vector performance variable, thus, the attitude-error $\tilde{R}$ given by Poisson's equation (5.30) cannot be used directly. As in [70], we reformulate the attitude-error dynamics using the vector parameter S presented in [58].

For $i = 1, 2, 3$, let e_i denote the ith column of the 3×3 identity matrix, and let $A_{\text{att}} = \text{diag}(a_1, a_2, a_3)$ be a diagonal positive-definite matrix. Then

$$S \triangleq \sum_{1}^{3} a_i \left(\tilde{R}^{\mathrm{T}} e_i \right) \times e_i \in \mathbb{R}^3 \tag{5.33}$$

is a vector measure of attitude-error. Thus, we define the performance variable for the attitude control problem as

$$z \triangleq \begin{bmatrix} \tilde{\omega} \\ S \end{bmatrix} \in \mathbb{R}^6. \tag{5.34}$$

5.2.1 Baseline Markov Parameter

We utilize the procedure outlined in [70] to compute a baseline Markov parameter for the spacecraft system through linearization of the error dynamics in (5.30) and (5.32). We parameterize the SO(3) attitude-error $\tilde{R}$ using the vector

$$\tilde{r} \triangleq \begin{bmatrix} \tilde{r}_1 & \tilde{r}_2 & \tilde{r}_3 \end{bmatrix}^{\mathrm{T}} \in \mathbb{R}^9, \tag{5.35}$$

where $\tilde{r}_i \in \mathbb{R}^{1\times 3}$ is the ith row of the rotation matrix $\tilde{R}$. Then, the attitude-error dynamics in (5.30) become

$$\dot{\tilde{r}} = \begin{bmatrix} -\tilde{\omega}^{\times} & & \\ & -\tilde{\omega}^{\times} & \\ & & -\tilde{\omega}^{\times} \end{bmatrix} \tilde{r}. \tag{5.36}$$

We rewrite Euler's equation in (5.31) as

$$\begin{aligned} J\dot{\tilde{\omega}} = &\left[J\left(\tilde{\omega} + \mathcal{D}(\omega_{\mathrm{d}})\tilde{r}\right) - B_{\mathrm{sc}}\nu\right] \times \left[\tilde{\omega} + \mathcal{D}(\omega_{\mathrm{d}})\tilde{r}\right] \\ &+ J\left[\tilde{\omega} \times \mathcal{D}(\omega_{\mathrm{d}})\tilde{r} - \mathcal{D}(\dot{\omega}_{\mathrm{d}})\tilde{r}\right] + B_{\mathrm{sc}}u + z_{\mathrm{dist}}. \end{aligned} \tag{5.37}$$

The operator $\mathcal{D}(x) : \mathbb{R}^3 \to \mathbb{R}^{3\times 9}$ is

$$\mathcal{D}(x) \triangleq \begin{bmatrix} x_1 I_3 & x_2 I_3 & x_3 I_3 \end{bmatrix}, \tag{5.38}$$

where x_i for $i = 1, 2, 3$, is the ith component of x.

We construct a state vector by stacking the angular-velocity error $\tilde{\omega}$, the attitude-error $\tilde{r}$, and the reaction-wheel angular-rates ν. We define our system using this state vector and the rewritten error dynamics in (5.36) and (5.37) combined with the reaction wheel dynamics in (5.26).

We linearize the system by computing a Jacobian about the equilibrium $x_{\mathrm{e}}^{\mathrm{T}} = \begin{bmatrix} \tilde{\omega}_{\mathrm{e}}^{\mathrm{T}} & \tilde{r}_{\mathrm{e}}^{\mathrm{T}} & \nu_{\mathrm{e}}^{\mathrm{T}} \end{bmatrix}^{\mathrm{T}}$. The derivative of (5.37) with respect to $\tilde{\omega}$, $\tilde{r}$, and ν are

$$\begin{aligned} \frac{\partial \dot{\tilde{\omega}}}{\partial \tilde{\omega}} = &J^{-1}\left[-\left(\tilde{\omega}_e + \mathcal{D}(\omega_d)\tilde{r}_e\right)^{\times} J \right. \\ &\left. + \left[J\left(\tilde{\omega}_e + \mathcal{D}(\omega_d)\tilde{r}_e\right) - B_{\mathrm{sc}}\nu\right]^{\times}\right] - \left(\mathcal{D}(\omega_d)\tilde{r}_e\right)^{\times}, \end{aligned} \tag{5.39}$$

$$\begin{aligned} \frac{\partial \dot{\tilde{\omega}}}{\partial \tilde{r}} = &J^{-1}\left[-\left(\tilde{\omega}_e + \mathcal{D}(\omega_d)\tilde{r}_e\right)^{\times} J\mathcal{D}(\omega_d) \right. \\ &+ \left[J\left(\tilde{\omega}_e + \mathcal{D}(\omega_d)\tilde{r}_e\right) - B_{\mathrm{sc}}\nu\right]^{\times} \mathcal{D}(\omega_d)\Big] \\ &+ \tilde{\omega}_e^{\times}\mathcal{D}(\omega_d) - \mathcal{D}(\dot{\omega}_d), \end{aligned} \tag{5.40}$$

$$\frac{\partial \dot{\tilde{\omega}}}{\partial \nu} = -J^{-1}\left[\tilde{\omega}_e + \mathcal{D}(\omega_d)\tilde{r}_e\right]^{\times} B_{\mathrm{sc}}. \tag{5.41}$$

Next, we write the derivative for each row $\tilde{r}_i$ of $\tilde{R}$ as

$$\dot{\tilde{r}}_i = \left(\tilde{r}_i \times \tilde{\omega}\right)^{\mathrm{T}}. \tag{5.42}$$

Then, the derivatives of (5.42) with respect to $\tilde{\omega}$, $\tilde{r}_j$, and ν are,

$$\frac{\partial \dot{\tilde{r}}_i}{\partial \tilde{\omega}} = -\tilde{r}_{e,i}^{\times}, \text{ for } i = 1, 2, 3, \tag{5.43}$$

$$\frac{\partial \dot{\tilde{r}}_i}{\partial \tilde{r}_j} = \left[-\tilde{\omega}^{\times} \frac{\partial \tilde{r}_i}{\partial \tilde{r}_j} + \tilde{r}_i^{\times} \frac{\partial \tilde{\omega}}{\partial \tilde{r}_j} \right]^{\mathrm{T}}, \tag{5.44}$$

$$\frac{\partial \dot{\tilde{r}}_i}{\partial \nu} = 0, \text{ for } i = 1, 2, 3. \tag{5.45}$$

where

$$\frac{\partial \tilde{r}_i}{\partial \tilde{r}_j} = \begin{cases} I_3, & i = j, \\ 0_{3\times 3}, & i \neq j, \end{cases}$$

$$\frac{\partial \tilde{\omega}}{\partial \tilde{r}_j} = \begin{cases} \mathcal{D}(\omega_d) \begin{bmatrix} I_3 & 0 & 0 \end{bmatrix}^{\mathrm{T}}, & j = 1, \\ \mathcal{D}(\omega_d) \begin{bmatrix} 0 & I_3 & 0 \end{bmatrix}^{\mathrm{T}}, & j = 2, \\ \mathcal{D}(\omega_d) \begin{bmatrix} 0 & 0 & I_3 \end{bmatrix}^{\mathrm{T}}, & j = 3. \end{cases}$$

Finally, the Jacobian for the reaction-wheel dynamics (5.26) is

$$\frac{\partial \dot{\nu}}{\partial x} = 0. \tag{5.46}$$

We obtain the input matrix by differentiating (5.37), (5.42), and (5.26) with respect to the control input u which yields

$$B_{\mathrm{c}} = \begin{bmatrix} J^{-1} B_{\mathrm{sc}} \\ 0_{9\times n_w} \\ R_{W_1} e_{W_1} \\ \vdots \\ R_{W_{n_w}} e_{W_{n_w}} \end{bmatrix}. \tag{5.47}$$

We rewrite the attitude parameter S in terms of the attitude state $\tilde{r}$ to compute the output matrices.

$$S = -M_a R_a \tilde{r}, \tag{5.48}$$

where

$$M_a \triangleq \begin{bmatrix} e_1^\times & e_2^\times & e_3^\times \end{bmatrix}, R_a \triangleq \begin{bmatrix} a_1 I_3 & & \\ & a_2 I_3 & \\ & & a_3 I_3 \end{bmatrix}.$$

Thus,

$$C = \begin{bmatrix} I_3 & 0_{3\times 9} & 0_{3\times n_w} \\ 0_{3\times 3} & M_a & 0_{3\times n_w} \end{bmatrix}. \tag{5.49}$$

We obtain the discrete-time dynamics matrix from

$$A = e^{A_c h}, \tag{5.50}$$

where A_c is the Jacobian constructed from the derivatives in (5.39) - (5.46) and h is the controller time step. The discrete-time input matrix is given by

$$B = \int_0^h e^{A\tau} d\tau B_c. \tag{5.51}$$

The discrete-time output matrices are $E_1 = C$ and $D_d = 0$.

5.3 M2R Examples

Consider a rigid body whose inertia matrix relative to its center of mass resolved in the body frame is

$$J_0 = \begin{bmatrix} 5 & -0.1 & -0.5 \\ -0.1 & 2 & 1 \\ -0.5 & 1 & 3.5 \end{bmatrix} \text{ kg-m}^2. \tag{5.52}$$

We use $n_w = 3$ reaction wheels whose rotational-axis moments of inertia are $\alpha_{0_i} = 0.1$ kg/m^2 for $i = 1, 2, 3$. The wheel spin axes are chosen such that $e_{W_i} = e_1$, for $i = 1, 2, 3$, are aligned orthogonally. Thus, the actuator matrix $B_{\rm sc}$ in (5.32) becomes

$$B_{\rm sc} = -0.1 I_3. \tag{5.53}$$

The spacecraft's initial motion is described by

$$\omega(0) = \frac{0.1}{\sqrt{3}} \begin{bmatrix} 1 & -1 & 1 \end{bmatrix}^{\rm T} \text{ rad/sec} \tag{5.54}$$

with the reaction-wheels initially at rest so that

$$\nu_i(0) = \begin{bmatrix} 0 & 0 & 0 \end{bmatrix}^{\rm T} \text{ rad/sec, for } i = 1, 2, 3. \tag{5.55}$$

The spacecraft's initial attitude is given by $R(0) = I_3$. The goal of the controller is to bring the spacecraft to rest with an attitude corresponding to an eigenaxis rotation of 40° about the body direction $\begin{bmatrix} 1 & 1 & 1 \end{bmatrix}^{\rm T}$.

The controller order is set to $n_c = 3$, the recursive cost weighting $R = I$, the initial controller coefficients and the initial covariance are set to $\theta(0) = 0$ and $P(0) = 100I$, and the attitude parameter weights for S in (5.33) are given by $a_1 = 1, a_2 = 2$, and $a_3 = 3$. To compute the baseline Markov parameter, we compute the Jacobian about the equilibrium $\tilde{\omega}_{\rm e} = 0$, $\tilde{R}_{\rm e} = I_3$, $\nu_{\rm e} = 0$. Then, the first Markov parameter for the linearized system is

$$\mathcal{H}_1 \triangleq E_1 B = \begin{bmatrix} hJ^{-1}B_{\rm sc} \\ \\ \frac{1}{2}h^2 M_a R_a M_a^{\rm T} J^{-1} B_{\rm sc} \end{bmatrix}. \tag{5.56}$$

As in [70], we saturate the control input proportionally, by scaling the control vector as

$$u_{\rm sat} = \begin{cases} u, & u \in \mathcal{B}, \\ \\ \eta u, & u \notin \mathcal{B}, \end{cases} \tag{5.57}$$

where $\mathcal{B}$ is a boundary defined by the saturation limits and η is the maximum scaling possible such that $u_{\rm sat} \in \mathcal{B}$, that is,

$$\eta = \max_{\eta \in (0,1]} \{\eta : \eta u \in \mathcal{B}\}. \tag{5.58}$$

we limit the magnitude of the angular acceleration of each wheel to 1 rad/sec^2.

5.3.1 Robustnes to Inertia Uncertainty

To evaluate the robustness of RCAC to inertia uncertainty, we examine the relationship between the Markov parameter and the spacecraft and reaction wheel inertias. We introduce two inertia-free Markov parameters $\hat{\mathcal{H}}_1$ and $\hat{\mathcal{H}}_1'$. The first inertia-free Markov parameter $\hat{\mathcal{H}}_1$, does not have information about the spacecraft inertia J, that is

$$\hat{\mathcal{H}}_1 \triangleq \left[\begin{array}{c} hB_{\rm sc} \\ \\ \frac{1}{2}h^2 M_a R_a M_a^{\rm T} B_{\rm sc} \end{array} \right]. \tag{5.59}$$

The second inertia-free Markov parameter, $\hat{\mathcal{H}}_1'$ does not contain information about either the spacecraft inertia J or the reaction wheel inertias α_{0_i}, thus

$$\hat{\mathcal{H}}_1' \triangleq \left[\begin{array}{c} h\hat{B}_{\rm sc} \\ \\ \frac{1}{2}h^2 M_a R_a M_a^{\rm T} \hat{B}_{\rm sc} \end{array} \right], \tag{5.60}$$

where the columns of the inertia-free $\hat{B}_{\rm sc}$ are given by

$$\hat{b}_i = -R_{{\rm W}_i} e_{{\rm W}_i}. \tag{5.61}$$

Thus, the Markov parameter $\hat{\mathcal{H}}_1'$ is inertia-free but uses the actuator alignment information in $\hat{B}_{\rm sc}$. Figure 5.2 compares the eigenaxis attitude error,

$$\theta_{\rm eig} \triangleq \cos^{-1}\frac{1}{2}\left(\mathrm{tr}\ \tilde{R} - 1\right), \tag{5.62}$$

using the baseline and inertia-free Markov parameters $\mathcal{H}_1$, $\hat{\mathcal{H}}_1$, and $\hat{\mathcal{H}}_1'$.

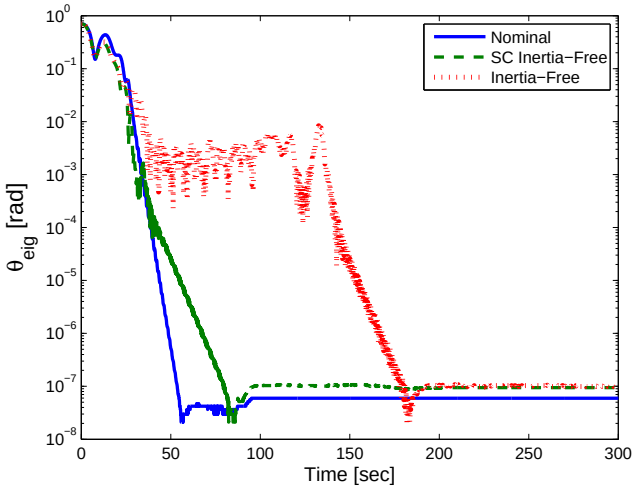

Figure 5.2: Eigenaxis attitude-error for a M2R maneuver on a log scale. RCAC reaches the commanded attitude using the baseline Markov parameter $\mathcal{H}_1$, the spacecraft-inertia-free parameter $\hat{\mathcal{H}}_1$, and the inertia-free parameter $\hat{\mathcal{H}}_1'$.

Figure 5.2 shows that removing the inertia information affects increases the steady state error. Furthermore, also removing the reaction wheel inertia approximately doubles the settling time.

Next, we scale the inertia matrix and compare the settling time for various spacecraft inertias given by $J_{\rm sc} = \beta J_0$ for $\beta > 0$. To evaluate the closed-loop performance, we define the settling time $t_{\rm ss}$ as the time needed to bring the eigenaxis attitude-error within a bound $\theta_{\rm ss}$, that is,

$$\theta_{\rm eig}(t) \leq \theta_{\rm ss}, \quad \text{for all } t \geq t_{\rm ss}.$$

In the following examples $\theta_{\rm ss} = 1$ deg and we use the inertia-free Markov parameter $\hat{\mathcal{H}}_1'$ in (5.60).

Figure 5.3 shows that, for the Markov parameter $\hat{\mathcal{H}}_1'$, the settling time increases as the inertia of the spacecraft increases. This result is expected and is due to the decrease of control authority of the fixed-size reaction wheels. As the spacecraft inertia increases, the reaction wheels have a smaller effect on the angular acceleration $\dot{\omega}$. However, the steady

state error is less than 1×10^{-7} radians and the settling time is within 200 seconds which is acceptable for many spacecraft applications.

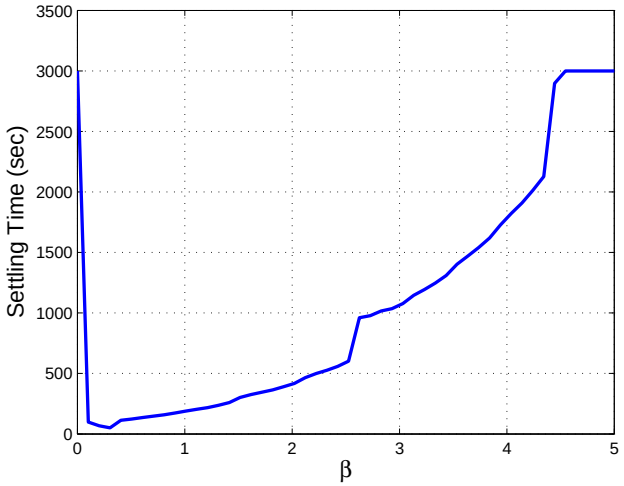

Figure 5.3: M2R settling time t_{ss} as a function of spacecraft inertia scaling β for fixed wheel inertias α_{0_i}. As the spacecraft inertia increases, RCAC requires more time to reach the commanded attitude.

5.3.1.1 Unmodeled Inertia Changes

We examine the effect unmodeled variations in the spacecraft inertia J_{sc} and the wheel inertias J_{W_i} have on the settling time of the M2R maneuver. Let the centroid inertia matrix be given by $J_3 = \text{diag}\,(10, 8.33, 5)$. Then we set the spacecraft inertia to be a value between J_3 and other inertias according to

$$J = (1 - \alpha)J_3 + \alpha J_i, \text{ for} \tag{5.63}$$

where, for $i = 1, 2, 4, 5$, J_i is given by

$$J_1 = 10I_3, \quad J_2 = \text{diag}\,(10, 10, 5) \quad J_4 = \text{diag}(10, 5, 5) \quad J_5 = \text{diag}(10, 10, 0.1).$$

J_1 represents a sphere, J_2 is a cylinder, J_4 is a thin disk and J_5 is a thin cylinder.

Figure 5.4 shows the settling time for the M2R maneuver as we vary the weighting α.

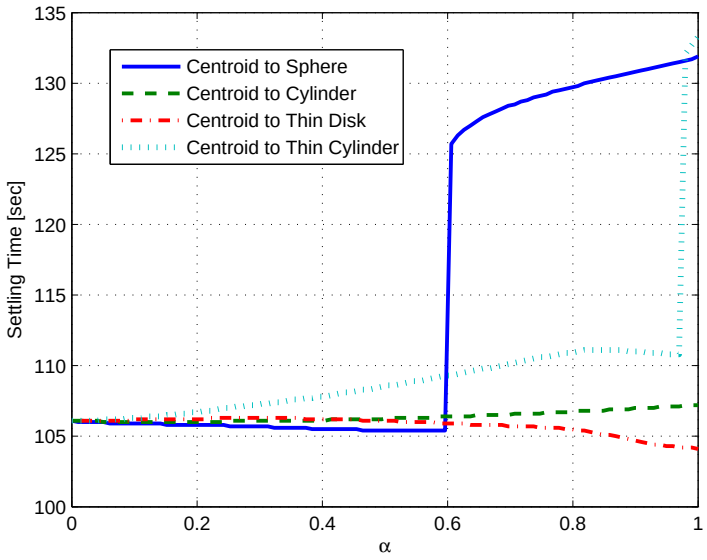

Figure 5.4: M2R settling time for RCAC using reaction wheels. The inertia J starts at the centroid value J_3 and moves toward the sphere J_1, cylinder J_2, thin disk J_4, and thin cylinder J_5 according to (4.56). The saturation level is set at 0.1 rad/sec^2.

Next, let $J = J_3$ and let the reaction wheel spin axis inertias $J_{\mathrm{W}_i} = \alpha_J$. Figure 5.5. shows the effect of changes in the reaction wheel inertia on the settling time of the M2R maneuver.

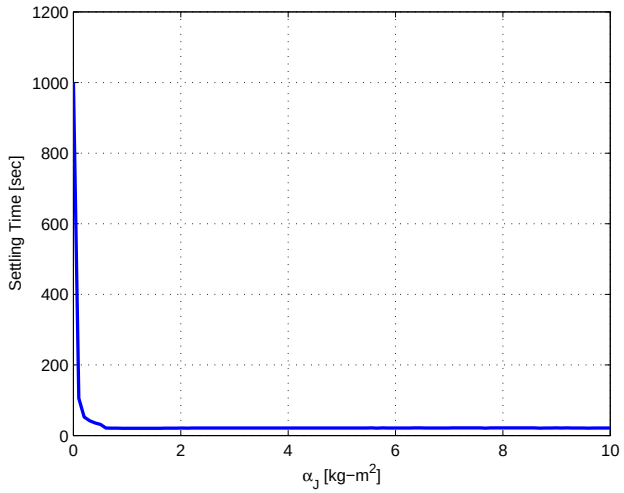

Figure 5.5: M2R closed-loop performance for RCAC using reaction wheels. Settling time as a function of the reaction wheel spin axis inertia α_J. The saturation level is set at 0.1 rad/sec^2.

5.3.2 Frame Rotation and Actuator Misalignment

We evaluate the robustness of RCAC to unknown inertia rotations for the M2R maneuver. First, we examine the effect of unmodeled off-diagonal inertia terms in J on the M2R settling time. This is equivalent to unmodeled rotation of the $\mathrm{F_B}$ relative to a principal axis frame. Let

$$J = \mathcal{R} J_0 \mathcal{R}^{\mathrm{T}}, \tag{5.64}$$

where J_0 is given by (5.52) and $\mathcal{R}(\phi, \hat{n}) \in \mathbb{R}^{3\times 3}$ is given by

$$\mathcal{R}(\phi, \hat{n}) = \cos(\phi) I_3 + [1 - \cos(\phi)]\hat{n}\hat{n}^{\mathrm{T}} + \sin(\phi)\hat{n}^{\times}, \tag{5.65}$$

where ϕ is the misalignment angle and $\hat{n}$ is the misalignment axis. Figure 5.6 shows that RCAC can complete the M2R maneuver for all possible single-axis rotations of $\mathrm{F_B}$ relative to a principal axis frame.

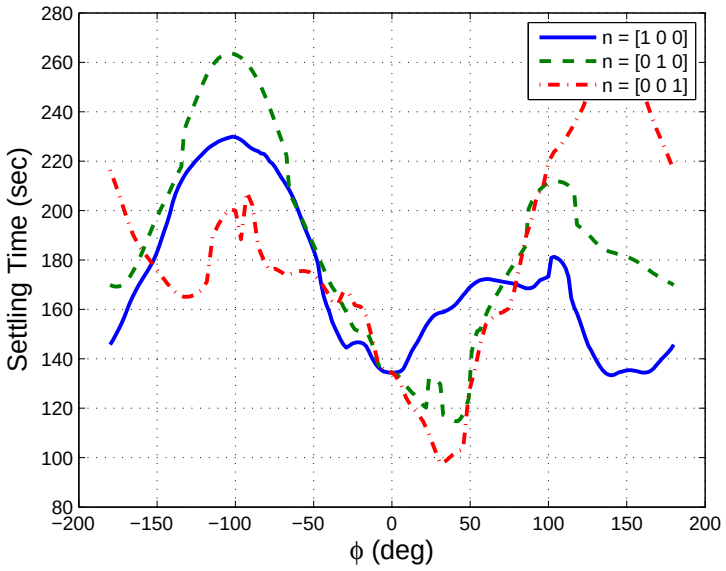

Figure 5.6: Settling time t_{ss} as a function of the angle ϕ for different rotation axes $\hat{n}$. RCAC can complete the maneuver for all single axis rotations of the actuator and sensor axes.

Next, we misalign the reaction-wheels by applying an unknown rotation $\mathcal{R}$ according to (5.65) so that the columns of the actuator matrix $B_{\rm sc}$ become

$$b_i = -\alpha_i \mathcal{R} R_{W_i} e_{W_i}. \tag{5.66}$$

We vary the angle ϕ and consider the misalignment axes

$$\hat{n}_1 = e_1, \qquad \hat{n}_2 = e_2, \qquad \hat{n}_3 = e_3.$$

We use the Markov parameter $\hat{\mathcal{H}}_1'$ in (5.60), which does not assume knowledge of the misalignment information $\mathcal{R}$ or the inertia $J_{\rm sc}$. Figure 5.7 shows that, as the misalignment angle increases, RCAC requires more time to settle, which reflects the lack of alignment information in the Markov parameter $\hat{\mathcal{H}}_1'$.

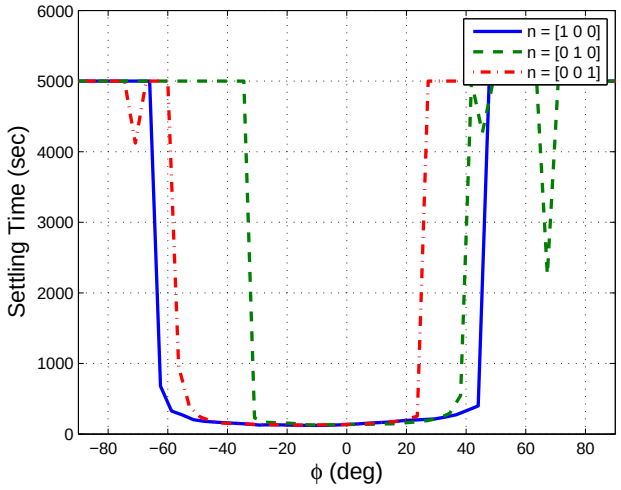

Figure 5.7: Settling time $t_{\rm ss}$ as a function of the actuator misalignment angle ϕ. RCAC is robust to single-axis misalignments up to 20 deg about all three axes.

5.3.3 Constant Disturbance Torque

We examine the performance of RCAC under the presence of a disturbance torque that is inertially constant such as solar radiation pressure. We test three different cases using the constant magnitude disturbance

$$\tau_{\rm dist} = R^{\rm T} d_0 \hat{n}_d, \tag{5.67}$$

where d_0 is the disturbance magnitude and $\hat{n}$ is the disturbance vector direction resolved in the inertial frame. Figure 5.8 shows the eigenaxis attitude-error for a disturbance of magnitude $d_0 = 1 \times 10^{-4}$ N-m with various inertial directions.

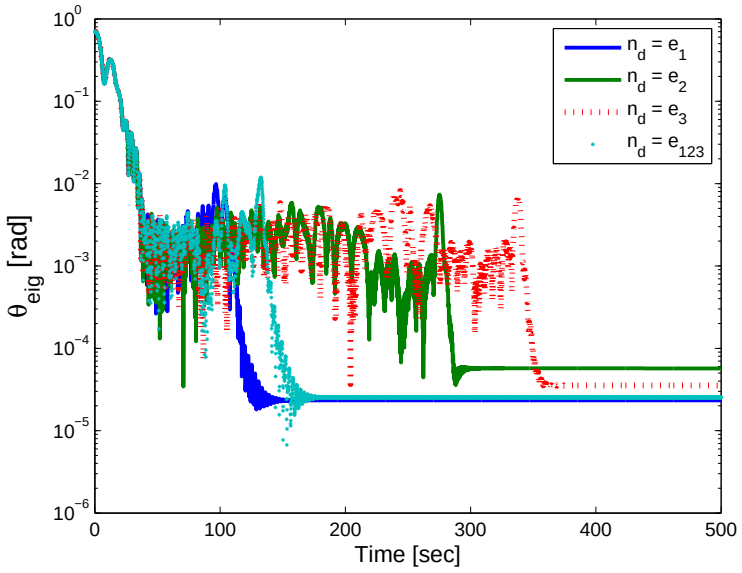

Figure 5.8: Eigenaxis attitude-error on a log scale for an inertially constant disturbance torque with magnitude $d_0 = 1 \times 10^{-4}$ N-m and for different inertial directions $\hat{n}_d$; the direction $e_{123} = \frac{1}{\sqrt{3}}[1\ 1\ 1]^{\mathrm{T}}$. RCAC can complete the maneuver under a constant, single-axis disturbance torque using the inertia-free Markov parameter $\hat{\mathcal{H}}_1'$.

5.3.4 Noise and Bias

We introduce noise and bias into the angular-velocity measurement and examine the impact on the settling time. Let the measured angular velocity be given by

$$y_\omega = \omega + b + \nu_\omega, \tag{5.68}$$

where $b \in \mathbb{R}^3$ is a constant bias and ν_ω is white Gaussian noise. Figure 5.9 shows the eigenaxis attitude error when the angular velocity measurement is corrupted by a constant biases $b = b_0 \begin{bmatrix} 1 & 1 & 1 \end{bmatrix}^{\mathrm{T}}$ and Gaussian white noise with variance $\sigma_\omega^2 = 10^{-12}$ rad/sec. Since the angular-velocity measurement is included in the performance variable, the steady-state error increases as the bias magnitude increases.

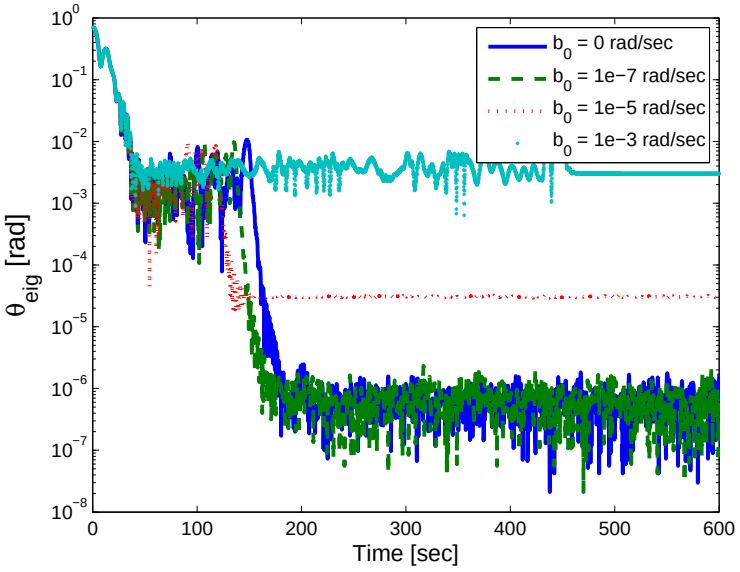

Figure 5.9: Eigenaxis attitude error on a log scale for noise and bias in the angular-velocity measurement. As the bias increases, the steady-state error increases.

5.3.5 M2S Maneuvers Using Reaction Wheels

For the M2S maneuver, we again take the spacecraft inertia to be $J = J_3$, the reaction wheel inertias $J_{\mathrm{W}_i} = 0.1$ kg-m^2 and let the spacecraft be initially at rest so that $R(0) = I$. As in the thruster examples, we test four maneuvers: spins about each of the principal axes and a spin about a non-principal axis.

For the desired attitude, we command an 40 deg eigenaxis rotation about the vector $\begin{bmatrix} 1 & 1 & 1 \end{bmatrix}^{\mathrm{T}}$. The desired attitude evolves according to $\dot{R}_{\mathrm{d}} = R_{\mathrm{d}}\omega^{\times}$. Figure 5.10 shows the closed-loop response for the M2S maneuver.

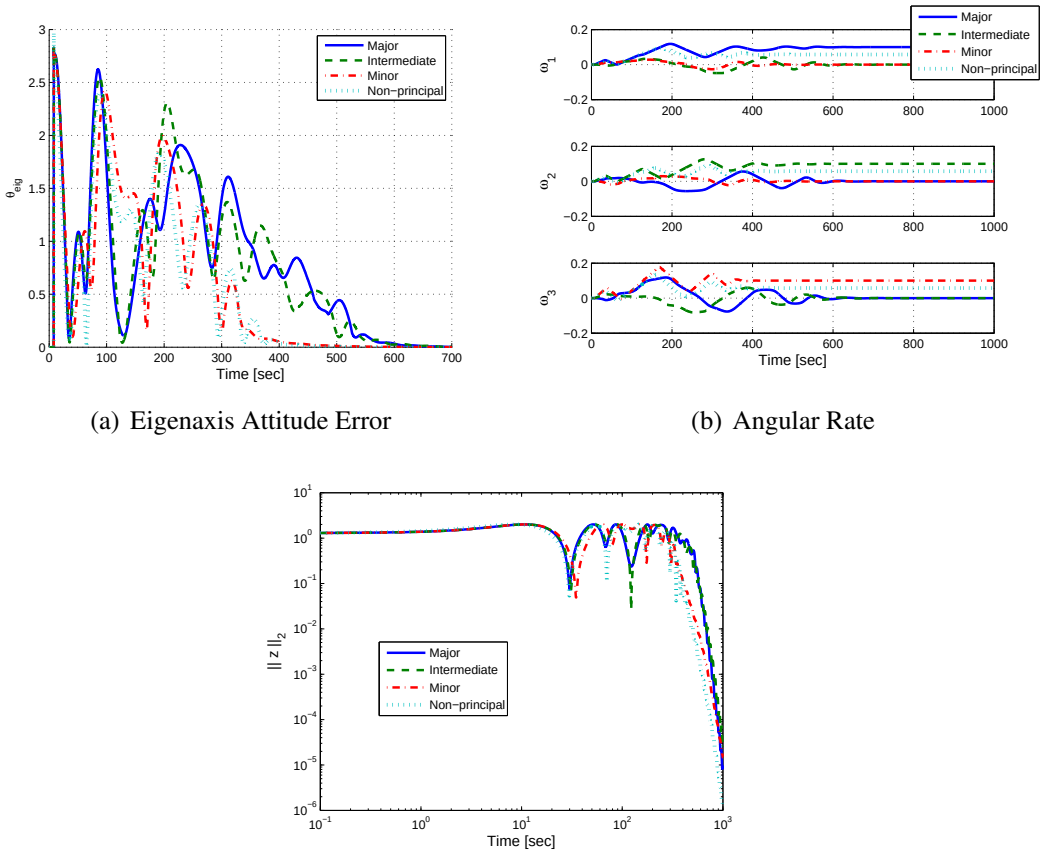

(a) Eigenaxis Attitude Error

(b) Angular Rate

(c) Euclidean Norm of Performance Variable

Figure 5.10: M2S performance for RCAC using reaction wheels. The spacecraft is commanded to spin about each principal axis as well as a non-principal axis. The number of previous time steps in the retrospective cost is set to $s = 1$ and use the inertia-free Markov parameter $\hat{\mathcal{H}}_1'$ in (5.60). The saturation level is set at 0.1 rad/sec^2.

5.4 Conclusion

RCAC was shown to achieve attitude command following for motion-to-rest maneuvers using reaction wheels. Dependence on the inertia of the spacecraft bus and the spin axis moment of inertia of the reaction wheels was removed from the Markov parameter. Therefore, an inertia-free controller was shown to achieve command following for spacecraft under various off-nominal conditions.

The inertia-free Markov parameter enabled RCAC to reach the desired attitude with acceptable levels of steady state error (10^{-8}rad) and settling time (< 30sec). Numerical studies demonstrated robustness to scaling errors in the spacecraft inertia model as well as robustness to unknown single-axis misalignments of the reaction wheel spin axes. Furthermore, RCAC is able to handle unmodeled inertially constant disturbances.

Finally, we introduced Gaussian white noise and bias in the angular-velocity measurement and showed that the controller is stable can reach the desired attitude.

CHAPTER 6

Magnetic Torquers

Magnetic coils are commonly used to reduce momentum in spacecraft that use momentum storage devices such as reaction wheels [82]. Magnetic actuators are also used to de-spin spacecraft after launch vehicle separation [83]. However, the torque produced by the coils is constrained to the plane orthogonal to the Earth's local magnetic field vector. This lack of instantaneous controllability along with low-torque capability, and low pointing accuracy make magnetic coils impractical for three-axis attitude control of large spacecraft. Yet, as the size of the spacecraft decreases and pointing accuracy requirements are relaxed, the benefits of magnetic coils, such as small size, ease of manufacturing, and low power consumption, outweigh the challenges in the design and operation of these control systems [84]. Thus, the application of active magnetic coils for three-axis attitude control of small spacecraft has gained interest in recent years [85].

Attitude regulation methods for magnetic control typically rely on a model of the spacecraft dynamics and kinematics, the spacecraft mass properties, and a model of the magnetic field. Control techniques include proportional-derivative control, optimal control, and nonlinear methods [86]. However, these methods may fail when accurate modeling information is not available. Thus, a control law that reduces the required modeling information is desired.

We develop a controller that utilizes measurements of the local magnetic field without knowledge of the mass properties. We apply retrospective cost adaptive control (RCAC) to spacecraft attitude control using magnetic torquers. Specifically, we modify the RCAC formulation to accommodate the rank deficiency of the input matrix. We compare two approaches to address the rank deficiency and time-varying nature of the input matrix. The first approach utilizes an average of the magnetic field based on a-priori knowledge, whereas the second approach uses three multi-input, single-output controllers. RCAC uses no information about the spacecraft inertia, and model information is limited to the input-output relation given by the first Markov parameter, which is computed from an inertia-free linearization of Euler's and Poisson's equations. We compare the performance of both

algorithm variants. Given a spacecraft with arbitrary initial angular rate and initial attitude, the objective of the first maneuver to bring the spacecraft to rest at a specified attitude. For the second maneuver we wish to spin about an inertially pointed body axis.

6.1 Spacecraft Model

Magnetic torquers are composed of electric coils which generate a current which in turn creates a local magnetic field. The magnetic field created by the coils interacts with the Earth's magnetic field $\vec{b}$ and produces a torque on the spacecraft,

$$\vec{M}_{\text{coil}} = -\vec{b}^{\times}\vec{d} \tag{6.1}$$

where $\vec{d}$ is the combined magnetic dipole produced by the magnetic torquers.

Since magnetic torquers do not store momentum, Euler's equation for a spacecraft controlled by magnetic torquers is given by

$$\vec{J}_{\text{b/c}}\,\overset{\text{B}\bullet}{\vec{\omega}}_{\text{B/I}} = -\vec{\omega}_{B/I} \times \vec{J}_{\text{b/c}}\vec{\omega}_{\text{B/I}} - \vec{b}^{\times}\vec{d} + \vec{M}_{\text{sc}}. \tag{6.2}$$

We define the notation,

$$J_{\text{sc}} \triangleq \vec{J}_{\text{b/c}}\Big|_{\text{B}}, \quad \omega \triangleq \vec{\omega}_{\text{B/I}}\Big|_{\text{B}}, \quad d \triangleq \vec{d}\Big|_{\text{B}}, \quad b(t) \triangleq \vec{b}\Big|_{\text{B}}, \quad \tau_{\text{dist}} \triangleq \vec{M}_{\text{sc}}\Big|_{\text{B}}. \tag{6.3}$$

We resolve (6.2) in the body frame and obtain the dynamics for a spacecraft actuated by magnetic torquers

$$J_{\text{sc}}\omega = -\omega^{\times}J_{\text{sc}}\omega - b(t)^{\times}d + \tau_{\text{dist}}. \tag{6.4}$$

The attitude is given by

$$\dot{R} = R\omega^{\times}. \tag{6.5}$$

The vector τ_{dist} represents disturbance torques, that is, all internal and external torques applied to the spacecraft aside from control torques. These disturbances may be due to onboard components, gravity gradients, solar pressure, atmospheric drag, or the ambient magnetic field. For convenience in (6.4) and (6.5) we omit the argument t, recognizing that ω, R, d, and τ_{dist} are time-varying quantities.

6.1.1 Magnetic Dipole Allocation

Let the command u computed by RCAC be the desired torque. The magnetic coils must generate the desired torque u using a magnetic dipole command d. The resulting dipole creates a torque vector that is orthogonal to the local, time-varying magnetic field $b(t) \in \mathbb{R}^3$. Given the control torque u commanded by RCAC we must compute the required dipole d.

The torque obtained from a magnetic dipole $d(t)$ and the Earth's magnetic field $b(t)$ is given by

$$\tau(t) = -b(t)^{\times} d(t). \tag{6.6}$$

Replacing τ in (6.6) with the desired control torque u and solving for d yields

$$d(t) = -b(t)^{\times +} u = \frac{b(t)^{\times}}{b(t)^{\mathrm{T}} b(t)} u. \tag{6.7}$$

where the generalized inverse of the skew-symmetric matrix $b(t)^{\times}$ is given by

$$b(t)^{\times +} = -\frac{b(t)^{\times}}{b(t)^{\mathrm{T}} b(t)}. \tag{6.8}$$

The generalized inverse $b(t)^{\times +}$ projects the desired torque onto the plane orthogonal to $b(t)$ and allocates the necessary dipole $d(t)$. Thus, the control torque applied to the spacecraft is given by

$$\tau(t) = -b(t)^{\times} d(t) = B_{\mathrm{sc}}(t) u, \tag{6.9}$$

where

$$B_{\mathrm{sc}}(t) \triangleq \frac{-b(t)^{\times} b(t)^{\times}}{b(t)^{\mathrm{T}} b(t)}. \tag{6.10}$$

Note that, for all t, $\mathrm{rank}\, B_{\mathrm{sc}}(t) = 2$. Using (6.9) we write (6.4) as

$$J_{\mathrm{sc}} \omega = -\omega^{\times} J_{\mathrm{sc}} \omega + B_{\mathrm{sc}} u + \tau_{\mathrm{dist}}. \tag{6.11}$$

6.2 Modifications to RCAC for Magnetic Control

Let the performance z be given by

$$z = \begin{bmatrix} \tilde{\omega} \\ \sum_{i=1}^{3} a_i e_i \times \tilde{R} e_i \end{bmatrix}. \tag{6.12}$$

where $\tilde{R} = R_{\mathrm{d}}^{\mathrm{T}} R$, and for $i = 1, 2, 3,\ e_i$ is the ith column of the 3×3 identity matrix, and the positive scalars a_i are distinct. Linearizing the spacecraft dynamics and using convolution we can write (6.12) as

$$z(k) = E_1 A x(k-1) + \mathcal{H} u(k-1), \tag{6.13}$$

where

$$A = \begin{bmatrix} I_3 & 0_{3\times9} \\ -hM_a^{\mathrm{T}} & I_9 \end{bmatrix}, \tag{6.14}$$

$$B = \begin{bmatrix} hJ_{\mathrm{SC}}^{-1} B_{\mathrm{SC}} \\ -\frac{h^2}{2} M_a^{\mathrm{T}} J_{\mathrm{SC}}^{-1} B_{\mathrm{SC}} \end{bmatrix}, \tag{6.15}$$

$$E_1 = \begin{bmatrix} I_3 & 0_{3\times9} \\ 0_{3\times3} & -M_a R_a \end{bmatrix}. \tag{6.16}$$

The Markov parameter for the linearized spacecraft equations controlled by magnetic torquers is given by

$$\mathcal{H} = E_1 B = \begin{bmatrix} hJ_{\mathrm{sc}}^{-1} B_{\mathrm{sc}} \\ \frac{1}{2} h^2 M_a R_a M_a^{\mathrm{T}} J_{\mathrm{sc}}^{-1} B_{\mathrm{sc}} \end{bmatrix}, \tag{6.17}$$

where

$$M_a = \begin{bmatrix} e_1^\times & e_2^\times & e_3^\times \end{bmatrix} \in \mathbb{R}^{3\times 9}, \tag{6.18}$$

$$R_a = \begin{bmatrix} a_1 I_3 & & \\ & a_2 I_3 & \\ & & a_3 I_3 \end{bmatrix} \in \mathbb{R}^{9\times 9}. \tag{6.19}$$

We remove the inertia information from $\mathcal{H}$ and define

$$H \triangleq \alpha \begin{bmatrix} hB_{\mathrm{sc}} \\ \frac{1}{2}h^2 M_a R_a M_a^{\mathrm{T}} B_{\mathrm{sc}} \end{bmatrix}, \tag{6.20}$$

where α is a positive scalar.

6.2.1 Cost Function

The 2-step retrospective cost function is given by

$$J(\hat{U}(k-1), k) = \hat{\bar{U}}(k-1)^{\mathrm{T}} \mathcal{A}(k) \hat{\bar{U}}(k-1) + \hat{\bar{U}}^{\mathrm{T}}(k-1)\mathcal{B}^{\mathrm{T}}(k)\hat{\bar{U}} + \mathcal{C}(k), \tag{6.21}$$

where

$$\mathcal{A}(k) \triangleq \bar{H}^{\mathrm{T}} R_Z(k) \bar{H} + R_U(k), \tag{6.22}$$

$$\mathcal{B}(k) \triangleq 2\bar{H}^{\mathrm{T}} R_Z(k)[\bar{Z}(k) - \bar{H}\bar{U}(k-1)], \tag{6.23}$$

$$\mathcal{C}(k) \triangleq \bar{Z}^{\mathrm{T}}(k) R_Z(k) \bar{Z}(k) - 2\bar{Z}^{\mathrm{T}}(k) R_Z(k) \bar{H}\bar{U}(k-1) + \bar{U}^{\mathrm{T}}(k-1)\bar{H}^{\mathrm{T}} R_Z(k) \bar{H}\bar{U}(k-1), \tag{6.24}$$

R_Z, R_U are positive-definite, $\bar{H}$ contains the Markov parameters, and $\bar{U}(k)$, $\bar{Z}(k)$ are stacks of previous controls and previous performances, respectively. If $\mathcal{A}(k)$ is positive definite, the unique minimizer for $J(\bar{U}(k-1), k)$ is

$$\hat{\bar{U}}(k-1) = -\frac{1}{2}\mathcal{A}^{-1}(k)\mathcal{B}(k). \tag{6.25}$$

The magnetic constraints on the control torque introduce additional difficulties in the computation of the retrospective controls $\hat{\bar{U}}(k-1)$ in (6.25) and the implementation of

the control input $u(k)$. We develop two methods for managing the rank deficiency in the Markov parameter caused by the singular input matrix.

6.3 Rank deficiency of $B_{\rm sc}$

In previous approaches to spacecraft attitude control [70], [71], [73], RCAC was set up as a multi-input, multi-output controller. The input matrix $B_{\rm sc}(t)$ in (6.11) is used to compute the Markov parameter. However, since $b(t)^\times$ is skew symmetric, $\bar{H}$ is rank deficient, which prevents the inversion of $\mathcal{A}$ in (6.25) in the absence of the control weighting matrix R_U. Although it is possible to create a full rank $\mathcal{A}$ by using the control weighting matrix R_U, numerical studies suggest that this does not result in a successful control law.

Thus, to ensure that the product $\bar{H}^{\rm T} R_Z \bar{H}$ in (6.22) is invertible, we propose two modifications to the previous attitude control RCAC implementations. The first approach utilizes the average of the input matrix $B_{\rm sc}(t)$. This average matrix is shown in [87] to have full-rank for orbits that are non-equatorial, thus the resulting Markov parameter is left invertible. The second approach uses an alternate control architecture including three separate multi-input, single-output RCAC controllers instead of one multi-input, multi-output controller.

6.3.1 Averaged Markov parameter

Define the input matrix $B_{\rm sc}(t)$ resolved in the ECI frame as

$$B_{\rm sc}(t)\Big|_{\rm ECI} = B'_{\rm sc}(t) \triangleq \frac{-b'(t)^\times b'(t)^\times}{b'(t)^{\rm T} b'(t)} \tag{6.26}$$

where $b'(t)$ is the magnetic field vector resolved in the ECI frame. Next, we compute the average of $B'_{\rm sc}(t)$ over several orbits

$$\tilde{B}'_{\rm sc} = \lim_{T\to\infty} \frac{1}{T} \int_0^T B'_{\rm sc}(t) dt. \tag{6.27}$$

The averaged input matrix (6.27) is used to prove controllability and stability in [87]. We use this approach to obtain a full rank Markov parameter for RCAC. First, we transform the averaged input matrix into the spacecraft body frame

$$\tilde{B}_{\rm sc} \triangleq \tilde{B}'_{\rm sc}\Big|_B = R^{\rm T} \tilde{B}'_{\rm sc} R. \tag{6.28}$$

Then, using the average matrix in resolved in the body frame we construct the average Markov parameter

$$\tilde{\mathcal{H}} = \alpha \begin{bmatrix} hJ_{\rm sc}^{-1}\tilde{B}_{\rm sc} \\ \frac{1}{2}h^2 M_a R_a M_a^{\rm T} J_{\rm sc}^{-1}\tilde{B}_{\rm sc} \end{bmatrix}. \tag{6.29}$$

We remove the inertia and obtain,

$$\tilde{H} = \alpha \begin{bmatrix} h\tilde{B}_{\rm sc} \\ \frac{1}{2}h^2 M_a R_a M_a^{\rm T} \tilde{B}_{\rm sc} \end{bmatrix}, \tag{6.30}$$

which is left invertible for non-equatorial orbits.

6.3.2 Decentralized RCAC

For the second method, we synthesize the desired torque u using three independent multi-input single-output RCAC control loops. A similar architecture is used in [88] for angular velocity control using a heuristic approach to controller construction. We define the performance for each RCAC block as

$$z_i(k) \triangleq \begin{bmatrix} \tilde{\omega}_i \\ S_i \end{bmatrix} = C_i' z(k), \tag{6.31}$$

where S_i and $\tilde{\omega}_i$ are the ith components of S and $\tilde{\omega}$, respectively, and

$$C_i' \triangleq \begin{bmatrix} e_i^{\rm T} & 0_{1\times 3} \\ 0_{1\times 3} & e_i^{\rm T} \end{bmatrix}. \tag{6.32}$$

We rewrite (6.31) as

$$z_i(k) = C_i' E_1 A x(k-1) + \sum_{j=1}^{3} C_i' E_1 B e_j u_j(k-1), \tag{6.33}$$

where $u_j(k)$ is the jth component of $u(k)$.

To compute the Markov parameter we assume that the sensor and actuator frames are

Parameter	Value
Inclination	87°
Radius	450 [km]
Right ascension of ascending node	0
Argument of perigee	0
Mean anomaly	0
Period $(T_{\rm orbit})$	5615 [sec]

Table 6.1: Orbital parameters.

aligned and that each component of the performance $z(k)$ is only affected by the corresponding component of the control $u(k-1)$ such that

$$z_i(k) \approx C_i' E_1 A x(k-1) + C_i' E_1 B e_i u_i(k-1). \tag{6.34}$$

Thus, the Markov parameter for the ith multi-input, single-output RCAC is

$$\mathcal{H}_i(t) = C_i' E_1 B e_i \tag{6.35}$$

$$= \begin{bmatrix} h e_i^{\rm T} J_{\rm sc}^{-1} B_{\rm sc}(t) \\ \frac{1}{2} h^2 e_i^{\rm T} M_a R_a M_a^{\rm T} J_{\rm sc}^{-1} B_{\rm sc}(t) \end{bmatrix} e_i. \tag{6.36}$$

Removing the inertia yields

$$H_i'(t) \triangleq \begin{bmatrix} h e_i^{\rm T} B_{\rm sc}(t) \\ \frac{1}{2} h^2 e_i^{\rm T} M_a R_a M_a^{\rm T} B_{\rm sc}(t) \end{bmatrix} e_i, \tag{6.37}$$

which is left invertible. This approach ignores the coupling between axes and only requires knowledge of the alignment between actuators and sensors.

6.4 Numerical Examples

Consider a rigid spacecraft around a high-inclination circular orbit given by the orbital parameters in Table 6.1. The magnetic field is computed using the International Geomagnetic Reference Field (IGRF) model [89]. Furthermore, all disturbances $z_{\rm d}$ are assumed to

parameter	Value
n_c	10
P_0	$100I$
R_U	$10I$
s	$\frac{T_{\text{orbit}}}{h}$
θ_0	0
a_1	1
a_2	2
a_3	3
h	10 [sec]
α	0.1

Table 6.2: RCAC parameters.

be zero. The RCAC parameters used are shown in Table 6.2. Furthermore, the performance weighting is given by

$$R_Z = \begin{bmatrix} \epsilon I_3 & 0 \\ 0 & \epsilon^2 I_3 \end{bmatrix}, \tag{6.38}$$

where ϵ is a positive number. The scaling requirements between the angular velocity and attitude error terms is explained in [87]. For the M2R examples, we set $\epsilon = 10^{-5}$.

6.4.1 M2R Examples

Let the initial motion of the spacecraft be described by

$$\omega(0) = 0.001 \begin{bmatrix} 0 & -1 & 0 \end{bmatrix}^{\mathrm{T}} \text{ rad/sec.} \tag{6.39}$$

We describe the initial and desired attitudes using eigenaxis rotations as defined by Rodrigues' equation

$$\mathcal{R}(\theta_e, \hat{n}_e) = \cos(\theta_e) I_3 + (1 - \cos(\theta_e)) n_e n_e^{\mathrm{T}} + \sin(\theta_e) n_e^{\times}, \tag{6.40}$$

where θ_e is the eigenangle and $\hat{n}_e \in \mathbb{R}^3$ is the eigenaxis. Thus, the initial attitude be given by an eigenaxis rotation of $\theta_0 = 90^\circ$ about the vector

$$n_0 = \begin{bmatrix} -0.03 & -0.9 & 0.03 \end{bmatrix}^{\mathrm{T}}. \tag{6.41}$$

The goal of the controller is to bring the spacecraft to rest, that is, $\omega_d = 0$, at the inertial attitude given by the eigenaxis rotation of $\theta_d = 96^\circ$ about the vector

$$n_d = \begin{bmatrix} 1 & 1 & -1 \end{bmatrix}^{\mathrm{T}}. \tag{6.42}$$

We test the M2R maneuver on three different rigid bodies, namely, a sphere, a cylinder, and an arbitrary body.

We assume that the sensor and actuator axes are aligned such that the inertia matrices resolved in the body frame are given by

$$J_{\text{sphere}} = \operatorname{diag}(10, 10, 10) \text{ kg-m}^2, \tag{6.43}$$

$$J_{\text{cylinder}} = \operatorname{diag}(10, 10, 5) \text{ kg-m}^2, \tag{6.44}$$

$$J_{\text{arbitrary}} = \begin{bmatrix} 5 & -0.1 & -0.5 \\ -0.1 & 2 & 1 \\ -0.5 & 1 & 3.5 \end{bmatrix} \text{ kg-m}^2. \tag{6.45}$$

We compare the performance of both approaches to magnetic control for the M2R maneuver using the inertias in (6.43), (6.44), and (6.45). Figure 6.1 shows the results for the sphere inertia, Figure 6.2 shows the results for the cylinder inertia, and Figure 6.3 shows the results for the arbitrary inertia. The dipoles shown in the examples indicate that both implementations, averaged and decentralized, command dipoles of the same magnitude given the same tuning parameters in Table 6.2. Thus, we compare both approaches based on settling time of the eigenaxis attitude error θ_{eig}. For all three inertias, the centralized approach based on the average Markov parameter $\tilde{H}$ settles faster than the decentralized version based on the Markov parameter H_i'.

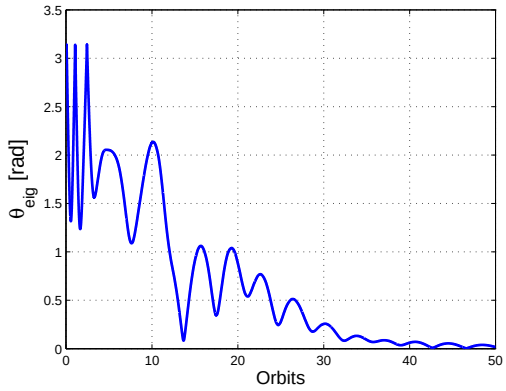

(a) Eigenaxis attitude errorfor MIMO RCAC using the average Markov parameter $\tilde{H}$

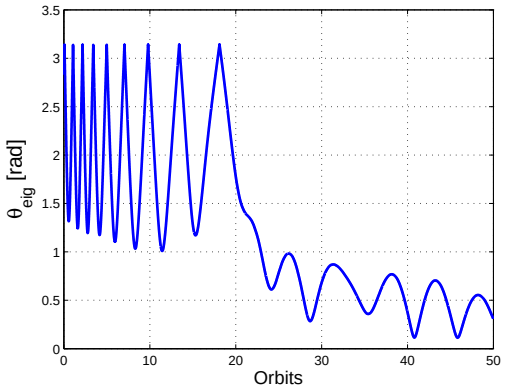

(b) Eigenaxis attitude error for decentralized RCAC

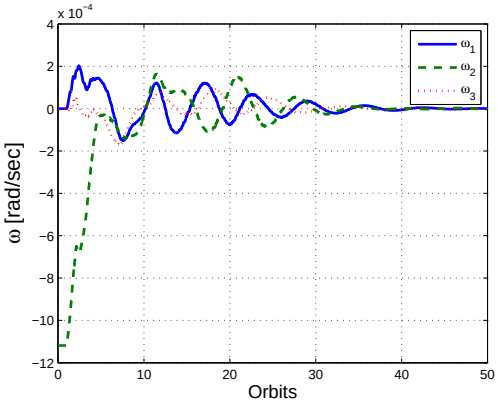

(c) Angular velocity for MIMO RCAC using the average Markov parameter $\tilde{H}$

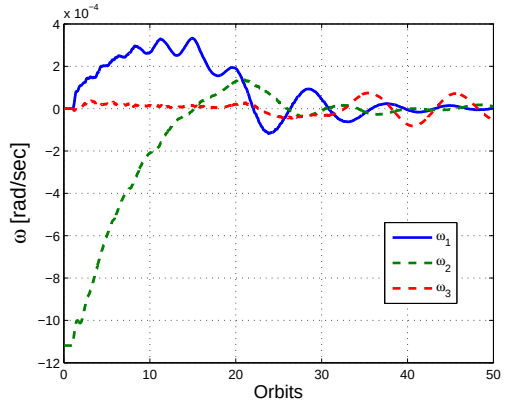

(d) Angular velocity for decentralized RCAC

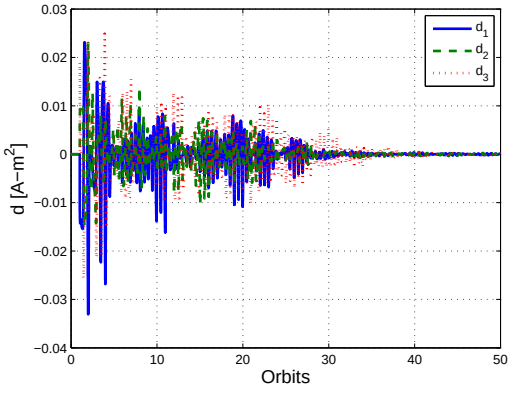

(e) Magnetic dipole for MIMO RCAC using the average Markov parameter $\tilde{H}$

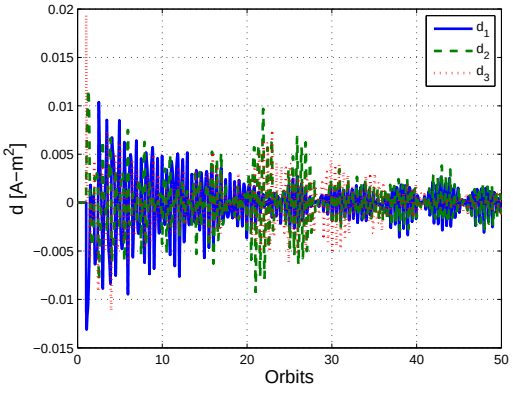

(f) Magnetic dipole for decentralized RCAC

Figure 6.1: Performance comparison of RCAC using the average Markov parameter $\tilde{H}$ versus the decentralized approach for the M2R maneuver for a spherical spacecraft with inertia J_{sphere} in (6.43).

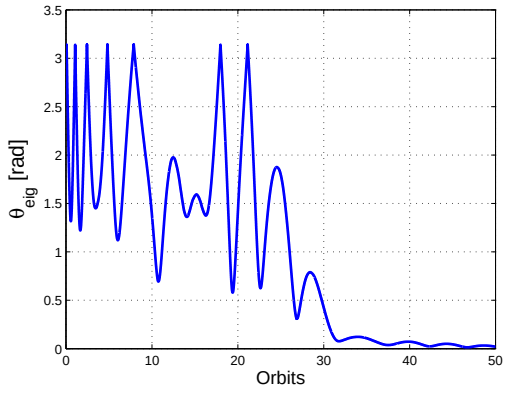

(a) Eigenaxis attitude errorfor MIMO RCAC using the average Markov parameter $\tilde{H}$

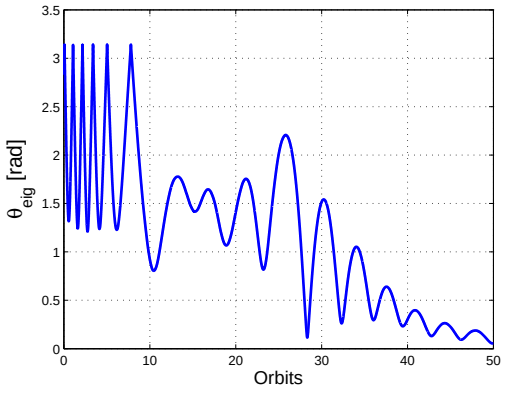

(b) Eigenaxis attitude error for decentralized RCAC

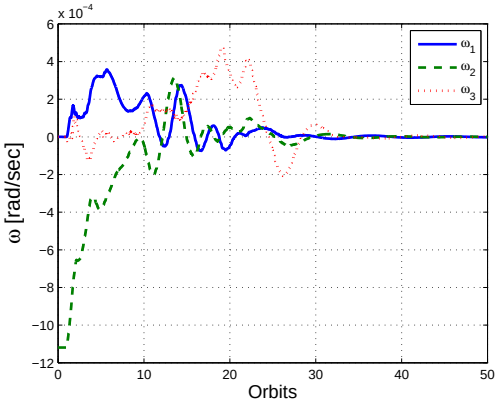

(c) Angular velocity for MIMO RCAC using the average Markov parameter $\tilde{H}$

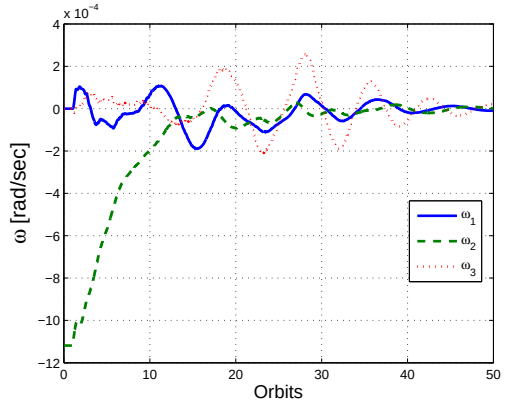

(d) Angular velocity for decentralized RCAC

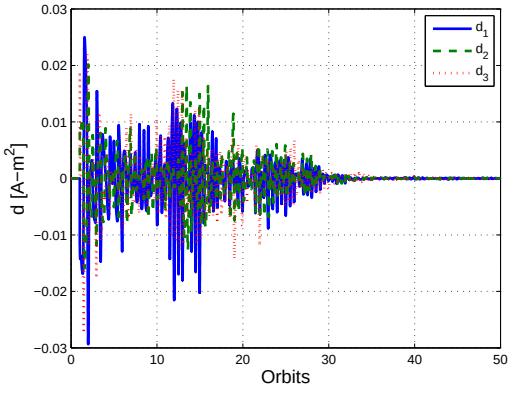

(e) Magnetic dipole for MIMO RCAC using the average Markov parameter $\tilde{H}$

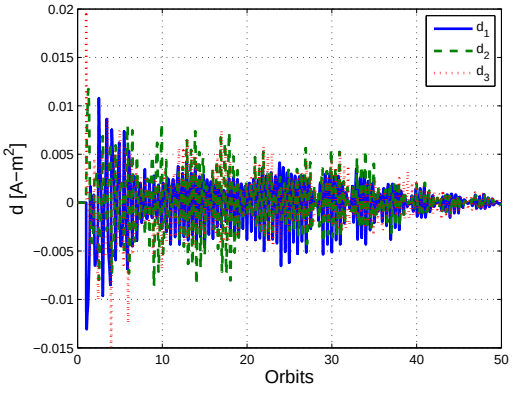

(f) Magnetic dipole for decentralized RCAC

Figure 6.2: Performance comparison of RCAC using the average Markov parameter $\tilde{H}$ versus the decentralized approach for the M2R maneuver for a cylindrical spacecraft with inertia J_{cylinder} in (6.44).

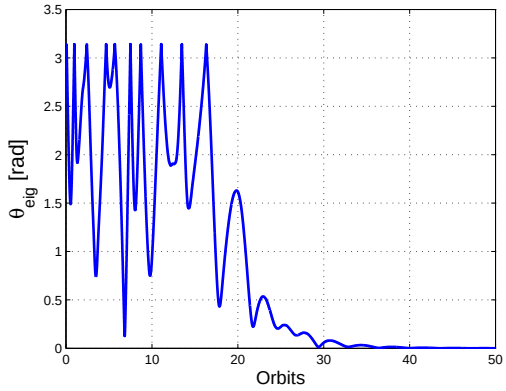

(a) Eigenaxis attitude errorfor MIMO RCAC using the average Markov parameter $\tilde{H}$

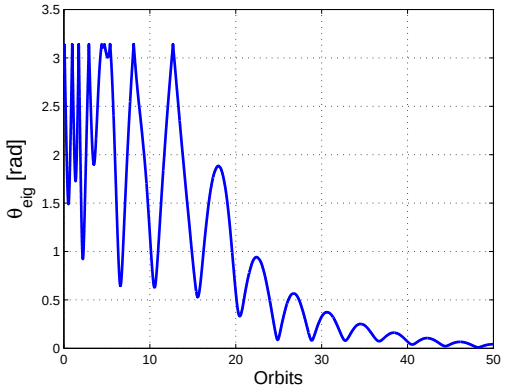

(b) Eigenaxis attitude error for decentralized RCAC

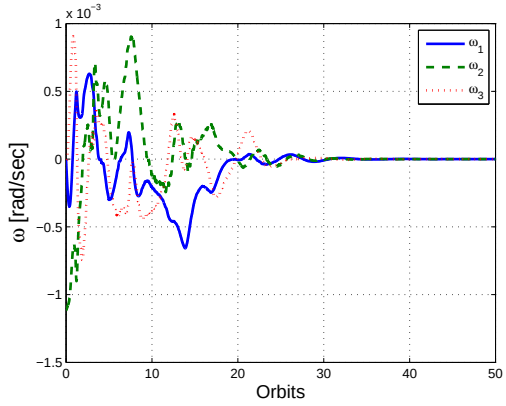

(c) Angular velocity for MIMO RCAC using the average Markov parameter $\tilde{H}$

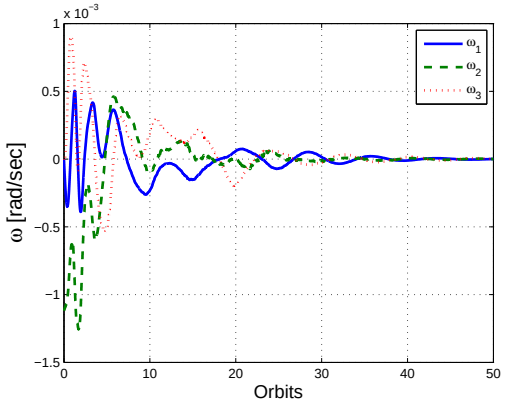

(d) Angular velocity for decentralized RCAC

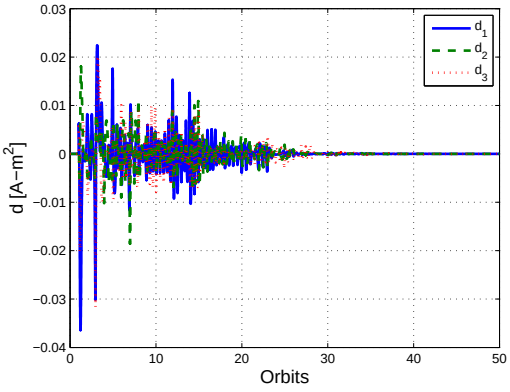

(e) Magnetic dipole for MIMO RCAC using the average Markov parameter $\tilde{H}$

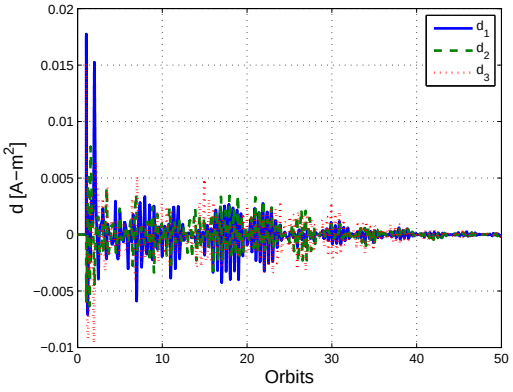

(f) Magnetic dipole for decentralized RCAC

Figure 6.3: Performance comparison of RCAC using the average Markov parameter $\tilde{H}$ versus the decentralized approach for the M2R maneuver for the arbitrary inertia $J_{\text{arbitrary}}$ in (6.45).

The advantage of the centralized controller can be attributed to the information about coupling of the axes in the average input matrix $\tilde{B}_{\rm sc}$. The loss of information caused by decoupling the input and output relations in (6.37) increases the settling time of the decentralized architecture in the presence of the real time input matrix $B_{\rm sc}(t)$.

We can also compare these approaches based on algorithm complexity and execution time. The order of the controller affects the memory requirements and time required to compute each control iteration. This is an important factor for the application of these control laws on small spacecraft. For a controller of order n_c, the averaged Markov parameter method needs to compute $l_u n_c(l_u + l_z) = 27n_c$ parameters. In contrast, the decentralized approach requires $3l_u n_c(l_u+l_z) = 9n_c$ parameters. Thus, the decentralized approach yields similar settling times for M2R maneuvers using a third of the computational cost.

6.4.2 M2S Examples

We command the spacecraft to spin about a body axis aligned in a specific inertial direction. Let the initial angular velocity and attitude of the spacecraft be as in Section6.46.4.1 The desired angular rate

$$\omega_d = 0.001 \begin{bmatrix} 0 & -1 & 0 \end{bmatrix}^{\rm T} \text{ rad/sec} \tag{6.46}$$

corresponds to an Earth-pointing attitude. The desired attitude evolves over time according to $\dot{R}_{\rm d} = R_{\rm d}\omega_{\rm d}^{\times}$ where the initial desired attitude $R_d(0)$ is described by an eigenaxis rotation of $\theta_d(0) = 96$ deg about the vector n_d in (6.42). We set the controller parameters as in Table 6.2. Unlike the M2S examples, we set $\alpha = 1$ in (6.30) and (6.37) and $\epsilon = 5 \times 10^{-5}$ in (6.38).

Figures 6.4 and 6.5 show that the decentralized approach is able to bring the both the spherical and cylindrical spacecraft into a Nadir pointing attitude, that is, a spin about an inertially pointed body axis.

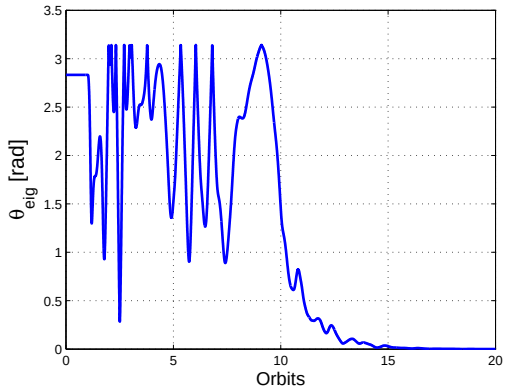

(a) Eigenaxis attitude error for decentralized RCAC

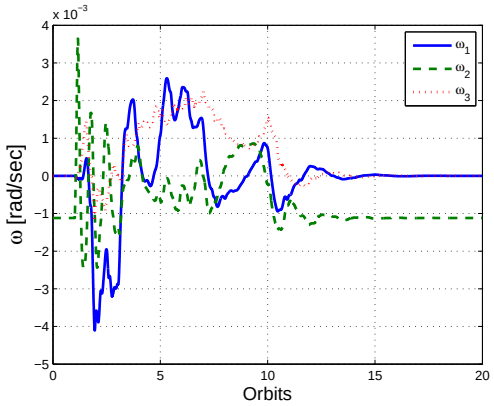

(b) Angular velocity for decentralized RCAC

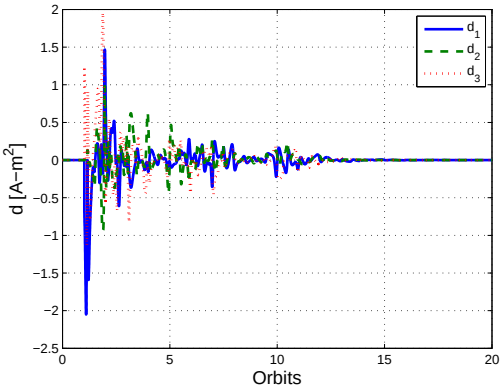

(c) Magnetic dipole for decentralized RCAC

Figure 6.4: Performance of RCAC using the decentralized approach for the M2S maneuver for the spherical spacecraft inertia J_{sphere} in (6.43).

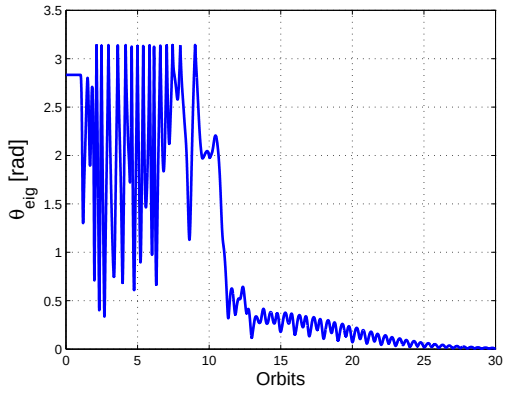

(a) Eigenaxis attitude error for decentralized RCAC

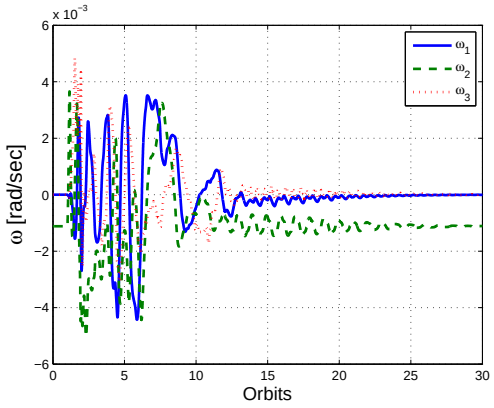

(b) Angular velocity for decentralized RCAC

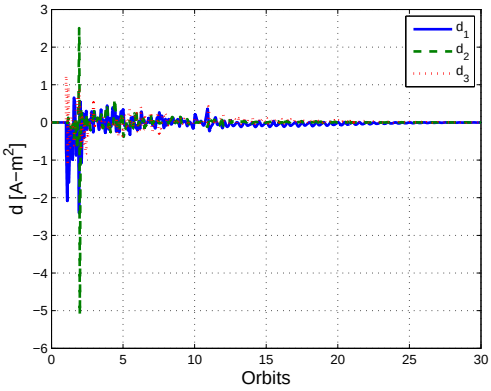

(c) Magnetic dipole for decentralized RCAC

Figure 6.5: Performance of RCAC using the decentralized approach for the M2S maneuver for the cylindrical spacecraft inertia J_{cylinder} in (6.44).

6.5 Conclusions

RCAC was used to control spacecraft angular velocity and attitude using magnetic torque actuators. The torque command computed by RCAC was allocated into magnetic dipoles based on the generalized inverse of the skew symetric cross-product matrix of the magnetic field vector. The Markov parameter for the magnetic torquer-controlled spacecraft was made left invertible through two different approaches, averaging and decentralized control.

Using the averaged Markov parameter an inertia-free control law was developed. Numerical simulations show that the algorithm can achieve a M2R maneuver and bring different spacecraft bus shapes to rest at an inertial attitude.

The decentralized control approach assumes that the sensor and actuator axes are aligned. The three control inputs are computed by independent RCAC controllers using different performance variables. This architecture results in three multi-input, single-output systems with left invertible Markov parameters. The decentralized RCAC approach was also shown to complete the M2R maneuver for different inertias.

Comparison of the numerical results indicate that the averaged Markov parameter approach has better settling time characteristics than the decentralized approach given similar RCAC tunings. However, the decentralized method uses one third of the computational capacity of the averaged Markov parameter approach. Thus, the decentralized method is better suitable for applications where computational capacity is limited and settling time requirements are flexible. Furthermore, the settling time of the decentralized approach could be improved by modifying the performance variable to account for the coupling present in the magnetic control formulation.

CHAPTER 7

Control Moment Gyros

CMG's are typically operated in torque mode, where the desired torque is determined by a separate control law. This torque is then realized by a steering law that commands the angular velocities of each CMG gimbal [90–93]. A difficulty of this approach is the fact that the CMG's may reach a singular configuration in which the torques that can be produced are confined to a plane. This situation manifests itself as a singularity in the input matrix. The singularity prevents the use of the matrix inverse required by some steering laws [94]. This actuation constraint is analogous to the constraint that arises with magnetic torquers. Variable speed CMG's can be used to overcome torque singularities [95], at a cost of greater actuation complexity.

In this chapter we consider spacecraft attitude control with CMG's using RCAC to directly command the gimbal velocities. Previous adaptive methods for single-gimbal CMG's include steering laws as part of the control synthesis to avoid singularities [96]. Other adaptive methods have focused on variable speed [44, 97] or double gimbaled CMG's [98].

The primary objective of this chapter is to assess the performance and robustness of RCAC in the presence of time-varying singularities in the input matrix for velocity-commanded CMG's. Furthermore, we examine the sensitivity to changes in the orientation of the principal axes relative to an arbitrary body-fixed frame. In Section 2, we review the equations of motion of a spacecraft controlled by three orthogonally mounted CMG's; further details are given in [99].

7.1 Spacecraft Model with CMG's

We derive the dynamics of a spacecraft sc consisting of a bus b actuated by n single-gimbal CMG's. For $i = 1, \ldots, n$, CMG_i is composed of wheel w_i mounted on gimbal g_i.

7.1.1 Kinematics

Define an inertial frame $\mathrm{F_I}$, a body frame $\mathrm{F_B}$ fixed to b, a frame $\mathrm{F_{G_i}}$ fixed to g_i, and a frame $\mathrm{F_{W_i}}$ fixed to w_i. The kinematics are described by Poisson's equation

$$\overset{\mathrm{B}\bullet}{\vec{R}}_{\mathrm{B/I}} = \vec{R}_{\mathrm{B/I}} \vec{\omega}^{\times}_{\mathrm{B/I}}, \tag{7.1}$$

where $\mathrm{B}\bullet$ denotes the derivative with respect to $\mathrm{F_B}$, $\vec{R}_{\mathrm{B/I}}$ is the physical rotation matrix that transforms $\mathrm{F_I}$ into $\mathrm{F_B}$, $\vec{\omega}_{\mathrm{B/I}}$ is the angular velocity of $\mathrm{F_B}$ relative to $\mathrm{F_I}$, and the superscript $\times$ denotes the skew-symmetric cross-product matrix.

7.1.2 Dynamics

We specify the following assumptions.

Assumption 1. *The spacecraft bus and wheels are rigid bodies.*

Assumption 2. *The gimbals are massless.*

Assumption 3. *For all $i = 1, \ldots, n$, the center of mass c_i of w_i is fixed in the spacecraft bus.*

Assumption 4. *For all $i = 1, \ldots, n$, w_i is rotationally symmetric about $\hat{\imath}_{\mathrm{W}_i}$.*

Assumption 5. *For all $i = 1, \ldots, n, \mathrm{F_{W_i}}$ spins at a constant speed about $\hat{\imath}_{\mathrm{W}_i}$ relative to $\mathrm{F_{G_i}}$.*

Assumption 6. *For all $i = 1, \ldots, n, \hat{\imath}_{\mathrm{W}_i}$ is fixed in $\mathrm{F_{G_i}}$.*

Assumption 7. *For all $i = 1, \ldots, n$, g_i is angular-velocity commanded about $\hat{\jmath}_{\mathrm{G}_i}$.*

Assumption 8. *For all $i = 1, \ldots, n$, there are no external torques or forces acting on w_i or g_i.*

Assumptions 1, 2, and 3 imply that the center of mass c of the spacecraft is fixed in b. Therefore, the angular momentum $\vec{H}_{\mathrm{b/c/I}}$ of b relative to c with respect to $\mathrm{F_I}$ is given by

$$\vec{H}_{\mathrm{b/c/I}} = \vec{J}_{\mathrm{b/c}} \vec{\omega}_{\mathrm{B/I}}, \tag{7.2}$$

where $\vec{J}_{\mathrm{b/c}}$ is the physical inertia matrix of the spacecraft bus relative to c. The angular momentum $\vec{H}_{\mathrm{w}_i\mathrm{/c/I}}$ of w_i relative to c with respect to $\mathrm{F_I}$ is given by

$$\vec{H}_{\mathrm{w}_i\mathrm{/c/I}} = \vec{H}_{\mathrm{w}_i\mathrm{/c}_i\mathrm{/I}} + \vec{r}_{\mathrm{c}_i\mathrm{/c}} \times m_i \overset{\mathrm{I}\bullet}{\vec{r}}_{\mathrm{c}_i\mathrm{/c}}, \tag{7.3}$$

where $\vec{H}_{\mathrm{w}_i/\mathrm{c}_i/\mathrm{I}}$ is the angular momentum of w_i relative to its the center of mass c_i with respect to F_I, $\vec{r}_{\mathrm{c}_i/\mathrm{c}}$ is the position of c_i relative to c, m_i is the mass of w_i, and $\mathrm{I}\bullet$ denotes the derivative with respect to F_I.

Applying the transport theorem to $\overset{\mathrm{I}\bullet}{\vec{r}}_{\mathrm{c}_i/\mathrm{c}}$ in (7.3) yields

$$\vec{H}_{\mathrm{w}_i/\mathrm{c}/\mathrm{I}} = \vec{H}_{\mathrm{w}_i/\mathrm{c}_i/\mathrm{I}} + \vec{r}_{\mathrm{c}_i/\mathrm{c}} \times m_i \left(\overset{\mathrm{B}\bullet}{\vec{r}}_{\mathrm{c}_i/\mathrm{c}} + \vec{\omega}_{\mathrm{B}/\mathrm{I}} \times \vec{r}_{\mathrm{c}_i/\mathrm{c}} \right), \tag{7.4}$$

where $\mathrm{B}\bullet$ denotes the derivative with respect to F_B. Since both c and c_i are fixed in b, it follows that $\overset{\mathrm{B}\bullet}{\vec{r}}_{\mathrm{c}_i/\mathrm{c}} = 0$. Therefore,

$$\begin{aligned} \vec{H}_{\mathrm{w}_i/\mathrm{c}/\mathrm{I}} &= \vec{H}_{\mathrm{w}_i/\mathrm{c}_i/\mathrm{I}} + m_i \vec{r}_{\mathrm{c}_i/\mathrm{c}} \times \left(\vec{\omega}_{\mathrm{B}/\mathrm{I}} \times \vec{r}_{\mathrm{c}_i/\mathrm{c}} \right) \\ &= \vec{H}_{\mathrm{w}_i/\mathrm{c}_i/\mathrm{I}} - m_i \vec{r}^{\times 2}_{\mathrm{c}_i/\mathrm{c}} \vec{\omega}_{\mathrm{B}/\mathrm{I}}. \end{aligned} \tag{7.5}$$

Since, by Assumption 1, c_i is fixed in w_i, the angular momentum $\vec{H}_{\mathrm{w}_i/\mathrm{c}_i/\mathrm{I}}$ of w_i relative to c_i with respect to F_I is given by

$$\vec{H}_{\mathrm{w}_i/\mathrm{c}_i/\mathrm{I}} = \vec{J}_{\mathrm{w}_i/\mathrm{c}_i} \vec{\omega}_{\mathrm{W}_i/\mathrm{I}}, \tag{7.6}$$

where $\vec{J}_{\mathrm{w}_i/\mathrm{c}_i}$ is the physical inertia matrix of w_i relative to c_i and $\vec{\omega}_{\mathrm{W}_i/\mathrm{I}}$ is the angular velocity of $\mathrm{F}_{\mathrm{W}_i}$ relative to F_I. Expanding $\vec{\omega}_{\mathrm{W}_i/\mathrm{I}}$ in (7.6) yields

$$\vec{H}_{\mathrm{w}_i/\mathrm{c}_i/\mathrm{I}} = \vec{J}_{\mathrm{w}_i/\mathrm{c}_i} \left(\vec{\omega}_{\mathrm{W}_i/\mathrm{B}} + \vec{\omega}_{\mathrm{B}/\mathrm{I}} \right), \tag{7.7}$$

where $\vec{\omega}_{\mathrm{W}_i/\mathrm{B}}$ is the angular velocity of $\mathrm{F}_{\mathrm{W}_i}$ relative to F_B. The angular velocity of $\mathrm{F}_{\mathrm{W}_i}$ relative to F_B is given by

$$\vec{\omega}_{\mathrm{W}_i/\mathrm{B}} = \vec{\omega}_{\mathrm{W}_i/\mathrm{G}_i} + \vec{\omega}_{\mathrm{G}_i/\mathrm{B}}, \tag{7.8}$$

where $\vec{\omega}_{\mathrm{W}_i/\mathrm{G}_i}$ is the angular velocity of $\mathrm{F}_{\mathrm{W}_i}$ relative to $\mathrm{F}_{\mathrm{G}_i}$ and $\vec{\omega}_{\mathrm{G}_i/\mathrm{B}}$ is the angular velocity of $\mathrm{F}_{\mathrm{G}_i}$ relative to F_B. By Assumption 7, the control vector for CMG_i is defined by

$$\vec{u}_i \triangleq \vec{\omega}_{\mathrm{G}_i/\mathrm{B}}. \tag{7.9}$$

Therefore, using (7.8) and (7.9) we rewrite (7.7) as

$$\vec{H}_{\mathrm{w}_i/\mathrm{c}_i/\mathrm{I}} = \vec{J}_{\mathrm{w}_i/\mathrm{c}_i}\left(\vec{\omega}_{\mathrm{W}_i/\mathrm{G}_i} + \vec{u}_i + \vec{\omega}_{\mathrm{B/I}}\right). \tag{7.10}$$

Substituting (7.10) into (7.5) yields

$$\begin{aligned}\vec{H}_{\mathrm{w}_i/\mathrm{c/I}} &= \vec{J}_{\mathrm{w}_i/\mathrm{c}_i}\left(\vec{\omega}_{\mathrm{W}_i/\mathrm{G}_i} + \vec{u}_i + \vec{\omega}_{\mathrm{B/I}}\right) - m_i \vec{r}^{\times 2}_{\mathrm{c}_i/\mathrm{c}}\vec{\omega}_{\mathrm{B/I}} \\ &= \vec{J}_{\mathrm{w}_i/\mathrm{c}_i}\left(\vec{\omega}_{\mathrm{W}_i/\mathrm{G}_i} + \vec{u}_i\right) + \vec{J}_{\mathrm{w}_i/\mathrm{c}}\vec{\omega}_{\mathrm{B/I}},\end{aligned} \tag{7.11}$$

where, by the parallel axis theorem,

$$\vec{J}_{\mathrm{w}_i/\mathrm{c}} = \vec{J}_{\mathrm{w}_i/\mathrm{c}_i} - m_i \vec{r}^{\times 2}_{\mathrm{c}_i/\mathrm{c}}. \tag{7.12}$$

By Assumption 2, the angular momentum $\vec{H}_{\mathrm{g}_i/\mathrm{c/I}}$ of g_i relative to c with respect to $\mathrm{F_I}$ is zero. Therefore, the combined angular momentum $\vec{H}_{\mathrm{sc/c/I}}$ of the bus and CMG's relative to c with respect to $\mathrm{F_I}$ is given by

$$\begin{aligned}\vec{H}_{\mathrm{sc/c/I}} &= \vec{H}_{\mathrm{b/c/I}} + \sum_{i=1}^{n}\vec{H}_{\mathrm{w}_i/\mathrm{c/I}} + \sum_{i=1}^{n}\vec{H}_{\mathrm{g}_i/\mathrm{c/I}} \\ &= \vec{H}_{\mathrm{b/c/I}} + \sum_{i=1}^{n}\vec{H}_{\mathrm{w}_i/\mathrm{c/I}}.\end{aligned} \tag{7.13}$$

Using (7.2) and (7.11) we rewrite (7.13) as

$$\begin{aligned}\vec{H}_{\mathrm{sc/c/I}} &= \vec{J}_{\mathrm{b/c}}\vec{\omega}_{\mathrm{B/I}} + \sum_{i=1}^{n}\left[\vec{J}_{\mathrm{w}_i/\mathrm{c}_i}\left(\vec{\omega}_{\mathrm{W}_i/\mathrm{G}_i} + \vec{u}_i\right) + \vec{J}_{\mathrm{w}_i/\mathrm{c}}\vec{\omega}_{\mathrm{B/I}}\right] \\ &= \vec{J}_{\mathrm{sc/c}}\vec{\omega}_{\mathrm{B/I}} + \sum_{i=1}^{n}\vec{J}_{\mathrm{w}_i/\mathrm{c}_i}\left(\vec{\omega}_{\mathrm{W}_i/\mathrm{G}_i} + \vec{u}_i\right),\end{aligned} \tag{7.14}$$

where

$$\vec{J}_{\mathrm{sc/c}} = \vec{J}_{\mathrm{b/c}} + \sum_{i=1}^{n}\vec{J}_{\mathrm{w}_i/\mathrm{c}}. \tag{7.15}$$

7.1.2.1 Euler's Equation

Let w be a particle that is not subject to any forces. Assumption 1 implies that the center of mass $\mathrm{c_b}$ of b is fixed in b. Thus, the derivative of the left side of (7.2) with respect to $\mathrm{F_I}$

is given by

$$\overset{\mathrm{I}\bullet}{\vec{H}}_{\mathrm{b/c/I}} = -m_{\mathrm{b}}\vec{r}_{\mathrm{c_b/c}}\times \overset{\mathrm{I}\bullet\bullet}{\vec{r}}_{\mathrm{c}/w} + \vec{M}_{\mathrm{b}} + \sum_{i=1}^{n}\vec{M}_{\mathrm{r}_i}, \tag{7.16}$$

where m_{b} is the mass of b, $\vec{r}_{\mathrm{c_b/c}}$ is the position of $\mathrm{c_b}$ relative to c, $\vec{r}_{\mathrm{c}/w}$ is the position of c relative to w, and $\overset{\mathrm{I}\bullet\bullet}{\vec{r}}_{\mathrm{c}/w}$ denotes the second derivative of $\vec{r}_{\mathrm{c}/w}$ with respect to $\mathrm{F_I}$. The sum of all external torques acting on the bus is given by $\vec{M}_{\mathrm{b}}$, and, for $i = 1, \ldots, n$, $\vec{M}_{\mathrm{r}_i}$ is the reaction torque between b and w_i acting on b. Likewise, Assumption 8 implies that the derivative of the left side of (7.11) with respect to $\mathrm{F_I}$ is given by

$$\overset{\mathrm{I}\bullet}{\vec{H}}_{\mathrm{w}_i\mathrm{/c/I}} = -m_i\vec{r}_{\mathrm{c}_i\mathrm{/c}}\times \overset{\mathrm{I}\bullet\bullet}{\vec{r}}_{\mathrm{c}/w} - \vec{M}_{\mathrm{r}_i}. \tag{7.17}$$

Summing (7.17) over all wheels and adding (7.16) yields

$$\begin{aligned}
\overset{\mathrm{I}\bullet}{\vec{H}}_{\mathrm{b/c/I}} + \sum_{i=1}^{n}\overset{\mathrm{I}\bullet}{\vec{H}}_{\mathrm{w}_i\mathrm{/c/I}} &= -m_{\mathrm{b}}\vec{r}_{\mathrm{c_b/c}}\times \overset{\mathrm{I}\bullet\bullet}{\vec{r}}_{\mathrm{c}/w} + \vec{M}_{\mathrm{b}} + \sum_{i=1}^{n}\vec{M}_{\mathrm{r}_i} - \sum_{i=1}^{n}\left(m_i\vec{r}_{\mathrm{c}_i\mathrm{/c}}\times \overset{\mathrm{I}\bullet\bullet}{\vec{r}}_{\mathrm{c}/w} + \vec{M}_{\mathrm{r}_i}\right) \\
&= \vec{M}_{\mathrm{b}} - \left(m_{\mathrm{b}}\vec{r}_{\mathrm{c_b/c}} + \sum_{i=1}^{n} m_i\vec{r}_{\mathrm{c}_i\mathrm{/c}}\right)\times \overset{\mathrm{I}\bullet\bullet}{\vec{r}}_{\mathrm{c}/w} \\
&= \vec{M}_{\mathrm{b}} - m_{\mathrm{sc}}\vec{r}_{\mathrm{c/c}}\times \overset{\mathrm{I}\bullet\bullet}{\vec{r}}_{\mathrm{c}/w} \\
&= \vec{M}_{\mathrm{b}},
\end{aligned} \tag{7.18}$$

where

$$m_{\mathrm{sc}} \triangleq m_{\mathrm{b}} + \sum_{i=1}^{n} m_i, \tag{7.19}$$

the third equality follows from the definition of the center of mass of the spacecraft, and the fourth equality is due to the fact that $\vec{r}_{\mathrm{c/c}} = 0$. Thus, differentiating (7.13) with respect to $\mathrm{F_I}$ and using (7.18) yields

$$\begin{aligned}
\overset{\mathrm{I}\bullet}{\vec{H}}_{\mathrm{sc/c/I}} &= \overset{\mathrm{I}\bullet}{\vec{H}}_{\mathrm{b/c/I}} + \sum_{i=1}^{n}\overset{\mathrm{I}\bullet}{\vec{H}}_{\mathrm{w}_i\mathrm{/c/I}} \\
&= \vec{M}_{\mathrm{b}}.
\end{aligned} \tag{7.20}$$

Applying the transport theorem to the left side of (7.20) yields

$$\overset{\mathrm{I}\bullet}{\vec{H}}_{\mathrm{sc/c/I}} = \overset{\mathrm{B}\bullet}{\vec{H}}_{\mathrm{sc/c/I}} + \vec{\omega}_{\mathrm{B/I}} \times \vec{H}_{\mathrm{sc/c/I}}. \tag{7.21}$$

Hence, (7.20) and (7.21) imply

$$\overset{\mathrm{B}\bullet}{\vec{H}}_{\mathrm{sc/c/I}} + \vec{\omega}_{\mathrm{B/I}} \times \vec{H}_{\mathrm{sc/c/I}} = \vec{M}_{\mathrm{b}}, \tag{7.22}$$

which is Euler's equation for the spacecraft.

7.1.2.2 Body-frame Derivatives

Differentiating (7.13) with respect to $\mathrm{F_B}$ yields

$$\overset{\mathrm{B}\bullet}{\vec{H}}_{\mathrm{sc/c/I}} = \overset{\mathrm{B}\bullet}{\vec{H}}_{\mathrm{b/c/I}} + \sum_{i=1}^{n} \overset{\mathrm{B}\bullet}{\vec{H}}_{\mathrm{w}_i\mathrm{/c/I}}. \tag{7.23}$$

Since, by Assumption 1, the inertia $\vec{J}_{\mathrm{b/c}}$ is constant with respect to $\mathrm{F_B}$, differentiating (7.2) with respect to $\mathrm{F_B}$ yields

$$\overset{\mathrm{B}\bullet}{\vec{H}}_{\mathrm{b/c/I}} = \vec{J}_{\mathrm{b/c}} \overset{\mathrm{B}\bullet}{\vec{\omega}}_{\mathrm{B/I}} . \tag{7.24}$$

Furthermore, differentiating (7.11) with respect to $\mathrm{F_B}$ and using (7.12) yields

$$\begin{aligned} \overset{\mathrm{B}\bullet}{\vec{H}}_{\mathrm{w}_i\mathrm{/c/I}} = {} & \overset{\mathrm{B}\bullet}{\vec{J}}_{\mathrm{w}_i\mathrm{/c}_i} \left(\vec{\omega}_{\mathrm{W}_i\mathrm{/G}_i} + \vec{u}_i \right) + \vec{J}_{\mathrm{w}_i\mathrm{/c}_i} \left(\overset{\mathrm{B}\bullet}{\vec{\omega}}_{\mathrm{W}_i\mathrm{/G}_i} + \overset{\mathrm{B}\bullet}{\vec{u}}_i \right) \\ & + \left(\overset{\mathrm{B}\bullet}{\vec{J}}_{\mathrm{w}_i\mathrm{/c}_i} - m_i \overset{\mathrm{B}\bullet}{\overbrace{\vec{r}^{\times 2}_{\mathrm{c}_i\mathrm{/c}}}} \right) \vec{\omega}_{\mathrm{B/I}} + \vec{J}_{\mathrm{w}_i\mathrm{/c}} \overset{\mathrm{B}\bullet}{\vec{\omega}}_{\mathrm{B/I}} . \end{aligned} \tag{7.25}$$

Using (7.9), the derivative of $\vec{J}_{\mathrm{w}_i\mathrm{/c}_i}$ with respect to $\mathrm{F_B}$ is given by

$$\begin{aligned} \overset{\mathrm{B}\bullet}{\vec{J}}_{\mathrm{w}_i\mathrm{/c}_i} &= \overset{\mathrm{G}_i\bullet}{\vec{J}}_{\mathrm{w}_i\mathrm{/c}_i} + \vec{\omega}^{\times}_{\mathrm{G}_i\mathrm{/B}} \vec{J}_{\mathrm{w}_i\mathrm{/c}_i} - \vec{J}_{\mathrm{w}_i\mathrm{/c}_i} \vec{\omega}^{\times}_{\mathrm{G}_i\mathrm{/B}} \\ &= \vec{\omega}^{\times}_{\mathrm{G}_i\mathrm{/B}} \vec{J}_{\mathrm{w}_i\mathrm{/c}_i} - \vec{J}_{\mathrm{w}_i\mathrm{/c}_i} \vec{\omega}^{\times}_{\mathrm{G}_i\mathrm{/B}} \\ &= \vec{u}^{\times}_i \vec{J}_{\mathrm{w}_i\mathrm{/c}_i} - \vec{J}_{\mathrm{w}_i\mathrm{/c}_i} \vec{u}^{\times}_i , \end{aligned} \tag{7.26}$$

where $\overset{\mathrm{G}_i\bullet}{\vec{J}}_{\mathrm{w}_i/\mathrm{c}_i} = 0$ due to Assumptions 1, 5. Furthermore, Assumptions 5 and 6 imply that $\overset{\mathrm{G}_i\bullet}{\vec{\omega}}_{\mathrm{W}_i/\mathrm{G}_i} = 0$. Thus, using (7.9), the angular acceleration of $\mathrm{F}_{\mathrm{W}_i}$ relative to $\mathrm{F}_{\mathrm{G}_i}$ with respect to F_{B} is given by

$$\begin{aligned}\overset{\mathrm{B}\bullet}{\vec{\omega}}_{\mathrm{W}_i/\mathrm{G}_i} &= \overset{\mathrm{G}_i\bullet}{\vec{\omega}}_{\mathrm{W}_i/\mathrm{G}_i} + \vec{\omega}_{\mathrm{G}_i/\mathrm{B}} \times \vec{\omega}_{\mathrm{W}_i/\mathrm{G}_i} \\ &= \vec{\omega}_{\mathrm{G}_i/\mathrm{B}} \times \vec{\omega}_{\mathrm{W}_i/\mathrm{G}_i} \\ &= \vec{u}_i^{\times} \vec{\omega}_{\mathrm{W}_i/\mathrm{G}_i}. \end{aligned} \tag{7.27}$$

Since $\overset{\mathrm{B}\bullet}{\vec{r}}_{\mathrm{c}_i/\mathrm{c}} = 0$, the derivative of the cross term in (7.25) with respect to F_{B} is given by

$$\begin{aligned}\overbrace{\vec{r}_{\mathrm{c}_i/\mathrm{c}}^{\times 2}}^{\mathrm{B}\bullet} &= \vec{r}_{\mathrm{c}_i/\mathrm{c}}^{\times} \overbrace{\vec{r}_{\mathrm{c}_i/\mathrm{c}}^{\times}}^{\mathrm{B}\bullet} + \overbrace{\vec{r}_{\mathrm{c}_i/\mathrm{c}}^{\times}}^{\mathrm{B}\bullet} \vec{r}_{\mathrm{c}_i/\mathrm{c}}^{\times} \\ &= \vec{r}_{\mathrm{c}_i/\mathrm{c}}^{\times} \left(\overset{\mathrm{B}\bullet}{\vec{r}}_{\mathrm{c}_i/\mathrm{c}} \right)^{\times} + \left(\overset{\mathrm{B}\bullet}{\vec{r}}_{\mathrm{c}_i/\mathrm{c}} \right)^{\times} \vec{r}_{\mathrm{c}_i/\mathrm{c}}^{\times} \\ &= 0. \end{aligned} \tag{7.28}$$

Therefore, substituting (7.26), (7.27), and (7.28) into (7.25) yields the derivative of (7.11) with respect to F_{B}, that is,

$$\begin{aligned}\overset{\mathrm{B}\bullet}{\vec{H}}_{\mathrm{w}_i/\mathrm{c}/\mathrm{I}} &= \left(\vec{u}_i^{\times} \vec{J}_{\mathrm{w}_i/\mathrm{c}_i} - \vec{J}_{\mathrm{w}_i/\mathrm{c}_i} \vec{u}_i^{\times} \right) \left(\vec{\omega}_{\mathrm{B}/\mathrm{I}} + \vec{\omega}_{\mathrm{W}_i/\mathrm{G}_i} + \vec{u}_i \right) + \vec{J}_{\mathrm{w}_i/\mathrm{c}_i} \left(\vec{u}_i^{\times} \vec{\omega}_{\mathrm{W}_i/\mathrm{G}_i} + \overset{\mathrm{B}\bullet}{\vec{u}}_i \right) \\ &\quad + \vec{J}_{\mathrm{w}_i/\mathrm{c}} \overset{\mathrm{B}\bullet}{\vec{\omega}}_{\mathrm{B}/\mathrm{I}} \\ &= \left(\vec{u}_i^{\times} \vec{J}_{\mathrm{w}_i/\mathrm{c}_i} - \vec{J}_{\mathrm{w}_i/\mathrm{c}_i} \vec{u}_i^{\times} \right) \vec{\omega}_{\mathrm{B}/\mathrm{I}} + \vec{u}_i^{\times} \vec{J}_{\mathrm{w}_i/\mathrm{c}_i} \left(\vec{\omega}_{\mathrm{W}_i/\mathrm{G}_i} + \vec{u}_i \right) \\ &\quad + \vec{J}_{\mathrm{w}_i/\mathrm{c}_i} \overset{\mathrm{B}\bullet}{\vec{u}}_i + \vec{J}_{\mathrm{w}_i/\mathrm{c}} \overset{\mathrm{B}\bullet}{\vec{\omega}}_{\mathrm{B}/\mathrm{I}}. \end{aligned} \tag{7.29}$$

7.1.2.3 Resolving the Equations of Motion in F_{B}

Resolving Poisson's equation (7.1) in F_{B} yields

$$\dot{R} = \frac{\mathrm{d}}{\mathrm{d}t} \left(\vec{R}_{\mathrm{B}/\mathrm{I}} \Big|_{\mathrm{B}} \right) = \overset{\mathrm{B}\bullet}{\vec{R}}_{\mathrm{B}/\mathrm{I}} \Big|_{\mathrm{B}} = \vec{R}_{\mathrm{B}/\mathrm{I}} \Big|_{\mathrm{B}} \vec{\omega}_{\mathrm{B}/\mathrm{I}} \Big|_{\mathrm{B}}^{\times} = R\omega^{\times}, \tag{7.30}$$

where

$$R \triangleq \vec{R}_{\mathrm{B/I}}\Big|_{\mathrm{B}}, \qquad \omega \triangleq \vec{\omega}_{\mathrm{B/I}}\Big|_{\mathrm{B}}. \tag{7.31}$$

Resolving (7.2) in $\mathrm{F_B}$ yields

$$\vec{H}_{\mathrm{b/c/I}}\Big|_{\mathrm{B}} = J_{\mathrm{b}}\omega, \tag{7.32}$$

where

$$J_{\mathrm{b}} \triangleq \vec{J}_{\mathrm{b/c}}\Big|_{\mathrm{B}}. \tag{7.33}$$

Furthermore, resolving (7.24) in $\mathrm{F_B}$ yields

$$\overset{\mathrm{B}\bullet}{\vec{H}}_{\mathrm{b/c/I}}\Big|_{\mathrm{B}} = \frac{\mathrm{d}}{\mathrm{d}t}\left(\vec{H}_{\mathrm{b/c/I}}\Big|_{\mathrm{B}}\right) = J_{\mathrm{b}}\dot{\omega}, \tag{7.34}$$

where

$$\dot{\omega} = \frac{\mathrm{d}\omega}{\mathrm{d}t} = \overset{\mathrm{B}\bullet}{\vec{\omega}}_{\mathrm{B/I}}\Big|_{\mathrm{B}}. \tag{7.35}$$

Using Figure 7.1 and Assumptions 4, 5, and 6 to resolve the angular velocity and acceleration of w_i and g_i in $\mathrm{F}_{\mathrm{G}_i}$ yields

$$\vec{\omega}_{\mathrm{W}_i/\mathrm{G}_i}\Big|_{\mathrm{G}_i} = \nu_i e_1, \quad \vec{u}_i\Big|_{\mathrm{G}_i} = \vec{\omega}_{\mathrm{G}_i/\mathrm{B}}\Big|_{\mathrm{G}_i} = u_i e_2, \quad \overset{\mathrm{G}_i\bullet}{\vec{u}_i}\Big|_{\mathrm{G}_i} = \dot{u}_i e_2, \tag{7.36}$$

where e_i is the ith column of the 3×3 identity matrix I_3, u_i is the scalar control command for CMG_i, and $\nu_i > 0$ is the spin rate of w_i about $\hat{\imath}_{\mathrm{W}_i}$ relative to $\mathrm{F}_{\mathrm{G}_i}$. Furthermore, Figure 1 and Assumptions 4 and 6 imply that the inertia matrix of w_i relative to c_i resolved in both $\mathrm{F}_{\mathrm{G}_i}$ and $\mathrm{F}_{\mathrm{W}_i}$ is given by

$$J_i \triangleq \vec{J}_{\mathrm{w}_i/\mathrm{c}_i}\Big|_{\mathrm{G}_i} = \vec{J}_{\mathrm{w}_i/\mathrm{c}_i}\Big|_{\mathrm{W}_i} = \begin{bmatrix} \alpha_i & 0 & 0 \\ 0 & \beta_i & 0 \\ 0 & 0 & \beta_i \end{bmatrix}, \tag{7.37}$$

where α_i is the moment of inertia of w_i about the spin axis and β_i is the moment of inertia

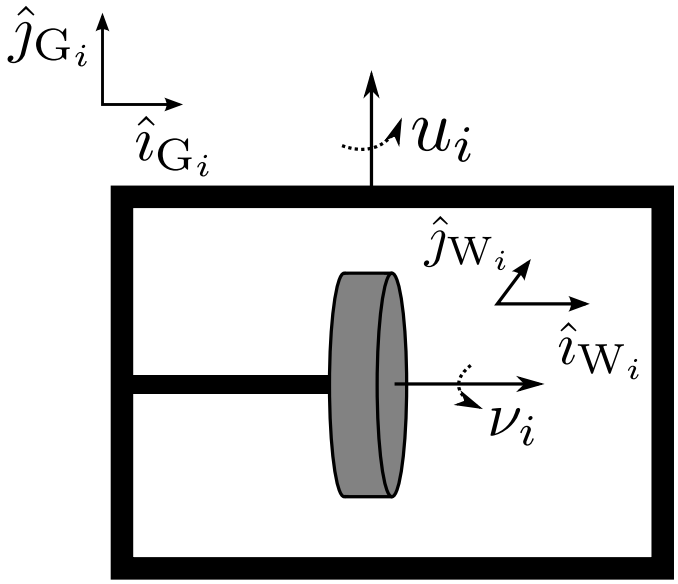

Figure 7.1: Wheel w_i mounted on gimbal g_i with frames $\mathrm{F}_{\mathrm{W}_i}$ and $\mathrm{F}_{\mathrm{G}_i}$. The wheel spins about $\hat{\imath}_{\mathrm{W}_i}$ with constant angular speed $\nu_i > 0$ relative to $\mathrm{F}_{\mathrm{G}_i}$. The gimbal angular velocity command u_i is about $\hat{\jmath}_{\mathrm{G}_i}$. Note that $\hat{\imath}_{\mathrm{W_i}}$ is aligned with $\hat{\imath}_{\mathrm{G_i}}$

about the remaining axes of $\mathrm{F}_{\mathrm{W}_i}$ and $\mathrm{F}_{\mathrm{G}_i}$.

Resolving (7.36) and (7.37) in F_{B} yields

$$\vec{\omega}_{\mathrm{W}_i/\mathrm{G}_i}\Big|_{\mathrm{B}} = \nu_i \mathcal{O}_i e_1, \qquad \vec{u}_i\Big|_{\mathrm{B}} = u_i \mathcal{O}_i e_2, \qquad \overset{\mathrm{G}_i\bullet}{\vec{u}_i}\Big|_{\mathrm{B}} = \dot{u}_i \mathcal{O}_i e_2, \tag{7.38}$$

$$\vec{J}_{\mathrm{w}_i/\mathrm{c}_i}\Big|_{\mathrm{B}} = \mathcal{O}_i \, \vec{J}_{\mathrm{w}_i/\mathrm{c}_i}\Big|_{\mathrm{G}_i} \mathcal{O}_i^{\mathrm{T}} = \mathcal{O}_i J_i \mathcal{O}_i^{\mathrm{T}}, \tag{7.39}$$

where $\mathcal{O}_i$ transforms a vector resolved in $\mathrm{F}_{\mathrm{G}_i}$ into the same vector resolved in F_{B}. The orientation matrix $\mathcal{O}_i$ is given by

$$\mathcal{O}_i \triangleq \vec{R}_{\mathrm{G}_i/\mathrm{B}}\Big|_{\mathrm{G}_i} \tag{7.40}$$

where $\vec{R}_{\mathrm{G}_i/\mathrm{B}}$ is the physical rotation matrix that transforms F_{B} into $\mathrm{F}_{\mathrm{G}_i}$. Define a reference

gimbal frame $\mathrm{F}_{\mathrm{G}_i'}$ which is fixed relative to F_{B}, then (7.40) can be rewritten as

$$\mathcal{O}_i = \overrightarrow{R}_{\mathrm{G}_i/\mathrm{G}_i'}\Big|_{\mathrm{G}_i} \overrightarrow{R}_{\mathrm{G}_i'/\mathrm{B}}\Big|_{\mathrm{G}_i} = \mathcal{O}_i' \begin{bmatrix} \cos\theta_i & 0 & \sin\theta_i \\ 0 & 1 & 0 \\ -\sin\theta_i & 0 & \cos\theta_i \end{bmatrix}, \tag{7.41}$$

where $\overrightarrow{R}_{\mathrm{G}_i'/\mathrm{B}}$ is the physical rotation matrix that transforms F_{B} into $\mathrm{F}_{\mathrm{G}_i'}$, θ_i is the gimbal angle that rotates $\mathrm{F}_{\mathrm{G}_i'}$ into $\mathrm{F}_{\mathrm{G}_i}$, and

$$\mathcal{O}_i' \triangleq \overrightarrow{R}_{\mathrm{G}_i'/\mathrm{B}}\Big|_{\mathrm{B}}. \tag{7.42}$$

Note that

$$\dot{\mathcal{O}}_i = \overset{\mathrm{G}_i\bullet}{\overrightarrow{R}}_{\mathrm{G}_i/\mathrm{B}}\Big|_{\mathrm{G}_i} = u_i \mathcal{O}_i e_2^{\times}, \tag{7.43}$$

$$\dot{\theta}_i = \frac{\mathrm{d}\theta_i}{\mathrm{d}t} = u_i. \tag{7.44}$$

Resolving (7.11) in F_{B} and using the fact that $\mathcal{O}_i^{\mathrm{T}}\mathcal{O}_i = I_3$ yields

$$\begin{aligned} \overrightarrow{H}_{\mathrm{w}_i/\mathrm{c}/\mathrm{I}}\Big|_{\mathrm{B}} &= \mathcal{O}_i J_i \mathcal{O}_i^{\mathrm{T}} \left(\nu_i \mathcal{O}_i e_1 + u_i \mathcal{O}_i e_2\right) + \left(\mathcal{O}_i J_i \mathcal{O}_i^{\mathrm{T}} - m_i r_i^{\times 2}\right)\omega \\ &= \mathcal{O}_i \left(\nu_i J_i e_1 + u_i J_i e_2\right) + J_i'\omega \\ &= \mathcal{O}_i \left(\alpha_i \nu_i e_1 + \beta_i u_i e_2\right) + J_i'\omega, \end{aligned} \tag{7.45}$$

where

$$J_i' \triangleq \overrightarrow{J}_{\mathrm{w}_i/\mathrm{c}}\Big|_{\mathrm{B}} = \mathcal{O}_i J_i \mathcal{O}_i^{\mathrm{T}} - m_i r_i^{\times 2}, \qquad r_i \triangleq \overrightarrow{r}_{\mathrm{c}_i/\mathrm{c}}\Big|_{\mathrm{B}}. \tag{7.46}$$

Using (7.119) to resolve the sum in (7.13) in $\mathrm{F_B}$ yields

$$\begin{aligned}\sum_{i=1}^{n} \vec{H}_{\mathrm{w}_i/\mathrm{c/I}}\Big|_{\mathrm{B}} &= \sum_{i=1}^{n} \left[\mathcal{O}_i \left(\alpha_i \nu_i e_1 + \beta_i u_i e_2\right) + J_i' \omega\right] \\ &= \sum_{i=1}^{n} \left(\alpha_i \nu_i \mathcal{O}_i e_1 + B_{1i} u_i + J_i' \omega\right) \\ &= \sum_{i=1}^{n} \left(\alpha_i \nu_i \mathcal{O}_i e_1 + J_i' \omega\right) + B_1 u, \end{aligned} \tag{7.47}$$

where,

$$u \triangleq \dot{\theta} = \begin{bmatrix} \dot{\theta}_1 \\ \vdots \\ \dot{\theta}_n \end{bmatrix} = \begin{bmatrix} u_1 \\ \vdots \\ u_n \end{bmatrix}, \tag{7.48}$$

and, for $i = 1, \ldots, n$, the ith column of $B_1 \in \mathbb{R}^{3\times n}$ is given by

$$B_{1i} \triangleq \beta_i \mathcal{O}_i e_2 = \beta_i \mathcal{O}_i' e_2 \in \mathbb{R}^{3\times 1}. \tag{7.49}$$

Note that B_{1i} does not change as the gimbals rotate.

The derivative of (7.119) is given by (7.29) resolved in $\mathrm{F_B}$, that is,

$$\begin{aligned}\frac{\mathrm{d}}{\mathrm{d}t}\left(\vec{H}_{\mathrm{w}_i/\mathrm{c/I}}\Big|_{\mathrm{B}}\right) &= \overset{\mathrm{B}\bullet}{\vec{H}}_{\mathrm{w}_i/\mathrm{c/I}}\Big|_{\mathrm{B}} \\ &= \mathcal{O}_i \left[(u_i e_2)^{\times} J_i - J_i (u_i e_2)^{\times}\right] \mathcal{O}_i^{\mathrm{T}} \omega \\ &\quad + (\mathcal{O}_i u_i e_2)^{\times} \mathcal{O}_i J_i \mathcal{O}_i^{\mathrm{T}} \left(u_i \mathcal{O}_i e_2 + \nu_i \mathcal{O}_i e_1\right) + \mathcal{O}_i J_i \mathcal{O}_i^{\mathrm{T}} \dot{u}_i \mathcal{O}_i e_2 + J_i' \dot{\omega} \\ &= u_i \mathcal{O}_i \left(e_2^{\times} J_i - J_i e_2^{\times}\right) \mathcal{O}_i^{\mathrm{T}} \omega + \mathcal{O}_i (u_i e_2)^{\times} \mathcal{O}_i^{\mathrm{T}} \mathcal{O}_i J_i \left(u_i e_2 + \nu_i e_1\right) \\ &\quad + \dot{u}_i \mathcal{O}_i J_i e_2 + J_i' \dot{\omega} \\ &= u_i \mathcal{O}_i \left(e_2^{\times} J_i - J_i e_2^{\times}\right) \mathcal{O}_i^{\mathrm{T}} \omega + u_i \mathcal{O}_i e_2^{\times} \left(u_i J_i e_2 + \nu_i J_i e_1\right) \\ &\quad + \dot{u}_i \mathcal{O}_i J_i e_2 + J_i' \dot{\omega} \\ &= u_i \mathcal{O}_i \left(e_2^{\times} J_i - J_i e_2^{\times}\right) \mathcal{O}_i^{\mathrm{T}} \omega + u_i \mathcal{O}_i \left(e_2^{\times} \beta_i u_i e_2 + e_2^{\times} \alpha_i \nu_i e_1\right) \\ &\quad + \dot{u}_i \mathcal{O}_i \beta_i e_2 + J_i' \dot{\omega} \\ &= u_i \mathcal{O}_i \left(e_2^{\times} J_i - J_i e_2^{\times}\right) \mathcal{O}_i^{\mathrm{T}} \omega - u_i \alpha_i \nu_i \mathcal{O}_i e_3 + \beta_i \dot{u}_i \mathcal{O}_i e_2 + J_i' \dot{\omega} \\ &= \left[\mathcal{O}_i \left(e_2^{\times} J_i - J_i e_2^{\times}\right) \mathcal{O}_i^{\mathrm{T}} \omega - \alpha_i \nu_i \mathcal{O}_i e_3\right] u_i + \beta_i \dot{u}_i \mathcal{O}_i e_2 + J_i' \dot{\omega}. \end{aligned} \tag{7.50}$$

Using (7.50) to resolve the sum in (7.23) in $\mathrm{F_B}$ yields

$$\sum_{i=1}^{n} \overset{\mathrm{B}\bullet}{\vec{H}}_{\mathrm{w}_i/\mathrm{c/I}}\Big|_{\mathrm{B}} = \sum_{i=1}^{n} J_i'\dot{\omega} + B_{1i}\dot{u}_i + B_{2i}u_i$$
$$= \sum_{i=1}^{n} J_i'\dot{\omega} + B_1\dot{u} + B_2 u, \tag{7.51}$$

where, for $i = 1, \ldots, n$, the ith column of $B_2 \in \mathbb{R}^{3\times n}$ is given by

$$B_{2i} \triangleq \mathcal{O}_i \left(e_2^{\times} J_i - J_i e_2^{\times}\right) \mathcal{O}_i^{\mathrm{T}}\omega - \alpha_i\nu_i\mathcal{O}_i e_3 \in \mathbb{R}^{3\times 1}, \tag{7.52}$$

Using (7.32) and (7.47) to resolve (7.13) in $\mathrm{F_B}$ yields

$$H_{\mathrm{sc}} \triangleq \vec{H}_{\mathrm{sc/c/I}}\Big|_{\mathrm{B}} = J\omega + \sum_{i=1}^{n} \alpha_i\nu_i\mathcal{O}_i e_1 + B_1 u, \tag{7.53}$$

where, using (7.15),

$$J \triangleq \vec{J}_{\mathrm{sc/c}}\Big|_{\mathrm{B}} = J_{\mathrm{b}} + \sum_{i=1}^{n} J_i'. \tag{7.54}$$

Using (7.34) and (7.51) to resolve (7.23) in $\mathrm{F_B}$ yields

$$\dot{H}_{\mathrm{sc}} = \frac{\mathrm{d}}{\mathrm{d}t}\left(\vec{H}_{\mathrm{sc/c/I}}\Big|_{\mathrm{B}}\right) = \overset{\mathrm{B}\bullet}{\vec{H}}_{\mathrm{sc/c/I}}\Big|_{\mathrm{B}} = J\dot{\omega} + B_1\dot{u} + B_2 u. \tag{7.55}$$

Resolving (7.22) in $\mathrm{F_B}$ using (7.53) and (7.55) yields

$$J\dot{\omega} + B_1\dot{u} + B_2 u = -\omega \times \left(J\omega + \sum_{i=1}^{n} \alpha_i\nu_i\mathcal{O}_i e_1 + B_1 u\right) + \tau, \tag{7.56}$$

where

$$\tau \triangleq \vec{M}_{\mathrm{sc}}\Big|_{\mathrm{B}}. \tag{7.57}$$

Rearranging (7.56) yields the dynamics for a spacecraft actuated by n velocity-commanded,

single-gimbal, fixed-speed CMG's, that is,

$$J\dot{\omega} = -\omega^{\times}\left(J\omega + \sum_{i=1}^{n} \alpha_i \nu_i \mathcal{O}_i e_1\right) + B_{\rm sc}u - B_1\dot{u} + \tau, \tag{7.58}$$

where

$$B_{\rm sc} \triangleq -\left(\omega^{\times}B_1 + B_2\right) \in \mathbb{R}^{3\times n}. \tag{7.59}$$

Note that J and $B_{\rm sc}$ depend on $\mathcal{O}_i$ as shown by (7.46), (7.54) and (7.49), (7.52), and (7.59), respectively. The orientation matrix $\mathcal{O}_i$ depends on the control u_i due to the kinematics (7.41). Thus, both J and $B_{\rm sc}$ are possibly time-varying.

7.1.3 Special Cases

We explore two special cases, namely, a spacecraft with three orthogonally arranged gimbals and gimbal configurations that result in constant spacecraft inertia.

7.1.3.1 Orthogonal 3-gimbal Configuration

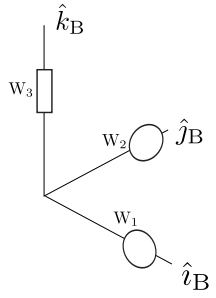

Figure 7.2: Sketch of 3-gimbal arrangement.

Consider a spacecraft actuated by $m = 3$ gimbals arranged in an orthogonal configuration as shown in Figure 7.2. The gimbals are arranged such that

$$\hat{\jmath}_{\rm G_1} = \hat{\imath}_{\rm B}, \quad \hat{\jmath}_{\rm G_2} = \hat{\jmath}_{\rm B}, \quad \hat{\jmath}_{\rm G_3} = \hat{k}_{\rm B}. \tag{7.60}$$

The orientation matrices corresponding to this gimbal arrangement are given by

$$\mathcal{O}_1 = \mathcal{R}(\frac{\pi}{2}, e_3)\mathcal{R}(\theta_1, e_2)^{\rm T}, \quad \mathcal{O}_2 = \mathcal{R}(\frac{\pi}{2}, e_2)\mathcal{R}(\theta_2, e_2)^{\rm T}, \quad \mathcal{O}_3 = \mathcal{R}(-\frac{\pi}{2}, e_1)\mathcal{R}(\theta_3, e_2)^{\rm T}, \tag{7.61}$$

where, given an eigenaxis $n_{\mathrm{e}} \in \mathbb{R}^3$ and an eigenangle $\theta_{\mathrm{e}} \in (-\pi, \pi]$,

$$\mathcal{R}(\theta_{\mathrm{e}}, n_{\mathrm{e}}) \stackrel{\triangle}{=} I_3 \cos\theta_{\mathrm{e}} + n_{\mathrm{e}} n_{\mathrm{e}}^{\mathrm{T}} (1 - \cos\theta_{\mathrm{e}}) - n_{\mathrm{e}}^{\times} \sin\theta_{\mathrm{e}}. \tag{7.62}$$

Consequently, for $i = 1, 2, 3$, the arrangement in (7.61) yields

$$\mathcal{O}_i e_2 = e_i. \tag{7.63}$$

Thus, the ith column of B_1 is given by

$$B_{1i} = \beta_i \mathcal{O}_i e_2 = \beta_i e_i, \tag{7.64}$$

and thus

$$B_1 = \left[\begin{array}{ccc} \beta_1 e_1 & \beta_2 e_2 & \beta_2 e_3 \end{array} \right]. \tag{7.65}$$

Furthermore, if $\beta_1 = \beta_2 = \beta_3 = \bar{\beta}$, then

$$B_1 = \bar{\beta} I_3. \tag{7.66}$$

7.1.3.2 Constant Spacecraft Inertia

Assume that, for all $i = 1, \ldots, n$, $\alpha_i = \beta_i$. Then, the wheel inertia resolved in $\mathrm{F}_{\mathrm{G}_i}$ and $\mathrm{F}_{\mathrm{W}_i}$ is given by

$$J_{\mathrm{w}_i}|_{\mathrm{G}_i} = J_{\mathrm{w}_i}|_{\mathrm{W}_i} = \alpha_i I_3. \tag{7.67}$$

Thus,

$$\vec{J}_{\mathrm{w}_i/\mathrm{c}_i}\Big|_{\mathrm{B}} = \mathcal{O}_i \, \vec{J}_{\mathrm{w}_i/\mathrm{c}_i}\Big|_{\mathrm{G}_i} \mathcal{O}_i^{\mathrm{T}} = \mathcal{O}_i \left(\alpha_i I_3\right) \mathcal{O}_i^{\mathrm{T}} = \alpha_i I_3 \tag{7.68}$$

and

$$J_i' = \mathcal{O}_i J_i \mathcal{O}_i^{\mathrm{T}} - m_i r_i^{\times 2} = \alpha_i I_3 - m_i r_i^{\times 2} \tag{7.69}$$

are constant. Consequently, the spacecraft inertia (7.54) relative to c resolved in $\mathrm{F_B}$ is given by

$$J = J_{\mathrm{b}} + \sum_{i=1}^{n} J_i' = J_{\mathrm{b}} + \sum_{i=1}^{n} \left(\alpha_i I_3 - m_i r_i^{\times 2} \right), \tag{7.70}$$

which is constant. The special case of spherical wheels is considered in [74].

Furthermore, the ith columns of B_1 and B_2 are given by

$$B_{1i} = \alpha_i \mathcal{O}_i e_2, \tag{7.71}$$

$$B_{2i} = \mathcal{O}_i \left[e_2^{\times} \left(\alpha_i I_3 \right) - \left(\alpha_i I_3 \right) e_2^{\times} \right] \mathcal{O}_i^{\mathrm{T}} \omega - \alpha_i \nu_i \mathcal{O}_i e_3 = -\alpha_i \nu_i \mathcal{O}_i e_3. \tag{7.72}$$

Therefore, the ith column of B_{sc} is given by

$$B_{\mathrm{sc},i} = -\left(\omega^{\times} B_{1i} + B_{2i} \right) = \alpha_i \left(\nu_i \mathcal{O}_i e_3 - \omega^{\times} \mathcal{O}_i e_2 \right). \tag{7.73}$$

If, in addition, the wheel speeds are much larger than the norm of the spacecraft angular velocity, that is, $|\nu_i| >> \|\omega\|_\infty$, then (7.73) implies that

$$B_{\mathrm{sc},i} \approx \alpha_i \nu_i \mathcal{O}_i e_3. \tag{7.74}$$

The simplified input matrix (7.74) is the Jacobian typically used in the CMG literature to formulate steering laws and analyze singularities [90, 91, 94].

7.1.4 Reachable Attitudes

Although singularities do not affect the controllability of the CMG-actuated spacecraft, they do limit the reachable states [100]. For a spacecraft at rest, the initial gimbal configuration, that is, the reference orientation matrices $\mathcal{O}_i'$ and the initial gimbal angles $\theta(0)$, defines the reachable set of rest attitudes.

In the absence of disturbance torques, the angular momentum $\vec{H}_{\mathrm{sc/c/I}}$ remains constant with respect to $\mathrm{F_I}$, that is,

$$\overset{\mathrm{I}\bullet}{\vec{H}}_{\mathrm{sc/c/I}} = 0. \tag{7.75}$$

Let the angular momentum of the spacecraft relative to c with respect to $\mathrm{F_I}$ resolved in $\mathrm{F_I}$

be given by

$$\mu \triangleq \vec{H}_{\mathrm{sc/c/I}}\Big|_{\mathrm{I}} = R\mu_{\mathrm{B}}(\theta). \tag{7.76}$$

where, for a spacecraft at rest,

$$\mu_{\mathrm{B}}(\theta) \triangleq \vec{H}_{\mathrm{sc/c/I}}\Big|_{\mathrm{B}} = \sum_{i=1}^{n} \alpha_i \nu_i \mathcal{O}_i e_1 + B_1 u. \tag{7.77}$$

Assume the gimbals are initially at rest so that $u = 0$, then, using (7.41) and (7.77) yields

$$\mu_{\mathrm{B}}(\theta) = \sum_{i=1}^{n} \alpha_i \nu_i \mathcal{O}_i' \begin{bmatrix} \cos\theta_i \\ 0 \\ -\sin\theta_i \end{bmatrix}. \tag{7.78}$$

Thus, when the gimbals and spacecraft are at rest, the gimbal angles define the momentum envelope of the spacecraft.

Lemma 3. *Define the momentum volume of the CMG array $\mathcal{V}$ as the set of all possible angular momentum vectors $\mu_{\mathrm{B}}(\theta)$ and let $\hat{n} \in \mathbb{R}^3$ be a unit vector. Therefore, for all $\hat{n} \in \mathbb{R}^3$, if*

$$\|\mu\|_2 \hat{n} \in \mathcal{V} \tag{7.79}$$

then all desired rest attitudes $R = R_{\mathrm{d}}, \omega = 0$ are reachable [100].

Combinations of initial attitude and gimbal configuration which violate violate (7.79) limit the set of reachable attitudes R_{d}.

Proposition 1. *Consider a spacecraft controlled by n CMG's initially at rest with $\omega = u = 0$ and initial attitude $R = R_0$. Let the desired attitude, angular velocity, and gimbal angular velocity be given by $R = R_{\mathrm{d}}, \omega = u = 0$. Let the angular momentum of the spacecraft resolved in $\mathrm{F_B}$ be given by* (7.78)*. If*

$$\|R_{\mathrm{d}}^{\mathrm{T}} R_0 \mu_{\mathrm{B}}(\theta_0)\|_\infty > \max_{\theta} \left\| \sum_{i=1}^{n} \alpha_i \nu_i \mathcal{O}_i' \begin{bmatrix} \cos\theta_i \\ 0 \\ -\sin\theta_i \end{bmatrix} \right\|_\infty \tag{7.80}$$

then R_{d} is not reachable from R_0.

Proof. Assume $R = R_{\mathrm{d}}, \omega = u = 0$ is reachable from $R = R_0, \omega = u = 0$. Then, there exists a combination of gimbal angles θ_{d} such that the spacecraft angular momentum when $R = R_{\mathrm{d}}$ resolved in $\mathrm{F_B} = \mathrm{F_d}$ is given by

$$\mu_{\mathrm{d}} = R_{\mathrm{d}}^{\mathrm{T}}\mu = R_{\mathrm{d}}^{\mathrm{T}}R_0\mu_{\mathrm{b}}(\theta_0) = \sum_{i=1}^{n} \alpha_i\nu_i\mathcal{O}_i' \begin{bmatrix} \cos\theta_{\mathrm{d}_i} \\ 0 \\ -\sin\theta_{\mathrm{d}_i} \end{bmatrix} \in \mathcal{V}. \tag{7.81}$$

Therefore,

$$\|\mu_{\mathrm{d}}\|_\infty \leq \max_\theta \left\| \sum_{i=1}^{n} \alpha_i\nu_i\mathcal{O}_i' \begin{bmatrix} \cos\theta_{\mathrm{d}_i} \\ 0 \\ -\sin\theta_{\mathrm{d}_i} \end{bmatrix} \right\|_\infty \tag{7.82}$$

which contradicts (7.80). Thus, R_{d} is not reachable. □

7.1.5 The Effect of Singularities

Consider a spacecraft at rest actuated by three orthogonal gimbals as in (7.61). Let all gimbals have the same spin axis inertia $\bar{\alpha}$ and the same wheel speed $\bar{\nu}$. Then the angular momentum of the spacecraft (7.78) is given by

$$\mu_{\mathrm{B}}(\theta) = \bar{\alpha}\bar{\nu} \begin{bmatrix} \cos\theta_{0_3} - \sin\theta_{0_2} \\ \cos\theta_{0_1} + \sin\theta_{0_3} \\ -\cos\theta_{0_2} - \sin\theta_{0_1} \end{bmatrix}. \tag{7.83}$$

For this configuration, $\max_\theta \|\mu_{\mathrm{B}}(\theta)\|_\infty = 2\bar{\alpha}\bar{\nu}$, therefore, the momentum volume $\mathcal{V}$ is a sphere of radius $2\bar{\alpha}\bar{\nu}$.

7.1.5.1 Example 1: Singularity in the x-axis

Given the singular configuration $\theta_0 = \begin{bmatrix} 0 & \frac{\pi}{2} & 0 \end{bmatrix}$ (7.52) yields

$$B_{\text{sc}}(0) = \bar{\alpha}\bar{\nu} \begin{bmatrix} e_3 & e_3 & -e_2 \end{bmatrix}. \tag{7.84}$$

Thus, the CMG's cannot produce torque about the e_1 axis of $\mathrm{F_B}$. Let $R_0 = I_3$, then

$$\|R_0 \mu_{\text{B}}(\theta_0)\|_2 > 2\bar{\alpha}\bar{\nu} \tag{7.85}$$

and thus $\|\mu\|_2 \hat{n} \notin \mathcal{V}$. Thus, Lemma 3 suggests that some desired attitudes $R = R_{\text{d}}$ are not reachable. Let $R_{\text{d}} = \mathcal{R}(-\frac{3\pi}{4}, e_3)$, then

$$\|R_{\text{d}}^{\text{T}} R_0 \mu_{\text{B}}(\theta_0)\|_\infty = \frac{3}{\sqrt{2}}\bar{\alpha}\bar{\nu} > \max_\theta \|\mu_{\text{B}}(\theta)\|_\infty. \tag{7.86}$$

Therefore, due to Proposition 1, R_{d} is unreachable from R_0.

7.1.5.2 Example 2: Singularity in the y-axis

Next, consider the singular gimbal configuration $\theta_0 = \begin{bmatrix} 0 & 0 & \frac{\pi}{2} \end{bmatrix}$ then the input matrix (7.52) is given by

$$B_{\text{sc}}(0) = \bar{\alpha}\bar{\nu} \begin{bmatrix} e_3 & -e_1 & e_1 \end{bmatrix} \tag{7.87}$$

and the CMG's cannot produce torque about the e_2 axis of $\mathrm{F_B}$. The 2-norm of the angular momentum is given by

$$\|R_0 \mu_{\text{B}}(\theta_0)\|_2 = \frac{1}{2}\bar{\alpha}\bar{\nu}. \tag{7.88}$$

Thus $\|\mu\|_2 \hat{n} \in \mathcal{V}$ and, due to Lemma 3, all desired attitudes $R = R_{\text{d}}$ are reachable regardless of the initial singular configuration.

Examples 1 and 2 show that there are different types of singularities. Therefore, a controller will be able to complete any rest-to-rest maneuver when the condition in Lemma 3 is met. Furthermore, if that condition is not met we can discard unreachable attitudes using Proposition 1. Henceforth we refer to singularities that satisfy Proposition 1 as *obstructing* singularities whereas cases that satisfy Lemma 3 are referred to as *non-obstructing* singularities.

7.2 Control Law

Let the control input be given by

$$u(k) = \Phi(k)\Theta(k) \tag{7.89}$$

where the regresor matrix is given by We can express the update law for $\Theta(k)$ recursively as

$$\Theta(k) = \Theta(k-1) + \mathcal{K}(k)\varepsilon(k), \tag{7.90}$$

where

$$\mathcal{K}(k) \triangleq \mathcal{P}(k-1)X(k)^{\mathrm{T}}\Gamma(k)^{-1}, \tag{7.91}$$

$$\varepsilon(k) \triangleq Z(k) - X(k)\Theta(k-1), \tag{7.92}$$

$$\Gamma(k) \triangleq \lambda\bar{R}(k)^{-1} + X(k)\mathcal{P}(k-1)X(k)^{\mathrm{T}}, \tag{7.93}$$

$$X(k) \triangleq \begin{bmatrix} H_1\Phi(k) \\ \Phi(k) \end{bmatrix}, \quad \bar{R}(k) \triangleq \begin{bmatrix} I_{l_z} & 0 \\ 0 & \eta_u(k)I_{l_u} \end{bmatrix}, \quad Z(k) \triangleq \begin{bmatrix} H_1u(k-1) - z(k) \\ 0 \end{bmatrix}. \tag{7.94}$$

The information matrix update is given by

$$\mathcal{P}(k) = \frac{1}{\lambda}\left[I_{l_\theta} - \frac{1}{\lambda}\mathcal{K}(k)X(k)\right]\mathcal{P}(k-1). \tag{7.95}$$

7.3 Performance Variable for Attitude Control

The objective of the attitude control problem is to determine control inputs that align $\mathrm{F_B}$ with the desired frame $\mathrm{F_d}$. That is given the desired attitude R_d and the desired angular velocity ω_d how do we choose a control u such that $R = R_\mathrm{d}, \omega = \omega_\mathrm{d}$. We define the corresponding performance variable z to achieve attitude control using RCAC.

Lemma 4. *Let the attitude error $\tilde{R} = R_\mathrm{d}^{\mathrm{T}}R$ and $S = \sum_{i=1}^{3} a_i e_i \times \tilde{R}^{\mathrm{T}}e_i$. Given distinct positive scalars a_1, a_2, a_3, then, $S = 0$ if and only if $\tilde{R} \in \{I_3,\ \mathrm{diag}(\ 1,\ -1,\ 1),\ \mathrm{diag}(\ -1,\ 1,\ 1),\ \mathrm{diag}(\ 1,\ 1,\ -1)\}$.*

Lemma 1 shows that using S as the sole measure of attitude error gives rise to spurious attitude equilibria [58]. To remove these equlibria, we define a scalar measure of attitude error that depends on the diagonal entries of $\tilde{R}$, namely,

$$s \stackrel{\triangle}{=} \mathrm{trace}(A_{\mathrm{att}} - A\tilde{R}) = a_1(1 - \tilde{R}_{11}) + a_2(1 - \tilde{R}_{22}) + a_3(1 - \tilde{R}_{33}). \tag{7.96}$$

where $A = \mathrm{diag}\,(a_1, a_2, a_3)$ is positive definite.

Lemma 5. *Let R_{ij} be the (i, j) entry of a rotation matrix R. Then $|R_{ij}| \leq 1$.*

Proposition 2. *Let $a_1, a_2, a_3 > 0$. Then $s = 0$ if and only if $\tilde{R} = I_3$.*

Proof. For necessity, note that $s = 0$ implies

$$0 = \mathrm{trace}(A - A\tilde{R}) = a_1(1 - \tilde{R}_{11}) + a_2(1 - \tilde{R}_{22}) + a_3(1 - \tilde{R}_{33}).$$

Lemma 2 implies that, for $i = 1, 2, 3$,

$$a_i(1 - \tilde{R}_{ii}) \geq 0. \tag{7.97}$$

Thus, $s = 0$ if and only if $a_i(1 - \tilde{R}_{ii}) = 0$. Since $a_1, a_2, a_3 > 0$, it follows that $\tilde{R}_{11} = \tilde{R}_{22} = \tilde{R}_{33} = 1$ and thus $\tilde{R} = I_3$. Conversely, let $\tilde{R} = I_3$. Then, by (7.96), $s = 0$.

□

The performance variable z for the attitude control problem is defined by

$$z \stackrel{\triangle}{=} \begin{bmatrix} \tilde{\omega} \\ S \\ s \end{bmatrix}. \tag{7.98}$$

where $\tilde{\omega} = \omega - \tilde{R}^{\mathrm{T}}\omega_{\mathrm{d}}$.

Proposition 3. *$z = 0$ if and only if $\omega = \omega_{\mathrm{d}}$ and $R = R_{\mathrm{d}}$.*

Proof. For necessity, assume $z = 0$. Then $s = 0$ and Proposition 1 implies that $\tilde{R} = I_3$. Therefore, (5.29) yields

$$R = R_{\mathrm{d}}\tilde{R} = R_{\mathrm{d}}.$$

If, in addition, $\tilde{\omega} = 0$, then

$$\omega = \tilde{R}^{\mathrm{T}}\omega_{\mathrm{d}} + \tilde{\omega} = \omega_{\mathrm{d}}.$$

Thus, $R = R_{\mathrm{d}}$ and $\omega = \omega_{\mathrm{d}}$.

To prove sufficiency, assume $R_{\mathrm{d}} = R$. Then (5.29) implies $\tilde{R} = I_3$. Thus, Lemma 1 implies $S = 0$ and Proposition 1 implies $s = 0$. Next, let $\omega = \omega_{\mathrm{d}}$. Then $\tilde{\omega} = \omega - \tilde{R}^{\mathrm{T}}\omega_{\mathrm{d}} = \omega - \omega_{\mathrm{d}} = 0$. Thus, $R = R_{\mathrm{d}}$ and $\omega = \omega_{\mathrm{d}}$ imply $s = 0$ and $S = \tilde{\omega} = 0$. Hence, $z = 0$. □

7.4 Markov Parameters

Markov parameters for attitude control are obtained by linearizing the expression for $\dot{\tilde{\omega}}$ and a 9×1 vector parameterization of the attitude error $\tilde{R}$ [70–72] . An alternative attitude parameterization can be achieved by using variations [101]. For the CMG attitude control problem we linearize the kinematics (7.30) and dynamics (7.58) and approximate the impulse response of the linear system. This approximation is used to construct the impulse response of the nonlinear performance z (7.98). The Markov parameter is constructed from the impulse response of the performance to a separate impulse from each CMG.

7.4.1 Markov Parameters as the Impulse Response

The Markov parameters of a linear discrete-time system correspond to the unit impulse response of the system. Consider the system defined by

$$x(k) = Ax(k-1) + Bu(k-1), \quad y(k) = Cx(k) \tag{7.99}$$

and let $x(0) = 0$. Applying a unit impulse at $k = 0$ yields the response at $k = q$,

$$z^j(q) = CA^q x(0) + \sum_{i=1}^{q} CA^{q-i}Bu^j(q-i) = CA^{q-1}B, \tag{7.100}$$

where the control input is given by

$$u^j(k) = \begin{cases} e_j', & k = 0, \\ \\ 0, & k > 0, \end{cases} \tag{7.101}$$

and e_j' is the jth column of the $l_u \times l_u$ identity matrix. Thus, the jth column of ith Markov parameter of the system (7.99) is given by

$$H_{k,j} = z^j(i). \tag{7.102}$$

7.4.2 Variations

The variation of a rotation matrix is given by

$$R^\epsilon = \bar{R}e^{\epsilon\eta^\times}, \tag{7.103}$$

where $\bar{R}$ is a reference attitude. Taking the derivative of (7.103) with respect to time yields.

$$\dot{R}^\epsilon = \dot{\bar{R}}e^{\epsilon\eta^\times} + \epsilon\bar{R}\dot{\eta}e^{\epsilon\eta^\times} = \bar{R}\bar{\omega}^\times e^{\epsilon\eta^\times} + \epsilon\bar{R}\dot{\eta}e^{\epsilon\eta^\times}, \tag{7.104}$$

Furthermore, substituting (7.103) into (7.30) and using (7.106) yields

$$\dot{R}^\epsilon = R^\epsilon\omega^{\epsilon\times} = \bar{R}e^{\epsilon\eta^\times}(\bar{\omega} + \epsilon\delta\omega)^\times, \tag{7.105}$$

where, given the reference angular velocity $\bar{\omega}$, the variation ω^ϵ is given by

$$\omega^\epsilon = \bar{\omega} + \epsilon\delta\omega. \tag{7.106}$$

Combining (7.104) and (7.105), differentiating with respect to ϵ, and evaluating at $\epsilon = 0$ yields the linear attitude kinematics

$$\dot{\eta} = \delta\omega - \bar{\omega}^\times\eta. \tag{7.107}$$

The variations of the gimbal angles, and control input are given by

$$\theta^\epsilon = \bar{\theta} + \epsilon\delta\theta, \tag{7.108}$$

$$u^\epsilon = \bar{u} + \epsilon\delta u, \tag{7.109}$$

where $\bar{\theta}$ and $\bar{u}$ are the reference gimbal angles and angular velocities, respectively. Substituting (7.108) and (7.109) into (7.58), differentiating with respect to ϵ, and evaluating at

$\epsilon = 0$ yields

$$\bar{J}\delta\dot{\omega} = \left[(\bar{J}\bar{\omega} + \bar{H}_{\mathrm{G}} + B_1\bar{u})^{\times} - \bar{\omega}^{\times}\bar{J} - B_{\omega}\right]\delta\omega - \left[\bar{\omega}^{\times}(M_{\omega} + M_H) + M_{\dot{\omega}} + B_{\theta}\right]\delta\theta - \bar{B}_2\delta u - B_1\delta\dot{u}, \tag{7.110}$$

where

$$\bar{J} = J_{\mathrm{b}} + \sum_{i=1}^{n} \bar{\mathcal{O}}_i J_i \bar{\mathcal{O}}_i^{\mathrm{T}} - m_i r_i^{\times 2}, \quad \bar{H}_{\mathrm{G}} = \sum_{i=1}^{n} \alpha_i \nu_i \bar{\mathcal{O}}_i e_1, \quad B_{\omega} = \sum_{i=1}^{n} \bar{\mathcal{O}}_i (e_2^{\times} J_i - J_i e_2^{\times}) \bar{\mathcal{O}}_i^{\mathrm{T}} \bar{u}_i,$$

and $\delta\dot{u} = \frac{\mathrm{d}}{\mathrm{d}t}\delta u$. For $i = 1, \ldots n$,

$$\bar{\mathcal{O}}_i = \mathcal{O}_i' \begin{bmatrix} \cos\bar{\theta}_i & 0 & \sin\bar{\theta}_i \\ 0 & 1 & 0 \\ -\sin\bar{\theta}_i & 0 & \cos\bar{\theta}_i \end{bmatrix} \tag{7.111}$$

and the ith column of $M_{\omega}, M_{\dot{\omega}}, M_H, B_{\theta}$, and $\bar{B}_2$ is given by

$$\begin{aligned}
M_{\omega_i} &= (\bar{\mathcal{O}}_i e_2^{\times} J_i \bar{\mathcal{O}}_i^{\mathrm{T}} - \bar{\mathcal{O}}_i J_i e_2^{\times} \bar{\mathcal{O}}_i^{\mathrm{T}})\bar{\omega}, \\
M_{\dot{\omega}_i} &= (\bar{\mathcal{O}}_i e_2^{\times} J_i \bar{\mathcal{O}}_i^{\mathrm{T}} - \bar{\mathcal{O}}_i J_i e_2^{\times} \bar{\mathcal{O}}_i^{\mathrm{T}})\dot{\bar{\omega}}, \\
M_{H_i} &= -\alpha_i \nu_i \bar{\mathcal{O}}_i e_3, \\
B_{\theta_i} &= [\bar{\mathcal{O}}_i e_2^{\times}(e_2^{\times} J_i - J_i e_2^{\times})\bar{\mathcal{O}}_i^{\mathrm{T}} - \bar{\mathcal{O}}_i (e_2^{\times} J_i - J_i e_2^{\times}) e_2^{\times} \bar{\mathcal{O}}_i^{\mathrm{T}}]\bar{\omega}\bar{u}_i + \alpha_i \nu_i \bar{\mathcal{O}}_i e_1 \bar{u}_i, \\
\bar{B}_{2i} &\triangleq \bar{\mathcal{O}}_i \left(e_2^{\times} J_i - J_i e_2^{\times}\right) \bar{\mathcal{O}}_i^{\mathrm{T}} \bar{\omega} - \alpha_i \nu_i \bar{\mathcal{O}}_i e_3,
\end{aligned}$$

respectively. Finally, take taking the time-derivative of (7.108) differentiating with respect to ϵ, and evaluating at $\epsilon = 0$ yields

$$\delta\dot{\theta} = \delta u. \tag{7.112}$$

7.4.3 Impulse response of the Linear System

Combining (7.107), (7.110), and (7.112) yields the linearized system dynamics

$$\begin{bmatrix} \dot{\eta} \\ \delta\dot{\omega} \\ \delta\dot{\theta} \end{bmatrix} = A_{\mathrm{c}} \begin{bmatrix} \eta \\ \delta\omega \\ \delta\theta \end{bmatrix} + B_u \delta u + B_{\dot{u}} \delta\dot{u}, \tag{7.113}$$

where

$$A_{\mathrm{c}} = \begin{bmatrix} A_1 & A_2 & A_3 \end{bmatrix}, \tag{7.114}$$

$$A_1 = \begin{bmatrix} -\bar{\omega}^{\times} \\ 0_{3\times 3} \\ 0_{n\times 3} \end{bmatrix}, \quad A_2 = \begin{bmatrix} I_3 \\ \bar{J}^{-1}\left[(\bar{J}\bar{\omega} + \bar{H}_{\mathrm{G}} + B_1\bar{u})^{\times} - \bar{\omega}^{\times}\bar{J} - B_{\omega}\right] \\ 0_{n\times 3} \end{bmatrix},$$

$$A_3 = \begin{bmatrix} 0_{3\times 3} \\ \bar{J}^{-1} - [\bar{\omega}^{\times}(M_{\omega} + M_H) + M_{\dot{\omega}} + B_{\theta}] \\ 0_{n\times n} \end{bmatrix},$$

$$B_u = \begin{bmatrix} 0_{3\times n} \\ -\bar{J}^{-1}\bar{B}_2 \\ I_n \end{bmatrix}, \quad B_{\dot{u}} = \begin{bmatrix} 0_{3\times n} \\ -\bar{J}^{-1}B_1 \\ 0_{n\times n} \end{bmatrix}. \tag{7.115}$$

For $i = 1, \ldots, n$, we can approximate the impulse response of (7.113) due to the ith CMG as

$$\begin{bmatrix} \eta^i \\ \delta\omega^i \\ \delta\theta^i \end{bmatrix} \approx (I_{6+l_u} + \frac{h^2}{2}A_{\mathrm{c}})B_u e_i'. \tag{7.116}$$

Using η^i we compute the resulting attitude

$$R^i = e^{\eta^{i\times}}. \tag{7.117}$$

Let $R_{\mathrm{d}} = I_3$ and $\omega_{\mathrm{d}} = 0_{3\times 1}$, then the impulse response of the performance (7.98) is given by

$$z^i = \begin{bmatrix} \delta\omega^i \\ \sum_{j=1}^{3} a_j e_j \times R^{i\mathrm{T}} e_j \\ \sum_{j=1}^{3} a_j e_j^{\mathrm{T}} R^i e_j \end{bmatrix} \tag{7.118}$$

Building the Markov parameter using (7.118) yields

$$H_1 = \begin{bmatrix} z^1 & \cdots & z^n \end{bmatrix} \in \mathbb{R}^{7\times n}. \tag{7.119}$$

Note that (7.119) is a function of the current spacecraft configuration, that is, different values of $\bar{\theta}$, $\bar{u}$, and $\bar{\omega}$ yield different Markov parameters. Therefore, unlike the controllers in [70] and [71], the Markov parameters and thus the filter $\bar{G}(\mathbf{q})$ in (2.6) are different at each iteration.

7.5 Numerical Examples

The spacecraft is given rest-to-rest commands, that is, at $t = 0$ the spacecraft is at rest with $R = I_3, \omega = u = 0$, and the desired attitude and angular velocity are given by $R = R_{\mathrm{d}}, \omega = 0$. We focus on the three orthogonal CMG configuration in (7.61). We examine maneuvers about both principal and non-principal axes. These maneuvers are commanded as either steps or ramps. We only consider maneuvers in which the initial CMG configuration is full rank.

Given $n = 3$, let the initial CMG configuration be given by $\theta = 0_{n\times 1}$ such that the input matrix B_2 in (7.52) is full rank. For $i = 1, \ldots, n$, the moments of inertia for w_i are given by

$$\alpha_i = 0.020 \text{ kg-m}^2, \quad \beta_i = 0.012 \text{ kg-m}^2, \tag{7.120}$$

and the spin rate of $\mathrm{F}_{\mathrm{W}_i}$ relative to $\mathrm{F}_{\mathrm{G}_i}$ is given by

$$\nu_i = 600 \text{ rad/sec}. \tag{7.121}$$

Figure 7.3 shows the performance of RCAC for a rest to rest maneuver of -90 deg about the eigenaxis $[1\ 0\ 0]$.

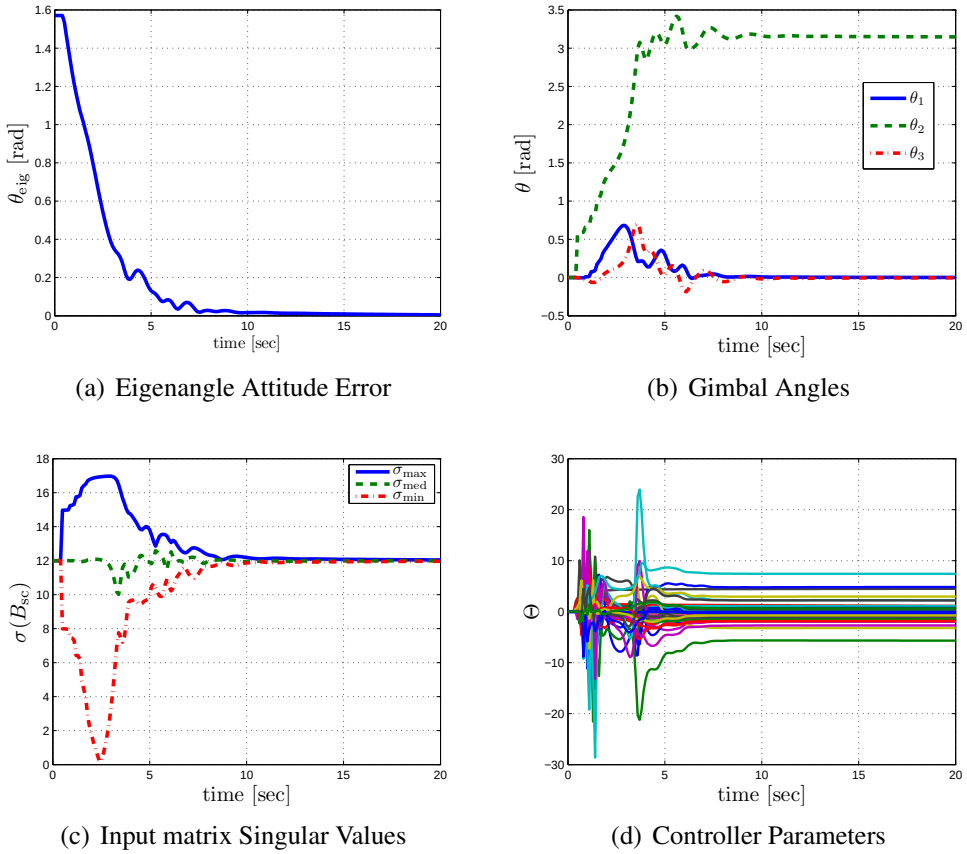

(a) Eigenangle Attitude Error (b) Gimbal Angles

(c) Input matrix Singular Values (d) Controller Parameters

Figure 7.3: R2R maneuver for $J_{\mathrm{b}} = J_1$. The control parameters are given by $\eta_u = 0.01, \eta_\theta = 10^{-5}$. All gains are initialized at $\Theta_0 = 0$.

7.5.1 Principal Axis Maneuvers

Consider three bus shapes with inertia matrix J_{b} given by

$$J_1 \triangleq \mathrm{diag}(10, 10, 10) \text{ kg-m}^2, \quad J_2 \triangleq \mathrm{diag}(10, 10, 5) \text{ kg-m}^2, \quad J_3 \triangleq \mathrm{diag}(10, 8.3, 5) \text{ kg-m}^2. \tag{7.122}$$

Note that, for J_1, J_2, J_3 the body frame is aligned with the principal axes of the bus. Then, for $i = 1, \ldots, 3$, let the desired attitude be given by

$$R_{\mathrm{d}}^{i}(\theta_{\mathrm{d}}) = \mathcal{R}(\theta_{\mathrm{d}}, e_i) \tag{7.123}$$

where e_i is the ith column of the 3×3 identity matrix. Figures 7.4, 7.5, and 7.6 show the maximum eigenangle error, the settling time, and the maximum control input for the inertias in (7.122) subjected to three different principal axis step commands of different magnitudes. Note that the "V" shape in Figure 7.4 shows that the controller does not exhibit any overshoot.

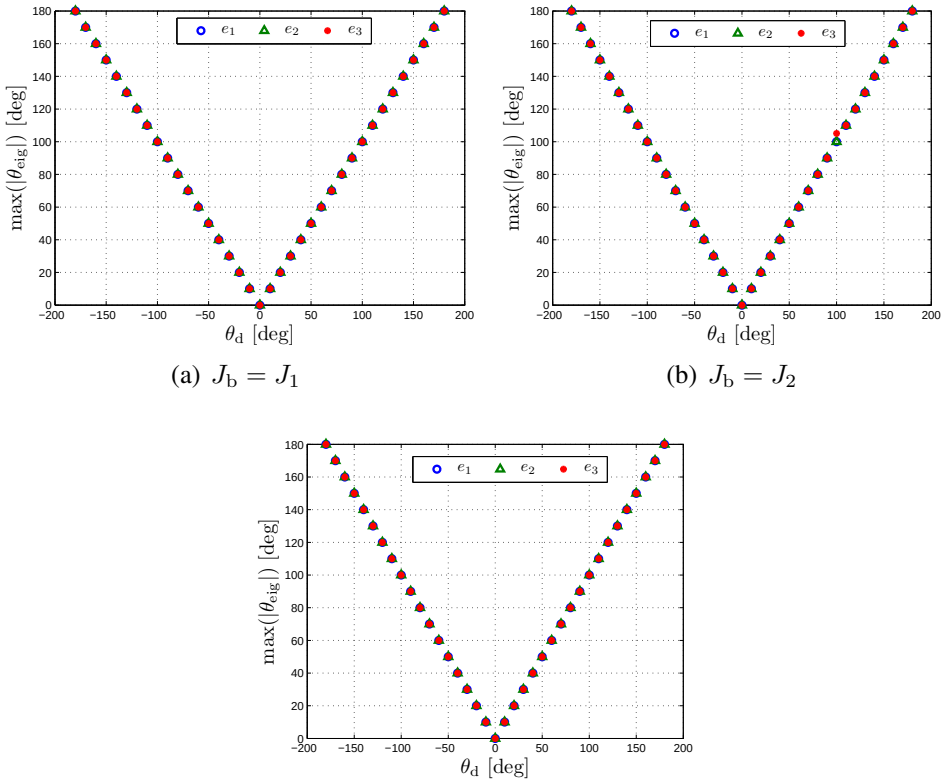

(a) $J_{\mathrm{b}} = J_1$ (b) $J_{\mathrm{b}} = J_2$

(c) $J_{\mathrm{b}} = J_3$

Figure 7.4: Maximum eigenangle error for R2R maneuvers of different magnitudes about principal axes e_1, e_2, e_3 for the bus inertias $J_{\mathrm{b}} = J_1, J_2, J_3$. The control parameters are given by $\eta_u = 0.01, \eta_\theta = 10^{-5}$. All gains are initialized at $\Theta_0 = 0$.

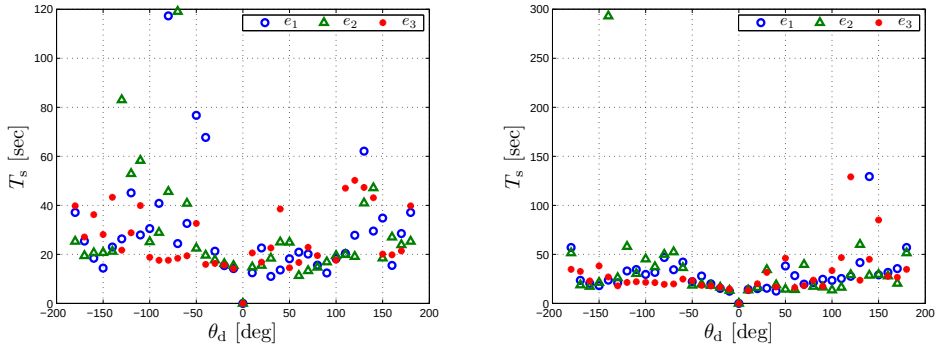

(a) $J_b = J_1$ (b) $J_b = J_2$

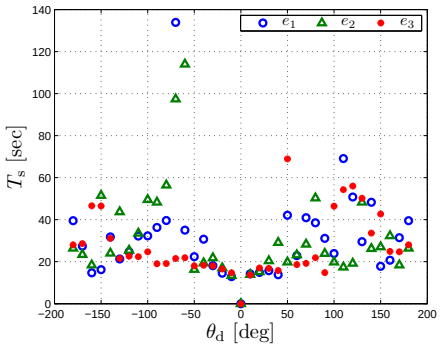

(c) $J_b = J_3$

Figure 7.5: Settling time to $\theta_{\text{eig}} \leq \theta_{\text{ss}} = \frac{1}{60}$ deg, for R2R maneuvers of different magnitudes about principal axes e_1, e_2, e_3 for the bus inertias $J_b = J_1, J_2, J_3$. The control parameters are given by $\eta_u = 0.01, \eta_\theta = 10^{-5}$. All gains are initialized at $\Theta_0 = 0$.

Next, consider an angular velocity command of the form

$$\omega_d^i = \begin{cases} \frac{\theta_d}{t_r} e_i, & 0 \leq t \leq t_r, \\ \\ 0, & t > t_r, \end{cases} \tag{7.124}$$

where t_r is the ramp duration such that for all $i = 1, 2, 3$, $R_d^i(t_r) = \mathcal{R}(\theta_d, e_i)$ and $R_d^i(0) = I_3$. Figure 7.7 shows the performance of RCAC for the rest-to-rest maneuver in Figure 7.3 commanded as a ramp of -90 deg about the eigenaxis $[1\ 0\ 0]$. Note that the control parameters adapt to the change in slope of the command at $t = 100$ sec.

Figures 7.8 and 7.9 show the maximum eigenangle error and maximum control input for the inertias in (7.122) subjected to three different principal axis ramp commands of different magnitudes. Note that the control inputs in Figure 7.9 are significantly lower than

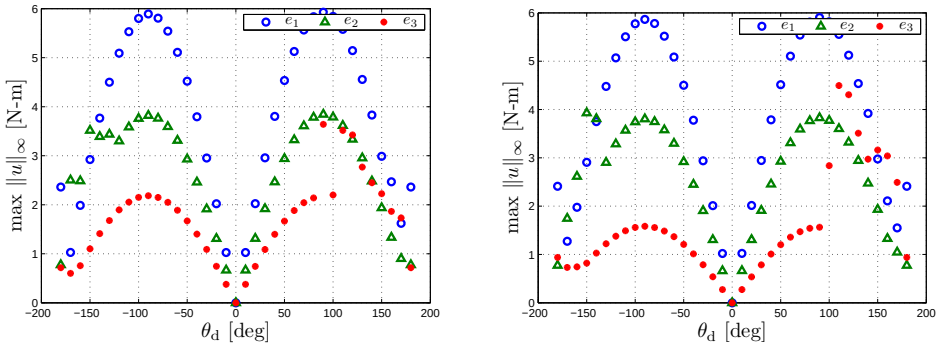

(a) $J_\mathrm{b} = J_1$ (b) $J_\mathrm{b} = J_2$

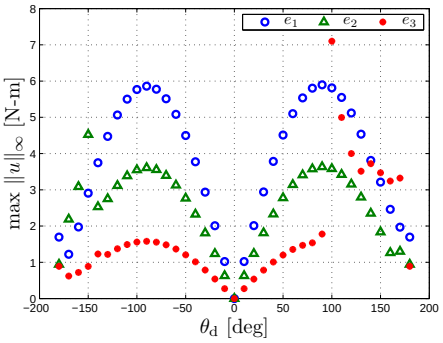

(c) $J_\mathrm{b} = J_3$

Figure 7.6: Maximum control input for R2R maneuvers of different magnitudes about principal axes e_1, e_2, e_3 for the bus inertias $J_\mathrm{b} = J_1, J_2, J_3$. The control parameters are given by $\eta_u = 0.01, \eta_\theta = 10^{-5}$. All gains are initialized at $\Theta_0 = 0$.

the control inputs for the step commands in Figure 7.6 which suggests that RCAC performs better when given ramp commands.

7.5.2 NonPrincipal Axis Maneuvers

Consider a R2R step command such that

$$R_\mathrm{d}(\theta_\mathrm{d}) = \mathcal{R}(\theta_\mathrm{d}, \frac{1}{\sqrt{3}}[1\ 1\ 1]^\mathrm{T}). \tag{7.125}$$

Note that the eigenaxis corresponding to R_d in (7.125) is not a principal axis of the inertias in (7.122). Figure 7.10 shows the maximum eigenangle error, settling time, and maximum control input for the bus inertias $J_\mathrm{b} = J_1, J_2, J_3$ subject to the non-principal axis step command in (7.125).

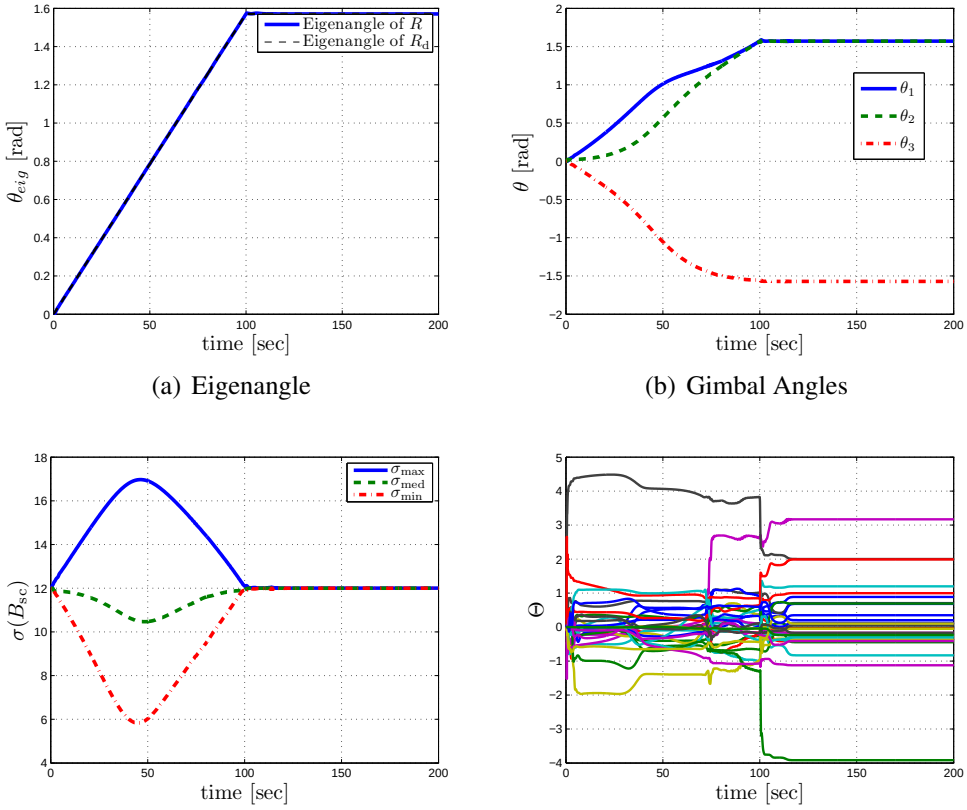

(a) Eigenangle

(b) Gimbal Angles

(c) Input matrix Singular Values

(d) Controller Parameters

Figure 7.7: R2R ramp maneuver for $J_{\rm b} = J_1$. The control parameters are given by $\eta_u = 0.01, \eta_\theta = 10^{-5}$. All gains are initialized at $\Theta_0 = 0$.

In addition to the diagonal bus inertias we consider the nondiagonal inertia

$$J_0 \triangleq \begin{bmatrix} 5 & -0.1 & -0.5 \\ -0.1 & 2 & 1 \\ -0.5 & 1 & 3.5 \end{bmatrix} \text{kg-m}^2. \tag{7.126}$$

We command the step R2R maneuver given by $R_{\rm d}^i$ in (7.123) for $i = 1, 2, 3$. Figure 7.11 shows the maximum eigenangle error, setting time, and maximum control input for the nondiagonal inertia subject to nonprincipal axis R2R step commands.

Next, we command the ramp R2R maneuver in (7.124). Figure 7.12 shows the maximum eigenangle error and maximum control input for the nonprincipal axis maneuvers given the bus inertia $J_{\rm b} = J_0$. Again, note that the control inputs in Figure 7.12 are smaller than the control inputs in Figure 7.11.

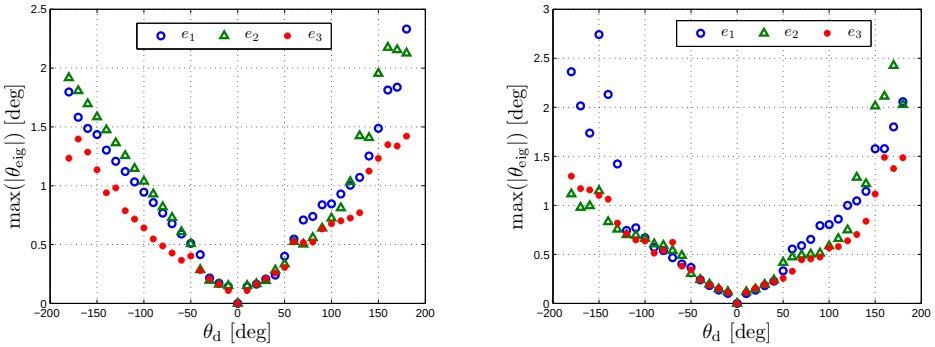

(a) $J_{\text{b}} = J_1$ (b) $J_{\text{b}} = J_2$

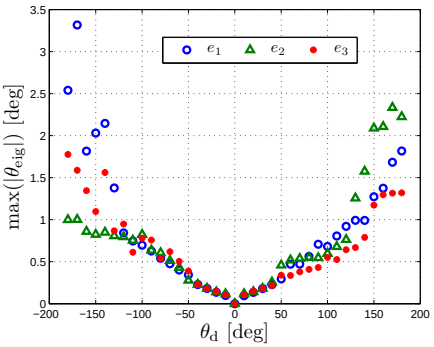

(c) $J_{\text{b}} = J_3$

Figure 7.8: Settling time to $\theta_{\text{eig}} \leq \theta_{\text{ss}} = \frac{1}{60}$ deg, for ramp commanded R2R maneuvers of different magnitudes about principal axes e_1, e_2, e_3 for the bus inertias $J_{\text{b}} = J_1, J_2, J_3$. The control parameters are given by $\eta_u = 0.01, \eta_\theta = 10^{-5}$. All gains are initialized at $\Theta_0 = 0$.

7.5.3 Singularities

We command a R2R maneuver starting at a singular configuration. Figure 7.13 shows the maximum component of the desired body-frame angular momentum $\|\mu_{\text{d}}\|_\infty$ in (7.81) corresponding with a rest state at R_{d}. The dotted line at $\|\mu_{\text{d}}\|_\infty = 24$N-m corresponds to the maximum value of (7.78) given the gimbal configuration and parameters in (7.120) and (7.121). Note that this is only a limited sample of the possible maneuvers and does not account for maneuvers about eigenaxes other than e_1, e_2, e_3 which might be required as the attitude error $\tilde{R}$ evolves "on the way" to R_{d}.

For the singularity examples we classify the behavior of the spacecraft after $t = 500$ sec in three categories

1. Stable: The steady state error $\theta_{\text{eig}} \leq \theta_{\text{ss}} = \frac{1}{60}$ deg
2. Steady State Error: The angular velocity at the end of the simulation is $\|\omega\|_2 \leq 1$ deg/sec.

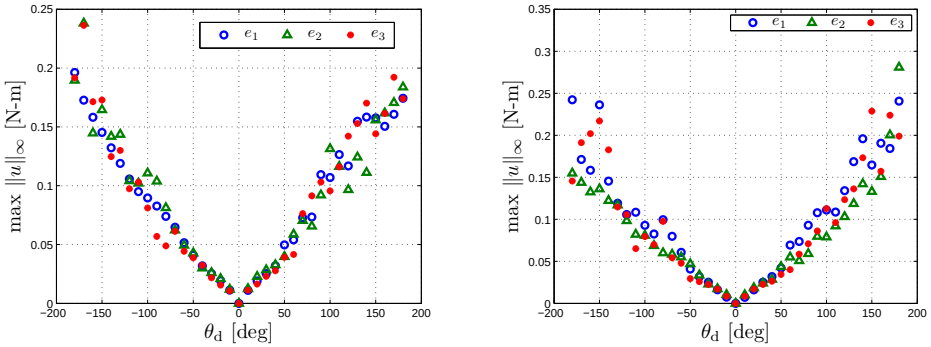

(a) $J_b = J_1$ (b) $J_b = J_2$

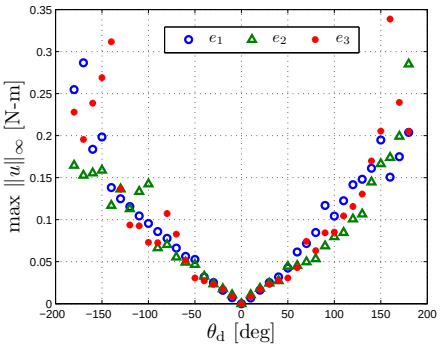

(c) $J_b = J_3$

Figure 7.9: Maximum control input for ramp commanded R2R maneuvers of different magnitudes about principal axes e_1, e_2, e_3 for the bus inertias $J_b = J_1, J_2, J_3$. The control parameters are given by $\eta_u = 0.01, \eta_\theta = 10^{-5}$. All gains are initialized at $\Theta_0 = 0$.

3. Unstable: Neither 1 or 2 above.

Figure 7.14 shows the results of for the R2R maneuver using the diagonal inertias J_1, J_2, J_3 for the case with initial gimbal singularity about $\hat{\imath}_B$ as in (7.84). According to Proposition 1, maneuvers in which $\|\mu_d\|_\infty > 24$N-M are unreachable. Therefore, Figure 7.13(a) suggests that a not insignificant number of the maneuvers in Figure 7.14(a) are physically impossible. This explains the large cluster of markers in the unstable and steady state error categories.

Figure 7.15 shows similar results for the case with initial gimbal singularity about $\hat{\jmath}_B$. Although according to Figure 7.13(b) all of the maneuvers in Figure 7.15 are reachable, there may be intermediate attitude errors $\tilde{R}$ which correspond to unreachable maneuvers.

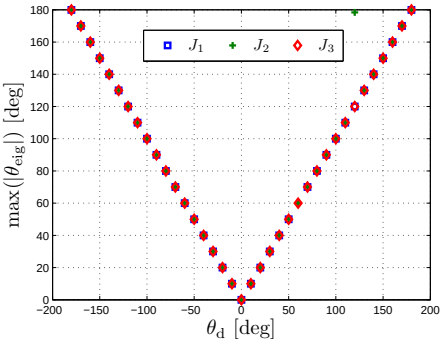

(a) Maximum Error

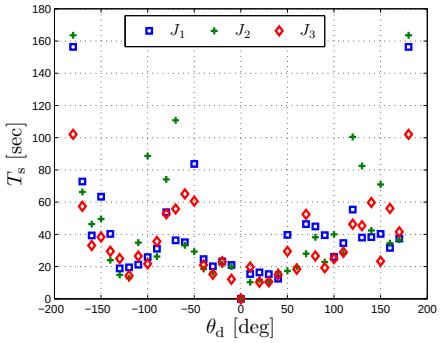

(b) Settling Time to $\theta_{\text{eig}} \leq \theta_{\text{ss}} = \frac{1}{60}$ deg

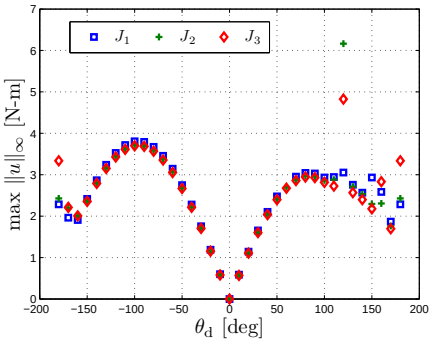

(c) Maximum Control Input

Figure 7.10: Maximum error, settling time, and maximum control input for R2R maneuvers of magnitude θ_{d} about the non-principal axis $[1\ 1\ 1]^{\text{T}}$. The diagonal bus inertias are given by $J_{\text{b}} = J_1, J_2, J_3$. The control parameters are given by $\eta_u = 0.01, \eta_\theta = 10^{-5}$. All gains are initialized at $\Theta_0 = 0$.

7.6 Conclusions

We apply RCAC to spacecraft attitude control with CMG's actuation. A detailed derivation of the CMG dynamics is obtained by using Newton-Euler methods. We developed a hybrid method to obtain the Markov parameter. First we used variations to obtain a linearized CMG model. The impulse response of the linear discrete-time model was used to obtain an impulse response rotation matrix which in turn is used to update the performance variable. The impulse response of the performance variable is used to construct the Markov parameter.

We test the controller on a spacecraft controlled by three orthogonally mounted CMG's. Several rest-to-rest maneuvers were examined about both principal and nonprincipal axes. Both step and ramp commands were considered. RCAC was able to successfully complete the maneuvers despite the presence of singularities. However, we must assume that the initial configuration of the gimbals is singularity-free.

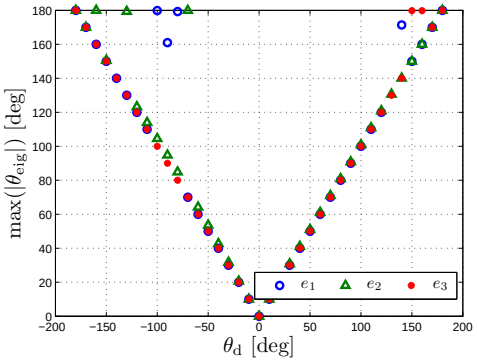

(a) Maximum Error

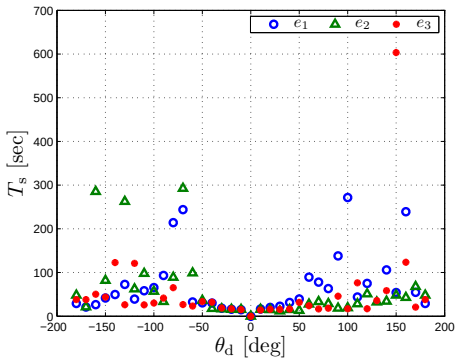

(b) Settling Time to $\theta_{\text{eig}} \leq \theta_{\text{ss}} = \frac{1}{60}$ deg

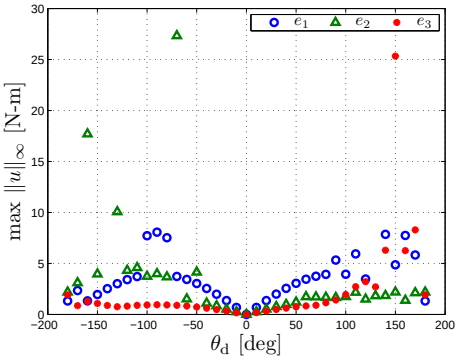

(c) Maximum Control Input

Figure 7.11: Maximum Error, settling time, and maximum control input for R2R maneuvers of magnitude θ_{d} about the non-principal axes e_1, e_2, e_3. The non-principal bus inertia is given by $J_{\text{b}} = J_0$. The control parameters are given by $\eta_u = 0.01, \eta_\theta = 10^{-5}$. All gains are initialized at $\Theta_0 = 0$.

For initially singular configurations, the results at first seem inconclusive. However careful thought and examination of the physical limitations imposed by singularities, namely unreachable attitudes, suggest that instabilities may arise even when the desired attitude is reachable. The angular momentum-based reachability condition in Proposition 1 can be used to prevent unfeasible commands from being given to the controller. We achieved direct control of CMG's. That is, RCAC controls the angular velocity of the gimbals directly without the use of steering laws. Furthermore, no saturated pseudo-inverse or similar methodologies to avoid singularities are used.

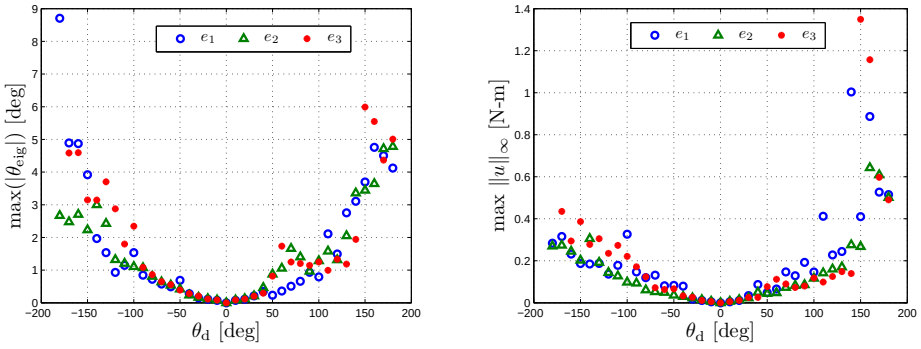

(a) Maximum Error (b) Maximum Control Input

Figure 7.12: Maximum eigenangle error and maximum control input for ramp commanded R2R maneuvers of magnitude θ_{d} about the non-principal axes e_1, e_2, e_3. The non-principal bus inertia is given by $J_{\text{b}} = J_0$. The control parameters are given by $\eta_u = 0.01, \eta_\theta = 10^{-5}$. All gains are initialized at $\Theta_0 = 0$.

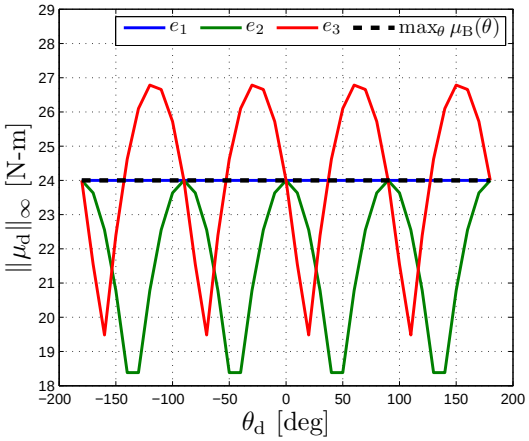

(a) Singularity about $\hat{\imath}_B$, $\theta(0) = \begin{bmatrix} 0 & \frac{\pi}{2} & 0 \end{bmatrix}$

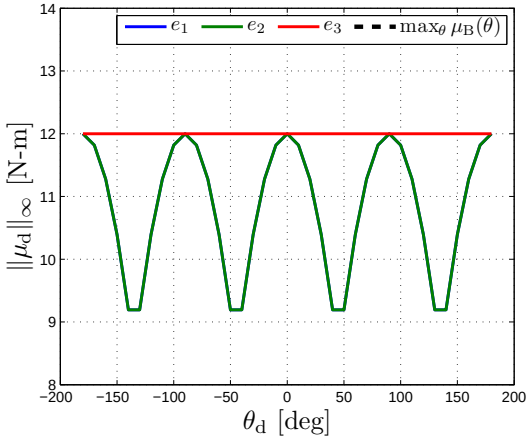

(b) Singularity about $\hat{\jmath}_B$, $\theta(0) = \begin{bmatrix} 0 & 0 & \frac{\pi}{2} \end{bmatrix}$

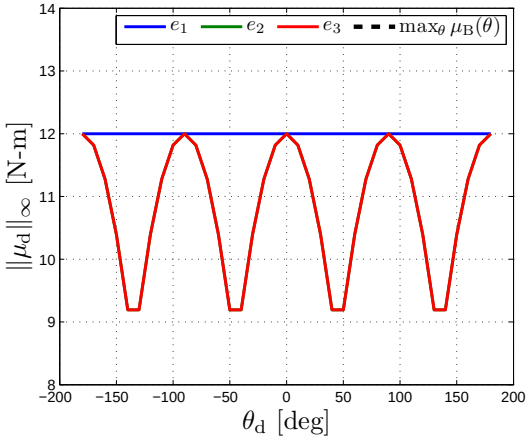

(c) Singularity about $\hat{k}_B$, $\theta(0) = \begin{bmatrix} \frac{\pi}{2} & 0 & 0 \end{bmatrix}$

Figure 7.13: Reachability for various rest attitudes $R_d = \mathcal{R}(\theta_d, e_i)$ for the $i = 1, 2, 3$ given the 3 orthogonal CMG configuration in Section 7.1.3.1.

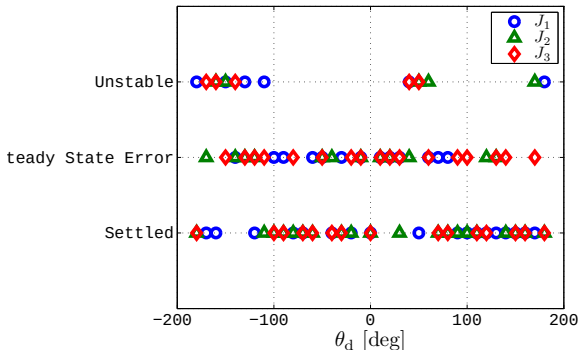

(a) $R_\mathrm{d} = R_\mathrm{d}^1$

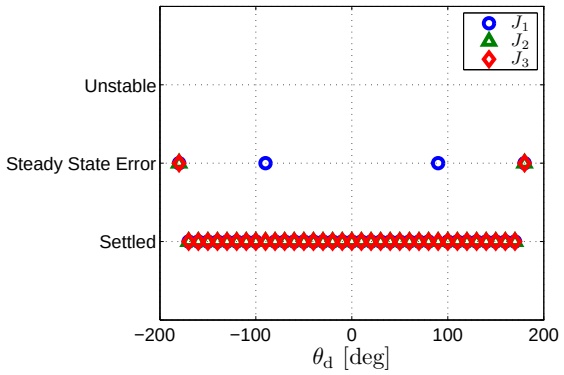

(b) $R_\mathrm{d} = R_\mathrm{d}^2$

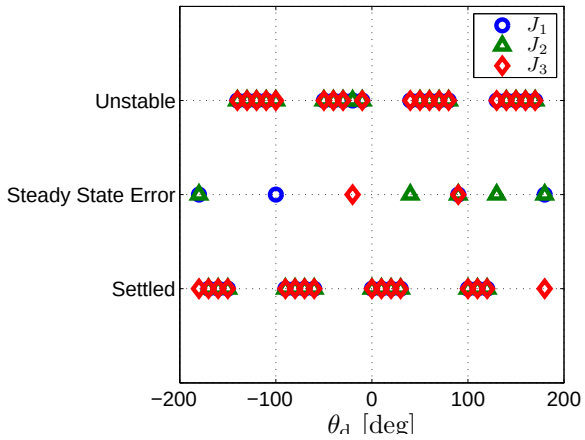

(c) $R_\mathrm{d} = R_\mathrm{d}^3$

Figure 7.14: Maneuver success for step commanded R2R maneuvers of magnitude θ_d about the principal axes e_1, e_2, e_3 given an initially singular gimbal configuration about $\hat{\imath}_\mathrm{B}$. The control parameters are given by $\eta_u = 0.01, \eta_\theta = 10^{-5}$. All gains are initialized at $\Theta_0 = 0$.

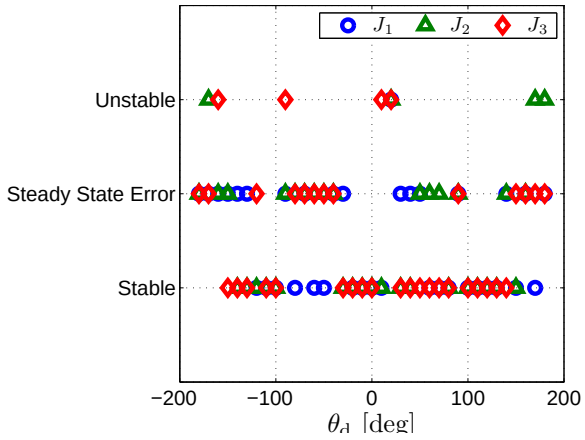

(a) $R_{\mathrm{d}} = R_{\mathrm{d}}^1$

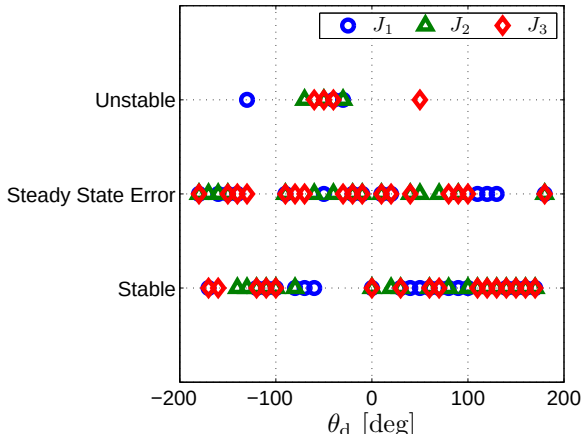

(b) $R_{\mathrm{d}} = R_{\mathrm{d}}^2$

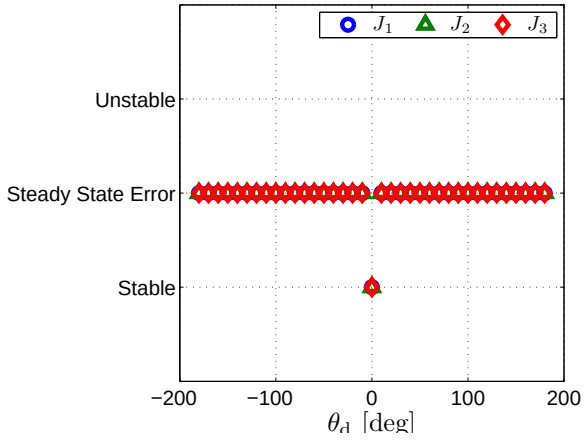

(c) $R_{\mathrm{d}} = R_{\mathrm{d}}^3$

Figure 7.15: Maneuver success for step commanded R2R maneuvers of magnitude θ_{d} about the principal axes e_1, e_2, e_3 given an initially singular gimbal configuration about $\hat{\jmath}_{\mathrm{B}}$. The control parameters are given by $\eta_u = 0.01, \eta_\theta = 10^{-5}$. All gains are initialized at $\Theta_0 = 0$.

CHAPTER 8

Planar Two-Body Linkage

We asses the performance of RCAC on a planar model of a multibody spacecraft. A previous study examined a rigid spacecraft with a single discrete flexible degree of freedom [102]. The spacecraft considered in [102] consists of a rigid base body connected by a compliance to a proof mass that can move along a single direction relative to the base body. The motion of the proof mass is assumed to be unmodeled and unknown, thereby providing a spacecraft model with flexible-mode uncertainty.

By removing the need for a continuum model of flexible dynamics, idealized discrete flexible models provide an exact nonlinear model of a flexible spacecraft under arbitrary motion. Thus, these idealized models provide a transparent setting for assessing the baseline performance of attitude control laws applied to flexible spacecraft.

We consider a planar spacecraft consisting of two components, a base body and an articulated appendage. These bodies are connected by a compliance that allows in-plane relative rotation but no translation. However, unlike [102], the performance objective for this model is to achieve attitude pointing of the appendage with actuation applied to the base body. This model may represent, for example, a telescope mounted on a spacecraft bus.

The challenging aspect of this problem is the fact that the actuation and performance variable are noncolocated. The implications of this control-system architecture are evident due to the fact that control torques applied to the base body to induce rotation in a given direction result in initial rotation of the appendage in the opposite direction. This phenomenon indicates nonminimum-phase behavior.

Adaptive control of nonminimum-phase plants remains a challenging problem [103]. As shown in [62], RCAC is applicable to nonminimum-phase systems as long as the plant is either open-loop asymptotically stable or the nonminimum-phase zeros are known. In [65,66], RCAC is applied to a linearized planar linkage with actuator/performance-variable noncolocation. However, unlike the linkage in [65], in this paper the base body is uncon-

strained. Thus, the system has a rigid body mode and is thus unstable and nonminimum-phase.

8.1 Spacecraft Model

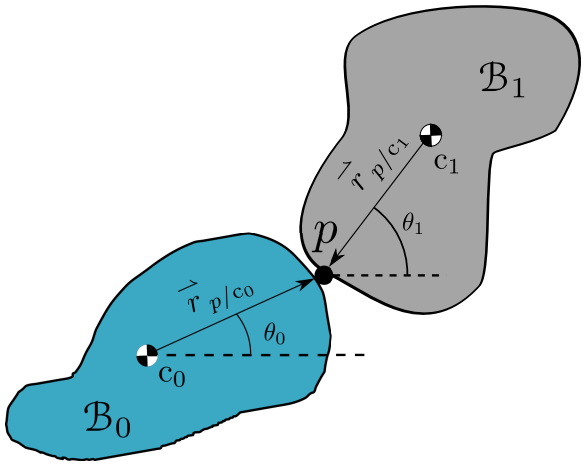

Figure 8.1: Planar two-body linkage with base body $\mathcal{B}_0$ and appendage $\mathcal{B}_1$. The angles θ_0 and θ_1 represent the attitude of $\mathcal{B}_0$ and $\mathcal{B}_1$ relative to a vector fixed in an inertial frame.

Consider the planar two-body linkage in Figure 8.1 composed of a base body $\mathcal{B}_0$ connected by a bending spring to an appendage $\mathcal{B}_1$. The linkage is controlled by a torque actuator attached to $\mathcal{B}_0$.

Define an inertial frame $\mathrm{F_I}$, a frame F_0 fixed to $\mathcal{B}_0$, and a frame F_1 fixed to $\mathcal{B}_1$. Assume that the center of mass c of the linkage is unforced. Then, define three additional reference points: the center of mass c_0 of $\mathcal{B}_0$, , the center of mass c_1 of $\mathcal{B}_1$, and the location of the flexible joint p, connecting $\mathcal{B}_0$ and $\mathcal{B}_1$.

Furthermore, for $i = 0, 1$, the attitude between $\mathrm{F_I}$ and F_i is given by $\vec{R}_{i/\mathrm{I}}$. Similarly, the angular velocity of F_i relative to $\mathrm{F_I}$ is given by $\vec{\omega}_{i/\mathrm{I}}$. The vector from c to c_i is given by $\vec{r}_{\mathrm{c}_i/\mathrm{c}}$ and the vector from c_i to p is given by $\vec{r}_{p/\mathrm{c}_i}$. Finally, the mass of $\mathcal{L}_i$ is m_i and its inertia relative to its center of mass c_i is given by $\vec{J}_{i/\mathrm{c}}$. Resolving the rotation matrices,

inertias, angular velocities, and position vectors in F_i yields,

$$R_i \triangleq \vec{R}_{i/\mathrm{I}}\Big|_i = \begin{bmatrix} \cos\theta_i & -\sin\theta_i & 0 \\ \sin\theta_i & \cos\theta_i & 0 \\ 0 & 0 & 1 \end{bmatrix}, \tag{8.1}$$

$$\vec{\omega}_{i/\mathrm{I}}\Big|_i = \omega_i e_3, \tag{8.2}$$

$$\vec{J}_{i/\mathrm{c}_i}\Big|_i = \mathrm{diag}(\alpha_i, \beta_i, J_i), \tag{8.3}$$

$$\vec{r}_{p/\mathrm{c}_0}\Big|_0 = r_0 e_2, \quad \vec{r}_{p/\mathrm{c}_1}\Big|_1 = -r_1 e_2 \tag{8.4}$$

where for $i = 1, 2$, $\theta_i, \omega_i \in \mathbb{R}$, $\alpha_i, \beta_i, J_i > 0$ are the principal moments of inertia of $\mathcal{L}_i$, $r_i > 0$ is the distance from c_i to p, and, for $j = 1, 2, 3$, e_j is the jth column of the 3×3 identity matrix.

8.1.0.1 Measurement Model

The control objective is to use the actuator on $\mathcal{B}_0$ to align F_1 at a desired angle θ_d relative to a direction fixed in F_I. Thus, the error angle is given by

$$\theta_\mathrm{e} \triangleq \theta_1 - \theta_\mathrm{d}, \tag{8.5}$$

where $-\pi \leq \theta_\mathrm{d} \leq \pi$ is the desired angle between F_1 and F_I. To avoid unwinding, that is, needless rotating for $\theta_e \geq 2\pi$, use the nonlinear measurement

$$y = 2\sin\left(\frac{\theta_\mathrm{e}}{2}\right). \tag{8.6}$$

Note that (8.6) is twice the third component of the error quaternion

$$\tilde{q} = \begin{bmatrix} 0 & 0 & \sin\frac{\theta_\mathrm{e}}{2} & \cos\frac{\theta_\mathrm{e}}{2} \end{bmatrix}^\mathrm{T}.$$

8.1.1 Lagrangian Mechanics

8.1.1.1 Kinetic Energy

The kinetic energy of $\mathcal{B}_0$ relative to c with respect to $\mathrm{F_I}$ is given by

$$T_0 = \frac{1}{2} J_0 \omega_0^2 + \frac{m_0}{2} \| \overset{\mathrm{I}\bullet}{\vec{r}}_{\mathrm{c_0/c}} \|^2 \tag{8.7}$$

Using the definition of the center of mass yields

$$\begin{aligned} \vec{r}_{\mathrm{c_0/c}} &\triangleq -\frac{1}{m_0 + m_1} \left(m_0 \vec{r}_{\mathrm{c_1/C_0}} + m_0 \vec{r}_{\mathrm{c_0/c_0}} \right) \\ &= -\frac{m_1}{m_0 + m_1} \vec{r}_{\mathrm{c_1/c_0}} \\ &= -\frac{m_1}{m_0 + m_1} \left(\vec{r}_{\mathrm{c_1}/p} + \vec{r}_{p/\mathrm{c_0}} \right), \end{aligned} \tag{8.8}$$

Using the transport theorem to take the derivative of (8.8) with respect to $\mathrm{F_I}$ and resolving in $\mathrm{F_I}$ yields

$$\begin{aligned} \left. \overset{\mathrm{I}\bullet}{\vec{r}}_{\mathrm{c_0/c}} \right|_{\mathrm{I}} &= -\frac{m_1}{m_0 + m_1} \left(\overset{\mathrm{I}\bullet}{\vec{r}}_{\mathrm{c_1}/p} + \overset{\mathrm{I}\bullet}{\vec{r}}_{p/\mathrm{c_0}} \right) \Bigg|_{\mathrm{I}} \\ &= -\frac{m_1}{m_0 + m_1} \left(\vec{\omega}^{\times}_{1/\mathrm{I}} \vec{r}_{\mathrm{c_1}/p} + \vec{\omega}^{\times}_{0/\mathrm{I}} \vec{r}_{p/\mathrm{c_0}} \right) \Bigg|_{\mathrm{I}} \\ &= \frac{m_1}{m_0 + m_1} \left(\vec{r}^{\times}_{\mathrm{c_1}/p} \vec{\omega}_{1/\mathrm{I}} + \vec{r}^{\times}_{p/\mathrm{c_0}} \vec{\omega}_{0/\mathrm{I}} \right) \Bigg|_{\mathrm{I}} \\ &= \frac{m_1}{m_0 + m_1} \left(r_1 \omega_1 R_1 + r_0 \omega_0 R_0 \right) e_1. \end{aligned} \tag{8.9}$$

Applying (8.9) to (8.7) and using the cosine addition identity yields

$$\begin{aligned} T_0 = &\frac{1}{2} J_0 \omega_0^2 + \frac{m_0}{2} \left(\frac{m_1}{m_0 + m_1} \right)^2 \cdot \\ &\left(r_1^2 \omega_1^2 + r_0^2 \omega_0^2 + 2 r_0 \omega_0 r_1 \omega_1 e_1^{\mathrm{T}} R_1^{\mathrm{T}} R_0 e_1 \right) \\ = &\frac{1}{2} J_0 \omega_0^2 + \frac{m_0}{2} \left(\frac{m_1}{m_0 + m_1} \right)^2 \cdot \\ &\left(r_0^2 \omega_0^2 + r_1^2 \omega_1^2 + 2 r_0 r_1 \omega_0 \omega_1 \cos \tilde{\theta} \right). \end{aligned} \tag{8.10}$$

where $\tilde{\theta} \triangleq \theta_0 - \theta_1$. Similarly, the kinetic energy of $\mathcal{B}_1$ relative to c with respect to $\mathrm{F_I}$ is given by

$$T_1 = \frac{1}{2} J_1 \omega_1^2 + \frac{m_1}{2} \left(\frac{m_0}{m_0 + m_1} \right)^2 \cdot \left(r_0^2 \omega_0^2 + r_1^2 \omega_1^2 + 2 r_0 r_1 \omega_0 \omega_1 \cos\tilde{\theta} \right). \tag{8.11}$$

Adding (8.7) to (8.11) yields the total kinetic energy

$$\begin{aligned} T &= \frac{1}{2} J_0 \omega_0^2 + \frac{1}{2} J_1 \omega_1^2 + \frac{(m_0 + m_1) m_0 m_1}{(m_0 + m_1)^2} \cdot \left(r_0^2 \omega_0^2 + r_1^2 \omega_1^2 + 2 r_0 r_1 \omega_0 \omega_1 \cos\tilde{\theta} \right) \\ &= \frac{1}{2} J_0' \omega_0^2 + \frac{1}{2} J_1' \omega_1^2 + \gamma r_0 r_1 \omega_0 \omega_1 \cos\tilde{\theta}, \end{aligned} \tag{8.12}$$

where

$$J_0' \triangleq J_0 + \gamma r_0^2, \quad J_1' \triangleq J_1 + \gamma r_1^2, \quad \gamma \triangleq \frac{m_0 m_1}{m_0 + m_1}. \tag{8.13}$$

8.1.1.2 Potential Energy

We assume that the joint is composed of a bending spring that exerts no torque when $\tilde{\theta} = 0$. The bending spring potential is given by

$$U = \frac{k'}{2} \tilde{\theta}^2, \tag{8.14}$$

where $k' > 0$ is the spring stiffness.

8.1.1.3 Lagrangian and Equations of Motion

The Lagrangian for the linkage is given by

$$\begin{aligned} L &= T - U \\ &= \frac{1}{2} J_0' \omega_0^2 + \frac{1}{2} J_1' \omega_1^2 + \gamma l_0 l_1 \omega_0 \omega_1 \cos\tilde{\theta} - \frac{k'}{2} \tilde{\theta}^2. \end{aligned} \tag{8.15}$$

Since $\dot{\theta}_0 = \omega_0$ and $\dot{\theta}_1 = \omega_1$, the equations of motion are then given by

$$\frac{d}{dt} \left(\frac{\partial L}{\partial \omega_0} \right) - \frac{\partial L}{\partial \theta_0} + \frac{\partial \tau}{\partial \omega_0} = u, \tag{8.16}$$

$$\frac{d}{dt}\left(\frac{\partial L}{\partial \omega_1}\right) - \frac{\partial L}{\partial \theta_1} + \frac{\partial \tau}{\partial \omega_1} = 0, \tag{8.17}$$

where $u \in \mathbb{R}$ is the control torque applied to $\mathcal{B}_0$. Computing the partial derivatives in (8.16) and (8.17) yields

$$J_0'\dot{\omega}_0 + b_2\dot{\omega}_1 + b_1\omega_1^2 + k'\tilde{\theta} + c\tilde{\omega} = u, \tag{8.18}$$

$$J_1'\dot{\omega}_1 + b_2\dot{\omega}_0 - b_1\omega_0^2 - k'\tilde{\theta} - c\tilde{\omega} = 0, \tag{8.19}$$

where

$$b_1 \triangleq \gamma r_0 r_1 \sin\tilde{\theta}, \quad b_2 \triangleq \gamma r_0 r_1 \cos\tilde{\theta}. \tag{8.20}$$

Combining the (8.18) and (8.19) into a matrix equation yields

$$M \begin{bmatrix} \dot{\omega}_0 \\ \dot{\omega}_1 \end{bmatrix} = \begin{bmatrix} k'E & cE \end{bmatrix} x + b_1 \begin{bmatrix} -\omega_1^2 \\ \omega_0^2 \end{bmatrix} + \begin{bmatrix} 1 \\ 0 \end{bmatrix} u. \tag{8.21}$$

where $x = \begin{bmatrix} \theta_0 & \theta_1 & \omega_0 & \omega_1 \end{bmatrix}^{\mathrm{T}}$,

$$M \triangleq \begin{bmatrix} J_0' & b_2 \\ b_2 & J_1' \end{bmatrix}, \quad E \triangleq \begin{bmatrix} -1 & 1 \\ 1 & -1 \end{bmatrix}. \tag{8.22}$$

Thus, the equations of motion for the linkage are given by

$$\begin{aligned} \dot{x} = & \begin{bmatrix} 0_{2\times 2} & I_2 \\ k'M^{-1}E & cM^{-1}E \end{bmatrix} x \\ & + \begin{bmatrix} 0_{2\times 1} \\ M^{-1}b_1 \begin{bmatrix} -\omega_1^2 \\ \omega_0^2 \end{bmatrix} \end{bmatrix} + \begin{bmatrix} 0_{2\times 1} \\ M^{-1} \begin{bmatrix} 1 \\ 0 \end{bmatrix} \end{bmatrix} u, \end{aligned} \tag{8.23}$$

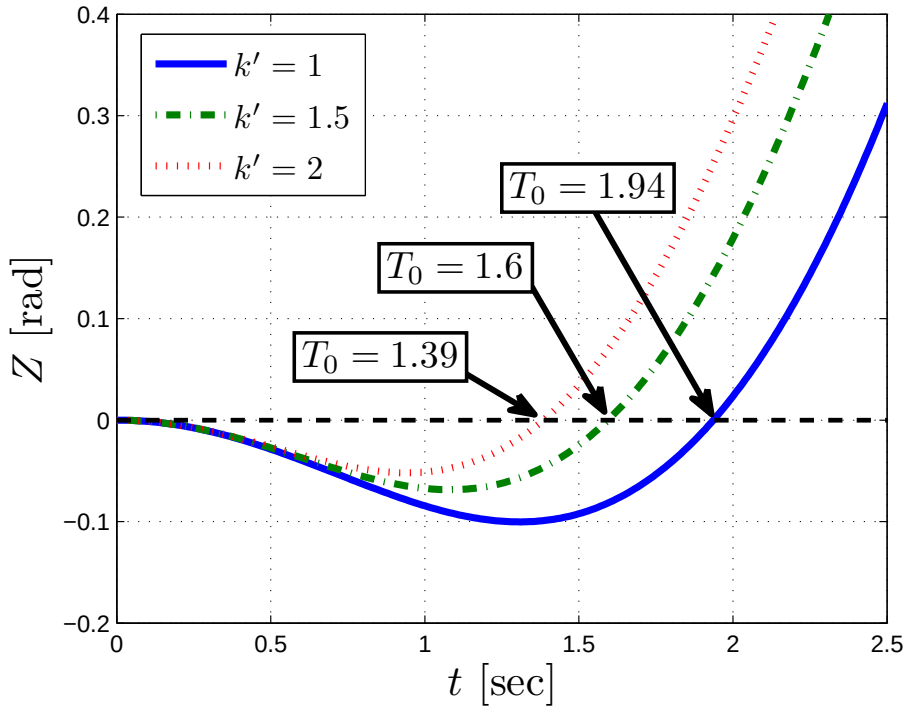

Figure 8.2: Step response Z for the nonlinear planar two-link mechanism for different values of the spring stiffness k'. The model parameters are $r_0 = r_1 = 1, J_0 = J_1 = 1, m_0 = m_1 = 1, c = 0$. T_0 indicates the zero-crossing time for each curve.

where the inverse of the mass matrix is given by

$$M^{-1} = \frac{1}{J_0' J_1' - b_2^2} \begin{bmatrix} J_1' & -b_2 \\ -b_2 & J_0' \end{bmatrix}. \tag{8.24}$$

8.1.2 Dynamical Analysis

Subjecting the system described by (8.18) and (8.19) to a unit step torque applied to $\mathcal{B}_0$ and measuring θ_1 yields the response shown in Figure 8.2. Note that $\theta_1 < 0$ before crossing zero to remain positive. This suggests the presence of a nonminimum-phase zero in the linear dynamics demonstrated below.

8.1.2.1 Linearization

Computing the Jacobian of (8.23) at the equilibrium $\bar{x} = 0_{4\times 1}$ yields

$$\delta\dot{x} = \begin{bmatrix} 0_{2\times 2} & I_2 \\ k'\bar{M}^{-1}E & c\bar{M}^{-1}E \end{bmatrix} \delta x + \frac{1}{d}\begin{bmatrix} 0_{2\times 1} \\ J_1' \\ -\gamma r_0 r_1 \end{bmatrix} u, \tag{8.25}$$

$$y = \begin{bmatrix} 0 & 1 & 0 & 0 \end{bmatrix} \delta x, \tag{8.26}$$

where $\delta x = x - \bar{x}$,

$$\bar{M}^{-1} \triangleq \frac{1}{d}\begin{bmatrix} J_1' & -\gamma r_0 r_1 \\ -\gamma l_0 l_1 & J_0' \end{bmatrix}, \quad d \triangleq J_0' J_1' - (\gamma r_0 r_1)^2. \tag{8.27}$$

Therefore, the transfer function for the linear system in (8.25), (8.26) is given by

$$G(s) = -\frac{\gamma r_0 r_1}{d} \frac{\left(s^2 - \frac{1}{\gamma r_0 r_1}k'\right)}{s^2\left[s^2 + \frac{k'}{d}\left(J_0' + J_1' + 2\gamma r_0 r_1\right)\right]}. \tag{8.28}$$

Note that $G(s)$ has a nonminimum-phase zero at

$$\bar{z}_{\mathrm{c}} = \frac{1}{2\gamma r_0 r_1}\sqrt{4k'\gamma r_0 r_1}. \tag{8.29}$$

8.1.3 Discretization

Since RCAC is a discrete-time method, we discretize the linearized equations of motion. The discrete-time system matrix is given by

$$A = e^{A_{\mathrm{c}}h} \approx I_4 + hA_{\mathrm{c}} = \begin{bmatrix} I_{2\times 2} & hI_2 \\ hk'\bar{M}^{-1}E & I_2 + hc\bar{M}^{-1}E \end{bmatrix}, \tag{8.30}$$

where h is the sample time and A_{c} is the system matrix in (8.26). The input and output matrices are given by

$$B = \int_0^h e^{A_{\mathrm{c}}\tau}\mathrm{d}\tau \begin{bmatrix} 0_{2\times 1} \\ B' \end{bmatrix} \approx \begin{bmatrix} \frac{h^2}{2}B' \\ hB' + \frac{h^2}{2}c\bar{M}^{-1}EB' \end{bmatrix}, \tag{8.31}$$

$$C = \begin{bmatrix} 0 & 1 & 0 & 0 \end{bmatrix}, \tag{8.32}$$

respectively, where $B' = d^{-1}\begin{bmatrix} J_1' & -\gamma r_0 r_1 \end{bmatrix}^{\mathrm{T}}$.

8.2 The Nonminimum-phase Problem

8.2.1 Laurent Expansion

The transfer function of an asymptotically stable system can be approximated using a truncated Laurent series expanded at the spectral radius of G_{zu}. The coefficients of this series are the Markov parameters. Therefore, the Markov parameters can be used to estimate the location of the nonminimum-phase zeros of G_{zu} [78],

$$\begin{aligned} G_{zu} &\approx G_{\mathrm{f}}(\mathbf{z}) \\ &= \frac{H_0\mathbf{z}^{n_H} + H_1\mathbf{z}^{n_H-1} + \cdots + H_{n_H}}{\mathbf{z}^{n_H}} \\ &= \frac{(\mathbf{z}-\hat{z}_1)\cdots(\mathbf{z}-\hat{z}_{n_z})\cdots(\mathbf{z}-\hat{z}_{n_H})}{\mathbf{z}^{n_H}}, \end{aligned}$$

where for $i = 1, \ldots n_H$, $\hat{z}_i$ is an estimated nonminimum-phase zero and n_z is the number of nonminimum-phase zeros in G_{zu}.

When $n_H > n_z + 1$, G_{f} in (8.33) has more zeros than G_{zu}. Figure 8.3(a) shows that the extra zeros of G_{f} are distributed along the unit circle. If the plant is unstable, As n_H increases, G_{f} develops real and imaginary zeros. Note that, for $n_H = 9$, the zeros of G_{f}, indicated by the triangular markers, are all imaginary. As we increase the filter order to $n_H = 9$ the filter exhibits a positive root. Eventually, as shown by the asterisks corresponding to $n_H = 17$, one of the real zeros of G_{f} approaches the location of the nonminimum-phase zero $\bar{z}$ of G_{zu}.

Figure 8.3(b) confirms that, as the order of G_{f} is increased, the error between the largest real root of G_{f} and the nonminimum-phase zero of G_{zu} decreases. The horizontal axis in

8.3(b) starts at $n_H = 10$ since lower order filters may not have real roots.

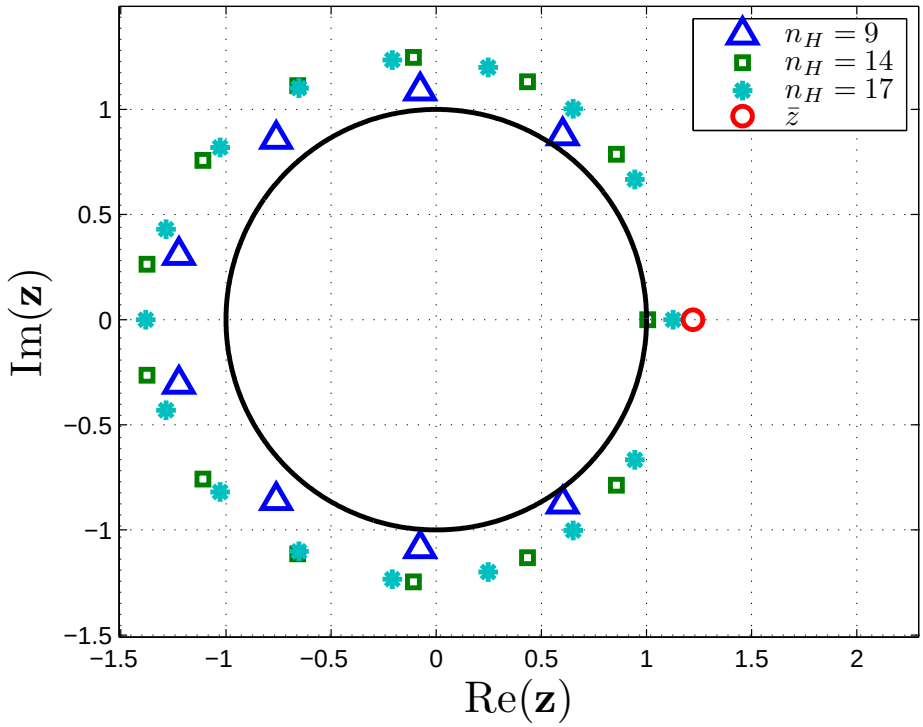

(a) Roots of G_{f} in (8.33) for different values of n_H and $k' = 2$. The location of the nonminimum-phase zero $\bar{z}$ of G_{zu} is represented by the circular marker to the right of the unit circle.

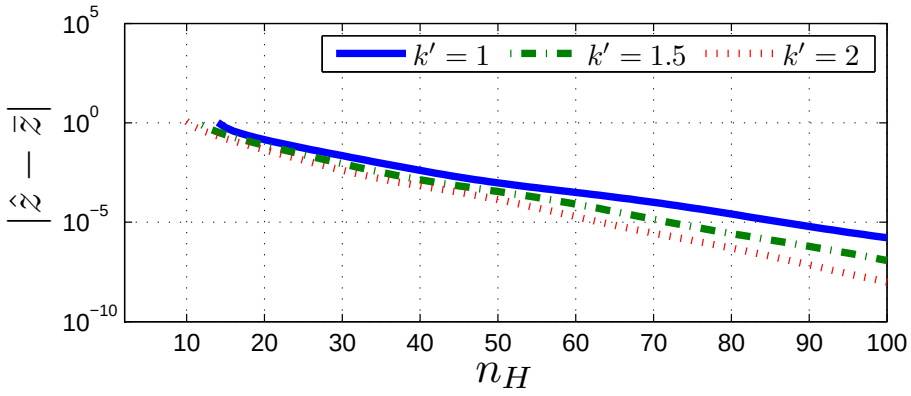

(b) Error in the estimate of $\bar{z}$ in (8.29) as a function of the filter order n_H for different values of k'.

Figure 8.3: Effects of increasing the order n_H of G_{f}, on the location of the nonminmum-phase zero estimate $\hat{z}$. As n_H increases $\hat{z}$ approaches the location of the nonminimum phase zero $\bar{z}$ of G_{zu}.The model parameters are $r_0 = r_1 = 1, J_0 = 1, J_1 = 1, m_0 = m_1 = 1, c = 0$. The time-step size is $h = 0.1$ sec.

8.2.2 Step and Impulse response

The impulse response is the derivative of the step response. Since the Markov parameters correspond to the impulse response, we can obtain the step response $Z(k)$ by adding the Markov parameters. That is,

$$Z(k) = \sum_{i=1}^{k} H_i. \tag{8.33}$$

In order to select the required Markov parameters we examine the sign of the estimated zero as the number of Markov parameters in the filter increases.

Figure 8.4 shows how the real zero in G_{f} crosses the unit circle and becomes nonminimum-phase as n_H increases. The arrows indicate the first step in which the step response is positive. For example, the solid line in Figure 8.2 indicates that the step response for $k' = 1$ crosses zero at $T_0 \approx 1.9$ sec. Given a step size of $h = 0.1$ sec, the step response is positive after $k_0 = 14$ steps as indicated by the solid line in Figure 8.4. Therefore, building a filter G_{f} using (8.33), requires $n_H \geq k_0 = 14$, in order to capture the nonminimum-phase behavior of the plant.

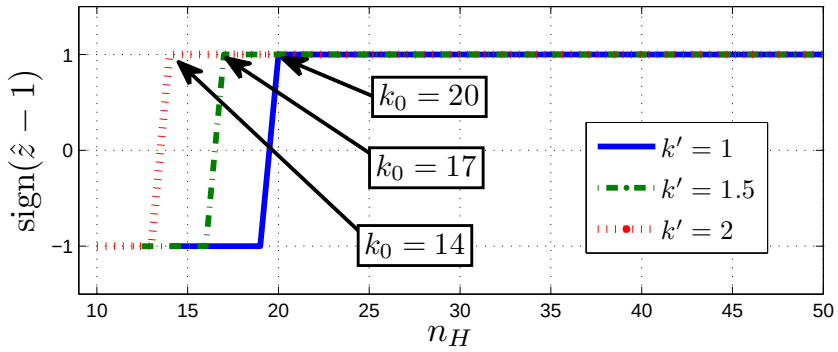

Figure 8.4: Minimum-phase status of the estimated zero, $\hat{z}$ as a function of n_H. The time-step $k_0 > \frac{T_0}{h}$ indicates the first time-step when the step response is positive. If $n_H \geq k_0$, $\hat{z}$ is nonminimum-phase. The model parameters are $r_0 = r_1 = 1, J_0 = J_1 = 1, m_0 = m_1 = 1, c = 0$. The time-step size is $h = 0.1$ sec, k indicates the time step at which the step response crosses zero.

Proposition 4. *It is possible to control a nonminimum-phase system using retrospective cost adaptive control (RCAC), by choosing the filter G_{f} using Markov parameters as in* (8.33)*. Furthermore, the order of this filter n_H must be such that*

$$n_H \geq k_0. \tag{8.34}$$

The zero-crossing step k_0 is defined such that

$$\text{for all } k \geq k_0,\ Z(k) > 0. \tag{8.35}$$

Otherwise the nonminimum-phase behavior of the plant is not captured leading to instability.

We demonstrate Proposition 4 numerically in the following section.

8.3 Numerical Examples

The following examples involve three maneuver types. Rest-to-Rest (R2R) maneuvers are step commands where the linkage begins at zero attitude error and $\mathcal{B}_0$ and $\mathcal{B}_1$ have zero angular velocity relative to $\mathrm{F_I}$. Motion-to-Rest (M2R) maneuvers the linkage starts at an arbitrary angular velocity and is commanded to stabilize at a specified attitude. Finally, a Rest-to-Spin (R2S) maneuver involves bringing the linkage from a stationary attitude to a non-constant desired attitude such as a constant spin or a sinusoidal motion.

8.3.1 Configuring RCAC

First, we choose $n_H > \frac{T_0}{h}$ such that the step response, $Z(n_H) > 0$. Therefore, the filter G_{f} contains a nonminimum-phase zero. For each k' in Figure 8.5, let $n_H = k_0$, the values indicated in Figure 8.4. The controller order is matched to the filter order so that $N_{\mathrm{c}} = n_H$. Finally, the control and transient penalties, R_u and R_θ, respectively, are chosen arbitrarily.

8.3.1.1 Choosing n_H

We examine the effect of n_H on RCAC to test Proposition 1. To achieve this, we fix the controller order and command the $\theta_{\mathrm{d}} = 180$ deg step for a given controller order. Figure 8.6 confirms the condition in (8.34). As n_H decreases, the settling time increases and eventually, when $n_H < k_0$ the controller diverges. Furthermore, increasing n_H reduces the settling time T_{s} and the steady state error Z_{ss}. In some cases a larger order filter can reduce transients $Z_{\max}$ although the effect is not clear from the Figure 8.6. Furthermore, increasing the filter order does not necessarily yield improved performance. However, closer examination of T_{s} and Z_{ss} in Figure 8.6 suggests that performance is improved when the controller order $n_H = N_{\mathrm{c}}$.

Figure 8.7 shows that, when $N_{\mathrm{c}} = n_H$, performance increases proportionally to n_H. As in Figure 8.6, the transient response may not always improve as n_H increases.

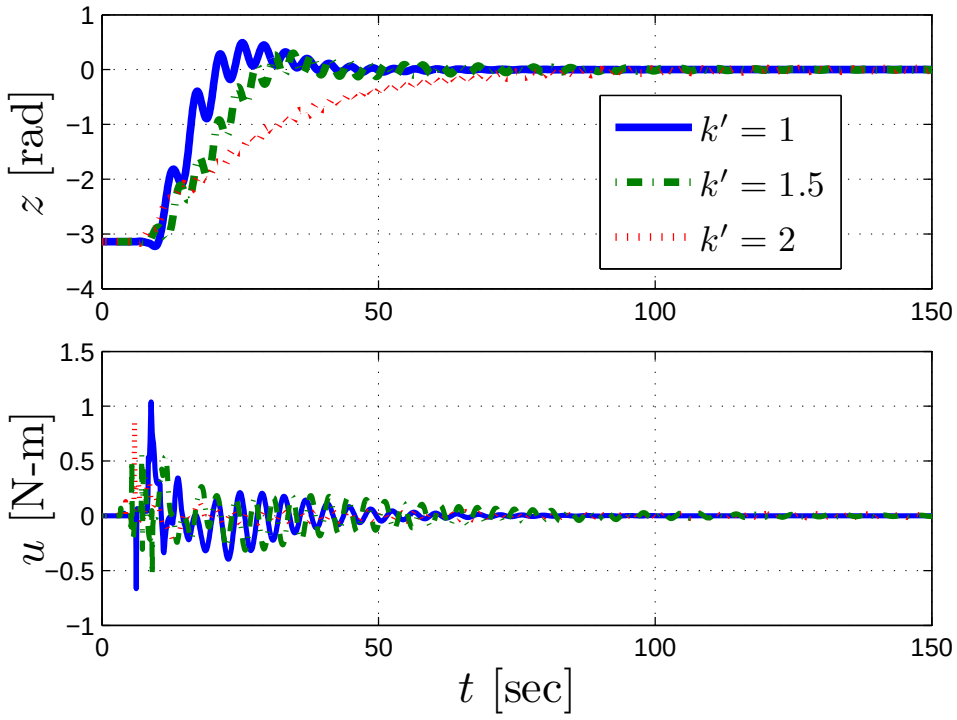

Figure 8.5: Performance z (top) and control u (bottom) for R2R maneuver to $\theta_{\rm d} = 180$ deg. The order of $G_{\rm f}$ is $n_H = 14, 17, 20$ for $k' = 1, 1.5, 2$, respectively. The controller parameters are $R_u = 0.1$, $R_\theta = 10^{-10}$ and the controller order $N_{\rm c} = n_H$. The model parameters are $r_0 = r_1 = 1, J_0 = 1, J_1 = 1, m_0 = m_1 = 1, c = 0, h = 0.1$.

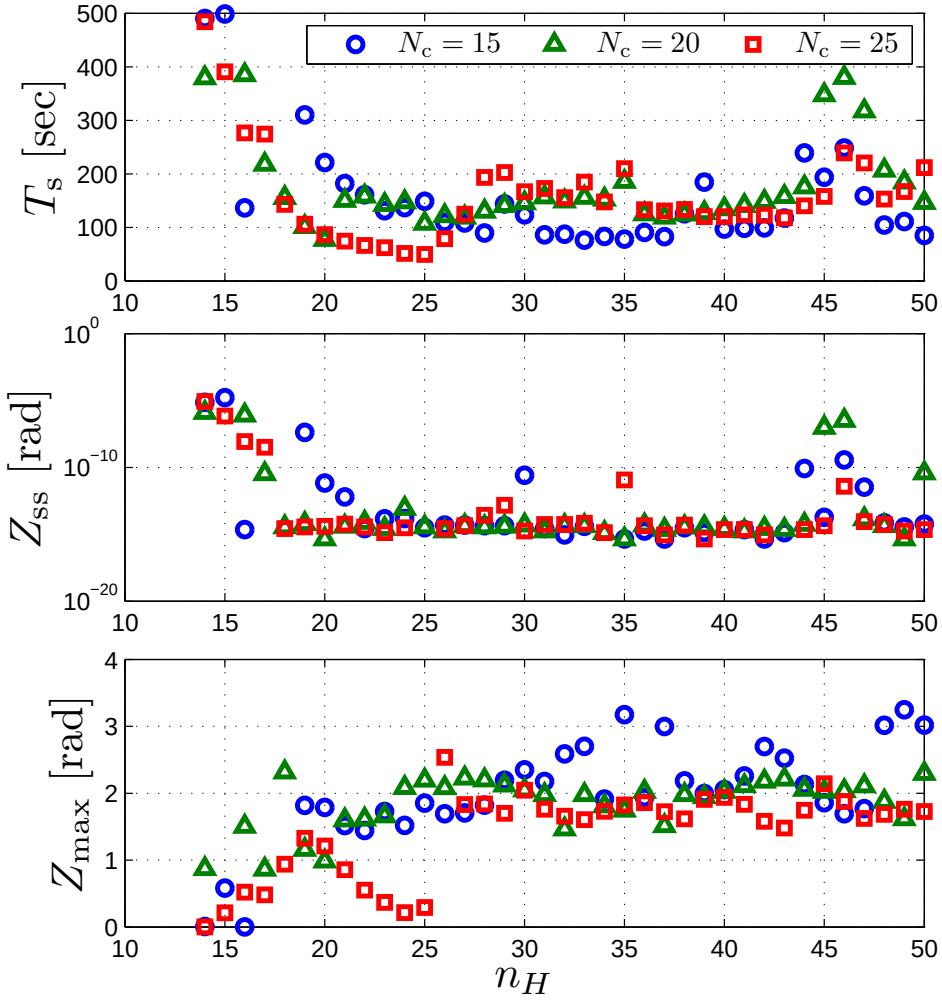

Figure 8.6: Comparison of settling time T_s (top), steady-state error Z_{ss} (middle) and overshoot Z_{max} as a function of the filter order n_H for the 180 degree R2R maneuver. The controller order N_c is fixed at the three values indicated by each marker. The controller parameters are $R_u = 0.1$, $R_\theta = 10^{-10}$ and the controller order $N_c = n_H$. The model parameters are $r_0 = r_1 = 1, J_0 = 1, J_1 = 1, m_0 = m_1 = 1, c = 0, h = 0.1$.

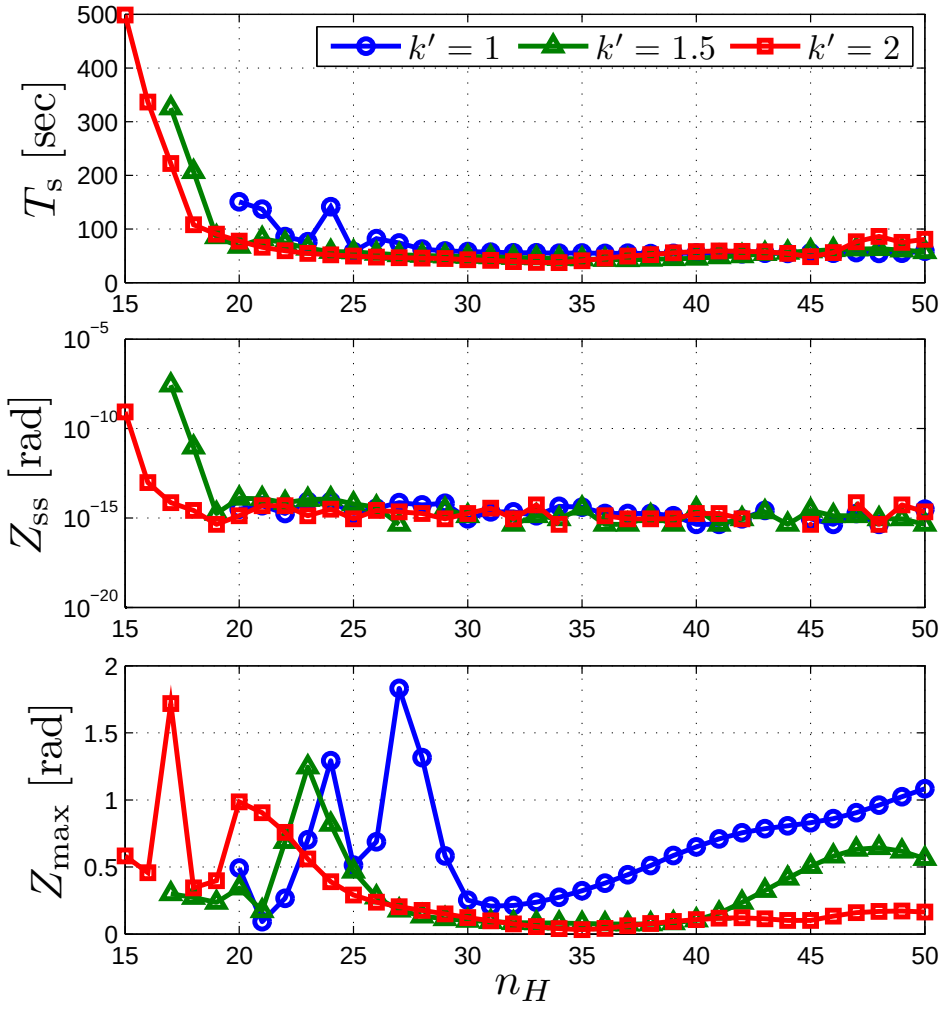

Figure 8.7: Comparison of settling time T_s (top), steady-state error Z_{ss} (middle) and overshoot Z_{max} as a function of the filter order n_H for the 180 degree R2R maneuver. The controller parameters are $R_u = 0.1$, $R_\theta = 10^{-10}$ and the controller order $N_c = n_H$. The model parameters are $r_0 = r_1 = 1, J_0 = 1, J_1 = 1, m_0 = m_1 = 1, c = 0, h = 0.1$.

8.3.2 Robustness Study

The examples in Figure 8.7 utilized perfect knowledge of the Markov parameters. We now study how uncertainty in the parameters affects performance for command following.

8.3.2.1 Parameter changes and the step response

We examine how the system behavior changes as different parameters are scaled. For $i = 0, 1$, define a baseline two-body linkage whose parameters are given by $r_i = \bar{r}, J_i = \bar{J}, m_i = \bar{m}, k' = \bar{k}'$. Then, the parameters are scaled one at a time according to

$$q = \alpha \bar{q}, \tag{8.36}$$

where $\bar{q}$ represents the baseline parameters and q represents the scaled parameter. Figure 8.8 shows how the zero-crossing time T_0 is affected by scaling each parameter. Note that the largest effects are due to variations in the spring stiffness k' and the distance r_i.

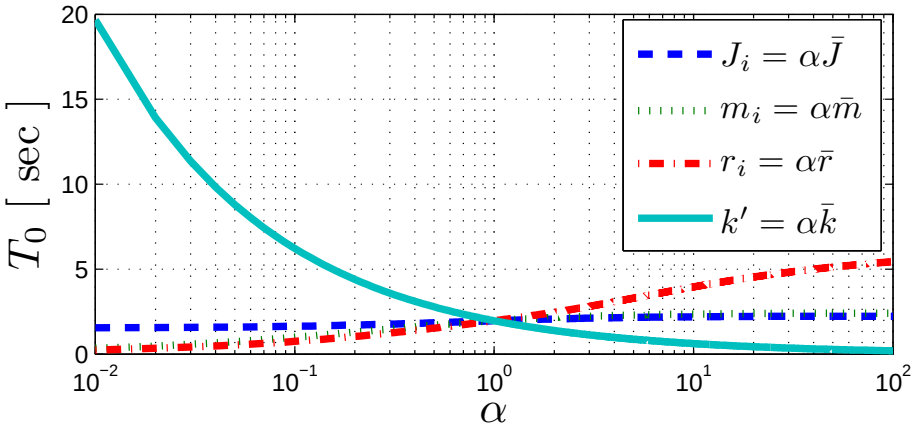

Figure 8.8: Effect of parameter scaling on the step-response zero-crossing T_0 for $i = 0, 1$. The baseline parameters are given by $\bar{r} = 1, \bar{J} = 1, \bar{m} = 1, \bar{k}' = 1$,.

The values of T_0 in Figure 8.8 can be used to select the minimum filter order for robustness to parameter scaling. For example, as k' increases, T_0 decreases. This suggest that a filter constructed for a smaller spring constant might contain sufficient information to account for the nonminimum-phase behavior. Similar logic suggests that in order to be robust to smaller than expected values of k', n_H should be large. The logic for robustness to scaling of r_i is similar; as r_i decreases T_0 decreases, suggesting that performance of a filter chosen for larger r_i should be acceptable.

8.3.2.2 Response to scaled stiffness k' and distance r_i

To test the robustness of the controller to uncertain plant information, we build the filter $G_{\rm f}$ from the Markov parameters for the baseline system using $\bar{r}, \bar{J}, \bar{m}, \bar{k}$. Independently scaling the stiffness or the center of mass location such that $k' = \alpha\bar{k}'$ and for $i = 0$ or $i = 1$, $r_i = \bar{r}$ provides a method of testing robustness to modeling error. Figures 8.9 and 8.10 show the steady state error $Z_{\rm ss}$ and the maximum control input $rmmax|u|$ for the $\theta_{\rm d} = 180$ deg R2R maneuver when either the stiffness k' or the center of mass location r_0 or r_1 are modeled incorrectly.

In Figure 8.9 the stiffness is less than the nominal and since the step response crosses zero later than when $k' = 1$, the system is more difficult to control. When the distance r_0 is less than the nominal distance RCAC can easily finish the maneuver since the step response crosses zero earlier than for $r = 1$. In Figure 8.10 although the stiffness is larger than $\bar{k}$ the system is easier to control. Conversely, as the distance r_0 increases, RCAC is less able to stabilize the system.

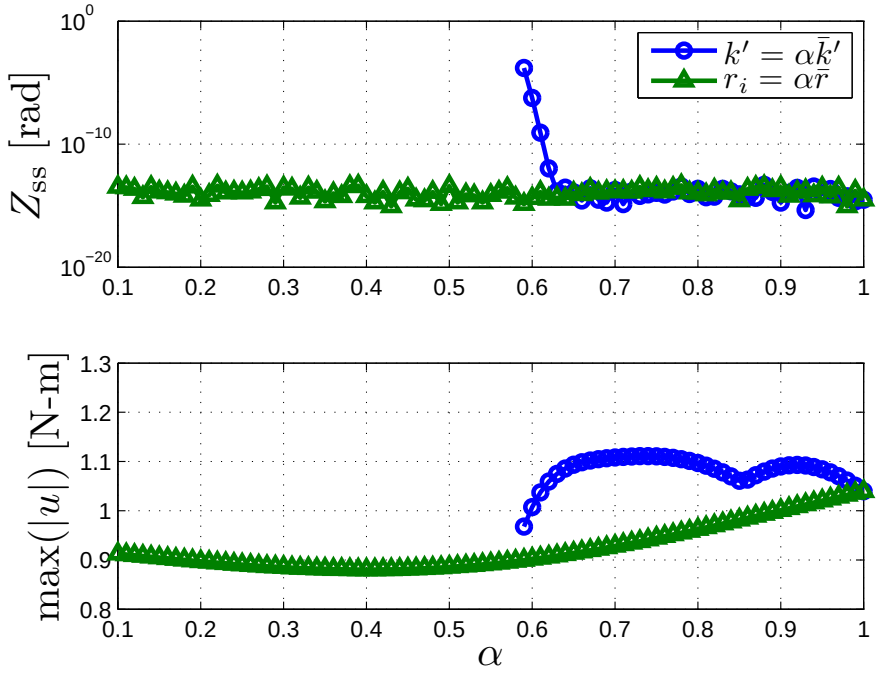

Figure 8.9: Effect of parameter scaling on the R2R maneuver. The baseline parameters are given by $\bar{r} = 1, \bar{J} = 1, \bar{m} = 1, \bar{k}' = 1$. The Controller parameters are $n_H = N_{\rm c} = 20, R_u = 0.1, R_\theta = 10^{-10}$.

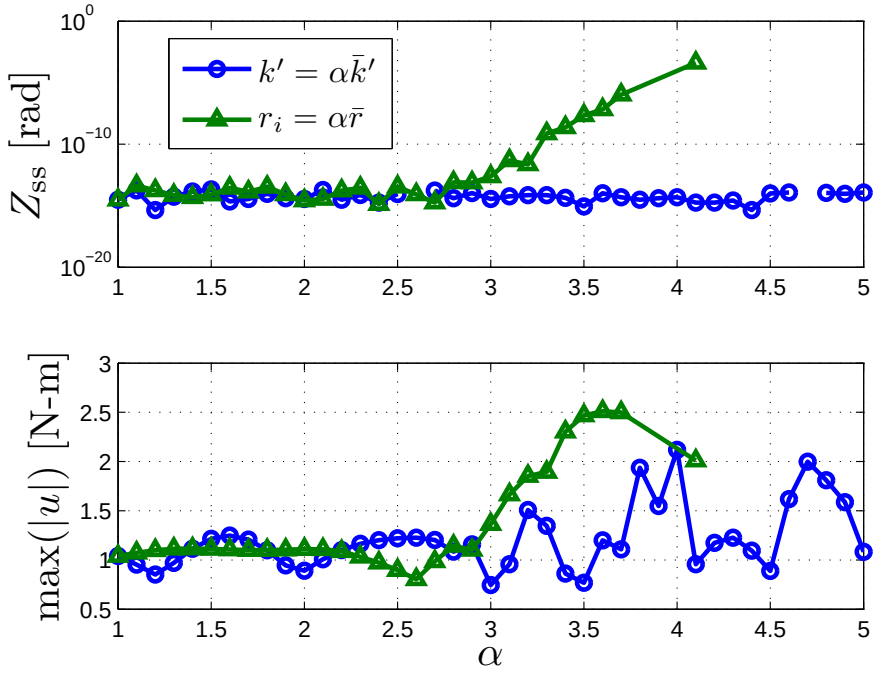

Figure 8.10: Effect of parameter scaling on the R2R maneuver. The baseline parameters are given by $\bar{r} = 1, \bar{J} = 1, \bar{m} = 1, \bar{k}' = 1$. The controller parameters are $n_H = N_c = 20, R_u = 0.1, R_\theta = 10^{-10}$.

8.4 Conclusions

We achieved command following of a two-body linkage with noncolocated sensors and actuators. Using RCAC enabled the application of a controller using only the Markov parameters of the system without the need to know the location of the nonminmum-phase (NMP) zero. Using the guidelines developed, we are able to construct a controller that can robustly deal with the NMP behavior and parameter uncertainty.

Although the Markov parameters may be obtained through linearization, if the system parameters are not readily available the impulse response of the nonlinear system can be used instead. By integrating the impulse response we also obtain the step response which provides the necessary information to capture the NMP behavior of the system.

Numerical simulations show that the method is robust to scaling of the spring stiffness and distance from the center of mass of both bodies to the flexible joint. Saturation limits can be accommodated through a control penalty in the cost function.

CHAPTER 9

Conclusions and Future Research

We considered the problem of retrospective-cost based adaptive spacecraft attitude control. We successfully applied retrospective cost adaptive control (RCAC) to spacecraft simulations controlled using thrusters, reaction wheels, magnetic torquers, and control moment gyros (CMG's). Furthermore, we extended the thruster results to the control of a simplified model of a flexible spacecraft with noncollocated sensors and actuators. The performance variable used for these control problems is based on rotation matrices and although two different vector attitude representations were used to compute the Markov parameters, the inherent issues with these parameterizations do not affect control synthesis since they are not used to propagate the attitude or to evaluate the attitude error.

9.1 Conclusions

For thrusters and reaction wheels, RCAC was applied as an inertia-free controller. Using numerical simulations we demonstrated the robustness of RCAC to mass property uncertainty, actuator nonlinearities and misalignment, as well as unknown disturbances, measurement noise and bias. The Markov parameter for thrusters and reaction wheels was derived through the linearization of Euler and Poisson's equations using a vector representation of the attitude. These controllers were then made inertia-free by removing all mass property information from the Markov parameters.

In order to extend the approach to magnetic torquers the Markov parameter has to be updated in real-time. However, the input matrix singularity inherent in magnetic torquers necessitated the development of two alternate Markov parameter formulations. First, we examined an averaging technique inspired by [87] and utilized an averaged input matrix which was rotated at each time step based on the current spacecraft attitude. Then, we implemented a multi-input-single-output decentralized control structure which did not require matrix inversion and thus avoided the problem of input matrix singularities. Both

methods were successfully applied in simulation to control spacecraft in polar orbits with known inertia alignment information, that is, the alignment between the principal axes and the actuators is known a priori.

Singularities and time varying input matrix issues also affected the development of the retrospective cost-based controller for CMG's. We applied the 1-Step implementation of RCAC to sidestep the matrix rank requirements of the 2-Step implementation. Furthermore, we addressed the inherent limitation of the off-diagonal element-based performance, namely the existence of spurious equilibria, is addressed through the addition of the matrix trace-based performance variable. Given these challenges we took a different approach to linearization and Markov parameter generation, we replaced the row parameterization of the rotation matrix in favor of the rotation matrix variations. Using the propagated unit impulse response of the linear system the impulse response of the rotation matrix was computed. This impulse response rotation matrix yielded the impulse response of the performance variables and thus the columns of the time-varying Markov parameter.

Last but not least, we accomplished control of a dual-rigid body model of a flexible spacecraft with noncolocated sensors and actuators without knowledge of the location of the nonminimum-phase zeros. Guidelines for constructing a Markov parameter-based filter are developed experimentally from the qualities of the step response of the linearized system. Robustness to model uncertainty was demonstrated through system analysis and numerical simulations. The

The main contribution of this work is a unified framework for the application of RCAC to spacecraft attitude control. The adaptive controller uses performance variables which are functions of the rotation matrices. Thus, the controller does not need any extra logic or discontinuities required by other attitude representations and necessary in most controllers in literature. Attitude control of rigid bodies using thrusters, reaction wheels, magnetic torquers, or CMG's is achieved only using the impulse response of the system. The first Markov parameter can be computed analytically from the system model. For thrusters and reaction wheels the Markov parameter can be also be obtained by applying a unit impulse to the system. Using the impulse response can be a useful approach in the absence of modeling information.

Another important contribution is the detailed development of CMG dynamics from Newton-Euler dynamics. Surprisingly, these equations are not found in the CMG literature. The effect of singularities was qualitatively evaluated through the development of a sufficient condition to test the reachability of desired attitudes.

The observations relating the zero crossing of the step response of NMP systems and the roots of the Markov parameter polynomial which are the basis for Chapter 8 can yield

new results on the problem of controlling other unstable NMP systems using RCAC. Other contributions which enabled these results are the new regularization term in cost function of the 1-Step implementation without which the results in Chapter 8 would not have been possible, and the implementation of sequential recursive least squares updates which significantly increase the numerical stability of RCAC for MIMO systems.

9.2 Future Research

First, the difference between the two implementations of RCAC should be examined, the numerical experiments in Chapters 3, 4, and 5 can be redone using the 1-Step method. The 2-Step approach was applied to the CMG problem in [74] with limited success.

A thorough investigation on the effects of singularities on the control gains as well as development of a necessary condition for resting attitude reachability given the initial and desired angular momenta should be explored. A reference governor could also be applied in conjunction with Proposition 1 in Chapter 7 to prevent unfeasible commands to the controller. Furthermore, CMG arrays which allow null motion, such as the 4 CMG pyramid or the 6 CMG rooftop arrangement, as well as variable speed CMG's should be examined.

The problem of magnetic control using RCAC is not fully investigated, lower inclination orbits, corrupted magnetic field measurements and a control implementation which accounts for the geometric torque constraints merits investigation.

Finally, the results in Chapter 8 can be extended to 3-dimensional rigid bodies as well as other NMP systems. We should also aim to obtain an analytical explanation for the behavior of the roots of the Markov parameter polynomial based on the polynomial order and the zero-crossing of the step response.

APPENDIX A

Useful Lemmas and Definitions

The derivation in Chapter 3 relies heavily on the following Lemmas and Definitions. They are presented in detail and proven in [81].

Definition 1. *Let* $\mathrm{F_X}, \mathrm{F_Y}$ *be frames defined by the frame vectors* $\hat{\imath}_\mathrm{X}, \hat{\jmath}_\mathrm{X}, \hat{k}_\mathrm{X}$*, and* $\hat{\imath}_\mathrm{Y}, \hat{\jmath}_\mathrm{Y}, \hat{k}_\mathrm{Y}$ *respectively. Then the physical rotation matrix which rotates* $\mathrm{F_X}$ *to* $\mathrm{F_Y}$ *is defined by*

$$\vec{R}_{\mathrm{Y/X}} \triangleq \hat{\imath}_Y \hat{\imath}_X^{\mathrm{T}} + \hat{\jmath}_Y \hat{\jmath}_X^{\mathrm{T}} + \hat{k}_Y \hat{k}_X^{\mathrm{T}}, \tag{A.1}$$

where the superscript T *indicates the transpose operator.*

Definition 2. *Let* $\vec{x}$ *be a physical vector. For all* $\vec{x}$*, the physical identity matrix* $\vec{U}$ *is defined by*

$$\vec{U}\vec{x} \triangleq \vec{x}. \tag{A.2}$$

Definition 3. *Let* $\vec{x}, \vec{y}$ *be a physical vectors. Then the physical cross product matrix* $\vec{x}^{\times}$ *is defined by*

$$\vec{x}^{\times} y \triangleq \vec{x} \times \vec{y} \tag{A.3}$$

Lemma 6. *Let* $\vec{x}^{\times}$ *be a physical cross product matrix then*

1. $\vec{x}^{\times}\vec{x} = 0$,
2. $\left(\vec{x}^{\times}\right)^{\mathrm{T}} = -\vec{x}^{\times}$,
3. $\vec{x}^{\mathrm{T}}\vec{x}^{\times} = 0$.

Lemma 7. *Let* $\vec{R}_{\mathrm{Y/X}}$ *be a physical rotation matrix. Then*

1. $\overrightarrow{R}^{\mathrm{T}}_{\mathrm{Y/X}} = \overrightarrow{R}_{\mathrm{X/Y}}$,

2. $\overrightarrow{R}_{\mathrm{Y/X}}\overrightarrow{R}_{\mathrm{X/Y}} = \overrightarrow{U}$,

Definition 4. *Let* $\mathrm{F_X}$ *be a frame and* $\overrightarrow{x}$ *be a physical vector expressed as*

$$\overrightarrow{x} = x_1\hat{\imath}_{\mathrm{X}} + x_2\hat{\jmath}_{\mathrm{X}} + x_3\hat{k}_{\mathrm{X}} \tag{A.4}$$

The frame derivative of $\overrightarrow{x}$ *with respect to* $\mathrm{F_X}$ *is defined by*

$$\overset{\mathrm{X}\bullet}{\overrightarrow{x}} \triangleq \dot{x}_1\hat{\imath}_{\mathrm{X}} + \dot{x}_2\hat{\jmath}_{\mathrm{X}} + \dot{x}_3\hat{k}_{\mathrm{X}} \tag{A.5}$$

Lemma 8. *Let* $\mathrm{F_X}$ *be a frame and* $\overrightarrow{x}$ *be a physical vector. Then*

$$\left(\overset{\mathrm{X}\bullet}{\overrightarrow{x}}\right)^{\mathrm{T}} \triangleq \left(\overrightarrow{x}^{\mathrm{T}}\right)^{\mathrm{X}\bullet} . \tag{A.6}$$

Lemma 9. *Let* $\overrightarrow{R}_{\mathrm{Y/X}}$ *be a physical rotation matrix and* $\overrightarrow{\omega}_{\mathrm{Y/X}}$ *be the angular velocity of* $\mathrm{F_X}$ *relative to* $\mathrm{F_Y}$*. The relation between frames* $\mathrm{F_X}$ *and* $\mathrm{F_Y}$ *are evolves according to Poisson's equation*

$$\overset{\mathrm{Y}\bullet}{\overrightarrow{R}}_{\mathrm{Y/X}} = \overrightarrow{R}_{\mathrm{Y/X}}\overrightarrow{\omega}^{\times}_{\mathrm{Y/X}}, \tag{A.7}$$

where $\mathrm{Y}\bullet$ *denotes a frame derivative.*

Definition 5. *Let* $\mathrm{F_X}$ *be a frame and define a physical vector* $\overrightarrow{x}$*, then* $\overrightarrow{x}\Big|_{\mathrm{X}}$ *is the physical vector* $\overrightarrow{x}$ *resolved in* $\mathrm{F_X}$*.*

Definition 6. *Let* $\mathrm{F_X}$ *be a frame and define a physical matrix* $\overrightarrow{M}$*, then* $\overrightarrow{M}\Big|_{\mathrm{X}}$ *is the physical matrix* $\overrightarrow{M}$ *resolved in* $\mathrm{F_X}$*.*

Definition 7. *Let* $\mathrm{F_X}, \mathrm{F_Y}$ *be a frames and* $\overrightarrow{R}_{\mathrm{Y/X}}$ *be a physical rotation matrix. The rotation matrix from* $\mathrm{F_X}$ *to* $\mathrm{F_Y}$ *is defined by*

$$R_{\mathrm{Y/X}} \triangleq \overrightarrow{R}_{\mathrm{Y/X}}\Big|_{\mathrm{X}} = \overrightarrow{R}_{\mathrm{Y/X}}\Big|_{\mathrm{Y}} = \begin{bmatrix} \hat{\imath}^{\mathrm{T}}_{\mathrm{X}}\hat{\imath}_{\mathrm{Y}} & \hat{\imath}^{\mathrm{T}}_{\mathrm{X}}\hat{\jmath}_{\mathrm{Y}} & \hat{\imath}^{\mathrm{T}}_{\mathrm{X}}\hat{k}_{\mathrm{Y}} \\ \hat{\jmath}^{\mathrm{T}}_{\mathrm{X}}\hat{\imath}_{\mathrm{Y}} & \hat{\jmath}^{\mathrm{T}}_{\mathrm{X}}\hat{\jmath}_{\mathrm{Y}} & \hat{\jmath}^{\mathrm{T}}_{\mathrm{X}}\hat{k}_{\mathrm{Y}} \\ \hat{k}^{\mathrm{T}}_{\mathrm{X}}\hat{\imath}_{\mathrm{Y}} & \hat{k}^{\mathrm{T}}_{\mathrm{X}}\hat{\jmath}_{\mathrm{Y}} & \hat{k}^{\mathrm{T}}_{\mathrm{X}}\hat{k}_{\mathrm{Y}} \end{bmatrix} . \tag{A.8}$$

Definition 8. *Let* $\mathrm{F_X}, \mathrm{F_Y}$ *be a frames and* $\vec{R}_{\mathrm{Y/X}}$ *be a physical rotation matrix. The orientation matrix of* $\mathrm{F_X}$ *relative to* $\mathrm{F_Y}$ *is defined by*

$$\mathcal{O}_{\mathrm{X/Y}} \triangleq R_{\mathrm{Y/X}} = R_{\mathrm{X/Y}}^{\mathrm{T}}. \tag{A.9}$$

Lemma 10. *Let* $\mathrm{F_X}, \mathrm{F_Y}$ *be a frames,* $\vec{x}$ *a physical vector, and* $\mathcal{O}_{\mathrm{X/Y}}$ *the orientation matrix of* $\mathrm{F_X}$ *relative to* $\mathrm{F_Y}$*. Then*

$$\vec{x}\Big|_{\mathrm{X}} = \mathcal{O}_{\mathrm{X/Y}}\, \vec{x}\Big|_{\mathrm{Y}}. \tag{A.10}$$

Lemma 11. *Let* $\mathrm{F_X}, \mathrm{F_Y}$ *be a frames,* $\vec{M}$ *a physical matrix, and* $\mathcal{O}_{\mathrm{X/Y}}$ *orientation matrix of* $\mathrm{F_X}$ *relative to* $\mathrm{F_Y}$*. Then*

$$\vec{M}\Big|_{\mathrm{X}} = \mathcal{O}_{\mathrm{X/Y}}\, \vec{M}\Big|_{\mathrm{Y}}\, \mathcal{O}_{\mathrm{X/Y}}^{\mathrm{T}}. \tag{A.11}$$

Lemma 12. *Let* $\mathrm{F_X}$ *be a frame and* $\vec{x}^{\times}$ *a physical cross product matrix. The physical cross product matrix resolved in* $\mathrm{F_X}$ *is given by*

$$\vec{x}^{\times}\Big|_{\mathrm{X}} = \vec{x}\Big|_{\mathrm{X}}^{\times} = \begin{bmatrix} 0 & -\hat{k}_X^{\mathrm{T}}\vec{x} & \hat{\jmath}_X^{\mathrm{T}}\vec{x} \\ \hat{k}_X^{\mathrm{T}}\vec{x} & 0 & -\hat{\imath}_X^{\mathrm{T}}\vec{x} \\ -\hat{\jmath}_X^{\mathrm{T}}\vec{x} & \hat{\imath}_X^{\mathrm{T}}\vec{x} & 0 \end{bmatrix}. \tag{A.12}$$

Lemma 13. *Let* $\mathrm{F_X}$ *be a frame and* $\vec{x}$ *a physical vector defined in* (A.4)*. The frame derivative of* $\vec{x}$ *with respect to* $\mathrm{F_X}$ *resolved in* $\mathrm{F_X}$ *is given by*

$$\overset{\mathrm{X}\bullet}{\vec{x}}\Big|_{\mathrm{X}} \triangleq \begin{bmatrix} \dot{x}_1 \\ \dot{x}_2 \\ \dot{x}_3 \end{bmatrix}. \tag{A.13}$$

Definition 9. *Let* $\mathrm{F_X}$ *be a frame,* $\mathcal{B}$ *a collection of rigid bodies* $\mathcal{B}_1, \mathcal{B}_2 \ldots, \mathcal{B}_n$*, and let* w *be a point. The, angular momentum of* $\mathcal{B}$ *relative to* w *with respect to* $\mathrm{F_X}$ *is defined by*

$$\vec{H}_{\mathcal{B}/w/\mathrm{X}} \triangleq \sum_{i=1}^{n} \vec{H}_{\mathcal{B}_i/w/\mathrm{X}}, \tag{A.14}$$

where, for $i = 1, \ldots, n$, the angular momentum $\vec{H}_{\mathcal{B}_i/w/\mathrm{X}}$ is defined by

$$\vec{H}_{\mathcal{B}_i/w/\mathrm{X}} \triangleq \int_{\mathcal{B}_i} \vec{r}_{dm/w} \vec{v}_{dm/w/\mathrm{X}} dm. \tag{A.15}$$

Lemma 14. *Let F_Y be a frame attached to the rigid body $\mathcal{B}$, define a frame F_X, and let w be a point fixed in $\mathcal{B}$. Then the angular momentum of $\mathcal{B}$ relative to w with respect to F_X is given by*

$$\vec{H}_{\mathcal{B}/w/\mathrm{X}} = \vec{J}_{\mathcal{B}/w} \vec{\omega}_{\mathrm{Y}/\mathrm{X}}, \tag{A.16}$$

where positive-definite physical inertia matrix, $\vec{J}_{\mathcal{B}/w}$ of $\mathcal{B}$ relative to w is defined by

$$\vec{J}_{\mathcal{B}/w} \triangleq \int_{\mathcal{B}} \|\vec{r}_{dm/w}\|^2 \vec{U} - \vec{r}_{dm/w} \vec{r}^{\mathrm{T}}_{dm/w} dm. \tag{A.17}$$

Lemma 15. *Let $\mathcal{B}$ be a rigid body of mass $m_\mathcal{B}$ with center of mass c, define a frame F_X, and let w be a point fixed in $\mathcal{B}$. The angular momentum of $\mathcal{B}$ relative to c with respect to F_X is given by*

$$\vec{H}_{\mathcal{B}/c/\mathrm{X}} = \vec{H}_{\mathcal{B}/w/\mathrm{X}} + \vec{r}_{\mathrm{c}/w} \times m_\mathcal{B} \vec{v}_{\mathrm{c}/w/\mathrm{X}}. \tag{A.18}$$

Lemma 16. *Let $\mathcal{B}$ be a rigid body of mass $m_\mathcal{B}$ with center of mass c, define a frame F_X, and let w be a point fixed in $\mathcal{B}$. Then the physical inertia matrix of $\mathcal{B}$ relative to w is given by*

$$\vec{J}_{\mathcal{B}/w} = \vec{J}_{\mathcal{B}/\mathrm{c}} - m_\mathcal{B} (\vec{r}^{\times}_{w/\mathrm{c}})^2. \tag{A.19}$$

BIBLIOGRAPHY

[1] Chaturvedi, N. A., Sanyal, A. K., and McClamroch, N. H., "Rigid-body attitude control," *Control Systems, IEEE*, Vol. 31, No. 3, 2011, pp. 30–51.

[2] Stuelpnagel, J., "On the parametrization of the three-dimensional rotation group," *SIAM review*, Vol. 6, No. 4, 1964, pp. 422–430.

[3] Markley, F. L., "Attitude error representations for Kalman filtering," *Journal of guidance, control, and dynamics*, Vol. 26, No. 2, 2003, pp. 311–317.

[4] Wertz, J. R., Everett, D. F., and Puschell, J. J., *Space Mission Engineering: The New SMAD*, Microcosm Press, 2011.

[5] Bhat, S. P. and Bernstein, D. S., "A topological obstruction to continuous global stabilization of rotational motion and the unwinding phenomenon," *Systems & Control Letters*, Vol. 39, No. 1, 2000, pp. 63–70.

[6] Mayhew, C. G., Sanfelice, R. G., and Teel, A. R., "On path-lifting mechanisms and unwinding in quaternion-based attitude control," *Automatic Control, IEEE Transactions on*, Vol. 58, No. 5, 2013, pp. 1179–1191.

[7] Park, G., Seagraves, S., and McClamroch, N. H., "A Dynamic Model of a Passive Magnetic Attitude Control System for the RAX Nanosatellite," *Guidance, Navigation, and Control Conference*, AIAA, Toronto, Ontario.

[8] Hughes, P. C., *Spacecraft Attitude Dynamics*, Wiley, 1986.

[9] Lovera, M., "Optimal magnetic momentum control for inertially pointing spacecraft," *European Journal of Control*, Vol. 7, No. 1, 2001, pp. 30–39.

[10] Chen, X., Steyn, W. H., Hodgart, S., and Hashida, Y., "Optimal combined reaction-wheel momentum management for Earth-pointing satellites," *Journal of guidance, control, and dynamics*, Vol. 22, No. 4, 1999, pp. 543–550.

[11] Carpenter, M. D. and Peck, M. A., "Reducing Base Reactions With Gyroscopic Actuation of Space-Robotic Systems," *Robotics, IEEE Transactions on*, Vol. 25, No. 6, 2009, pp. 1262–1270.

[12] Curti, F., Romano, M., and Bevilacqua, R., "Lyapunov-based thrusters' selection for spacecraft control: analysis and experimentation," *Journal of guidance, control, and dynamics*, Vol. 33, No. 4, 2010, pp. 1143–1160.

[13] Rui, C., Kolmanovsky, I. V., and McClamroch, N. H., "Nonlinear attitude and shape control of spacecraft with articulated appendages and reaction wheels," *Automatic Control, IEEE Transactions on*, Vol. 45, No. 8, 2000, pp. 1455–1469.

[14] Psiaki, M. L., "Magnetic torquer attitude control via asymptotic periodic linear quadratic regulation," *Journal of Guidance, Control, and Dynamics*, Vol. 24, No. 2, 2001, pp. 386–394.

[15] Arduini, C. and Baiocco, P., "Active magnetic damping attitude control for gravity gradient stabilized spacecraft," *Journal of Guidance, Control, and Dynamics*, Vol. 20, No. 1, 1997, pp. 117–122.

[16] Krishnan, S. and Vadali, S. R., "An inverse-free technique for attitude control of spacecraft using CMGs," *Acta Astronautica*, Vol. 39, No. 6, 1996, pp. 431–438.

[17] Wen, J.-Y. and Kreutz-Delgado, K., "The attitude control problem," *Automatic Control, IEEE Transactions on*, Vol. 36, No. 10, 1991, pp. 1148–1162.

[18] Tsiotras, P., Corless, M., and Longuski, J., "A novel approach to the attitude control of axisymmetric spacecraft," *Automatica*, Vol. 31, No. 8, 1995, pp. 1099–1112.

[19] Joshi, S., Kelkar, A., and Wen, J.-Y., "Robust attitude stabilization of spacecraft using nonlinear quaternion feedback," *Automatic Control, IEEE Transactions on*, Vol. 40, No. 10, 1995, pp. 1800–1803.

[20] Coverstone-Carroll, V., "Detumbling and reorienting underactuated rigid spacecraft," *Journal of guidance, control, and dynamics*, Vol. 19, No. 3, 1996, pp. 708–710.

[21] Avanzini, G. and Giulietti, F., "Magnetic detumbling of a rigid spacecraft," *Journal of Guidance, Control, and Dynamics*, Vol. 35, No. 4, 2012, pp. 1326–1334.

[22] Kim, K.-S. and Kim, Y., "Robust backstepping control for slew maneuver using nonlinear tracking function," *Control Systems Technology, IEEE Transactions on*, Vol. 11, No. 6, 2003, pp. 822–829.

[23] Wie, B. and Lu, J., "Feedback control logic for spacecraft eigenaxis rotations under slew rate and control constraints," *Journal of Guidance, Control, and Dynamics*, Vol. 18, No. 6, 1995, pp. 1372–1379.

[24] Bilimoria, K. D. and Wie, B., "Time-optimal three-axis reorientation of a rigid spacecraft," *Journal of Guidance, Control, and Dynamics*, Vol. 16, No. 3, 1993, pp. 446–452.

[25] Wie, B. and Barba, P. M., "Quaternion feedback for spacecraft large angle maneuvers," *Journal of Guidance, Control, and Dynamics*, Vol. 8, No. 3, 1985, pp. 360–365.

[26] Lo, S.-C. and Chen, Y.-P., "Smooth sliding-mode control for spacecraft attitude tracking maneuvers," *Journal of Guidance, Control, and Dynamics*, Vol. 18, No. 6, 1995, pp. 1345–1349.

[27] Sharma, R. and Tewari, A., "Optimal nonlinear tracking of spacecraft attitude maneuvers," *Control Systems Technology, IEEE Transactions on*, Vol. 12, No. 5, 2004, pp. 677–682.

[28] Byrnes, C. I. and Isidori, A., "On the attitude stabilization of rigid spacecraft," *Automatica*, Vol. 27, No. 1, 1991, pp. 87–95.

[29] Bang, H., Myung, H.-S., and Tahk, M.-J., "Nonlinear momentum transfer control of spacecraft by feedback linearization," *Journal of Spacecraft and Rockets*, Vol. 39, No. 6, 2002, pp. 866–873.

[30] Pittelkau, M. E., "Optimal periodic control for spacecraft pointing and attitude determination," *Journal of Guidance, Control, and Dynamics*, Vol. 16, No. 6, 1993, pp. 1078–1084.

[31] Kwon, S., Shimomura, T., and Okubo, H., "Pointing control of spacecraft using two SGCMGs via LPV control theory," *Acta Astronautica*, Vol. 68, No. 7, 2011, pp. 1168–1175.

[32] Vadali, S., Kraige, L., and Junkins, J., "New results on the optimal spacecraft attitude maneuver problem," *Journal of Guidance, Control, and Dynamics*, Vol. 7, No. 3, 1984, pp. 378–380.

[33] Krstic, M. and Tsiotras, P., "Inverse optimal stabilization of a rigid spacecraft," *Automatic Control, IEEE Transactions on*, Vol. 44, No. 5, 1999, pp. 1042–1049.

[34] Dwyer, III, T. A. and Sira-Ramirez, H., "Variable-structure control of spacecraft attitude maneuvers," *Journal of Guidance, Control, and Dynamics*, Vol. 11, No. 3, 1988, pp. 262–270.

[35] Egeland, O. and Godhavn, J.-M., "Passivity-based adaptive attitude control of a rigid spacecraft," *Automatic Control, IEEE Transactions on*, Vol. 39, No. 4, 1994, pp. 842–846.

[36] Xiao, B., Hu, Q., and Zhang, Y., "Fault-tolerant attitude control for flexible spacecraft without angular velocity magnitude measurement," *Journal of Guidance, Control, and Dynamics*, Vol. 34, No. 5, 2011, pp. 1556–1561.

[37] Gasbarri, P., "A two-dimensional approach to multibody free dynamics in space environment," *Acta Astronautica*, Vol. 51, No. 12, 2002, pp. 831–842.

[38] Vu-Quoc, L. and Simo, J. C., "Dynamics of earth-orbiting flexible satellites with multibody components," *Journal of Guidance, Control, and Dynamics*, Vol. 10, No. 6, 1987, pp. 549–558.

[39] Nichkawde, C., Harish, P., and Ananthkrishnan, N., "Stability analysis of a multi-body system model for coupled slosh–vehicle dynamics," *Journal of Sound and Vibration*, Vol. 275, No. 3, 2004, pp. 1069–1083.

[40] Åström, K. J. and Wittenmark, B., *Adaptive control*, Courier Dover Publications, 2013.

[41] Landau, I. D., Lozano, R., and M'Saad, M., *Adaptive control*, Vol. 51, Springer Berlin, 1998.

[42] Ioannou, P. and Sun, J., "Theory and design of robust direct and indirect adaptive-control schemes," *International Journal of Control*, Vol. 47, No. 3, 1988, pp. 775–813.

[43] Junkins, J. L., Akella, M. R., and Robinett, R. D., "Nonlinear adaptive control of spacecraft maneuvers," *Journal of Guidance, Control, and Dynamics*, Vol. 20, No. 6, 1997, pp. 1104–1110.

[44] Yoon, H. and Tsiotras, P., "Spacecraft Adaptive Attitude and Power Tracking with Variable Speed Control Moment Gyroscopes," *Journal of Guidance, Control and Dynamics*, Vol. 25, 2002, pp. 1081–1090.

[45] Ahmed, J., Coppola, V. T., and Bernstein, D. S., "Adaptive asymptotic tracking of spacecraft attitude motion with inertia matrix identification," *Journal of Guidance, Control, and Dynamics*, Vol. 21, No. 5, 1998, pp. 684–691.

[46] Costic, B., Dawson, D., De Queiroz, M., and Kapila, V., "Quaternion-based adaptive attitude tracking controller without velocity measurements," *Journal of Guidance, Control, and Dynamics*, Vol. 24, No. 6, 2001, pp. 1214–1222.

[47] Slotine, J. and Di Benedetto, M., "Hamiltonian adaptive control of spacecraft," *Automatic Control, IEEE Transactions on*, Vol. 35, No. 7, 1990, pp. 848–852.

[48] Seo, D. and Akella, M. R., "High-performance spacecraft adaptive attitude-tracking control through attracting-manifold design," *Journal of guidance, control, and dynamics*, Vol. 31, No. 4, 2008, pp. 884–891.

[49] Schaub, H., Akella, M. R., and Junkins, J. L., "Adaptive control of nonlinear attitude motions realizing linear closed loop dynamics," *Journal of Guidance, Control, and Dynamics*, Vol. 24, No. 1, 2001, pp. 95–100.

[50] Luo, W., Chu, Y.-C., and Ling, K.-V., "Inverse optimal adaptive control for attitude tracking of spacecraft," *Automatic Control, IEEE Transactions on*, Vol. 50, No. 11, 2005, pp. 1639–1654.

[51] Chen, Z. and Huang, J., "Attitude tracking and disturbance rejection of rigid spacecraft by adaptive control," *IEEE Transactions on Automatic Control*, Vol. 54, No. 3, 2009, pp. 600–605.

[52] Zeng, Y., Araujo, A. D., and Singh, S. N., "Output feedback variable structure adaptive control of a flexible spacecraft," *Acta Astronautica*, Vol. 44, No. 1, 1999, pp. 11–22.

[53] Boškovic, J. D., Li, S.-M., and Mehra, R. K., "Robust adaptive variable structure control of spacecraft under control input saturation," *Journal of Guidance, Control, and Dynamics*, Vol. 24, No. 1, 2001, pp. 14–22.

[54] Cai, W., Liao, X., and Song, D. Y., "Indirect robust adaptive fault-tolerant control for attitude tracking of spacecraft," *Journal of Guidance, Control, and Dynamics*, Vol. 31, No. 5, 2008, pp. 1456–1463.

[55] BoSkoviC, J. D., Li, S.-M., and Mehra, R. K., "Intelligent control of spacecraft in the presence of actuator failures," *Decision and Control, 1999. Proceedings of the 38th IEEE Conference on*, Vol. 5, IEEE, 1999, pp. 4472–4477.

[56] Jiang, Y., Hu, Q., and Ma, G., "Adaptive backstepping fault-tolerant control for flexible spacecraft with unknown bounded disturbances and actuator failures," *ISA transactions*, Vol. 49, No. 1, 2010, pp. 57–69.

[57] Chaturvedi, N., Sanyal, A. K., and McClamroch, N. H., "Rigid Body Attitude Control: Using rotation matrices for continuous, singularity-free control laws," *IEEE Contr. Sys. Mag.*, Vol. 31, No. 3, 2011, pp. 30–51.

[58] Sanyal, A., Fosbury, A., Chaturvedi, N., and Bernstein, D. S., "Inertia-Free Spacecraft Attitude Tracking with Disturbance Rejection and Almost Global Stabilization," *AIAA J. Guid. Contr. Dyn.*, Vol. 32, 2009, pp. 1167–1178.

[59] Weiss, A., Yang, X., Kolmanovsky, I., and Bernstein, D. S., "Inertia-Free Spacecraft Attitude Control with Reaction-Wheel Actuation," *Proc. AIAA Guid. Nav. Contr. Conf.*, Toronto, August 2010, AIAA-2010-8297-163.

[60] Hoagg, J. B. and Bernstein, D. S., "Retrospective Cost Model Reference Adaptive Control for Nonminimum-Phase Discrete-Time Systems, Part 1: The Adaptive Controller; Part 2: Stability Analysis," *Proc. Amer. Contr. Conf.*, San Francisco, CA, June 2011, pp. 2927–2938.

[61] D'Amato, A. M., Sumer, E. D., and Bernstein, D. S., "Retrospective Cost Adaptive Control for Systems with Unknown Nonminimum-Phase Zeros," *AIAA Guid. Nav. Contr. Conf.*, Portland, OR, August 2011, AIAA-2011-6203.

[62] D'Amato, A. M., Sumer, E. D., and Bernstein, D. S., "Frequency-Domain Stability Analysis of Retrospective-Cost Adaptive Control for Systems with Unknown Nonminimum-Phase Zeros," *Proc. of 50th IEEE Conf. on Decision and Control*, Orlando, FL, December 2011, pp. 1098–1103.

[63] Yan, J., D'Amato, A. M., Sumer, D., Hoagg, J. B., and Bernstein, D. S., "Adaptive Control of Uncertain Hammerstein Systems Using Auxiliary Nonlinearities," *Proc. Conf. Dec. Contr.*, Maui, HI, December 2012.

[64] Al Janaideh, M., Yan, J., DAmato, A., and Bernstein, D., "Retrospective-cost adaptive control of uncertain Hammerstein-Wiener systems with memoryless and hysteretic nonlinearities," *Proceedings of AIAA Guidance, Navigation, and Control Conference, Minneapolis, MN, Paper No. AIAA-2012-4449-671*, 2012, pp. 1–26.

[65] Morozov, A., Hoagg, J. B., and Bernstein, D. S., "Retrospective Adaptive Control of a Planar Multilink Arm with Nonminimum-Phase Zeros," *Proc. of 49th IEEE Conf. on Decision and Control*, Atlanta, GA, December 2010, pp. 3706–3711.

[66] Isaacs, M. W., Hoagg, J. B., Morozov, A., and Bernstein, D. S., "A Numerical Study on Controlling a Nonlinear Multilink Arm Using a Retrospective Cost Model Reference Adaptive Controller," *Proc. of 50th IEEE Conf. on Decision and Control*, Orlando, FL, December 2011, pp. 8008–8013.

[67] Santillo, M. A., Holzel, M. S., Hoagg, J. B., and Bernstein, D. S., "Adaptive Control of the NASA Generic Transport Model Using Retrospective Cost Optimization," *AIAA Guidance, Navigation, and Control Conf., AIAA Paper*, Vol. 5616, 2009.

[68] D'Amato, A. M., Sumer, E. D., Mitchell, K. S., Morozov, A. V., Hoagg, J. B., and Bernstein, D. S., "Adaptive Output Feedback Control of the NASA GTM Model with Unknown Nonminimum-Phase Zeros," *AIAA Guid. Nav. Contr. Conf.*, Portland, OR, August 2011, AIAA-2011-6204.

[69] Coffer, B. C., Hoagg, J. B., and Bernstein, D. S., "Retrospective Cost Adaptive Control of the NASA GTM Model," *AIAA Guid. Nav. Contr. Conf.*, Toronto, August 2010, AIAA-2010-8404-212.

[70] Cruz, G., D'Amato, A. M., and Bernstein, D. S., "Retrospective Cost Adaptive Control of Spacecraft Attitude," *Proc. AIAA Guid. Nav. Contr. Conf.*, Minneapolis, MN, August 2012, AIAA-2012-4624-236.

[71] Cruz, G. and Bernstein, D. S., "Adaptive Spacecraft Attitude Control with Reaction Wheel Actuation," *Proc. Amer. Contr. Conf.*, Washington, DC, June 2013, pp. 4839–4844.

[72] Cruz, G. and Bernstein, D. S., "Retrospective Cost Adaptive Control of Spacecraft Attitude Using Magnetic Actuators," *Proc. AIAA Guid. Nav. Contr. Conf.*, Boston, MA, August 2013, AIAA-2013-4563.

[73] Weiss, A., Cruz, G., Agarwal, K., Rahman, Y., Medikeri, M., Xie, A., Camblor, M., Kolmanovsky, I., and Bernstein, D. S., "Inertia-free Attitude Control Laws Based on Rotation Matrices for Spacecraft with Torquers, Thrusters, and Wheels," *Proc. Itzhack Y. Bar-Itzhack Memorial Symposium on Estimation, Navigation, and Spacecraft Control*, 2012.

[74] Camblor, M., Cruz, G., Esteban, S., Leve, F. A., and Bernstein, D. S., "Retrospective cost adaptive spacecraft attitude control using control moment gyros," *American Control Conference (ACC), 2014*, June 2014, pp. 2492–2497.

[75] Cruz, G. and Bernstein, D. S., "Retrospective Cost-based Adaptive Spacecraft Attitude Control using Control Moment Gyros," Unpublished.

[76] Cruz, G. and Bernstein, D. S., "Noncolocated Adaptive Attitude Control of a Planar Two-Body Linkage with Nonminimum-Phase Dynamics," *American Control Conference (ACC)*, Chicago, IL, June 2015, Submitted.

[77] Hoagg, J. B. and Bernstein, D. S., "Retrospective Cost Adaptive Control for Nonminimum-Phase Discrete-Time Systems Part 1: The Ideal Controller and Error System, Part 2: The Adaptive Controller and Stability Analysis," *Proc. Conf. Dec. Contr.*, Atlanta, GA, December 2010, pp. 893–904.

[78] Santillo, M. A. and Bernstein, D. S., "Adaptive Control Based on Retrospective Cost Optimization," *Journal of Guidance, Control, and Dynamics*, Vol. 33, 2010, pp. 289–304.

[79] Sumer, E. D. and Bernstein, D. S., "Retrospective Cost Adaptive Control with Error-Dependent Regularization for MIMO Systems with Uncertain Nonminimum-Phase Transmission Zeros," *AIAA Guid. Nav. Contr. Conf., Minneapolis, MN*, 2012, AIAA-2012-4670.

[80] Simon, D., *Optimal state estimation: Kalman, H infinity, and nonlinear approaches*, John Wiley & Sons, 2006.

[81] Bernstein, D. S., *Geometry, Kinematics, Statics, and Dynamics*, 2013, Unpublished.

[82] Ismail, Z. and Varatharajoo, R., "A study of reaction wheel configurations for a 3-axis satellite attitude control," *Advances in Space Research*, Vol. 45, No. 6, 2010, pp. 750–759.

[83] Stickler, A. C. and Alfriend, K. T., "Elementary Magnetic Attitude Control System," *Journal of Spacecraft and Rockets*, Vol. 13, 1976, pp. 282–287.

[84] Marteru, F., Gabriel, S. R., and Rogers, E., "Attitude determination and control for small spacecraft," *Control '96, UKACC International Conference on (Conf. Publ. No. 427)*, Vol. 1, sept. 1996, pp. 620 – 625 vol.1.

[85] Reyhanoglu, M. and Hervas, J. R., "Three-axis magnetic attitude control algorithms for small satellites," *Recent Advances in Space Technologies (RAST), 2011 5th International Conference on*, IEEE, 2011, pp. 897–902.

[86] Silani, E. and Lovera, M., "Magnetic spacecraft attitude control: a survey and some new results," *Control Engineering Practice*, Vol. 13, 2005, pp. 357–371.

[87] Lovera, M. and Astolfi, A., "Global Magnetic Attitude Control of Inertially Pointing Spacecraft," *Journal of Guidance Control and Dynamics*, Vol. 28, 2005, pp. 1065–1072.

[88] Bayat, F., Bolandi, H., and Jalali, A. A., "A heuristic design method for attitude stabilization of magnetic actuated satellites," *Acta Astronautica*, Vol. 65, No. 1112, 2009, pp. 1813 – 1825.

[89] Finlay, C. C., Maus, S., Beggan, C. D., Bondar, T. N., Chambodut, A., Chernova, T. A., Chulliat, A., Golovkov, V. P., Hamilton, B., Hamoudi, M., et al., "International geomagnetic reference field: the eleventh generation," *Geophysical Journal International*, Vol. 183, No. 3, 2010, pp. 1216–1230.

[90] Wie, B., "Singularity Analysis and Visualization for Single-Gimbal Control Moment Gyro Systems," *Journal of Guidance, Control, and Dynamics*, Vol. 27, No. 2, 2004, pp. 271–282.

[91] Kurokawa, H., "A Geometry Study of Single Gimbal Control Moment Gyros–Singularity Problem and Steering Law," *TR 175*, Mechanical Engineering Lab., Tsukuba, Ibaraki, Japan, 1998.

[92] Takada, K., Kojima, H., and Matsuda, N., "Control Moment Gyro Singularity-Avoidance Steering Control Based on Singular-Surface Cost Function," *Journal of Guidance, Control, and Dynamics*, Vol. 33, No. 5, 2010, pp. 1442–1450.

[93] Paradiso, J. A., "Global Steering of Single Gimbaled Control Moment Gyroscopes using a Directed Search," *Journal of Guidance, Control, and Dynamics*, Vol. 15, No. 5, 1992, pp. 1236–1244.

[94] Leve, F. A., "Evaluation of Steering Algorithm Optimality for Single-Gimbal Control Moment Gyroscopes," *IEEE Transactions on Control Systems Technology*, 2013.

[95] Yoon, H. and Tsiotras, P., "Singularity Analysis of Variable-Speed Control Moment Gyros," *Journal of Guidance, Control, and Dynamics*, Vol. 27, 2004, pp. 374–386.

[96] MacKunis, W., Dupree, K., Fitz-Coy, N., and Dixon, W. E., "Adaptive satellite attitude control in the presence of inertia and CMG gimbal friction uncertainties," *The Journal of the Astronautical Sciences*, Vol. 56, No. 1, 2008, pp. 121–134.

[97] Yoon, H. and Agrawal, B., "Adaptive Control of Uncertain Hamiltonian Multi-Input Multi-Output Systems: With Application to Spacecraft Control," *Control Systems Technology, IEEE Transactions on*, Vol. 17, No. 4, 2009, pp. 900–906.

[98] Cui, P. and Liu, F., "Attitude-Tracking Control with Path Planning for Agile Satellite Using Double-Gimbal Control Moment Gyros," *Mathematical Problems in Engineering*, Vol. 2012, 2012.

[99] Agarwal, K., Weiss, A., Kolmanovsky, I., and Bernstein, D. S., "Inertia-Free Spacecraft Attitude Control with Control-Moment-Gyro Actuation," *Proc. AIAA Guid. Nav. Contr. Conf.*, Minneapolis, MN, August 2012, AIAA-2012-5003-282.

[100] Bhat, S. and Tiwari, P., "Controllability of Spacecraft Attitude Using Control Moment Gyroscopes," *Automatic Control, IEEE Transactions on*, Vol. 54, No. 3, March 2009, pp. 585–590.

[101] Lee, T., McClamroch, N., and Leok, M., "A lie group variational integrator for the attitude dynamics of a rigid body with applications to the 3D pendulum," *Control Applications, 2005. CCA 2005. Proceedings of 2005 IEEE Conference on*, Aug 2005, pp. 962–967.

[102] Camblor, M., Xie, A., Cruz, G., Esteban, S., Lee, T., and Bernstein, D. S., "A Numerical Comparison of Inertia-Free Attitude Control Laws for a Spacecraft with a Discrete Flexible Mode," *Proc. AIAA Guid. Nav. Contr. Conf.*, Boston, MA, August 2013, AIAA-2013-4562.

[103] Clarke, D., "Self-tuning control of nonminimum-phase systems," *Automatica*, Vol. 20, No. 5, 1984, pp. 501–517.